SYNTHESIS AND CHARACTERIZATION OF CERAMICS IN THE Ti-B-N-C SYSTEM

A Thesis Submitted for the Degree
of
Doctor of Philosophy

by
SU-JONG YOON

DEPARTMENT OF MATERIALS TECHNOLOGY
BRUNEL
THE UNIVERSITY OF WEST LONDON

January 1994

ABSTRACT

Titanium and boron nitride and carbide, titanium diboride were synthesized by carbothermic reduction as single phase as well as mixtures intended to form composite materials. The aims of the project is to study the physical chemistry of carbothermic reduction for the production of pure non-oxide ceramic powders and also for the in-situ formation of ceramic/ceramic partially-densified composites. The thermodynamic and kinetic factors that govern the phase constituents are discussed and the effect of processing parameters on the morphology and extent of reduction are also established.

The first part of the present investigation is aimed at the production of titanium nitride, carbonitride and carbide powders and the in-situ formation of TiN/TiC partially-densified composites by the carbothermic reduction of titania in suitable nitriding atmospheres. The investigation includes the aspects of the thermodynamics and kinetics of the nitriding reaction and points out the reaction mechanism by identifying the phase formed after the nitridation process. The microstructures produced after the reduction-nitridation process have been correlated with the thermodynamic and kinetic parameters.

The synthesized titanium nitride powder was identified as the carbonitride phase, $Ti(C_xN_{1-x})$, having a range of composition. The rate of reduction of TiO_2 was found to be determined by the rate of oxygen diffusion in the sub-oxide lattice and the derived value of activation energy in the temperature range 1473K to 1773K from the Arrhenius plot is 120 $kJ \cdot mole^{-1}$ of TiO_2. Ti_3O_5 was found as a high temperature precursor phase for the formation of titanium nitride. The use of iron chloride as catalyst and activated charcoal in the mixtures of oxide increased the yield of titanium nitride phase by enhancing the rate of reduction of titanium oxides. The morphology of titanium carbonitride particles was dependent upon the reactivity of carbon and the temperature. The calculated equilibrium phase fields were found to be in agreement with the experimental data and provide a means to select the variables for the reduction condition for designing a required ceramic microstructure.

The microstructure of boron nitrides is closely related to the structural chemistry of carbon and nitriding agent. The main aim of the second part of

the project was to synthesize boron nitride and carbide powders and whiskers by carbothermic reduction of boric anhydride (B_2O_3) in nitrogen atmosphere and also to understand a relation between the processing parameters and the phases produced. The effect of processing conditions such as the gas composition, reactivity of carbon, reaction temperature and time as well as the composition of starting materials on the synthesis of boron nitride and carbide phases were studied.

The reactivity of carbon, B/C ratio and gas composition were the most important variables that determined the formation, structure and morphology of the nitride. During the nitridation process, boron carbide phase also formed and played a significant role. The investigation also reports the evidence for the formation of metastable forms of BN i.e wurtzite and cubic BN. We also report the results of the solubility of nitrogen in C-saturated B_4C structure.

The third part of the present work is aimed at the production of TiB_2 powders. Aspects of the formation of two or three ceramic phase mixtures were also examined together with the relative stability of the single phase mixed diborides with respect to pure diboride phase. The central aim of this part is to establish the mechanism of the synthesis reaction leading to the formation of uniform size of titanium diboride crystals.

Titanium boride (TiB_2) powder was produced in the powder form by the reduction of ingredient oxides with carbon via a gas-solid phase reaction. For the production of the composite microstructure, the nitrogen partial pressure was found to be the most critical factor. In the composite microstructure, the titanium nitride particles have a submicrometer size whereas the boride particle size is only a few micrometers with predominantly hexagonal morphology. Some calculated equilibrium phase fields have been experimentally verified. The empirical verification is a useful tool to establish the correctness of the calculated phase diagram. The theoretical approach therefore enable to identify the condition for the formation of phase mixtures. The constituent phases depend on the reduction conditions. For example, nitrides in equilibrium with TiB_2 can only form above a critical nitrogen partial pressure whereas TiC or B_4C form in the inert atmospheres. This results is applicable to all other ceramics. The investigation also shows the viability of production of the composite powder mixture via the oxide co-reduction technique. The synthesis of TiB_2/TiN, TiB_2/TiC, TiB_2/TiN/BN and mixed diboride composites is possible by employing the reduction route.

CONTENTS

LIST OF FIFURES

CHAPTER. III

CHAPTER. IV

LIST OF TABLES

CHAPTER. II

CHAPTER. III

CHAPTER. IV

LIST OF PHOTOGRAPHS

CHAPTER I. GENERAL INTRODUCTION

Non-oxide ceramics, such as borides, carbides, nitrides and silicides, are known for their excellent mechanical strength, hardness, corrosion and oxidation resistance, thermal shock stability, and for a wide variation in electronic properties. Until recently, these compounds have received less attention than oxide ceramics partly due to difficulties encountered in routinely obtaining pure materials with well-defined bulk properties, grain characteristics and micro-structures. However, a rapid increase in demand for rugged ceramics has led to greater interest in non-oxide materials, and their development is now a key element in the design of advanced ceramics and their composites.

Titanium nitride and carbide have extremely high melting point and hardness, high chemical and thermal stability. They can also be used as a part of high temperature structure materials and for integrated circuitry for tailoring the electrical and thermal properties. By TiN dispersion in Si_3N_4[1], the properties of monolithic Si_3N_4 ceramics, such as strength and wear resistance, have been improved. Boron nitride (BN) has the superior thermal shock resistance, erosion resistance to molten metals and demonstrates improved machinability. The material has a low density, chemical inertness, low electric conductivity and high thermal conductivity. Because of its unique combination of properties, BN is increasingly used, for example, as evaporation boats and crucible materials. The major industrial use of boron carbide (B_4C) is for its excellent hardness; namely as abrasive grits and for wear-resistant engineering components. It is also used in nuclear industry. The borides constitute a group of ceramic materials with attractive and unusual combination of properties. Their extreme hardness and high melting points resemble those of covalently bonded ceramics, while their high thermal and electrical conductivity, positive temperature coefficient of resistivity and lustre are typical of metals. These unusual properties result from the simultaneous contributions of covalent and metallic bonding characteristics in the structure.[2] The diborides also exhibit

a considerable resistance to oxidation in air above 1373K. In the case of TiB_2, the oxidation resistance has been observed up to 1673K. TiB_2 is also an excellent reinforcing material for metal matrix composites. Its hardness (3400 HV) is greater than that of the more commonly used tungsten carbide (WC, 2000 HV) and is almost as hard as that of SiC (3500 HV).[3] The importance of these materials not only as monolithic materials but also as composite materials have been recognized. Ceramic-matrix composites, for example, based on silicon nitride, carbide and alumina have found applications as high performance materials structural parts, components and for cutting tools. Besides structural engineering applications, tribology is another area of application where the real potential of these materials have not been realised.

At present there are several methods for the preparation of metal nitride by the following reactions: 1) direct nitriding of the reactive metals and their hydrides lead to an exothermic reaction via which the metal nitrides form.[4] 2) Alternatively the oxides are reduced in the presence of nitrogen gas to form metal nitride.[5,6,20-22] Mixed interstitials can also be synthesised via this route. 3) Titanium nitride powder can also be synthesised by a chemical vapour reaction route[7] in which titanium tetrachloride and ammonia react in the vapour phase and yield high quality submicrometer size TiN powder. In addition to this, recently Tioxide has reported a process based on $TiCl_4$ vapour synthesis. The synthesis process, however, is rather expensive and the powder was marketed for 2 years and then withdrawn because of the unfavourable price competition. For the synthesis of carbides:[8] 1) direct reaction of the metal or their halides in an inert gas atmosphere or in a vacuum is carried out. 2) Reaction of the metal oxides and carbon to form metal carbide has been practised. 3) Alternatively the reaction of metal with a carburizing gas yield metal carbide. 4) Precipitation from the gas phase by reacting the metal halide or metal carbonyl in hydrogen lead to the formation of the carbide phase. For the synthesis of borides: 1) High-temperature reduction of the metal oxide by carbide and carbon has been one of the earliest routes for the synthesis of borides.[9] 2) Reaction of the metal halide with BH_3 in a plasma arc yields ultra-fine splat-cooled TiB_2 powders.[10,11] 3)The

reductive dehalogenation of halide with sodium metal as a low temperature route to boride precursors has also been developed.[12] 4) The hydrogen plasma arc process has been employed to carry out the reduction of the metal and boron oxides.[13] 5) TiB_2 powders with sub-borides of Ti has been synthesised by solid state reactions of metallic titanium and amorphous boron powder.[14] 6) The decomposition of metal borohydrides can also yield TiB_2 powder.[9] 7) The final category of synthesis reaction is the carbothermic reduction of oxides.[15]

Amongst all the above described processing techniques for non-oxide ceramics, the carbothermic reduction process is by far the cheapest because it relies on the supply of inexpensive raw materials such as coal and naturally occurring rutile, ilmenite, silica or borax. Also CO gas produced as a result of the reduction reaction can be used as a fuel to meet at least a part of the total energy cost of the process. The heat released from complete combustion of CO gas to CO_2 could therefore be utilised to meet the energy requirement of the materials fabrication process. Besides its favourable energy-economy, the process can be controlled to yield partially densified monolithic phases, ceramic/ceramic or metal/ceramic matrix composite materials which can be subsequently fully densified. Considerable cost incurred in making non-oxide ceramics from expensive starting materials such organometallic precursors and metal powders and a large energy cost means that the carbothermic reduction should be a more attractive method for the synthesis of non-oxide ceramics. The potential for the development of in-situ composite microstructure and of near-net shapes could also be realised by adopting this technique. In the majority of ceramic composite manufacturing processes, the cost of premixing ingredients is substantially large. For example, the premixing cost of Al_2O_3 powder with SiC whiskers, as cited by Cales[16], is approximately 37% of the total manufacturing cost. This is compared in **Figure I-1**. If a carbothermic reduction process is tailored for manufacturing SiC whisker-reinforced Al_2O_3 matrix composites, not only the mixing cost can be reduced but also the hot pressing cost. Additionally a finer microstructure could be designed that will yield a superior material for mechanical and wear properties. The finer

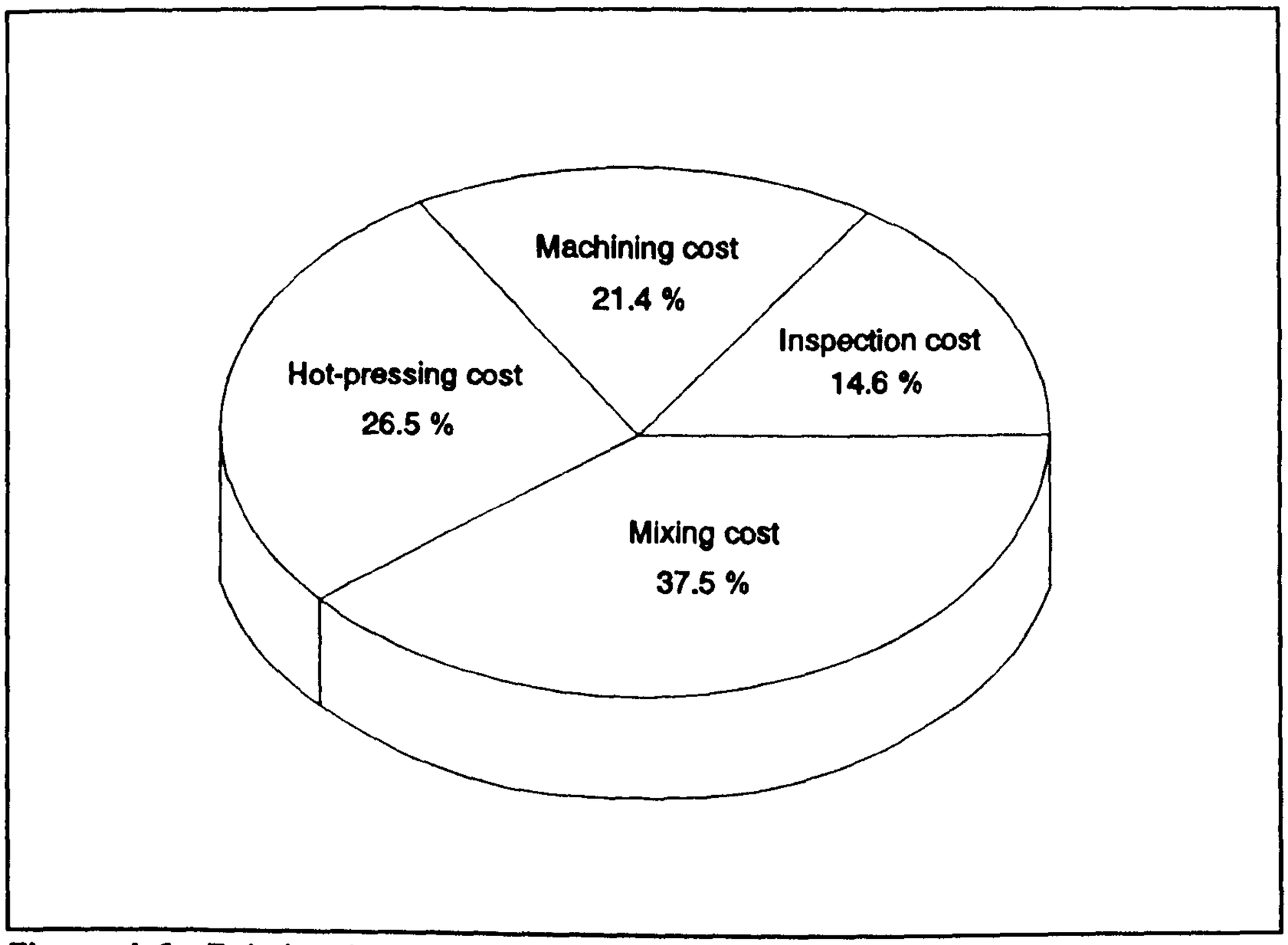

Figure I-1. Fabrication cost of alumina/SiC reinforced composite tool inserts.[16]

microstructure has an additional advantage in reducing the machining cost by the spark erosion technique. In this technique, the finer grain size improves the machinability.

It is important to compare the relative cost of powder at least for providing a production cost of each type of ceramic powders. Si_3N_4 is a widely used powder and is produced worldwide by several companies. On an industrial scale, it is produced by the reaction of silicon tetrachloride and ammonia. The process was developed by Ube company in Japan. The Starck powder is produced by direct nitridation of metallic silicon. Both types of powder sell for more than US$80 per kilogram. Recently Dow chemical company announced the production of quality silicon nitride by a carbothermic reduction process.[17] Dow anticipates to sell ceramic powder by December 1994 at a cost of US$20 per pound and $15 by the end of 1996. Although ceramic-composite materials are value-added products, yet the product price is prohibitively high to acquire a reasonable share of the engineering materials market. It is therefore essential that in order to keep the production cost low,

new manufacturing strategies based on novel scientific principles have to be adopted.

The present investigation cites several examples of a ceramic powder mixture manufacturing procedure that can be subsequently sintered and densified by either suitable pressureless or high-pressure densification techniques. The morphology based on the co-reduction of refractory oxide mixtures also provides a mechanism to control the microstructural characteristics of powder mixtures that is often difficult to manipulate without substantially increasing the raw materials cost. Besides an anticipated large reduction in the powder manufacturing cost, a further cut in the price of finished product is also possible because of the better sinterability of co-reduced powders. The principle behind co-reduction of refractory metal oxides (M_xO_y) is their thermal decomposition behaviour at elevated temperature which intensifies in the presence of a reducing atmosphere, i.e the reaction $M_xO_y = xM + y/2O_{2(g)}$ is thermodynamically less favourable than the reaction $M_xO_y + yC = xM + yCO$. The latter reaction in the presence of excess stoichiometric carbon (i.e x+y amount of C) will yield 'x' amount of MC carbide plus CO gas. The above thermodynamic principle has been adopted to produce nitride, boride and carbide ceramic powders and their mixtures.

The aim of the project is to study the physical chemistry of carbothermic reduction for the production of non-oxide ceramic powders, whiskers and the in-situ formation of ceramic/ceramic partially-densified composites. Also it intend to reduce the producing cost and to meet requirement for the final applications by adopting above process. A further aim is to identify the thermodynamic and kinetic parameters for ceramic powder synthesis and their relation with the resultant microstructure.

CHAPTER II. SYNTHESIS OF TITANIUM NITRIDE BY CARBOTHERMIC REDUCTION OF RUTILE (TiO_2)

1. INTRODUCTION

In the last 20 years, there has been an increasing need for new types of materials that can withstand large mechanical stress at higher temperatures and under severe environmental condition. The potential of nitride ceramics as structural engineering materials have been realised particularly for high temperature applications. In particular, silicon nitride and sialon ceramics including SiC have found applications as high temperature structural materials and also as tribological materials.[18] However, for temperatures above 1473K, the structural integrity of these materials drop rapidly due to their enhanced oxidation rate and creep, the latter arising due to the presence of a weak grain boundary phase.[18,19] Metal and metalloid nitrides exhibit thermal properties and good wettability towards most metals. Combined with their superior thermal and mechanical properties, nitride ceramic powders and whiskers could offer a new range of high performance materials for various engineering applications.

The major difficulty, however, arises in synthesising these materials economically in pure form and also with some suitable densifying agent that would aid further sintering process. The sintering behaviour of ceramics and consequently their microstructure and properties are influenced by the various processing steps involved as well as by the characteristics of the raw materials used during fabrication. Currently the cost of production of these materials is high which raises the manufacturing cost of the finished engineering components. Polycrystalline samples of nitrides are usually prepared by powder metallurgy. The synthesis routes are described in previous Chapter I.

Titanium nitride (TiN) is used as wear-resistant coating materials, as a diffusion barrier in semiconductor technology, and as hard refractory material

in powder metallurgy. TiN, as a reinforced dispersion material, has been utilised in Al_2O_3 matrix[23] for improving toughness. Norton/Quartz et Silice company have used TiN for rapid electrodischarge machining (EDM) of Si_3N_4. The addition of TiN is also known to improve toughness as well as the EDM properties for machining complex shapes. The properties of monolithic Si_3N_4 ceramics, such as for better strength and wear resistance or electrical conductivity have been improved by TiN dispersion.[1,24,25]

In the Chapter I, the benefits of carbothermic reduction process has been provided. The technique has been adopted previously by Coley et al[26,27] and Terry et al[3,28]. They have shown the production of ceramic dispersion (TiC, TiOC) in the matrix of either iron or iron-titanium alloy. The interfacial aspects of chemical reactions have been invoked for explaining the mechanism of the dispersion of ceramic phase. Also for each mole of TiN produced by the carbothermic reduction, the process generates 2 moles of CO gas which when burnt with the stoichiometric amount of oxygen will release 230 kJ of energy. The energy available from CO gas will reduce the overall energy cost of the process. This will also be reflected in the price of the synthesised powder. Besides potential advantage in the area of energy cost, a substantial reduction in the cost of future processing of powders can be anticipated by designing a process that will yield an in-situ composite microstructure as well as partial densification of ceramic powders.

The present work is aimed at the production of TiN and TiC powders and the in-situ formation of TiC/TiN partially-densified composites by the carbothermic reduction process. The investigation in particular emphasises the role of thermodynamic and kinetic factors in determining the size of the powder.

2. LITERATURE REVIEW

2.1 Introduction

The attractive electrical, thermal and mechanical properties of titanium

nitride (TiN), titanium carbide (TiC) and their solid solution, titanium carbonitride (TiC_xN_y) phase have led to systematic investigation of the powder processing, powder treatment and the characterisation of the properties. For example, a wear resistant surface of TiN can be imparted to Ti parts by nitriding. In integrated circuits, nitride thin-films are easily deposited by reactive sputtering.[29] Another potential use for nitrides is in superconducting devices. Nitrides have been suggested as materials for thin-film miniature superconducting solenoids, high quality inductors, Josephson junctions, and bolometers. Titanium nitride is not a stoichiometric phase. The composition range is extensive, and hence their physical properties depend upon the non-metal to metal ratio and the vacancy concentration.

2.2 Production and Processing of Nitrides

2.2.1 Methods of powder synthesis

The most commonly practised techniques for the preparation of titanium nitride are as follows and their equations are shown in **Table II-1**:

(1) Nitridation of the titanium metal powder with nitrogen gas yields pure powder product.[4,30]

(2) The reaction of titanium hydride with ammonia produces a high purity product.[31] Typical temperature for reacting Ti(TiH_2) powder is 1473K.[32]

(3) The reaction of titanium tetrachloride with a mixture of hydrogen and nitrogen[33] or ammonia and hydrogen[34] is used to deposit thin films by chemical vapour deposition (CVD) on substrates. The method was also adopted by Tioxide company as described in the section 1.

(4) Carbothermic reduction and nitridation of titanium oxide powders yield nitride and carbonitride phase.[5,6,20-22]

Titanium nitride is usually prepared by power metallurgy. The metal or oxide powder is reacted with nitrogen, pressed, and sintered. All powder

Table II-1. A summary of chemical reactions for the synthesis of TiN phase.

Chemical reaction	ΔG^{o}(kJ)
(1) $Ti + 1/2N_2 = TiN$	-336.31+0.093T
(2) $Ti(TiH_2) + N_2 = 2TiN + H_2$	-265 kJ·mol^{-1} (at 1600K)
(3) $TiCl_4 + NH_3 = TiN + 3HCl + Cl$	199.12-0.164T
(4) $TiO_2 + 1/2N_2 + 2C = TiN + 2CO$	375.89-0.256T

synthesis methods can be subdivided into four groups, i.e. solid state reaction, solidification of melts, solution techniques and vapour phase reactions. Direct nitridation of metal or metal hydride powders with nitrogen is the most common laboratory method for the formation of nearly all nitrides. This technique is also one of the best for producing relatively pure powder. The preparation of high-purity homogeneous samples for research purpose is, however, a difficult task. Temperatures higher than 1400K and good vacuum conditions or highly purified gases are generally required. The preparation conditions furthermore vary according to the alloy system and what may be an acceptable procedure in one case may result in an impure or inhomogeneous powder sample in another.

The reaction between titanium metal and nitrogen gas for the synthesis of titanium nitride or carbide was investigated by several workers.[35-39] Self-propagating high temperature synthesis (SHS) is a method of producing ceramic materials from their constituent powders. It is a solid-state combustion process characterized by an exothermic release of heat. The reaction front propagates as a combustion front through the powder compact, completely consuming the reactant powders once ignition is achieved. The synthesis of a variety of materials by self-propagating reactions has been demonstrated by numerous investigators. The recently plasma method was also adopted for the synthesis of TiN[4,40,41] whereas exotic methods such as electron beam heating was employed as the heating source for the synthesis of ceramic powders.[42] In an investigation by Yoshimura et al[43], the arc image heating process was tested for the synthesis of TiN and TiC powders by reduction/nitridation method.

2.2.2 Whisker growth

Ceramic whiskers are an important material for the development of the composite materials for elevated temperature structure applications. The whiskers are used as the reinforcing constituent in ceramic, metal and polymer matrix composites. Whisker surface morphology and surface chemical state determine the mechanical and chemical bond that form with the matrix material. The morphology and structure of the whisker are also important for the intrinsic strength of the whiskers. There are several theories for the mechanism of whisker growth and nucleation. This can be classified broadly into two major categories. The first mechanism illustrated that there must be a vapour phase for the nucleation at energetically-favourable sites. The mass transport via vapour phase will then sustain the growth. In the first method, the growth of metallic whiskers as well as ceramic whiskers have been observed. For example, the presence of SiO gas favours the formation of whiskers. In the second method, the reducing gas such as CO or H_2 plays a critical role during the reduction of metallic oxides. As pointed out by Sears[44] the nucleation and growth can only be sustained as long as the overall chemical potential difference is not too large otherwise the reaction product will have a very large surface area with many nuclei and no filamentary growth. Sears also proposed that whiskers are perfect except that they contain a single axial screw dislocation. Whisker growth assisted by a single screw dislocation is well-understood subject area and has been observed on many occasions. The model and principles developed for whisker growth from the vapour phase can be applied to whisker growth during the reduction of metal oxides. Brenner's observation on the need for low supersaturation conditions during whisker growth was also observed by Wagner.[45] The Wagnerian mechanism is based on his investigation of the reduction of transition metal oxides and sulphides. A large number of these oxides are non-stoichiometric and with excess anions. During the course of reduction, the activity of metal ions increases as excess anions are removed from the

compound lattice. Once the condition for low supersaturation are attained, whiskers nucleate around an active surface e.g. dislocations. Wagner suggested that the degree of supersaturation required during the reduction of metal oxides is related with the chemical potential of the anionic species in the crystalline phase and the related gas molecule in the gas phase. In general, the favourable conditions for whisker growth can be stated as follows: (a) structural anisotropy in the crystal lattice should be small, (b) additive-induced growth due to the presence of impurities which assist the screw dislocation mechanism and, (c) active sites for nucleation. Titanium nitride whiskers from the TiO_2 by a vapour-liquid-solid process were produced by Nolan et al.[46] Bamberger et al[47] also produced TiN whiskers by reaction of sodium titanium bronze with molten sodium cyanide.

2.2.3 Sintering of nitride powders

Ceramic materials are usually fabricated by sintering which is basically a firing process of a powder compact at a suitable temperature until agglomeration of the particles occurs with a decrease in their surface area and also of the porosity of the compact. Sintering is complex and usually involves chemical reaction, crystal growth, formation of liquid phases and solid-state diffusion. In a more complex process, a vapour phase may also be involved. Pure crystalline solids with primarily covalent bonding are almost impossible to sinter, because the activation energy required for the movement of defects in solids such as silicon nitride having strong, directional, covalent bonding is very high and therefore the self-diffusivity of Si and N in the structure of ß and α-Si_3N_4 is very low. The densification of silicon nitride occurs via liquid phase sintering and almost all available powders can be sintered to high densities, provided the amount of liquid phase is optimised. A variety of sintering additives can be used, e.g. MgO[48,49], Y_2O_3[50], $Y_2O_3 + Al_2O_3$, $MgO + Nd_2O_3$[51] etc. Oxygen, the major impurity in these powders, is present as surface SiO_2 and is beneficial for sintering. However the surface contaminant decreases the high-temperature strength of the sintered material. High-carbon contents may

impede sintering due to the formation of CO and SiO.[52]

Two main types of fabrication techniques adopted for large-scale densification process are reaction bonded and hot-pressed products. It is generally considered that several simultaneous mechanisms contribute to densification during hot-pressing. The densification is enhanced by applied pressure, grain boundary sliding and plastic flow as well as by diffusion. Recently it was shown that two kinds of high-pressure processing techniques are useful in obtaining the desired high-density compact of non-oxide materials: (1) static load exerting very high pressure sintering induced a phase transformation[53], and (2) dynamic consolidation techniques. A typical example of static high-pressure sintering is α-silicon nitride powders. The alpha silicon nitride phase transforms to the ß-phase during sintering. Temperature and time are crucial variables in determining the final composition and homogeneity of the nitride. One common method for preparing homogeneous sub-stoichiometric nitrides is to nitride the metal powders at a lower temperature than the reaction temperature for the formation of refractory nitrides for a short period of time and then homogenise the powders at an elevated temperature in an inert atmosphere. Homogenisation, however, is best done under an equilibrium nitrogen partial pressure to control the final nitrogen composition.

The published literature on the sintering of TiN is rather sparse and most of literatures are indirectly related to the understanding of the sintering process. The sintering of TiN however has been studied in the matrix of Si_3N_4. The presence of TiN can virtually lead to 100% of the theoretical density. Bellosi and co-workers[24] observed that the addition of TiN in the silicon nitride matrix improves the fracture toughness (K_{IC}) from 4.8 ± 0.5 MPa$\cdot$m$^{1/2}$ in 100% Si_3N_4 to 9.6 ± 1.1 MPa$\cdot$m$^{1/2}$ in 35 vol.% TiN-containing Si_3N_4 composite. Other general trend in the properties suggest that the coefficient of thermal expansion rises from 3.25×10^{-6} °C^{-1} to almost 5.0×10^{-6} °C^{-1} with 0 to 35 volume % TiN. However the change in electrical resistivity is extremely non-linear. The compositional dependence of the properties are plotted in **Figure II-1** for hot pressing, gas pressure sintering and pressureless sintering

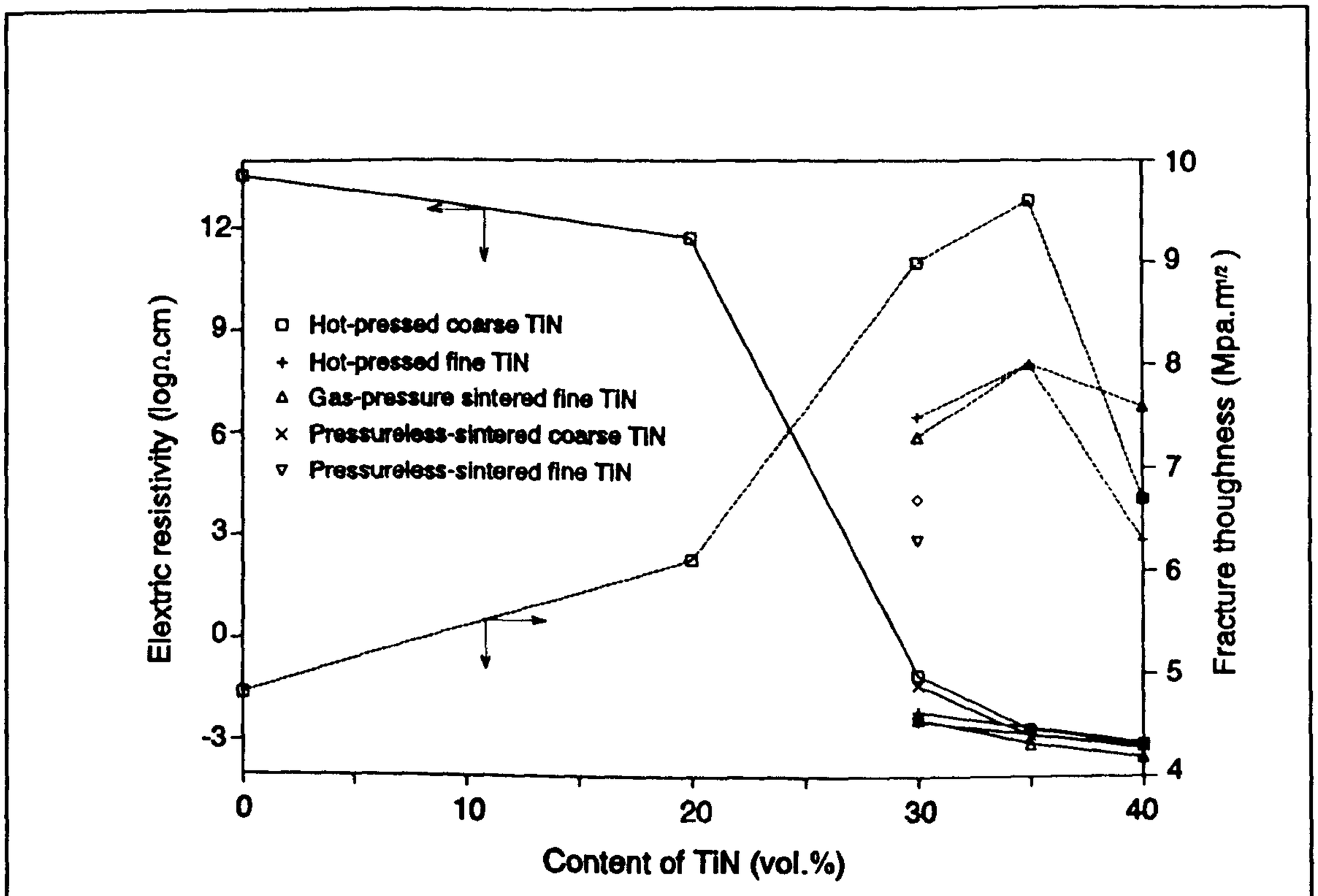

Figure II-1. Electrical resistivity and fracture toughness of the composites as a function of TiN content.[24]

conditions. A selected few key properties are also tabulated (see **Table II-2**). Martin and co-worker[54] have specially concentrated on the electrical conductivity of sintered Si_3N_4/TiN composites and the addition of up to 70% of volume fraction of TiN have been reported. Their investigation points out that the electrical conductivity rises non-linearly with the volume fraction of TiN and a sharp change takes place at 40 vol.% TiN which appears to be consistent with the resistivity measurement carried out by Belloisi et al.[24] The sintered microstructure reported by Martin et al[54] also indicates that the interconnection between the conducting particles seems to be possible around 30-35 volume %. Neither of the above two investigators have considered the possibility of either a complex titanium-silicon nitride phase or silicide phase. The latter appears to be more unlikely because the Ti_xSi_y type phase in equilibrium with N_2 gas is less stable than the $TiN + Si_3N_4$ phase combination. This definitely happens when FeCr alloy is dispersed in the Si_3N_4 matrix. Both Cr and Fe form ternary silicides as well as dissolve nitrogen. The micro-

Table II-2. Properties of the tested materials according to TiN content.[24]

Producing method	Sample		Electrical resistivity $\rho(\Omega cm)$	Fracture toughness $K_{IC}(MPa \cdot m^{1/2})$
	Type	TiN %		
Hot pressing	Si_3N_4	0%	3.6×10^{13}	4.8 ± 0.5
	coarse TiN powder	20%	5.0×10^{11}	6.1 ± 0.4
		30%	9.4×10^{-2}	9.0 ± 1.0
		35%	2.3×10^{-3}	9.6 ± 1.1
		40%	8.4×10^{-3}	6.7 ± 0.8
	fine TiN powder	30%	7.8×10^{-3}	7.5 ± 0.8
		35%	2.6×10^{-3}	8.0 ± 0.6
		40%	9.2×10^{-4}	6.3 ± 0.4
Gas-pressure sintering	fine TiN powder	30%	4.7×10^{-3}	7.3 ± 0.1
		35%	8.5×10^{-4}	8.0 ± 0.2
		40%	3.5×10^{-4}	7.6 ± 0.6
Pressureless sintering	coarse TiN powder	30%	4.7×10^{-3}	-
		35%	1.5×10^{-3}	-
		40%	7.6×10^{-4}	-
	fine TiN powder	30%	4.1×10^{-3}	6.3 ± 0.3
		35%	1.6×10^{-3}	-
		40%	6.5×10^{-4}	6.7 ± 0.8

structure of the sintered composites and the fractograph of the composite suggest that there is weak interfacial bonding between the TiN particulate and Si_3N_4 matrix. The high fracture toughness of TiN-reinforced composites is due to crack deflection, crack pinning and microcracking of the matrix.[24] The observed change in the electrical resistivity and K_{IC} of Si_3N_4-TiN composites suggest that the property changes are related to a phenomenon commonly known as the percolation.[55] According to the percolation theory, originally developed for explaining the electrical conductivity of metal-dispersed

composite materials, the change occurs non-linearly at a composition known as the percolation threshold. The technique requires further attention as it can be proved as a useful tool for non-destructive testing of ceramic materials.

2.3 Crystal Structure of Nitrides

2.3.1 Crystal chemistry

The close structural link between the nitrides and their metallic parent solid solutions is also a reflection of the relatively small size of the interstitial N atom. Hagg's rule[56] is well fulfilled for the nitrides[29] which is a set of empirical rules regulating the crystal structure types formed by transition-metal carbides, nitrides, borides, and hydrides. According to Hagg, the structure of transition-metal carbides, nitrides, borides, and hydrides is determined by the radius ratio $r = r_x/r_{Me}$. Here r_x and r_{Me} are the radius of the interstitial and transition-metal atoms, respectively. If r is less than 0.59, the metal atoms form very simple structures, ie, A_1, A_2, A_3 or simple hexagonal, where the letter A indicates an element, B an AB compound and C an AB_2 compound. A_1 is the structure of Cu (face centred cubic), A_2:α-Fe (BCC), A_3:Zn(HCP), B_1:NaCl structure. If r is greater than 0.59, the transition metal and interstitial elements form more complex structures than described above.

Compounds of nitrogen with transition metals have structures that may be simply described as a close-packed or nearly close packed-arrangement of metal atoms with smaller non-metal atoms occupying interstitial sites. For most structures, there are no apparent nitrogen-nitrogen localised interactions. An important characteristic of nitrides is the metal-non metal interaction and the geometry of the interstitial site. Nitrogen is normally located either in an octahedral interstitial site or in the centre of a trigonal prism. Filling all the octahedral interstitial sites in fcc results in the B_1(NaCl) structure. The metal substructure may also be described according to the sequential ordering of the close-packed metal-atom layers with the usual designations: -ABCABC- for

fcc, -AB,AB- for hcp, and -AA- for simple hexagonal. Nitride structures have the simple notations -AXBX'CX''- for B_1, -AXBX,AXBX- for L_3', and -AX,AX- for the WC type, where X represents a complete or partial filling of the interstitial sites (octahedral or trigonal prism) created by two adjacent metal layers. X' and X'' differ from X layers by a lateral shift.[29]

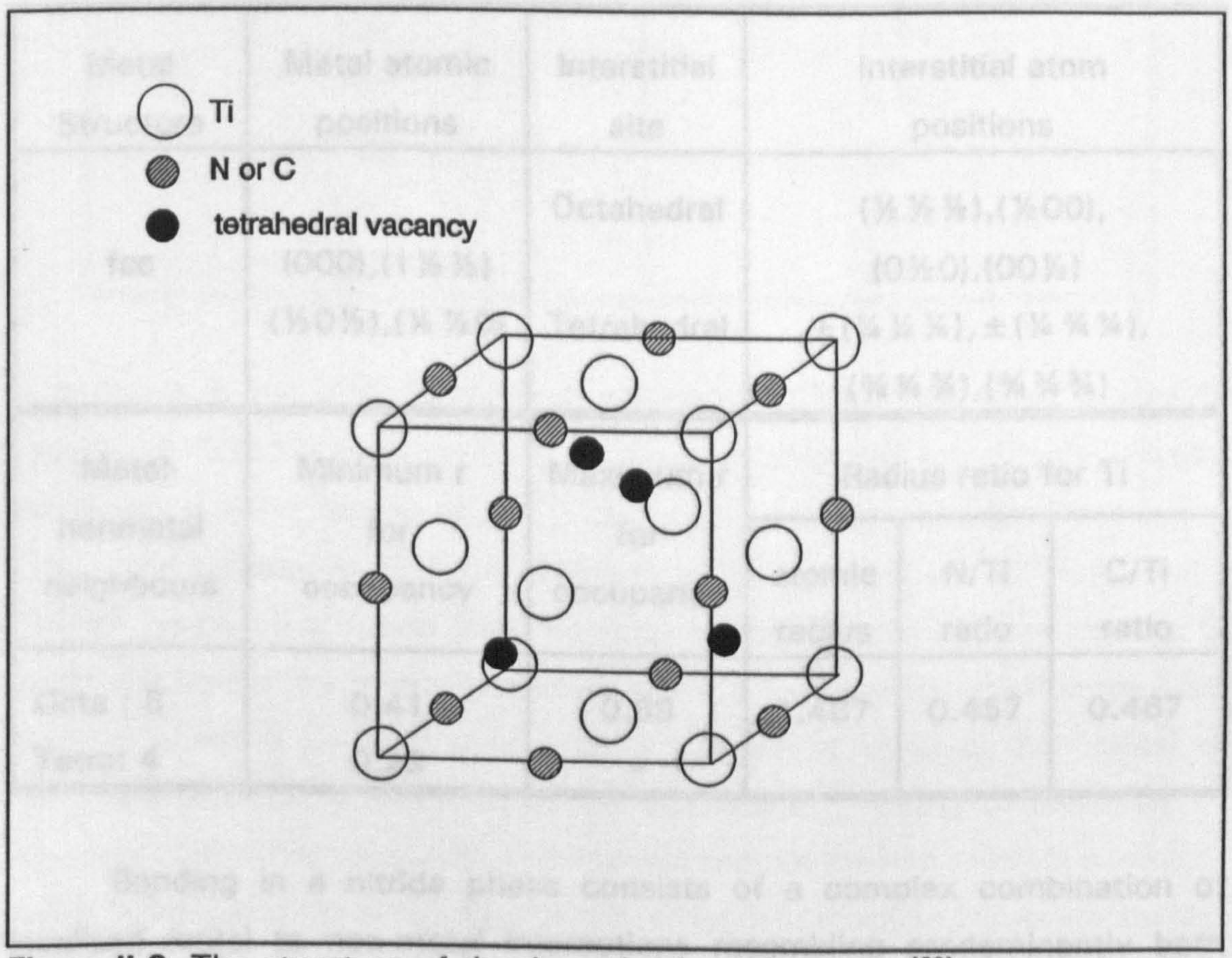

Figure II-2. The structure of titanium nitride and carbide.[29]

For the Ti element, the tetrahedral interstitial sites of the simple metal structures are too small to accommodate N, and only the octahedral and trigonal prism interstitial sites are occupied. Occupation of all the octahedral interstitial sites in a fcc metal lattice results in the B_1(NaCl) structure, which is very common among mononitrides. TiN is very similar to the TiC, such as in structure and properties. There is, however, a difference largely associated with the tri-valency of the nitrogen atom against quadri-valency of carbon which entails rather weaker bonds from metal to non-metal. The difference in

atomic size of carbon and nitrogen is relatively slight. (N = 0.69, C = 0.77Å radius). The structure of TiN or TiC, and metal lattices and interstitial sites for Hagg's fcc structures are shown in **Figure II-2** and **Table II-3**, respectively.

Table II-3. Metal lattices and interstitial sites for Hagg's simple crystal structure and radius ratio for Ti atoms.[29]

Metal Structure	Metal atomic positions	Interstitial site	Interstitial atom positions
fcc	(000),(1 ½ ½) (½ 0 ½),(½ ½ 0)	Octahedral Tetrahedral	(½ ½ ½),(½ 00), (0 ½ 0),(00 ½) ±(¼ ¼ ¼),±(¼ ¾ ¼), (¾ ¼ ¾),(¾ ¾ ¾)

Metal-nonmetal neighbours	Minimum r for occupancy	Maximum r for occupancy	Radius ratio for Ti		
			atomic radius	N/Ti ratio	C/Ti ratio
Octa : 6 Tetra: 4	0.41 0.23	0.59 -	1.467	0.457	0.467

Bonding in a nitride phase consists of a complex combination of localised metal to non-metal interactions resembling predominantly both covalent and metallic types of bonding. There is only a small amount of ionic bonding. The fraction of covalent bonding was calculated assuming the materials bonded only by covalent and ionic bonding as an approximation as shown in **Table II-4**. Titanium nitride, carbide and boride, and boron nitride and carbide ceramic materials have mainly covalent bonding compared with ionic bonding, i.e, fraction of covalent bonding is roughly 0.78 ~ 0.97 calculated by using the data of Pauling's electronegativity scale and electronegativity vs fractional ionic character derived by Pauling given in reference [57]. However, the essentially metallic nature of the bonding in TiN is similar to that in TiC but

Table II-4. The calculated data of fractional covalent bonding as an approximation by using the data given in reference [57]. (assumed $F_{covalent\ bonding} + F_{ionic\ bonding} = 1$, F:fraction)

Ceramic material	Fraction of covalent bonding
TiN	0.91
TiC	0.80
TiB_2	0.97
BN	0.78
B_4C	0.94

in contrast to the ionic bonding in isostructural TiO.[2] Nitrogen is able to dissolve in TiO both as an ion and as a covalent atom but, conversely, oxygen can dissolve in TiN only as an ion. A study of resistivity and microhardness of TiN_{1-x} as a function of its non-stoichiometry by Samsonov et al[58] showed a distinct tendency towards ionic bonding in the TiC, as against metallic in which the bond type begins to change within 30 ~ 50 atomic % N range from metallic towards ionic bonding with increasing N content. The metal to non-metal bonding is favoured by the octahedral grouping of metal atoms around a central nitrogen atom, but the presence of the non-metal in transition metal nitrides also tends to increase the strength of metal to non-metal bonds.

2.3.2 The Ti-N and Ti-C phase diagrams

It has been found that by nitriding Ti metal at low temperatures in ammonia produces a B1 structure mononitride Ti_xN where $x < 1$.[59] Density studies show that the phase produced is predominantly defective. Nitriding $Ti(TiH_2)$ in nitrogen or ammonia, however, produces a B1 structure mononitride TiN_x in which $x < 1$; that is, the nitrogen sublattice is predominantly defective. Density studies confirm the presence of the defective structure. However, even at the stoichiometry compositions appreciable vacancy concentrations

can exist on both metal and non-metal lattice sites and together due to the presence of vacancies, an enhanced mass transport even in the stoichiometric composition will be expected. In TiN the vacancy concentration at stoichiometry on both sublattices may be as high as 4 at%.[60] The phase diagram for Ti-N is so far incomplete. Two intermediate phases, TiN (B_1) and ϵ-Ti_2N, are known to exist.[60,61] TiN has a broad composition range from about $TiN_{0.6}$ to about $TiN_{1.0}$ at 1400°C. If TiN is prepared at low temperatures by reacting NH_3 with $TiCl_4$, a composition range of TiN to $TiN_{1.16}$ results.[62] TiN has the wide homogeneity range, and **Figure II-3** shows the variation of lattice

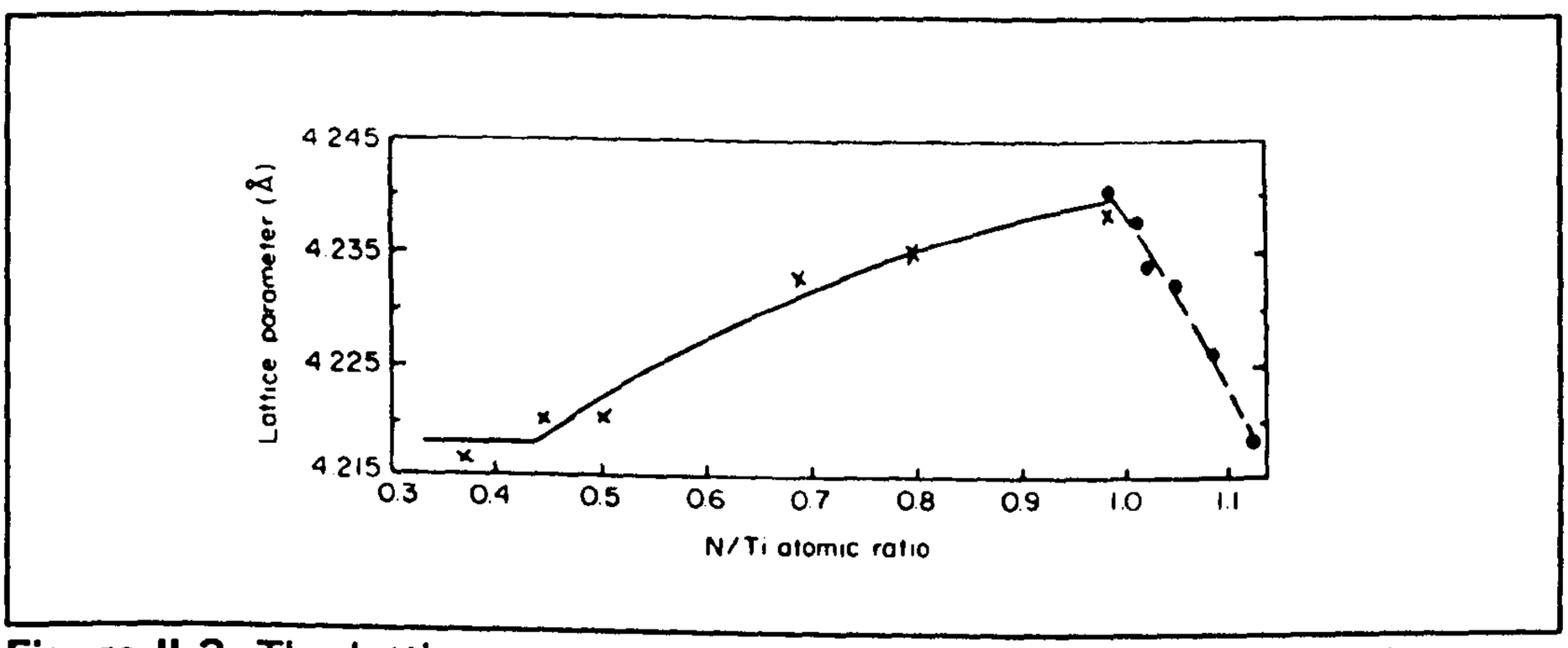

Figure II-3. The lattice parameter of the B_1 phase TiN_{1-x} is a maximum at the stoichiometric composition and decreases rapidly. (After Ehrlich[60] and Brager[62])

parameter with composition for TiN. The lattice parameter is maximum at the stoichiometric composition. **Figure II-4** attempts to piece together current literature on Ti-N phase relation.[29] Determining the vacancy concentration is difficult because of inaccuracies in determining the exact overall chemical composition. The vacancy concentration can be determined by comparing X-ray intensity with experimentally determined intensity. If the chemical composition is not exactly known, very large errors in estimating the vacancy concentration can be encountered. The phase diagram of the Ti metal with carbon is shown in **Figure II-5**. It is characterized by only one carbide phase, a monocarbide with B_1 structure with wide homogeneity range.

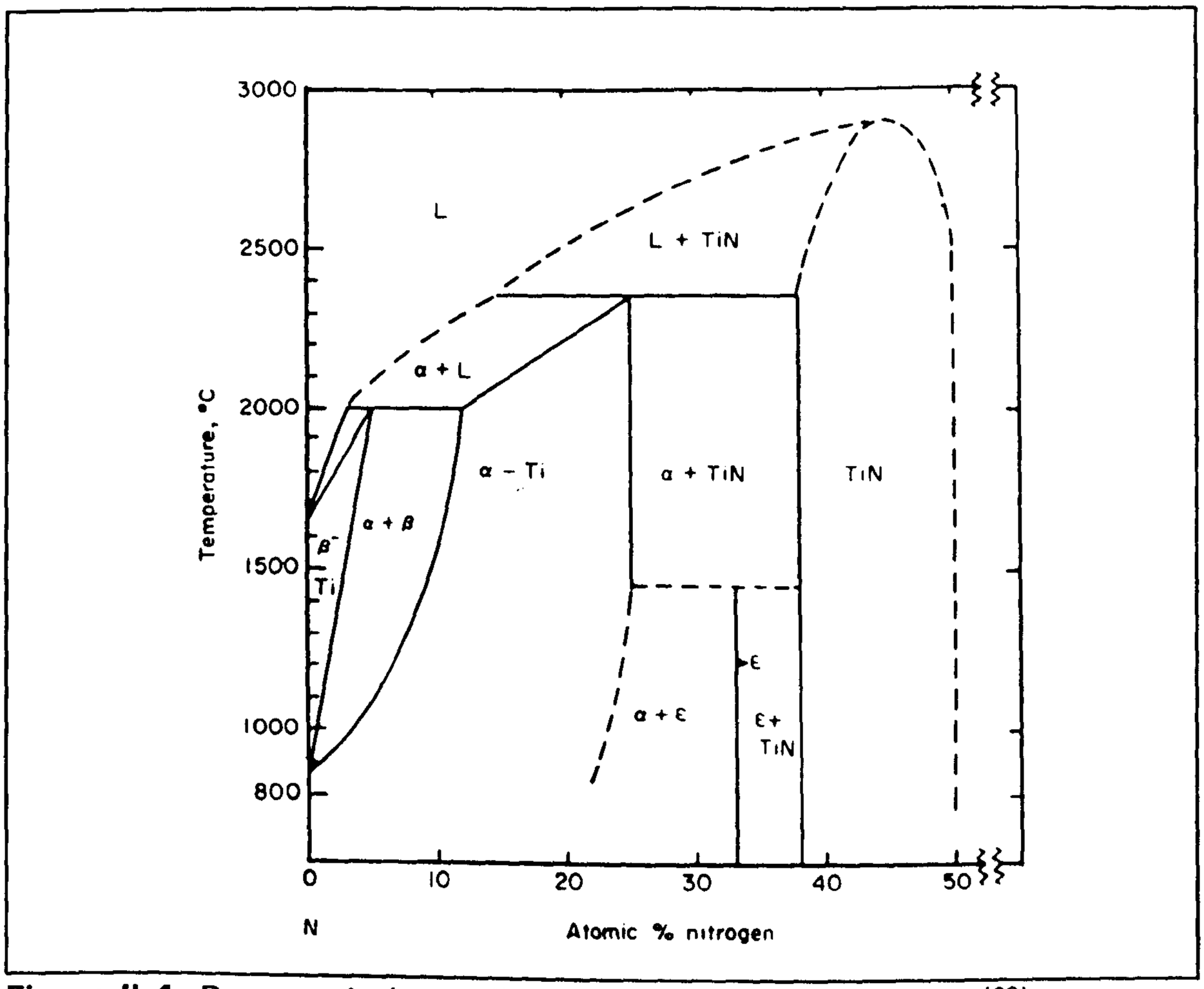

Figure II-4. Proposed phase diagram for titanium-nitrogen.[29]

2.4 Properties of Nitrides

The properties of nitrides are dependent upon a number of factors; crystal structure, lattice parameters, composition, non-metal to metal ratio, impurity concentration, and sample homogeneity. Porosity affects mechanical and electrical properties. The general properties of nitrides are as follows.[29] The important property of transition metal nitrides is their defect structure. Ideal stoichiometry is generally not found in these phases; deviations from stoichiometry are far more common. The phases exist over a broad composition range and appreciable vacancy concentrations can exist on the non-metal sub-lattice sites with lesser concentrations on metal-atom lattice sites. Even at the stoichiometric ratio appreciable vacancy concentrations (a few atomic percent) can exit on both sublattices in certain cases. When a large fraction of non-metal sites are vacant, the vacancies tend to exhibit a

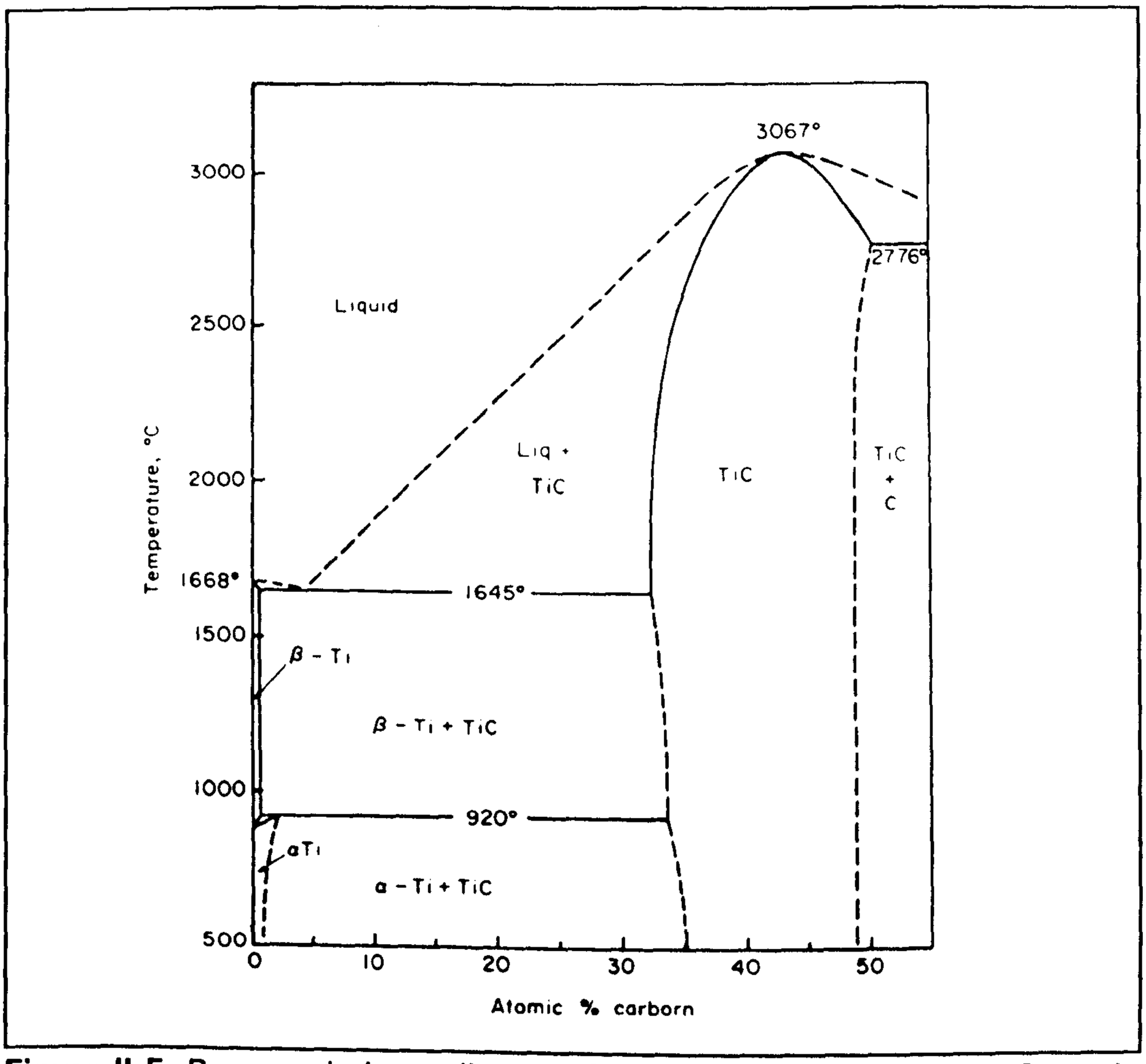

Figure II-5. Proposed phase diagram for titanium-carbon. (After Storm's evaluation.[8])

long-range order. This phenomenon is found in nearly all the subnitrides. Vacancy ordering in vanadium carbide is also well known and hence on this basis, the ordering of vacancies in subnitrides in not totally unexpected. The presence of a large concentration of vacancies, order or disorder, significantly affects properties, such a thermodynamic, mechanical, electrical, magnetic, superconducting, etc. Different processing techniques tend to produce different defect structures and hence properties. Because of the possibility of vacancy ordering in the defect structures, the crystal chemistry of nitrides is complex. Nitrogen, being a smaller atom than the metal element except boron, is always interstitially located. The covalency of nitrogen bonding results high melting point and hardness. The hardness of nitrides is inferior to their carbide. Titanium nitride is chemically stable at room temperatures. However at high temperatures they oxidise readily to form oxides. Both their chemical reactivity

and thermochemical properties are dependent on the non-metal to metal ratio. Titanium nitride has a wide range of compositions, therefore, this material is of interest for vacancy, particularly nitrogen vacancy studies. In **Table II-5**, the properties of titanium nitride and titanium carbide are compared.

Table II-5. Some properties of titanium nitride and carbide.[2,29,64-66]

Phase	Structure	Lattice parameters (nm)	X-ray density ($x10^3$,Kg/m^3)
TiN	B_1 (NaCl type)[29]	0.42417[64] 0.4240[29] 0.4244[2]	5.43[2] 5.39[29]
TiC	B_1 (NaCl type)	0.43274 0.4328 0.4328	4.94 4.91
Phase	Microhardness (kg/mm^2)	Melting temperature (K)	Heat conductivity ($x10^{-3}$, J/m·sec·K)
TiN	2000[29] 1900[2]	3220[65] 3222[29] 3223[2] 3218[66]	1.925[29]
TiC	2900 3200	3290 3340 3413 3340	2.092
Phase	Thermal expansion coef. ($x10^{-6}$, at r.t)	Enthalpy of formation ($\Delta_fH°$, kJ·mol^{-1})	Enthalpy of fusion($\Delta_{fus}H°$, kJ·mol^{-1})
TiN	9.35[29]	-337.65[65] -336.39[2]	66.944[29]
TiC	7.4	-184.10 -238.49	71.128

The understanding of these particular properties is generally based on the knowledge of the atomic diffusion parameters in the material. Abautret et al[63] determined the self-diffusion coefficient of nitrogen and activation energies for single crystals and in polycrystalline materials, and the results are as follows: for polycrystals, $D = 6.5x10^{-11}(cm^2/s)\cdot exp[-1.79 \pm 0.3\ (eV/at)/kT]$ for $T < 1773K$, $D = 1.4(cm^2/s)\cdot exp[-5.5 \pm 0.3(eV/at)/kT]$ for $T > 1773K$, and $D' = 17(cm^2/s)\cdot exp[-4.2 \pm 0.3\ (eV/at)/kT]$, where D is the bulk diffusion coefficient and D′ is grain boundary diffusion coefficient. For single crystals, $D = 1.8x10^{-9}(cm^2/s)\cdot exp[-1.8 \pm 0.3\,(eV/at)/kT]$ and $D' = 1x10^{-3}(cm^2/s)\cdot exp[-2.8$

$\pm$0.3(eV/at)/kT].

2.5 Previous Literature on the Reduction/Nitridation of TiO_2

There have been several investigations[6,20-22] on the reduction of TiO_2 in nitriding atmosphere in order to form titanium nitride. Although previous investigators[5,6] have reported their view that the reduction of the rutile phase progresses in sequence and some of the commonest lower oxides are Ti_3O_5, Ti_2O_3 and TiO; therefore, TiO phase is a precursor for the formation of Ti(ON) and TiN. Empirical evidence for the existence of TiO phase, however, has yet remained elusive. Andersson et al[67,68] reported the existence of a homogeneous series of oxides with the formula Ti_nO_{2n-1} with n from 4 up to 10. The homogeneity range of Ti_2O_3,[67] Ti_3O_5[69] is also reported. Stoichiometric TiO has been identified in two crystalline forms. High-temperature ß-TiO has a cubic NaCl-type structure,[67] while the low-temperature α-TiO has a closely related monoclinic structure.[70] Ideal α-TiO has an ordered array in which 1/6 of the lattice sites are vacant; half of the Ti and O atoms are missing alternately in every third (110) plane.[71] ß-TiO obtained at normal pressure appears to have a lower and somewhat variable ($\sim$14-15 %) vacancy concentration, depending on conditions of preparation. The transition temperature is believed to be 1198$\sim$1223K.[72] Licko et al[6] pointed out that in the final stage of reduction-nitridation, the TiO phase could progressively reduce to Ti(ON) and TiN phase. The oxygen atoms are replaced by nitrogen in the TiO lattice. There is also a possibility that the vacant interstitial sites are occupied by nitrogen atoms. Contrary to the hypothesis, Licko et al[6] only found Ti_4O_7 phase in the temperature range of 1443-1763K. Ouensanga[73] and White et al[74] found Ti_3O_5 phase as the last titanium suboxide by the carbothermic reduction at 1580K and in the temperature range of 1073-1573K, respectively. Liubimov et al[20] also reported "very small amount of Ti_2O_3" in the sample reacted at 1573K for a period of 10 minutes, and cubic phase along with Ti_5O_9, Ti_4O_7 and two different polymorphs of Ti_3O_5

phase. It was shown that the reduction of TiO_2 by carbon can produce titanium carbonitride (TiCN) or oxycarbonitride (TiOCN) phases. Licko et al[6] measured the composition of solid solution Ti(OCN) containing 17.2~19.6 mass% N, 1.5~6.4 mass% C and 0.9~4 mass% O. Yoshimura et al[43] estimated the composition of Ti(CN) solid solution in the range of $TiC_{0.06}N_{0.94}$ to $TiC_{0.66}N_{0.34}$ by comparing the measured lattice parameter with that of TiN and TiC.

It has been reported by several authors who have extensively studied the phase equilibria in the Fe-Ti-O system that the lower oxides of Ti are highly non-stoichiometric. The degree of non-stoichiometry of the lower oxides are shown in **Figure II-6** constructed by Wahlbeck and Gilles.[72] The Ti_2O_3 phase appears to be a more common intermediate oxide than TiO in the inert gas (argon) atmosphere. Terry et al[3] and Coley et al[27] have also reported that the Ti_2O_3 phase is the intermediate oxide prior to the formation of the oxycarbide phase. From their results it is evident that Ti_2O_3 phase is in equilibrium with Ti(O,C) but it is also in equilibrium with metallic iron. However Borowiec and Rosenqvist[75] have superimposed (TiO + Fe) calculated line on the empirically established univariant diagram ($\log Po_2$ vs 1/T). The reduction sequence and related equilibria with a particular reference to the stability of "TiO" phase will be discussed at length in the Discussion section.

Several studies[21,76] on the kinetic aspects of the reduction reaction have been undertaken and main features are described below:

(a) The kinetics of reduction-nitridation of naturally occurring minerals (rutile or anatase) appears to be dependent on the impurity oxide content of the minerals.[22] The reducibility is also dependent on the type of carbon used.

(b) The rate constant does not vary linearly over a wide range of temperature. There are two distinct regions: a large activation energy region at lower temperatures below 1373 K and at high temperature the activation energy is low.[76] Li and Riley[21] and White et al[76] have reported approximately 260 kJ of activation energy above 1373 K for the reduction of rutile to TiN phase and 280~390 kJ for anatase to TiN. Below 1373 K, the activation energy rises

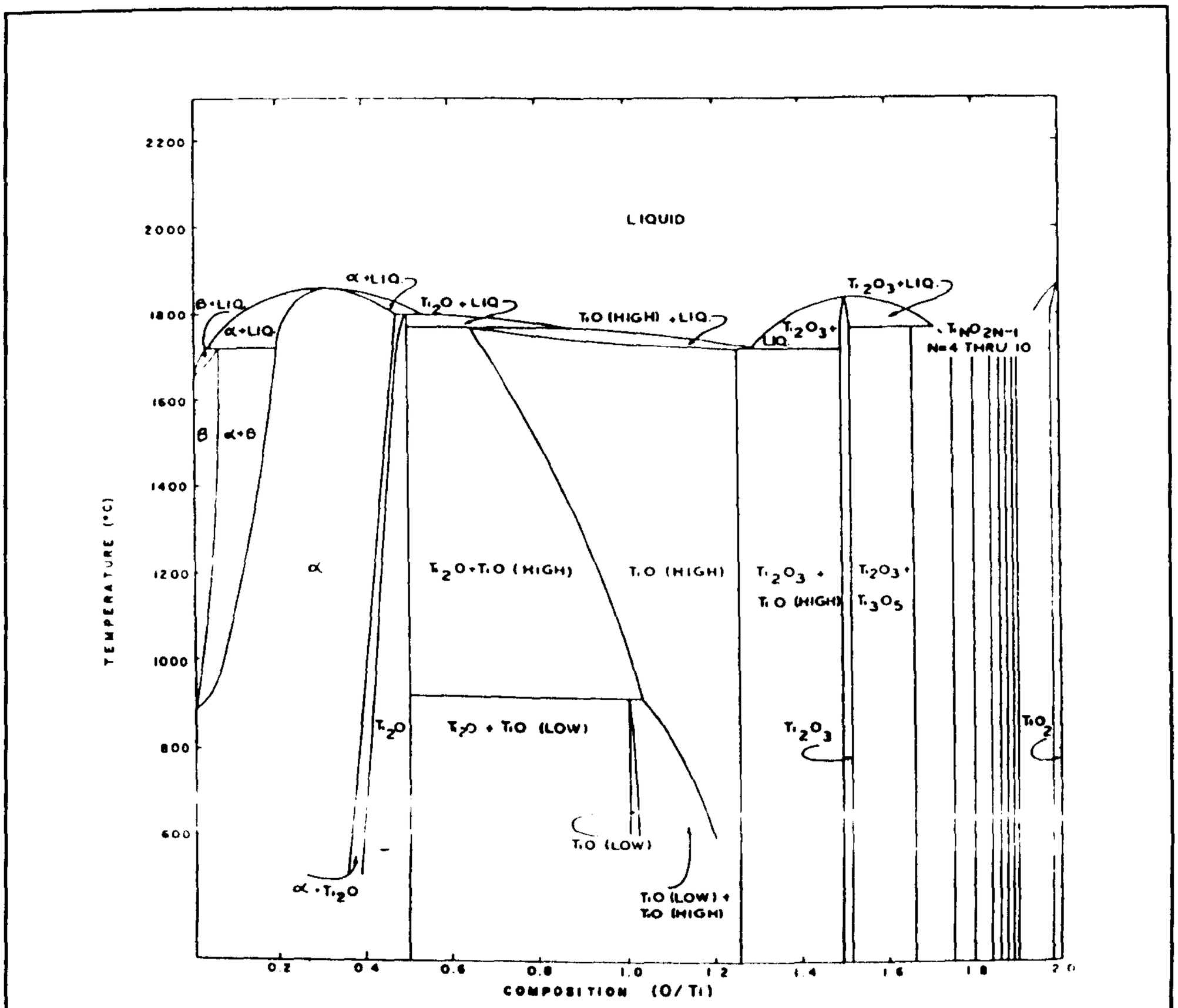

Figure II-6. Titanium-oxygen phase diagram.[72]

sharply to value of 715~970 kJ. Neither White et al[76] nor Li and Riley[21] present any conclusive view concerning the variations in the activation energy. Holt and Munir[37] have reported values in the vicinity of 120 kJ for the combustion synthesis of titanium carbide. Grami and Munir[35] also tested the effect of gas pressure and diluent content on the combustion synthesis of titanium nitride and gave an activation energy of 340 $kJ \cdot mol^{-1}$. Evidently further analysis is required to explain these results and the discrepancy that exists between them. The kinetics of the reduction results presented above will be examined in detail in the context of the present investigation.

3. THERMODYNAMICS OF THE SYNTHESIS REACTIONS

3.1 Thermodynamic Basis for Phase Stabilities

3.1.1 The stability of titanium suboxides in the oxygen atmosphere

The stability of titanium suboxides were calculated from their oxygen partial pressures. The complied thermodynamic data[77,66] were used to predict the phase stability of titanium oxides in equilibrium with oxygen gas and the calculated data is shown in **Table II-6**. The equilibrium between TiO_2 and Ti_4O_7, for example, is as follows:

$$4TiO_2 = Ti_4O_7 + 1/2O_2 \qquad \textbf{(2-1)}$$

The standard Gibbs free energy change (ΔG°) for the reaction equals 386530-111.33T (kJ). The equilibrium constant, K_1, can be expressed in terms of ΔG_1° as shown below.

$$K_1 = \exp\left(\frac{-\Delta G_1^o}{RT}\right) = \frac{a_{Ti_4O_7} \cdot (p_{O_2})^{1/2}}{a_{TiO_2}^{\ 4}} \qquad \textbf{(2-2)}$$

where p designates the partial pressure of the gaseous phase. For unit activities of the a_{TiO_2} and $a_{Ti_4O_7}$,,

$$K_1 = (p_{O_2})^{1/2} = \exp\left(\frac{-\Delta G_1^o}{RT}\right) \qquad \textbf{(2-3)}$$

The equilibrium partial pressure of oxygen (pO_2) at 1573K is 9.11×10^{-15}, which means above this pO_2, TiO_2 phase is stable, and TiO_2 will transform to Ti_4O_7 phase below this value. At 1773K, the equilibrium Po_2 is 7.12×10^{-12}, ie, at the higher temperature, titanium dioxide (TiO_2) will easily transforms to Ti_4O_7 at a relatively higher oxygen partial pressure than at 1573K. The stability of other titanium oxides were similarly calculated using Equation (b)~(f) in

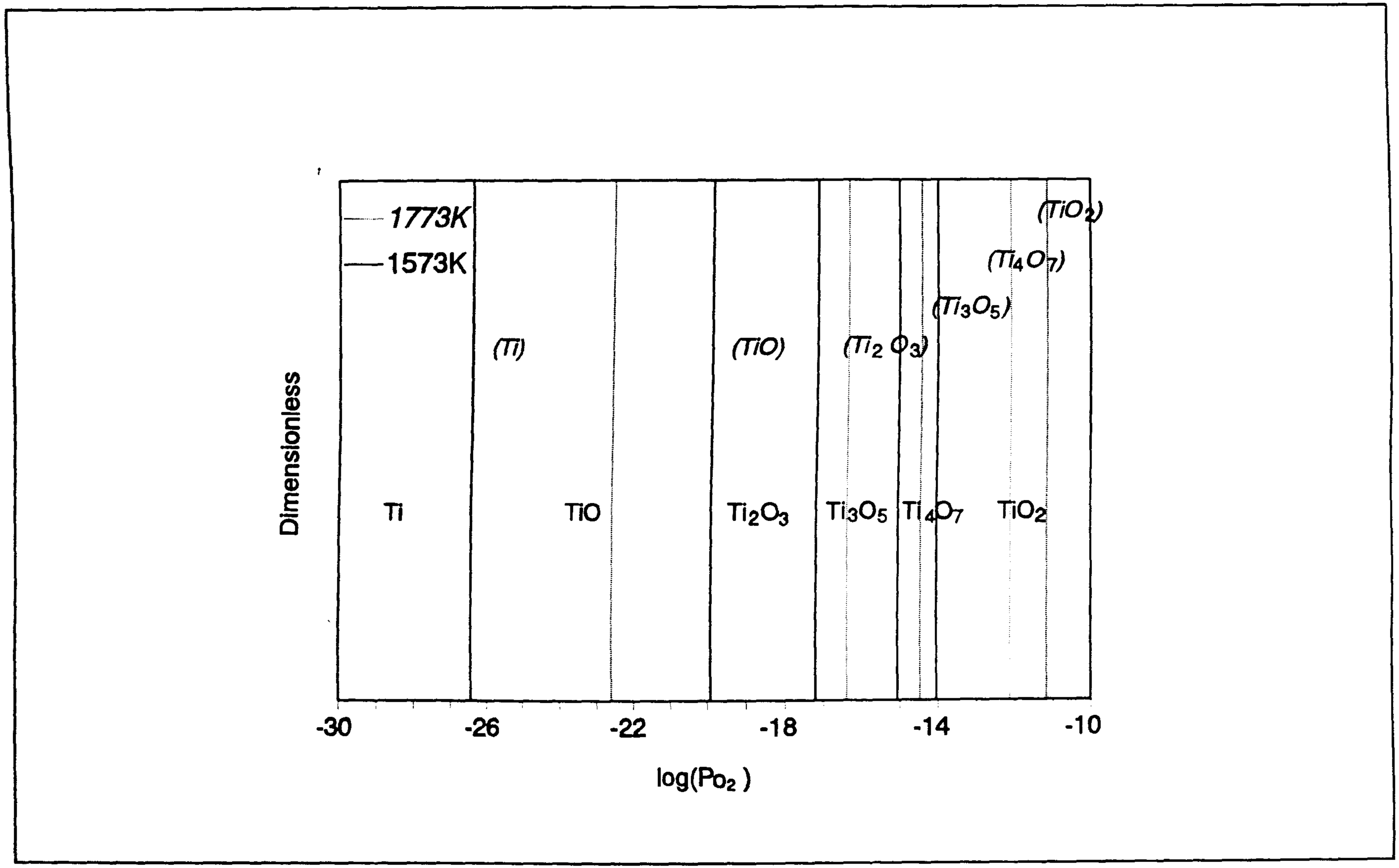

Figure II-7. The stability regions of titanium oxides on the oxygen partial pressure scale.

Table II-6. The stability diagram is also drawn in **Figure II-7**. In this figure, y axis has a dimensionless scale. Depending upon the partial pressure of oxygen, titanium oxide (TiO_2) changes to sub-oxides and the sequence which it follows is TiO_2, Ti_4O_7, Ti_3O_5, Ti_2O_3, TiO and Ti. In the process, it loses oxygen.

Table II-6. The thermodynamic data for the calculation of phase stability.

Reactions	$\Delta G^\circ(J) = \Delta H^\circ - \Delta S^\circ \cdot T$	Po_2 (atm, at 1573K)
(a) $4TiO_2 = Ti_4O_7 + 1/2O_2$	386530 -111.33T	9.11×10^{-15}
(b) $3Ti_4O_7 = 4Ti_3O_5 + 1/2O_2$	387350 -102.25T	9.05×10^{-16}
(c) $2Ti_3O_5 = 3Ti_2O_3 + 1/2O_2$	364008 - 66.78T	6.33×10^{-18}
(d) $Ti_2O_3 = 2TiO + 1/2O_2$	472792 -109.96T	1.22×10^{-20}
(e) $TiO = Ti + 1/2O_2$	514632 - 74.06T	3.62×10^{-27}

3.1.2 The stability of titanium nitride, carbide and oxide

The phase predominance area diagram at two temperatures 1573K and 1773K has been calculated by using the equilibrium thermodynamic data in **Table II-7**. The phase relationship are drawn in **Figure II-8**. The predominance diagram indicates that the phase stability of the carbide phase increases with increasing temperature and also that the carbide phase will always be in equilibrium with the Ti_3O_5 phase. Interestingly both TiO and Ti_2O_3 have much higher equilibrium oxygen partial pressure than Ti_3O_5/TiC equilibrium. This is the reason that the stability boundaries for TiO and Ti_2O_3 do not appear in the predominance diagram. This appears to be in contrast with the observation made by Terry et al[3] and Coley et al[27] who reported that the Ti_2O_3 phase is the intermediate oxide prior to the formation of the oxycarbide phase. We point out that the investigators considered ilmenite for their calculation and also in experiment which under a reducing condition yields metallic iron phase

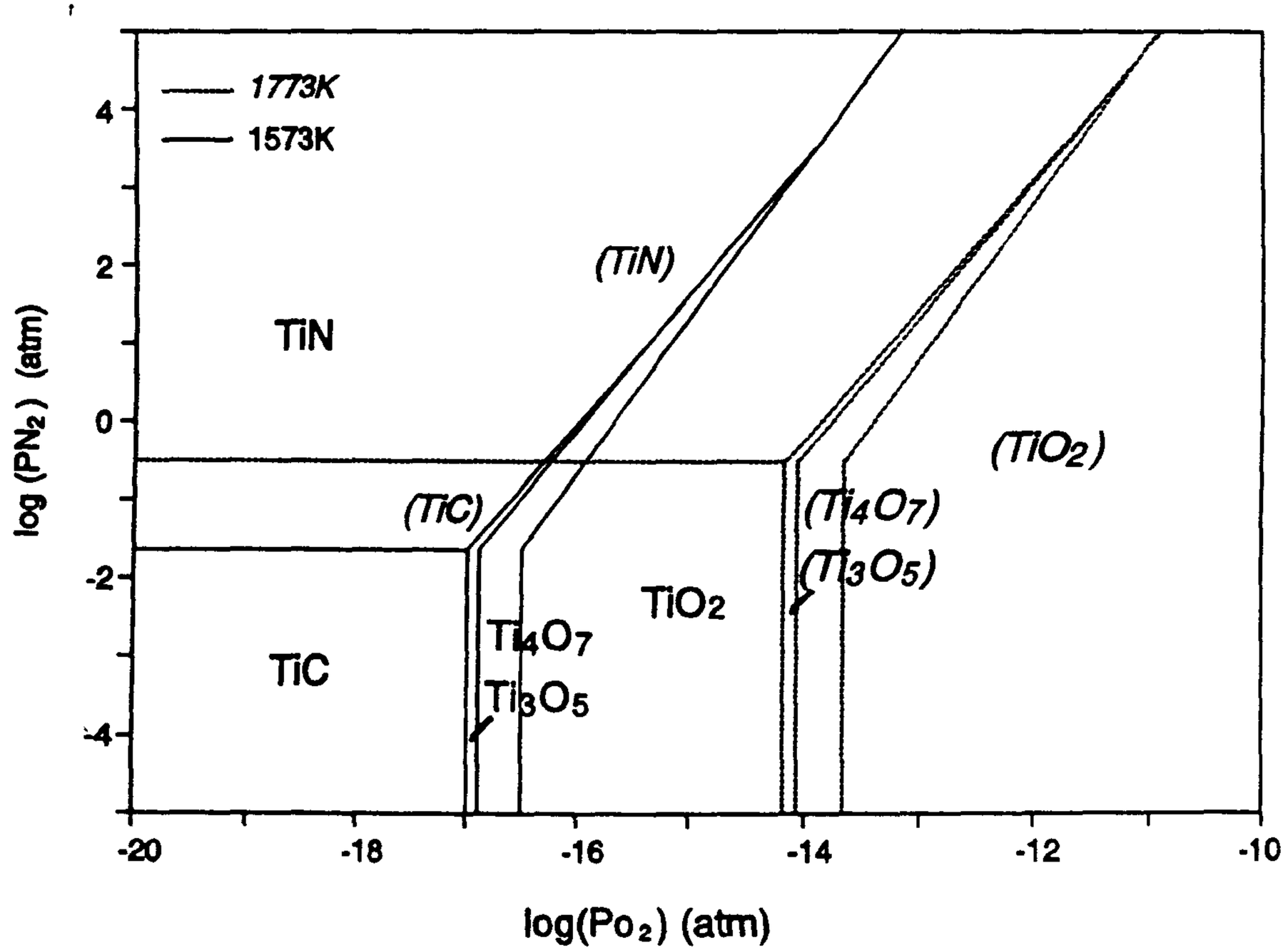

Figure II-8. The regions of phase stability for the titanium nitride, carbide and oxides showing the dependence on partial pressure of nitrogen, oxygen and temperature.

Table II-7. The thermodynamic data for the calculation of phase stability.

Reaction	$\Delta G^\circ(J) = \Delta H^\circ - \Delta S^\circ \cdot T$
(a) $TiO_2 + 1/2N_2 = TiN + O_2$	604672 - 87.31 T
(b) $Ti_4O_7 + 2N_2 = 4TiN + 7/2O_2$	2029309 - 221.60 T
(c) $Ti_3O_5 + 3/2N_2 = 3TiN + 5/2O_2$	1426158 - 140.71 T
(d) $Ti_2O_3 + N_2 = 2TiN + 3/2O_2$	829436 - 71.55 T
(e) $TiO + 1/2N_2 = TiN + 1/2O_2$	178322 + 19.20 T
(f) $TiN + C = TiC + 1/2N_2$	151544 - 80.71 T
(g) $TiO_2 + C = TiC + O_2$	756216 - 165.02 T
(h) $Ti_4O_7 + 4C = 4TiC + 7/2O_2$	2635794 - 547.01 T
(i) $Ti_3O_5 + 3C = 3TiC + 5/2O_2$	1880792 - 382.84 T
(j) $Ti_2O_3 + 2C = 2TiC + 3/2O_2$	1132525 - 232.97 T
(k) $TiO + C = TiC + 1/2O_2$	329867 - 61.50 T

containing disolved Ti. The process of the metallic phase allies the condition for oxygen potential. A similar procedure was adopted for defining the stability regions for the solid solution titanium carbonitride phase. These are drawn in **Figure II-9**. The mathematical procedure is described below. For the $TiC_{0.5}N_{0.5}$ phase, the following reactions were considered.

$$TiN + 1/2C = TiC_{0.5}N_{0.5} + 1/2N_2 \qquad \textbf{(2-4)}$$

$$TiC_{0.5}N_{0.5} + 1/2C = TiC + 1/2N_2 \qquad \textbf{(2-5)}$$

If we assume that the free energy change for the reaction (2-4) equals that of reaction (f) in Table II-7, then the equilibrium constant, K_4, can be expressed in terms of ΔG_4° as shown in **Equation (2-6)**,

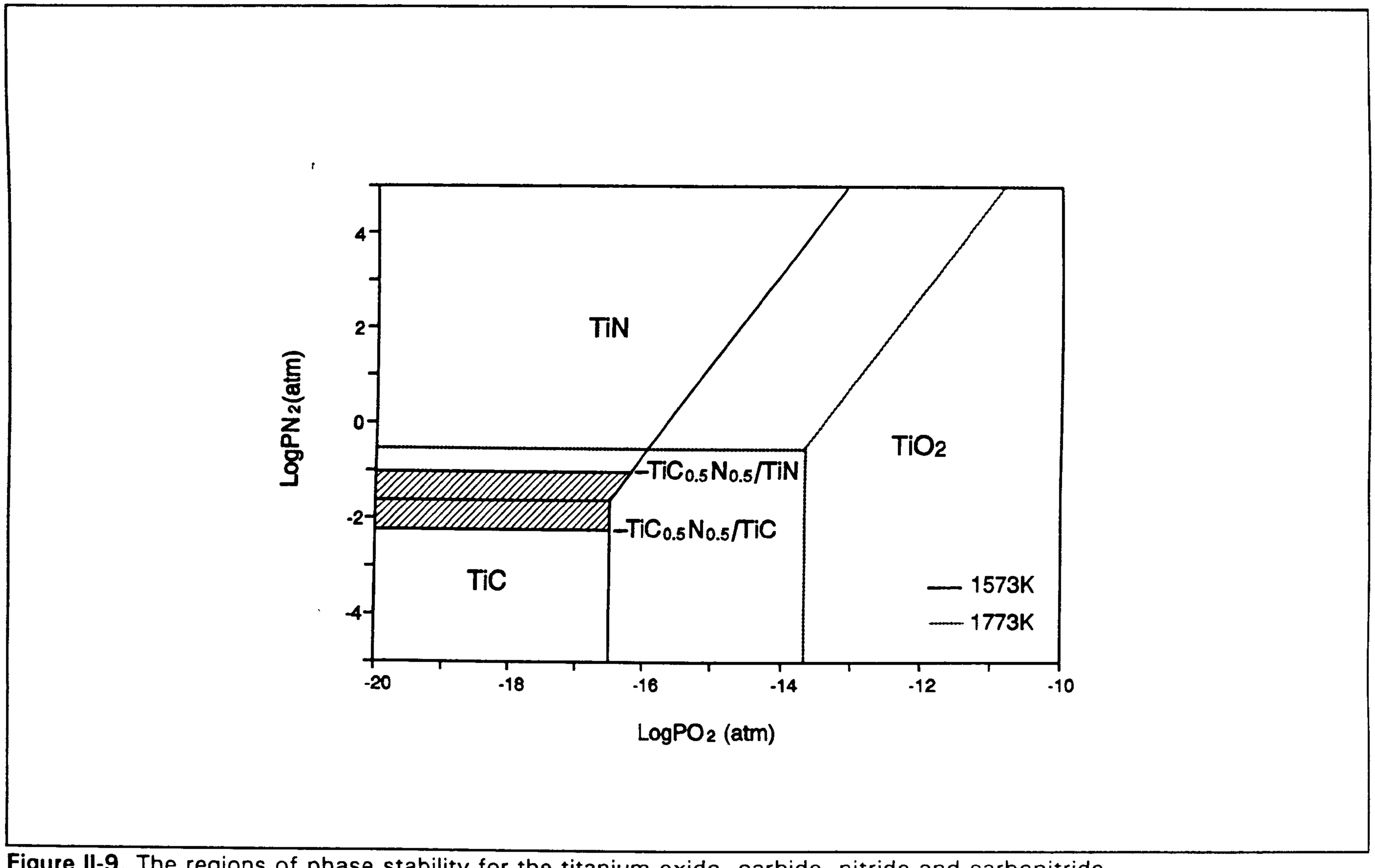

Figure II-9. The regions of phase stability for the titanium oxide, carbide, nitride and carbonitride.

$$K_4 = \exp(\frac{-\Delta G_1^o}{RT}) = \frac{a_{TiC_{0.5}N_{0.5}} \cdot (p_{N_2})^{1/2}}{a_{TiN} \cdot a_C^{1/2}} \qquad (2\text{-}6)$$

where p designates the partial pressure of the gaseous phase. By considering the activities of the $a_{TiC_{0.5}N_{0.5}}$ equals 0.5, because the TiC-TiN system forms an ideal solution. Then for the unity activity of carbon,

$$K_4 = 0.5 \cdot (p_{N_2})^{1/2} \qquad (2\text{-}7)$$

The equilibrium P_{N_2} equals 9.31×10^{-2} at 1573K. Similarly equilibrium P_{N_2} for **Equation (2-7)** equals 5.82×10^{-3} at 1573K. From Figure II-9, we find that the carbonitride phase which equilibrium with TiN and TiC phases has a stability region.

3.2 Thermodynamic Considerations for the Carbothermic Reduction

The thermodynamic feasibility for the formation of nitride phase by the carbothermic reduction process is considered below. Existing thermodynamic data can be used to predict the phase stability of nitrides in equilibrium as a function of temperature. The reduction of metal oxides with carbon to metal and their nitrides, carbides and borides is usually referred as the "carbothermic reduction" which for the production of TiN is defined below:

$$TiO_2(s) + 2C(s) + 1/2N_2(g) = TiN\ (s) + 2CO(g) \qquad (2\text{-}8)$$

The standard Gibbs free energy change ($\Delta G°$) for the reaction equals to $\Delta H° - T \cdot \Delta S°$; the values of enthalpy and entropy are 375.890 kJ $mole^{-1}$ and 0.256 kJ $mole^{-1}K^{-1}$, respectively. The equilibrium temperature (T_{eq}) equals to 1469K and below this temperature the oxide and carbon are in equilibrium and above 1469K, there is a tendency for reaction (2-8) to shift in the forward direction. Therefore the equilibrium constant, K_8, can be expressed in terms of $\Delta G_8°$ as shown below.

$$K_8 = \exp(\frac{-\Delta G_1^o}{RT}) = \frac{a_{TiN} \cdot (p_{CO})^2}{a_{TiO_2} \cdot a_C^2 \cdot (p_{N_2})^{1/2}} \qquad (2\text{-}9)$$

where p designates the partial pressure of the gaseous phase. For unit activities of the condensed phases, ie a_{TiN}, a_{TiO_2}, a_C and p_{N_2} equal 1.

$$K_8 = (p_{CO})^2 = \exp(\frac{-\Delta G_8^o}{RT}) \qquad (2\text{-}10)$$

which by combining with the $\Delta G°$ value yields

$$-RT\ln p_{co} = 187.945 - 0.128T \qquad (2\text{-}11)$$

The value of P_{CO} equal to 1 atm in Equation (2-8) represents the equilibrium temperature ($T_{eq.} = 1469K$) at which $\Delta G_1°$ equals to zero. From the Le Chatelier principle, the removal of CO gas from the reaction chamber by purging argon gas will ensure a shift in the equilibrium of reaction (2-8) in the forward direction, otherwise the backward equilibrium will dominate. Provided that the partial pressure of CO in the chamber is less than the equilibrium partial pressure, the reaction will proceed in the forward direction.

The formation of TiC by carbothermic reaction is also considered and are shown in Equations (2-8) and (2-12). By combining the relative stability of TiN and TiC phases, we have considered the following reaction (2-13):

$$TiO_2(s) + 3C(s) = TiC(s) + 2CO(g) \qquad (2\text{-}12)$$

$$TiN(s) + C(s) = TiC(s) + 1/2N_2(g) \qquad (2\text{-}13)$$

TiO_2 reacts with carbon in N_2 atmosphere to produce TiN, but TiN will be transformed to TiC when the temperature is higher than the stable equilibrium temperature for TiN or when the partial pressure of nitrogen is too low. Above 1864K, TiC is more stable than TiN, so TiN transforms to TiC as shown in reaction (2-13). The standard Gibbs free energy change vs temperature relationship for the carbothermic reduction of titanium dioxide to titanium

nitride and carbide phases is referred as the univarient diagram and on this basis, the stability range of the nitride and carbide ceramic phases under reducing atmosphere can be defined. This is summarized in **Figure II-10**.

4. EXPERIMENTS

4.1 Preparation

Titanium dioxide (TiO_2, rutile) was used as the starting material with carbon. Appropriate amounts of TiO_2 and carbon were weighed in stoichiometric proportions. The particle size of TiO_2 (Tioxide UK Ltd, pigment grade) was in the submicrometer range. In some mixtures, more than the stoichiometric amount of carbon was added. This was necessary for the sustenance of the reaction: $TiO_2 + 2C + 1/2N_2 = TiN + 2CO$. Two different kinds of carbon: graphite (Hopkins & Williams Ltd, synthetic powder, Assay > 98%) and activated charcoal (Fluka Chemie Ltd, ash < 1%) were used. In some mixtures, ferric chloride ($FeCl_3$, BDH Chemicals Ltd, > 96%) was also added up to 10 weight percent to investigate its role as catalyst during the reduction of TiO_2. Each sample weighed about 1.2 gram. The weighed materials were thoroughly dry-mixed, ground in an agate mortar and then pressed in a 6mm inner diameter steel mould to form cylindrical shape pellets. The pressure used was $3kN \cdot cm^{-2}$.

4.2 Fabrication

A silicon carbide resistance tube furnace (**Figure II-11**) was employed for heating the pelletised mixture. The alumina reaction tube was 70mm O.D x 60mm I.D x 800mm L. The temperature of furnace was controlled using a Eurotherm 818 controller connected to a Pt-Pt/Rh13% thermocouple placed adjacent to the furnace tube. The temperature was measured using Pt/Pt-Rh13% thermocouple placed inside the alumina tube at the bottom of the crucible which was also used as a support for the crucible. As shown in **Figure II-12**, a constant temperature region (±1°C) of 80~100mm long was obtained in the temperature range 1073K to 1773K. The compacted pellets were heated in the temperature range 1173 to 1773K. The pressed samples

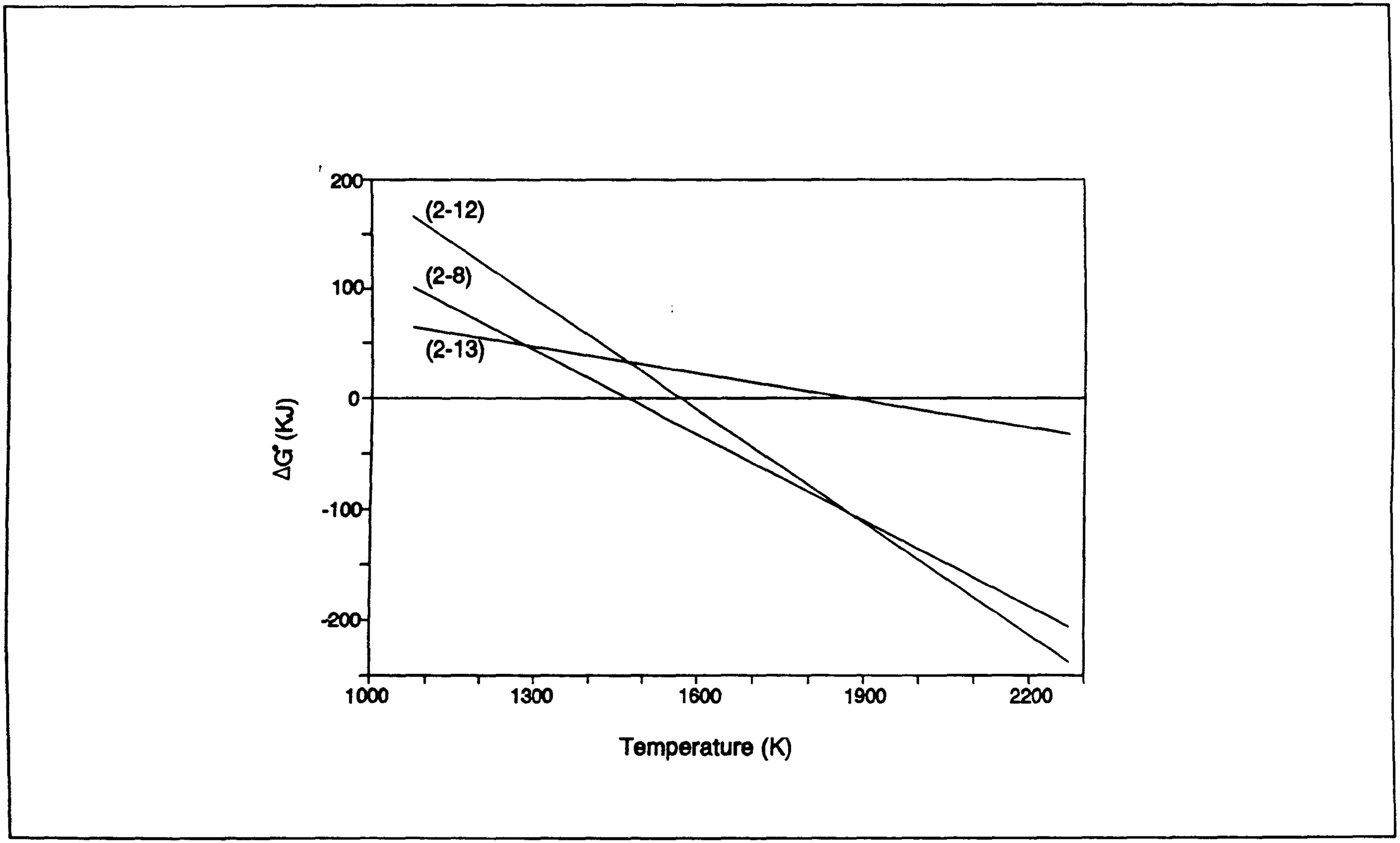

Figure II-10. The standard Gibbs free energy change diagram for the formation of TiN and TiC. ((*):Equation No.)

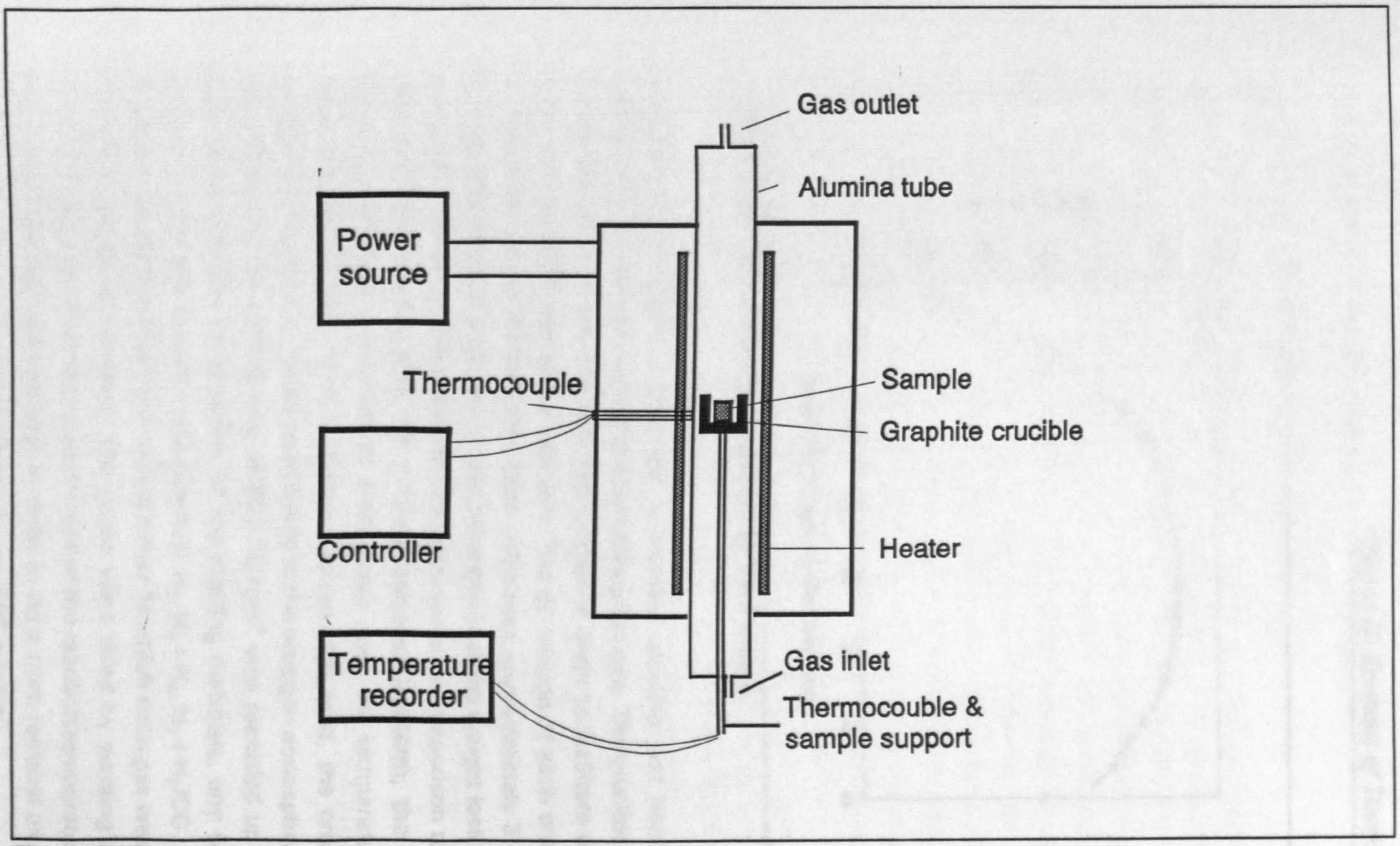

Figure II-11. A schematic diagram of the vertical tube furnace.

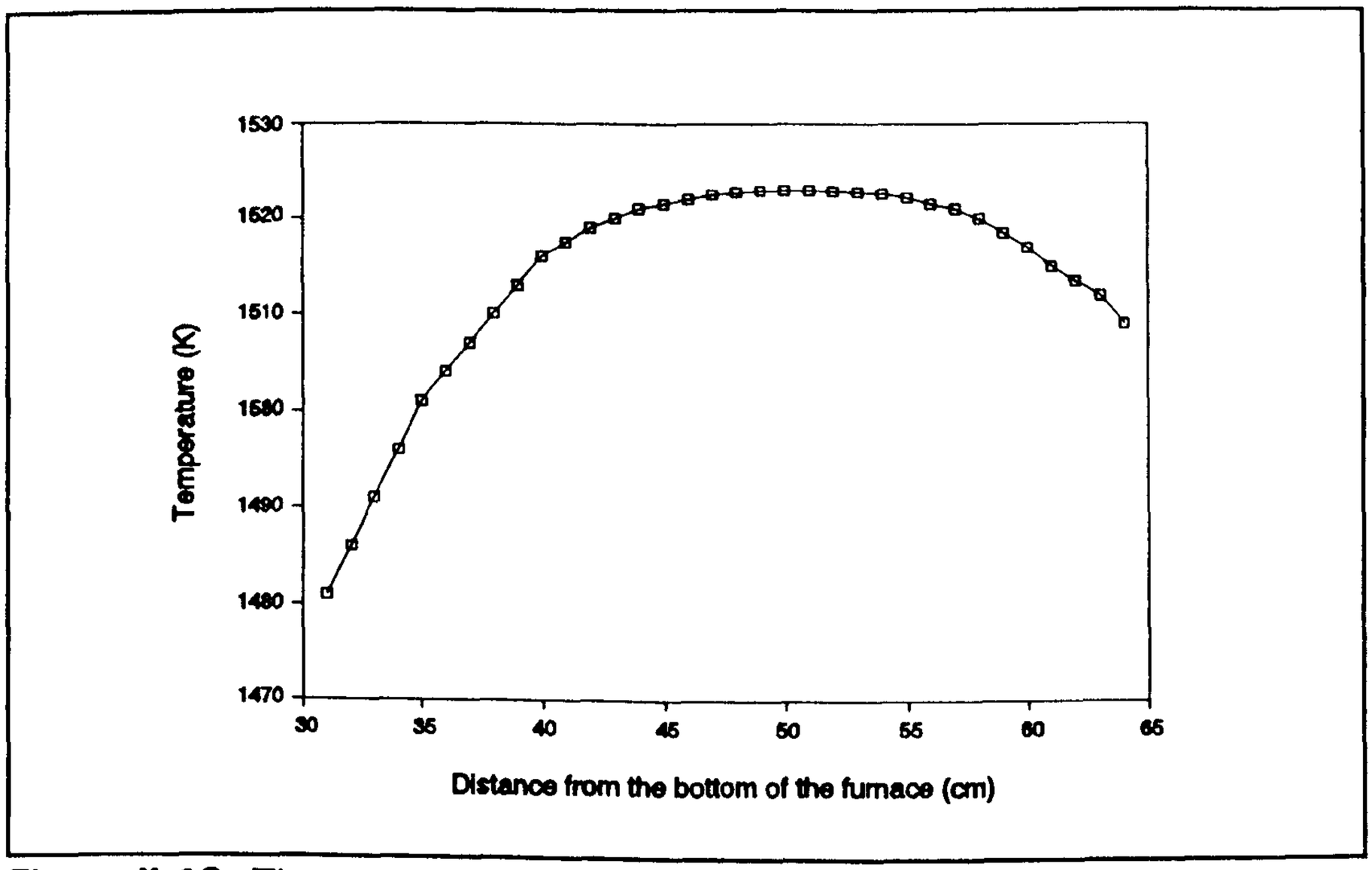

Figure II-12. The temperature profile of the furnace.

were transferred inside a graphite or alumina crucible and heated in the isothermally-maintained zone of the resistance furnace. The crucible had holes (3 mm diameter) on the side wall and bottom in order to facilitate the flow of gases around pellet during the reaction. The dimension of each crucible was 20 mm diameter and 20 mm long. Each pellet took approximately 3-4 minutes to reach the selected isotherm. It was recorded that the weight loss sustained by a pellet during heating was insignificantly small in comparison to the total expected weight loss. Also, for a lower selected isotherm, the reduction reaction seemed to commence at a slow rate once the temperature of the pellet reached 1273K. After a preselected reaction time, the crucible was lowered in order to cool the sample rapidly in the nitrogen atmosphere. During this procedure, the cooling rate of 250 °C·min^{-1} was recorded up to 673K. Depending upon the composition of the starting materials, any one of the following purge gas mixtures was selected: N_2, $N_2 + H_2$, $N_2 + H_2/CO$. A mixture of gases was obtained from the mixing tower to which each gas was provided through a set of flow meters. The gases were dried by passing through a column of silica gel. Prior to the attainment of the reaction temperature, N_2 gas was purged through the chamber in order to rid it from residual oxygen. The typical gas flow rate in all experiments was 500 ml·min^{-1}.

4.3 Analysis

After reaction, the pellets were weighed for determining the percentage reduction. The phases present in the reacted pellets were examined by X-ray powder diffraction technique by using Cu-kα radiation (0.15406nm) in a Philips PW1050 computer-controlled diffractometer. The two theta angles were measured after substracting the Cu-kα_2 value from the original data. The pellet after reaction was grounded to powder state and then mounted on a stainless steel stub. The selected 2θ (diffraction angle) scanning range was between 10° and 90°. For this, the pre-programmed step size and scan speed were 0.01 degree·min^{-1} and 0.015 degree·min^{-1}, respectively. In this way, the diffraction peaks from the powder reaction product were recorded. These results were compared with JCPDS card data to identify the phases produced. The reaction products were also examined by scanning electron microscopic technique using a JEOL 840 scanning electron microscope fitted with an energy dispersive X-ray (EDX) detector to study a morphology of the phases and their chemical composition. Prior to scanning microscopic examination the powder surface was coated with a trace of gold film in order to obtain a detailed surface topology of the new phase formed.

5. RESULTS

5.1 The Extent of TiO_2 Reduction with Graphite and Active Carbon and Phases Produced.

The degree of reduction (%R) was determined from the stoichiometry of the reaction shown below in **Equation (2-14)**:

$$TiO_2 + xC + \tfrac{1}{2}N_2 = TiN + 2CO + (x-2)C \qquad \textbf{(2-14)}$$

$$\text{Percentage reduction (\%R)} = \frac{\Delta W}{W_o} \times 100 \qquad \textbf{(2-15)}$$

where ΔW is the observed percentage weight loss in a pellet during the course of reaction at any arbitrarily chosen time 't' from the starting time $t = 0$, and W_o is the maximum expected stoichiometric percentage weight loss. The value of x is usually between 1 and 4. When $x = 3$ in Equation (2-14), for example,

total weight of the reactant is 115.93 gram, while that of the product should be 73.92 gram, from which a maximum weight loss of 42.01 gram is expected. This means that the theoretical maximum W_o is 36.24 %. If the weight loss of sample is 0.5 g and weight of the starting material was 1.5 g, ΔW will be 33 % so that the percentage reduction (%R) is 92. After collecting the %R data at various temperatures, the plots between %R and time 't' were constructed. These we call "the rate of reduction" curves. The rates of reduction of TiO_2 to TiN at different isotherms for graphite and activated charcoal are compared in **Figures II-13** and **II-14**, respectively, from which it is evident that the type of carbon, in this case active charcoal, has a pronounced effect in determining the speed of chemical reaction. When graphite was used as a reducing agent, for example, the reduction reaction virtually stopped at about 20 %R after 1 hour reaction at 1473K. Only partial reduction was achieved at 1573K after 4 hours. However at 1673K, the reduction continued at a steady rate even after 6 hours. A 100 % reduction was recorded with graphite at 1773K. Whereas in Figure II-14, which represents the reduction reaction with activated charcoal, about 80% reduction was achieved after 1 hour at 1573K. The reaction reached completion after 4 hours at 1573K. Activated charcoal has a very high surface area and its reactivity compared to graphite provides an increased number of active sites for the adsorption of oxygen, an essential requirement for the nucleation of CO gas. The mechanism has been proposed by Turkdogan and Vinters.[78] The reactivity of carbon surface area positively influences the rate of reduction, which may be due to a higher solid-solid and solid-gas interfacial surface area where reaction occurred. More intimate contact of the reactants significantly accelerates the reaction.

Pellets which were completely reduced yielded weight loss more than 100 %R. For this we have proposed two possible reasons. The titanium nitride produced is not stoichiometric TiN but it is a solid solution of titanium nitride and carbide, TiC_xN_{1-x}. If we consider the formation of $Ti(C_{0.5}N_{0.5})$ as shown in **Equation (2-17)**, the maximum theoretical value of %R is 117 when compared with **Equation (2-16)**.

$$TiO_2 + 3C + \tfrac{1}{2}N_2 = TiN + 2CO + C \qquad \textbf{(2-16)}$$

$$TiO_2 + 3C + \tfrac{1}{4}N_2 = Ti(C_{0.5}N_{0.5}) + 2CO + 0.5C \qquad \textbf{(2-17)}$$

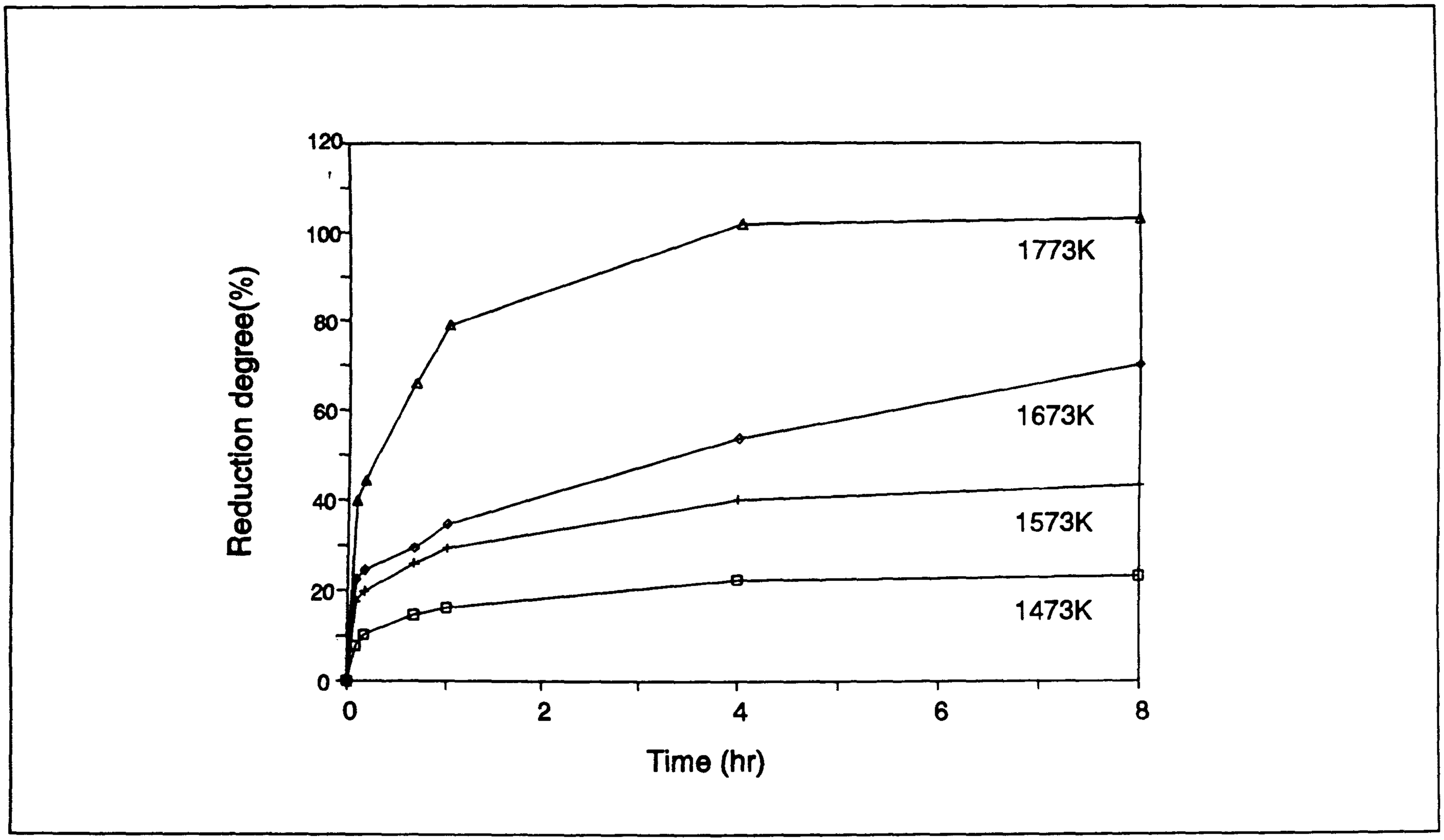

Figure II-13. Relationship between reduction degree (%R) and temperature for the nitriding reactions of TiO_2 with graphite. (Composition: $TiO_2 + 3C$)

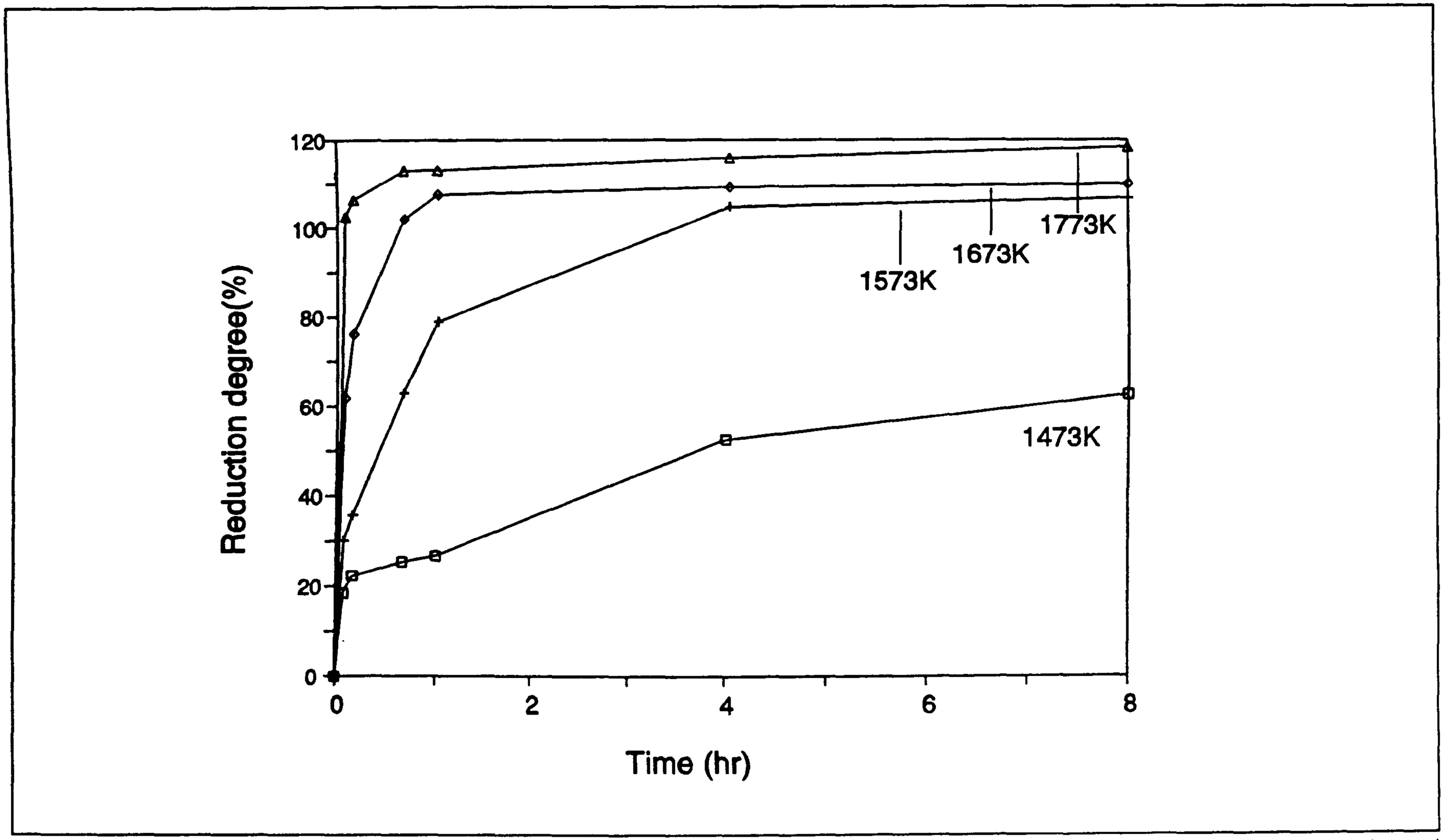

Figure II-14. Relationship between reduction degree (%R) and temperature for the nitriding reactions of TiO_2 with activated charcoal. (Composition: $TiO_2 + 3C$)

The data are shown in **Table II-8**. The second possible reason is the presence of air trapped in the pellet (starting material due to its high surface area) and some oxygen contamination from the gas phase. White et al[74] also observed more than stoichiometric value of %R, a maximum of 127 %R was recorded in their experiments.

Table II-8. The maximum percentage reduction according to phase produced.

Equation (2-16)				Equation (2-17)			
Weight loss($g \cdot mol^{-1}$)	Weight loss (ΔW,%)	Weight $loss_{max}$ (W_o,%)	% R	Weight loss($g \cdot mol^{-1}$)	Weight loss (ΔW,%)	Weight $loss_{max}$ (W_o,%)	% R
42.01	36.24	36.24	100	49.02	42.28	36.24	117

Figure II-13 and II-14 suggest that the reduction-nitridation of TiO_2 to TiN_x or $Ti(CN)_x$ takes place in three stages. The initial fast stage depends upon the temperature and constitutes a major part of the overall reduction process. This is evident whether we compare rate curves for either with graphite or with activated charcoal. The second stage is more distinguishable particularly at lower reduction temperatures and with graphite. Under these conditions the rate of reduction is slow. In the final stage, the reduction reaction proceeds very slowly.

The reduced pellets were examined by X-ray powder diffraction technique for the identification of the phases produced. **Tables II-9** and **II-10** below summarise the phases present at different temperatures and times intervals. In the table, various phases are arranged in the order of decreasing relative diffraction intensity. From these results, the relative stability of various phases at a particular temperature can be easily recognised. The data will be used later in the Discussion section for the interpretation of reduction reaction and the formation of interstitial ceramic phase. The removal of oxygen from rutile (TiO_2) lattice occurs during reduction leading to the formation of sub-oxide phases. Crystalline phases such as titanium carbonitride, $Ti(C_xN_{1-x})$, which is discussed below, titanium oxide (TiO_2), its sub-oxides, Ti_nO_{2n-1} ($Ti_{10}O_{19}$, Ti_9O_{17}, Ti_8O_{15}, Ti_7O_{13}, Ti_6O_{11}, Ti_5O_9, Ti_4O_7 and Ti_3O_5) and graphite were identified. Note that in most of our experiments, the nitride phase formed was impure. It is a solid-solution of nitride and carbide in the TiN lattice and

Table II-9. Produced phases for 8 hours reactions in the nitrogen atmosphere. (flow rate:0.5 $l \cdot min^{-1}$)

Starting Materials	Tempe-rature (K)	Time (hr)	Produced Phases	
			with Graphite	with Activated charcoal
TiO_2 + 3C	1173	8	TiO_2, C	TiO_2
	1273		TiO_2, C	TiO_2, $Ti_{10}O_{19}$*
	1373		C, $Ti_{10}O_{19}$, TiO_2*	Ti_3O_5, Ti_4O_7

(note: * indicate a very small trace of phase)

from here onwards, the phase will be referred as either carbonitride or TiCN type phase. The phases produced during the reduction of TiO_2 with graphite or activated charcoal in N_2 gas are summarised in **Table II-9**. Pellets that were reduced below 1373K over a period of 8 hours showed that only a small amount of reduction took place and no titanium carbonitride phase formed. Above 1473K, however, the presence of a titanium carbonitride (TiCN) with a series of titanium sub-oxide phases was recorded. This is shown in **Table II-10**. Some of the typical x-ray diffraction patterns are shown in **Figure II-15**. The relative intensity of diffraction peaks confirms the relative abundance of a specific phase in the reaction product. From TiO_2 phase, which has tetragonal structure, a series of the triclinic structure of sub-oxides ($2 > O/Ti \geq 7/4$) formed, which then transformed to Ti_3O_5 phase having a monoclinic structure. The crystal structure of titanium sub-oxides are compared in **Table II-11**. All triclinic phases have very similar lattice dimensions, indicating that the defect structures are rather similar except that their c-axis and ß-angle change. This further suggests that the oxygen vacancies are arranged along the c-axis and their distribution in the lattice space is compensated by the incremental angular change in the ß-angle of the defect structure.

Rutile (TiO_2), under reducing conditions, produces a series of titanium sub-oxide phases such as $Ti_{10}O_{19}$, Ti_9O_{17}, Ti_8O_{15}, Ti_7O_{13}, Ti_6O_{11}, Ti_5O_9, Ti_4O_7, Ti_3O_5, Ti_2O_3 and TiO, but in this investigation, Ti_2O_3 and TiO phases were not found. This is explained from the calculation of the predominance area diagram shown in the discussion section. The last sub-oxide that reduces to form $Ti(CN)_x$ is Ti_3O_5. The presence of Ti_3O_5 was also confirmed during the

reduction of TiO_2 with H_2+CO gas mixture. The above observations confirm that the reduction of TiO_2 to TiCN is a multi-stage process.

Table II-10. Synthesised phases depend on reaction temperature, time and the used type of carbon in the nitrogen atmosphere.
(N_2 flow rate: 0.5 $l \cdot min^{-1}$)

Starting Materials	Temp (K)	Time (hr)	Produced Phases	
			with Graphite	with Activated charcoal
TiO_2 + 3C	1473	0.1	C, Ti_9O_{17}, TiO_2*	Ti_5O_9, Ti_4O_7
		0.2	C, Ti_9O_{17}, Ti_8O_{15}	Ti_4O_7, Ti_5O_9
		0.3	C, Ti_6O_{11},Ti_7O_{13},Ti_8O_{15}	Ti_4O_7, Ti_3O_5
		0.7	C, Ti_6O_{11},Ti_5O_9,Ti_7O_{13}*	Ti_3O_5, TiCN
		1	C, Ti_5O_9, Ti_4O_7	Ti_3O_5, TiCN
		4	C, Ti_3O_5, TiCN*	Ti_3O_5, TiCN
		8	C, Ti_3O_5, TiCN	TiCN, Ti_3O_5
	1573	0.1	C, Ti_4O_7, Ti_3O_5	Ti_3O_5, TiCN
		0.2	C, $Ti3O_5$, Ti_4O_7	Ti_3O_5, TiCN
		0.7	C, Ti_3O_5, TiCN	TiCN, Ti_3O_5
		1	C, Ti_3O_5, TiCN	TiCN, Ti_3O_5
		4	C, Ti_3O_5, TiCN	TiCN
		8	C, Ti_3O_5, TiCN	TiCN
	1673	0.1	C, Ti_3O_5, TiCN	TiCN, Ti_3O_5
		0.2	C, Ti_3O_5, TiCN	TiCN, Ti_3O_5
		0.7	C, Ti_3O_5, TiCN	TiCN
		1	C, Ti_3O_5, TiCN	TiCN
		4	C, TiCN, Ti_3O_5	TiCN
		8	C, TiCN, Ti_3O_5	TiCN
		24	TiCN, C	TiCN
	1773	0.1	C, Ti_3O_5, TiCN	TiCN
		0.2	C, Ti_3O_5, TiCN	TiCN
		0.7	C, TiCN, Ti_3O_5	TiCN
		1	TiCN, C, Ti_3O_5	TiCN
		4	TiCN, C	TiCN
		8	TiCN, C	TiCN

(note: * indicate a small trace of phase)

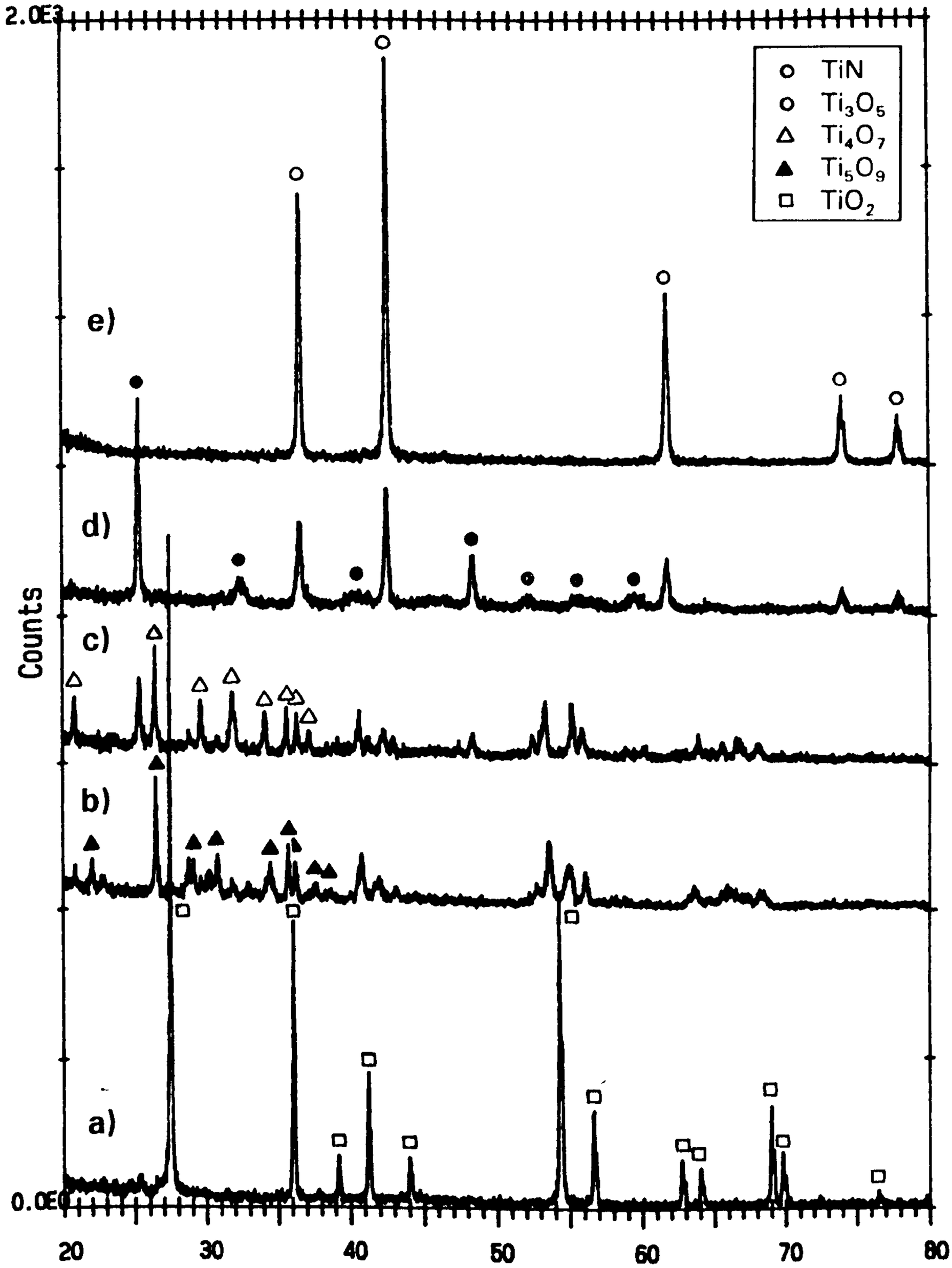

Figure II-15. The X-ray diffraction patterns of phases produced by reduction in a N_2 gas. (flow rate:0.5 $l \cdot min^{-1}$, $TiO_2 + 3C$:active carbon, (a) 8hrs, 1173K (b) 10min, 1473K (c) 20min, 1473K (d) 4hrs, 1473K (e) 4hrs, 1573K)

Table II-11. The structure and lattice parameter of titanium sub-oxides.[64]

Phase	Structure	Lattice parameter						JCPDS No.
		a_o(Å)	b_o(Å)	c_o(Å)	α(°)	ß(°)	γ(°)	
TiO_2	tetragonal	4.593	4.593	2.959	90.0	90.0	90.0	21-1276
$Ti_{10}O_{19}$	-	-	-	-	-	-	-	11-474
Ti_9O_{17}	triclinic	5.57	7.10	22.15	97.1	131.0	109.8	18-1405
Ti_8O_{15}	triclinic	5.57	7.10	37.46	97.2	128.8	109.6	18-1404
Ti_7O_{13}	triclinic	5.54	7.13	15.36	98.9	125.5	108.5	18-1403
Ti_6O_{11}	triclinic	5.56	7.14	24.04	98.5	120.8	108.5	18-1401
Ti_5O_9	triclinic	5.569	7.120	8.875	97.6	112.3	108.5	11-193
Ti_4O_7	triclinic	5.60	7.13	12.46	95.1	95.1	108.8	18-1402
Ti_3O_5	monoclinic	9.828	3.776	9.898	90.0	91.3	90.0	23-606
Ti_2O_3	trigonal	5.139		13.66				10-63
TiO-α	monoclinic	5.85	9.34	4.14	90.0	90.0	107.5	23-1078
TiO-ß	cubic	4.20	-	-	90.0	90.0	90.0	-

5.2 The Effect of Temperature and Time on the Reduction/Nitridation of TiO_2.

With increasing reduction temperature, the conversion of TiO_2 to a carbonitride phase occurred readily. Among the phases produced, titanium carbonitride was the main product of the reaction, as shown in Table II-10. For time intervals longer than 40 minutes, Ti_3O_5 had completely converted to a carbonitride phase at 1673K. However, decreasing the reduction isotherm by 100K to 1573K resulted into a much longer period of completion, in this case 8 hours. Significant nitriding begins above 22 %R and Ti_3O_5 begins to form from 18 %R, and exists in equilibrium with the carbonitride phase up to ~80 %R. Without carbon, no TiCN could be produced even though pellets were reduced in the N_2+H_2+CO gas atmosphere. Above the stoichiometric molar ratio of $C/TiO_2=2$, the rate of formation of TiCN becomes appreciable, and depends strongly upon the reactivity of carbon. The carbonitride phase was produced in less than 5 minutes of reaction time by carbothermic reduction above 1573K which is evident from Table II-10. Reaction temperatures can be reduced by nearly two hundreds of degree kelvin when activated charcoal replaced graphite as reducing agent.

5.3 The Effect of Gas Composition on the Reduction/Nitridation of TiO_2.

5.3.1 Reaction with $CO+H_2$ gas

A marginal improvement in the reducibility of titanium dioxide was observed with an increase in the carbon content both at low and high temperatures as a result of a small increase in the already-available oxide-carbon contact surface area. The present of CO gas in the purge gas however impedes the reduction reaction. From Le Chatelier principle which points out that the increasing CO partial pressure will lead to the reversion in equilibrium. The presence of hydrogen assists the reduction reaction. A small addition of iron in the starting materials also improved the extent of reduction. For the calculation of the theoretical value of percentage reduction (%R), iron content was not considered. The results are shown in **Table II-12**. Hydrogen gas when present in the nitriding atmosphere has a marked influence on the conversion

Table II-12. Synthesised phases according to gas composition.

Starting Materials	Temp (K)	Time (hr)	Gas composition	% R	Produced phases
TiO_2+1C	1673	4	N_2	56.05	Ti_3O_5, C, TiCN
			$N_2+[CO/H_2](35\%)$	45.35	Ti_3O_5, C, TiCN
			$N_2+[CO/H_2](45\%)$	32.73	C, Ti_3O_5, TiCN
TiO_2+1C*			N_2	63.85**	Ti_3O_5,TiO_2,TiCN
$TiO_2+1C+Fe(5wt\%)$			$N_2+[CO/H_2](50\%)$	75.85	TiCN, Ti_3O_5
TiO_2+2C			$N_2+[CO/H_2](45\%)$	30.64	C, Ti_3O_5, TiCN
TiO_2+3C			N_2	53.79	C, TiCN, Ti_3O_5
			$N_2+H_2(25\%)$	71.29	TiCN, C, Ti_3O_5
			$N_2+[CO/H_2](50\%)$	47.39	C, Ti_3O_5, TiCN
TiO_2+3C*			N_2	109.37	TiCN
			$N_2+H_2(25\%)$	119.16	TiCN
			$N_2+[CO/H_2](50\%)$	112.41	TiCN

(1. $CO:H_2$ = 50:50 mixture gas was used
2. Gas flow rate : N_2 = 0.5 $l \cdot min^{-1}$, mixed gas = 0.8 $l \cdot min^{-1}$)
3. * indicate activated charcoal, otherwise graphite unless specified.
4. ** indicate alumina crucible, otherwise graphite crucible unless specified)

Table II-13. Results of reduction degree according to reaction time.

Starting Materials	Temp (K)	Time (hr)	Gas composition	% R	Produced phases
TiO_2+1C	1673	3.5	$N_2+[CO/H_2](50\%)$	34.05	C, Ti_3O_5, TiCN
		15.0	(total:0.8 $l \cdot min^{-1}$)	41.47	C, TiCN, Ti_3O_5
		24.0		46.76	C, TiCN, Ti_3O_5

(* note: graphite was used for carbon source)

of TiO_2 to Ti(CN) or TiN. This is because of the competition between the water-shift reaction, $H_2+CO \rightarrow C+H_2O$, and the influence of CO gas on the suppression of the rate of reduction reaction. A higher percentage of CO in the gas phase tends to suppress the formation of TiCN phase. The presence of iron as catalyst improves the degree of reduction significantly in the $CO+H_2+N_2$ atmosphere even though the amount of carbon present in the mixture is only half of the stoichiometric amount. This is the reason that the effect of hydrogen on the reduction characteristic is even more significant than with CO. From these results we can conclude that hydrogen contributes to the reduction-nitridation of TiO_2 to TiCN. At longer reaction periods, as expected, the higher degree of reduction was achieved as shown in **Table II-13** at any temperatures. Comparison of the results of phase analysis indicated that the influence, of either in-situ generated oxygen potential as in the case of carbon, or externally imposed potential where $CO+H_2$ gas was used, has a similar effect on the phase combinations. Variation arises only in the final carbon content of the carbonitride phase. In the present investigation, the range of pO_2 (or pH_2O/pH_2) imposed during the reduction reaction has been estimated by using the Gibbs free energy change for the water-shift reaction. In the water-shift reaction, $C+H_2O=CO+H_2$, we have assumed the unit activity of carbon as an arbitrarily chosen value. This also appears to be true since in most of our direct reduction experiments, solid carbon was used as a reducing agent. The partial pressures of CO and H_2 were determined from the flow rate data at one atmosphere. The temperature dependence of pH_2O/pH_2 from the water-shift equilibrium is shown below in **Figure II-16** when pCO and pH_2 are 0.25. From the observed phase relationships and kinetic results, it is evident that the imposed oxygen potential gradient between the interface and the bulk gas promotes the mobility of oxygen and titanium ions leading to the formation of defective-structure sub-oxides.

5.3.2 Reaction with NH_3 gas

We also designed reduction experiments with ammonia as a nitriding

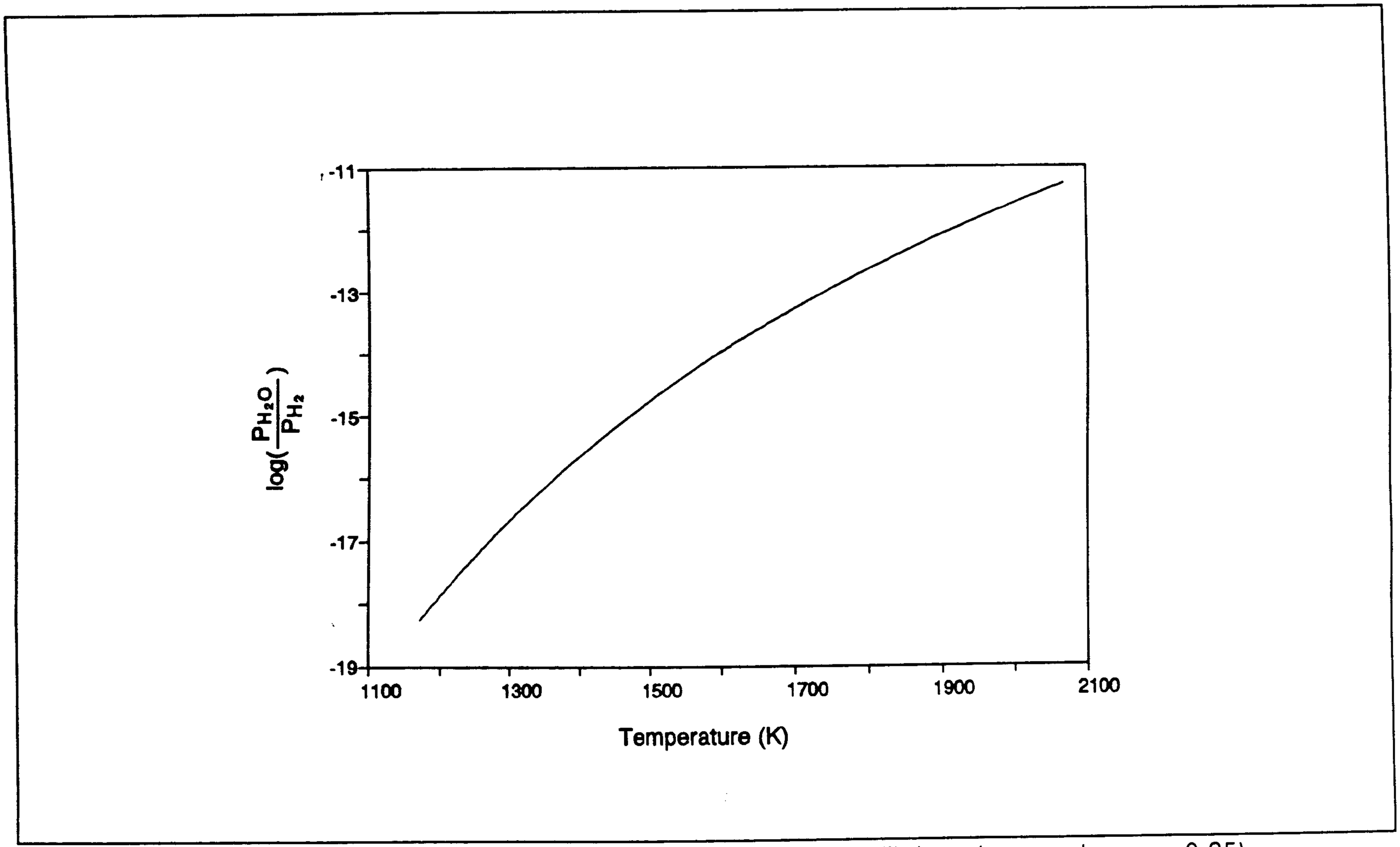

Figure II-16. The temperature dependence of pH_2O/pH_2 from water-shift equilibrium. (pCO and pH_2 are 0.25)

Table II-14. The results from ammonia nitridation.

Starting Materials	Temp (K)	Time (hr)	Gas composition	% R	Produced phases
TiO_2+2C	1673	2	N_2	88.33	TiCN, Ti_3O_5
	1473	2	$NH_3+[Ar/H_2](65\%)$	48.69	TiCN, Ti_3O_5
	1573	2	$NH_3+[Ar/H_2](65\%)$	51.80	TiCN, Ti_3O_5
		4	$NH_3+[Ar/H_2](75\%)$	74.57	TiCN, Ti_3O_5
	1673	2	$NH_3+[Ar/H_2](65\%)$	61.20	TiCN, Ti_3O_5
		4	$NH_3+[Ar/H_2](65\%)$	100.87	TiCN
TiO_2+1C	1473	2	$NH_3+[Ar/H_2](65\%)$	68.35	TiCN, Ti_3O_5
	1573	2	$NH_3+[Ar/H_2](65\%)$	75.44	TiCN, Ti_3O_5
	1673	2	$NH_3+[Ar/H_2](65\%)$	76.17	TiCN, Ti_3O_5

(* note : 1) carbon source: activated charcoal,
2) Gas flow rate : $N_2=0.5\ l{\cdot}min^{-1}$, $[Ar/H_2(4\%)]=0.1\ l{\cdot}min^{-1}$)

gas. A known volume percentage of NH_3 was mixed with the carrier gas mixture (Ar:96%/H_2:4%). The premixed carrier gas allows to select the nitrogen partial pressure in the reaction chamber by varying the concentrations of NH_3 and temperature. The control of nitrogen gas pressure is possible from the decomposition equilibrium of ammonia: $2NH_3(g) = N_2(g)+3H_2(g)$ which at a constant temperature yields $K=p_{N_2}\cdot p^3_{H_2}/p^2_{NH_3}$. The results from ammonia nitridation are summarised in **Table II-14**. The observed lattice parameters of TiCN are discussed in section 5.5.5.

5.4 The Effect of Catalyst ($FeCl_3$) on the Reduction Reaction

A number of experiments were carried out using $FeCl_3$ as a catalyst for the carbon oxidation reaction. As shown in section 5.3.1, its presence was also found to increase the rate of reduction reaction. The results are shown in **Figure II-17** and **18**. With increasing content of $FeCl_3$, the percentage reduction increased.

5.5 Lattice Parameter of Titanium Carbonitride

5.5.1 Determination of lattice parameters

The lattice parameter of the synthesised carbonitride was determined

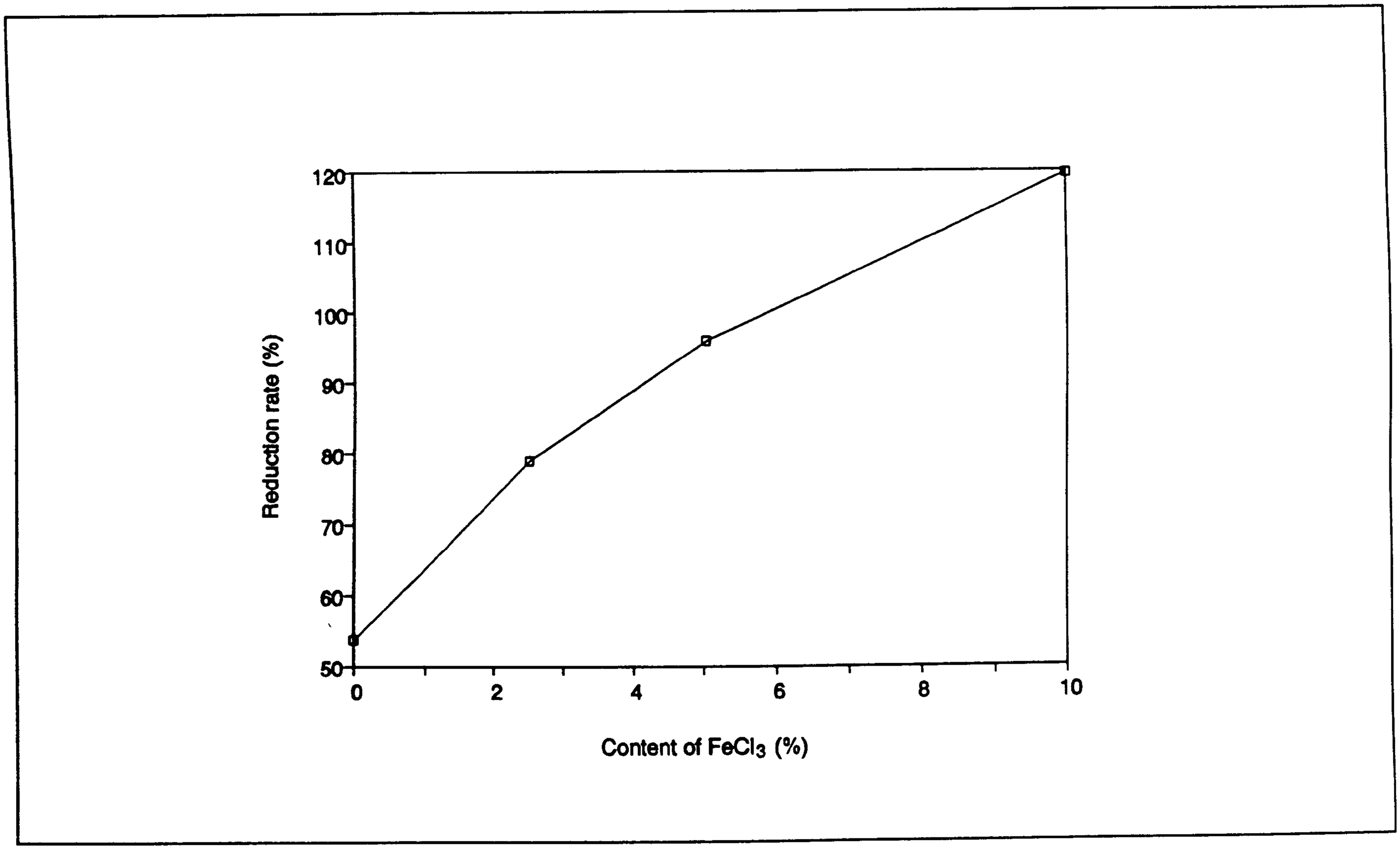

Figure II-17. The effect of $FeCl_3$ on the %R reacted at 1673K for 4 hours.

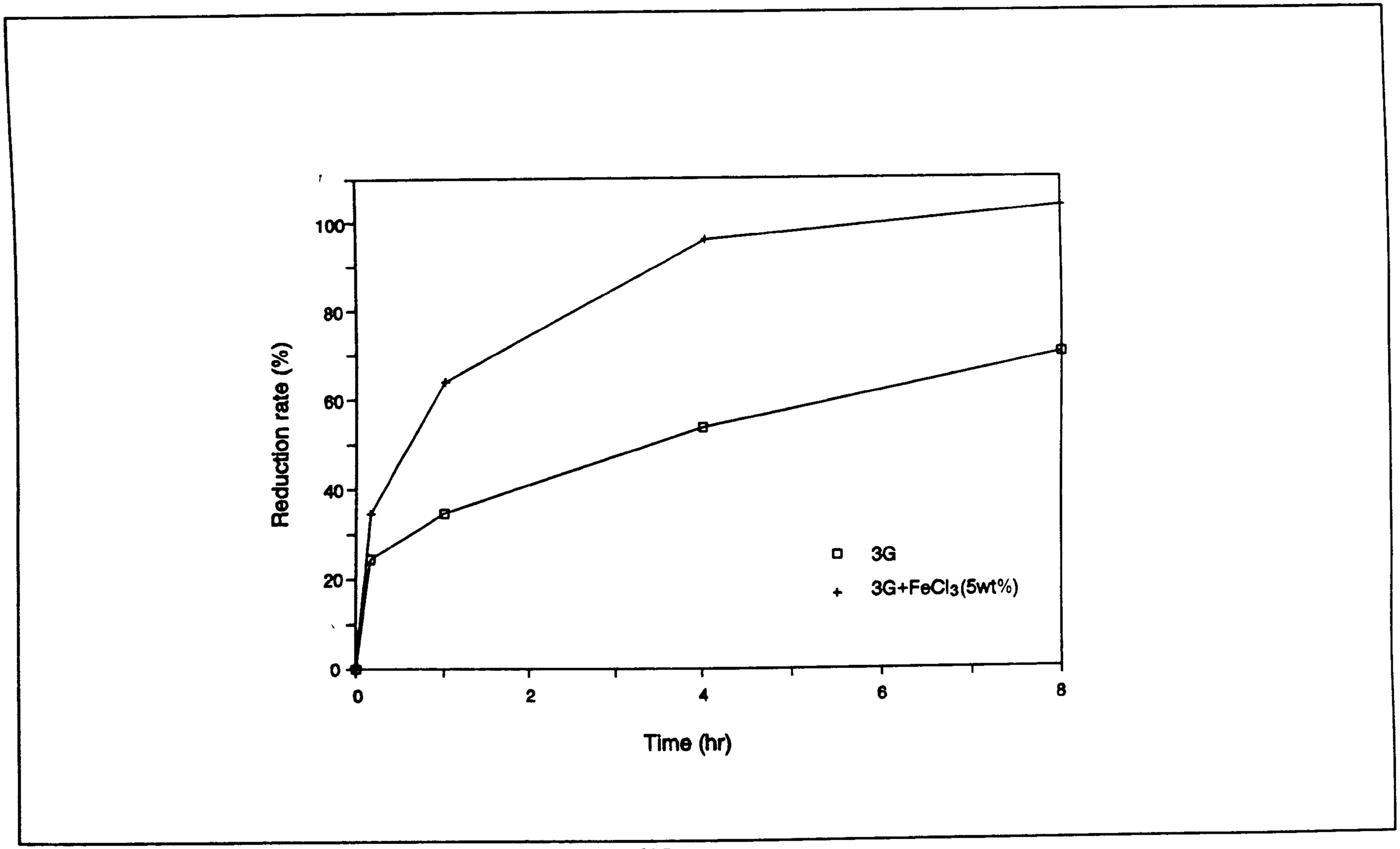

Figure II-18. Comparison of the effect of $FeCl_3$ on the %R.

from the measured d-spacing data derived from the powder diffraction and by using the following relationship. Titanium carbonitride has a face centred cubic structure (B1 NaCl) for which

$$\frac{1}{d^2} = \frac{h^2 + k^2 + l^2}{a^2} \qquad \textbf{(2-18)}$$

relationship is valid. The Bragg angle peaks corresponding to (111), (200), (220), (311) and (222) set of planes were used for evaluating the a-values. The data were statistically fitted to obtain a precise value of lattice parameter, '**a**', by extrapolating the straight line to $\sin^2\theta = 1$. The method adopted above has been recommended by Cullity.[79] The standard deviation for the values '**a**' determined from equation (2-18) was ± 0.0006 nm. The value of lattice parameter for each reduction experiment was compared with the values of the lattice parameters of stoichiometric TiN and TiC phases and are plotted against composition in **Figure II-19**. It was assumed that lattice constants varied linearly with composition, and $x+y$ equals to 1 in TiC_xN_y obtained in the present study. It is evident from this figure that the nitride of titanium formed as a result of the carbothermic reduction is carbonitride $Ti(C_xN_{1-x})$ and not the stoichiometric TiN phase. The non-stoichiometric $Ti_{1-x}N_x$ range is between 23 and 57 at.% N.[2] During the reaction, carbon dissolved in the lattice by occupying the available vacant interstitial sites hence producing a titanium carbonitride ($Ti(C_xN_{1-x})$) phase. The dissolution of C in the $Ti_{1-x}N_x$ lattice occurs because of the comparable atomic radii of the two interstitial atoms. Like the titanium nitride ($Ti_{1-x}N_x$), the carbide ($Ti_{1-x}C_x$) is also a non-stoichiometric phase (22 to 50 at% C) and hence allows a mutual random exchange of interstitial sites in the two identical crystalline structures. We noticed that when hydrogen gas was mixed with the bulk nitrogen gas during the reduction reaction, the tendency to form a carbonitride phase was significantly reduced. Also the containment material for the pellet seemed to be also important for the formation of oxynitride phase. For example, when an alumina crucible was used for reduction, the nitrogen concentration in the nitride phase then fell below 50 at.% i.e, to the right of TiN (100%) composition in Figure II-19. It is due to the extended mutual solid solubility of oxygen and nitrogen in the $Ti_{1-x}N_x$ lattice, the derived values of **a** for the non-stoichiometric $Ti_{1-x}(ON)_x$ compositions fall on the straight line joining the lattice parameter values of the stoichiometric carbide and nitride phases. However, it is difficult to ascertain the chemistry of the mixed interstitials on the basis of the lattice parameter

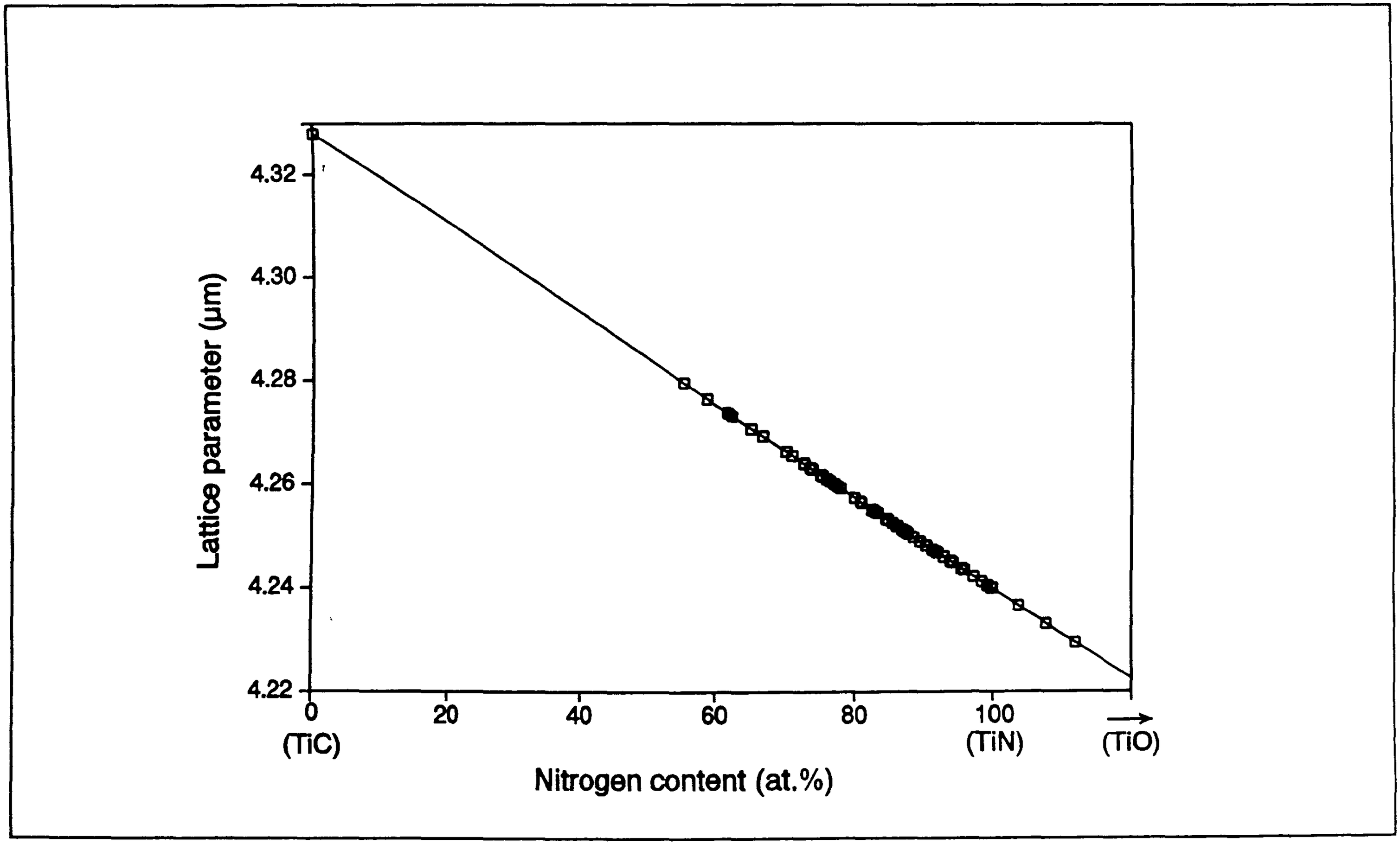

Figure II-19. The lattice parameter of synthesised titanium carbonitrides with varying nitrogen concentration.

data. Complex interstitials such as $Ti(C_xN_{1-x-y}O_y)$ are known to exist and their lattice parameters are suspiciously similar. Whether the oxygen-containing interstitials such as $Ti(O_xC_{1-x})$, $Ti(O_xN_{1-x})$ and $Ti(C_xN_{1-x-y}O_y)$ are stable under extremely low oxygen partial pressures ($3.22x10^{-17}$ to $3.29x10^{-16}$), as reported in the previous section, this is examined in the discussion section where we present the estimated and measured free energies of the interstitial compounds.

5.5.2 Variation of lattice parameters of Ti(CN) phase produced from the reduction with active carbon

Figure II-20 showed the lattice parameter change during reduction reaction. In the first stage of reduction, the lattice parameter of titanium carbonitride increased at short reaction time followed by a sharp decrease in the dimension (2nd stage), and then began to increase steadily (3rd stage). The rate of change varied accordingly with the reaction temperature. And it was much faster at a high temperature than observed at a lower temperature.

5.5.3. Variation of lattice parameters of Ti(CN) phase produced from the reduction with graphite

Earlier we pointed out under section 5.1 in Figure II-12 that at 1573K, the reduction reaction proceeded very slowly after 8 hours. During this period at this temperature, the lattice parameter of TiCN increased. However at 1673K, the lattice parameter followed a similar pattern as observed with active carbon (see above). At 1773K, the lattice parameter decreased continuously after an initial rise. These changes are summarised in **Figure II-21**.

5.5.4 The effect of reduction temperature on the lattice parameter of Ti(CN) phase

In **Figure II-22** which represents the reduction conditions, both with active carbon and graphite, the lattice parameter of TiCN phase formed in the initial stage of the reduction changes with rising temperature as well as with the reactivity of carbon. Empirical evidence indicates that the lattice parameter of the TiCN phase formed with graphite drops gradually with rising

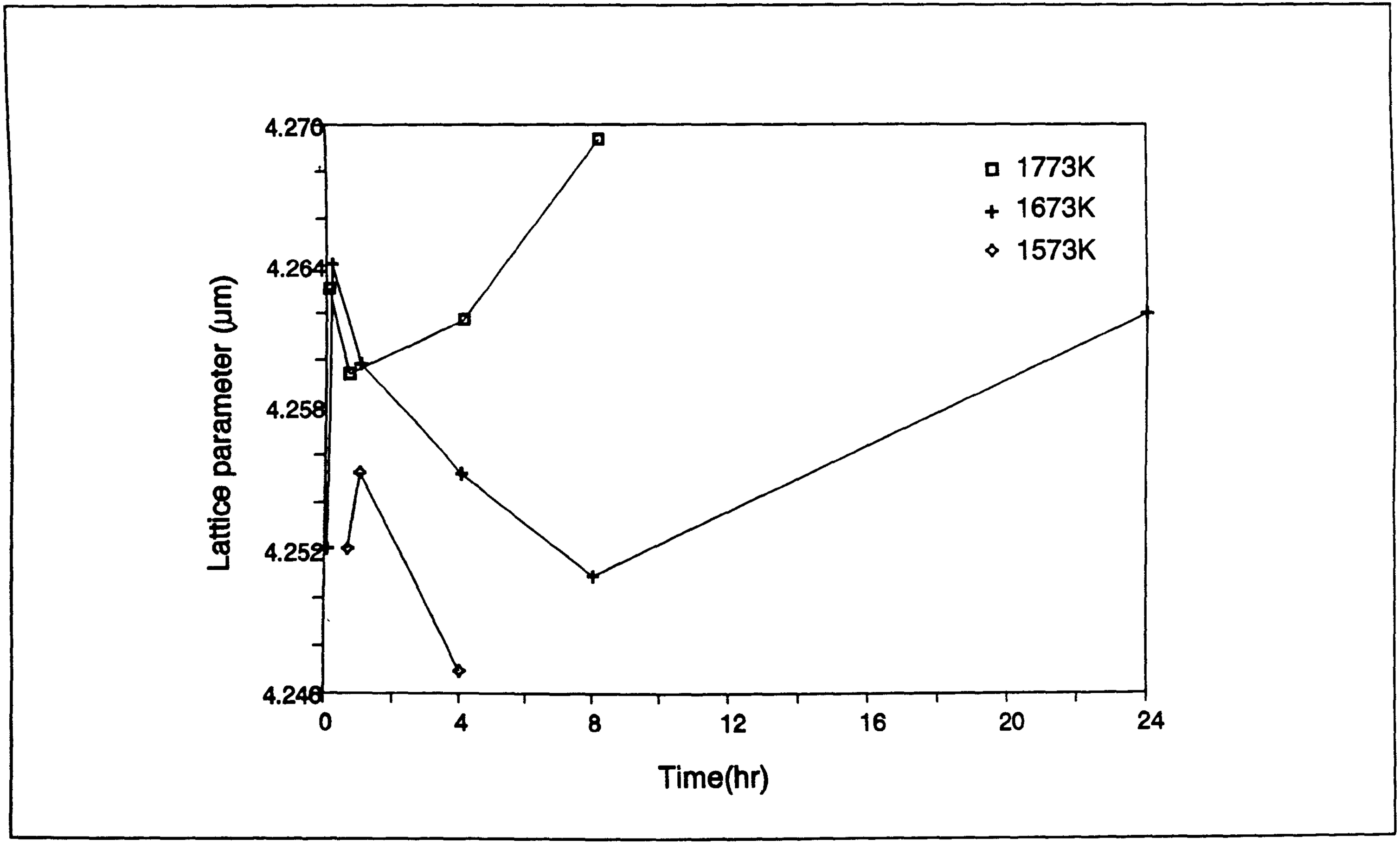

Figure II-20. Lattice parameter change of Ti(CN) phase produced with activated charcoal.

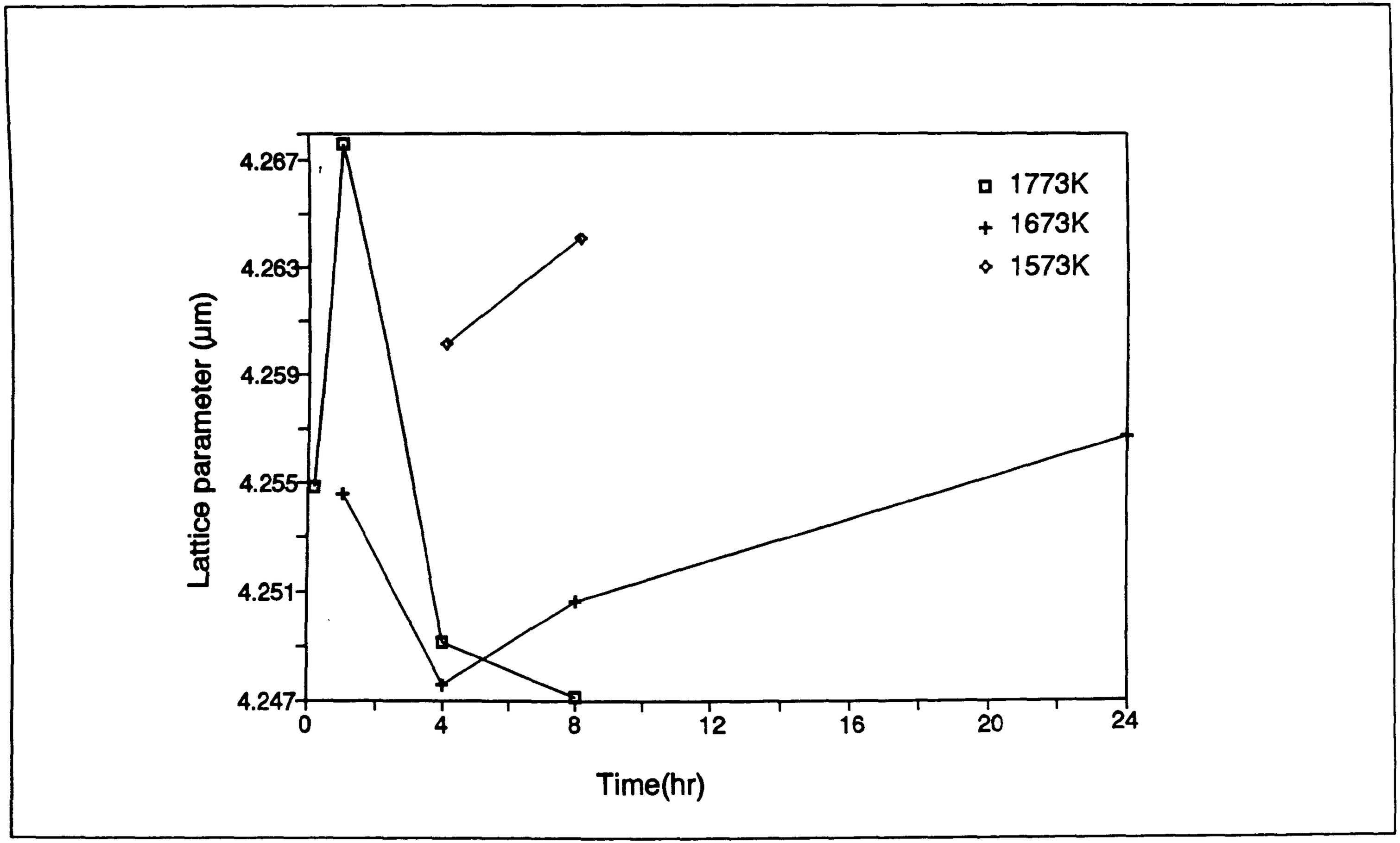

Figure II-21. Lattice parameter change of Ti(CN) phase produced with graphite.

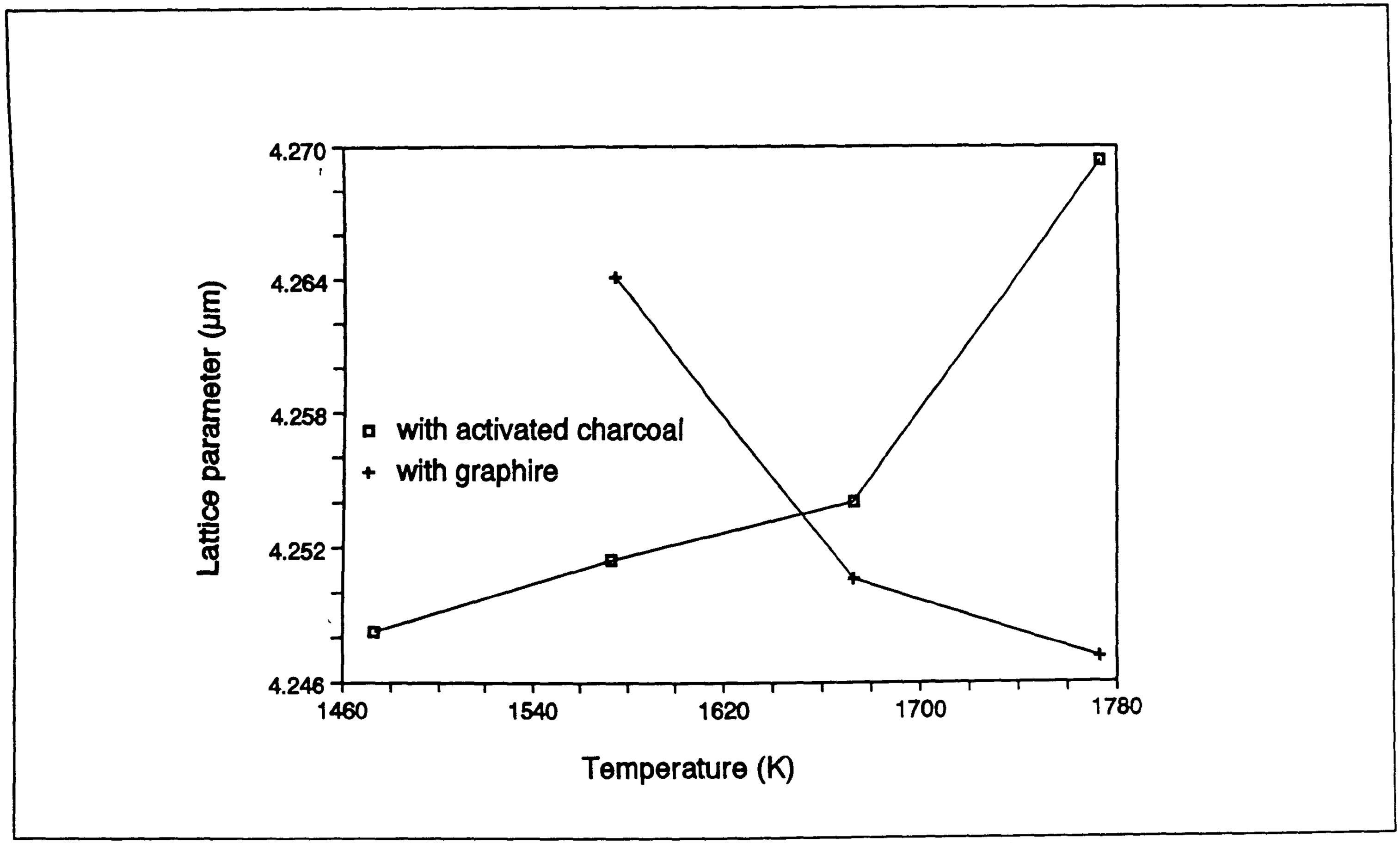

Figure II-22. Lattice parameter change with reduction temperature in the N_2 gas after 8 hours.

temperature, whereas on reaction with the active carbon, the change appears to take place in the reverse direction, in particular rising sharply above 1673K.

5.5.5 Lattice parameter change with the composition of the gas phase

Figure II-23 showed that as the content of CO increases in the reduction chamber, the lattice parameter of the TiCN phase rises. Whereas the presence of hydrogen leads to reduction in the cell dimension. This is true whether graphite or active carbon was used as reducing agent.

The effect of partial pressure of NH_3 and temperature on the lattice parameter of the titanium carbonitride phase is shown in **Figure II-24.** As the partial pressure of ammonia increases in the presence of carbon, which acts as a reducing agent, the experimentally determined lattice parameter appears to rise systematically. Also with the increasing temperature, the lattice parameter increases as this was also observed in the nitrogen gas atmosphere. In addition an experiment was also performed with NH_3 as a reducing and nitriding agent, but no nitride formed. In this experiment carbon was not present. This result showed that TiO_2 can not be reduced easily to either a carbonitride phase or an oxynitride phase without the presence of carbon.

5.6 Microstructure of Nitride

The scanning electron microscopic (SEM) examination showed that the morphology of titanium carbonitride particles is dependent upon the reactivity of carbon, temperature and reaction time.

5.6.1 The effect of reaction time and temperature

Photos II-1 and **II-2** show the microstructure of the reaction product produced during reduction with graphite and active carbon at different stages. The reduction temperature is 1673K. There is a strong evidence for sintering of titanium sub-oxides that exist in metastable equilibrium with TiCN phase. It is also evident that the titanium carbonitride phase grows from the surface of the oxide and has a distinct morphological feature. The carbonitride phase produced with graphite has a larger particle size than the carbonitride phase produced with active carbon. Additionally the phase has a facetted

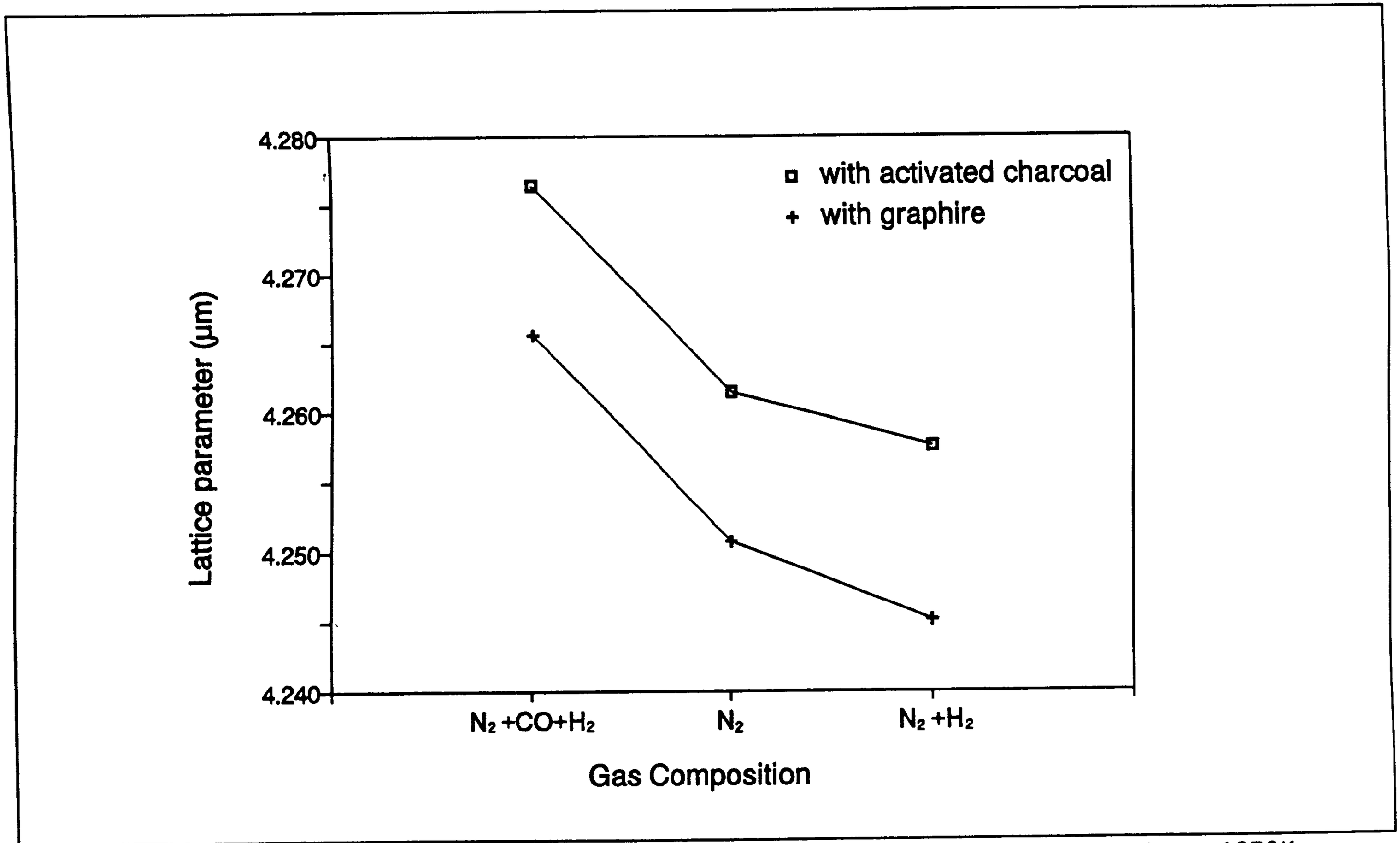

Figure II-23. Lattice parameter changes with the composition of the gas phase after 4 hours reaction at 1673K.

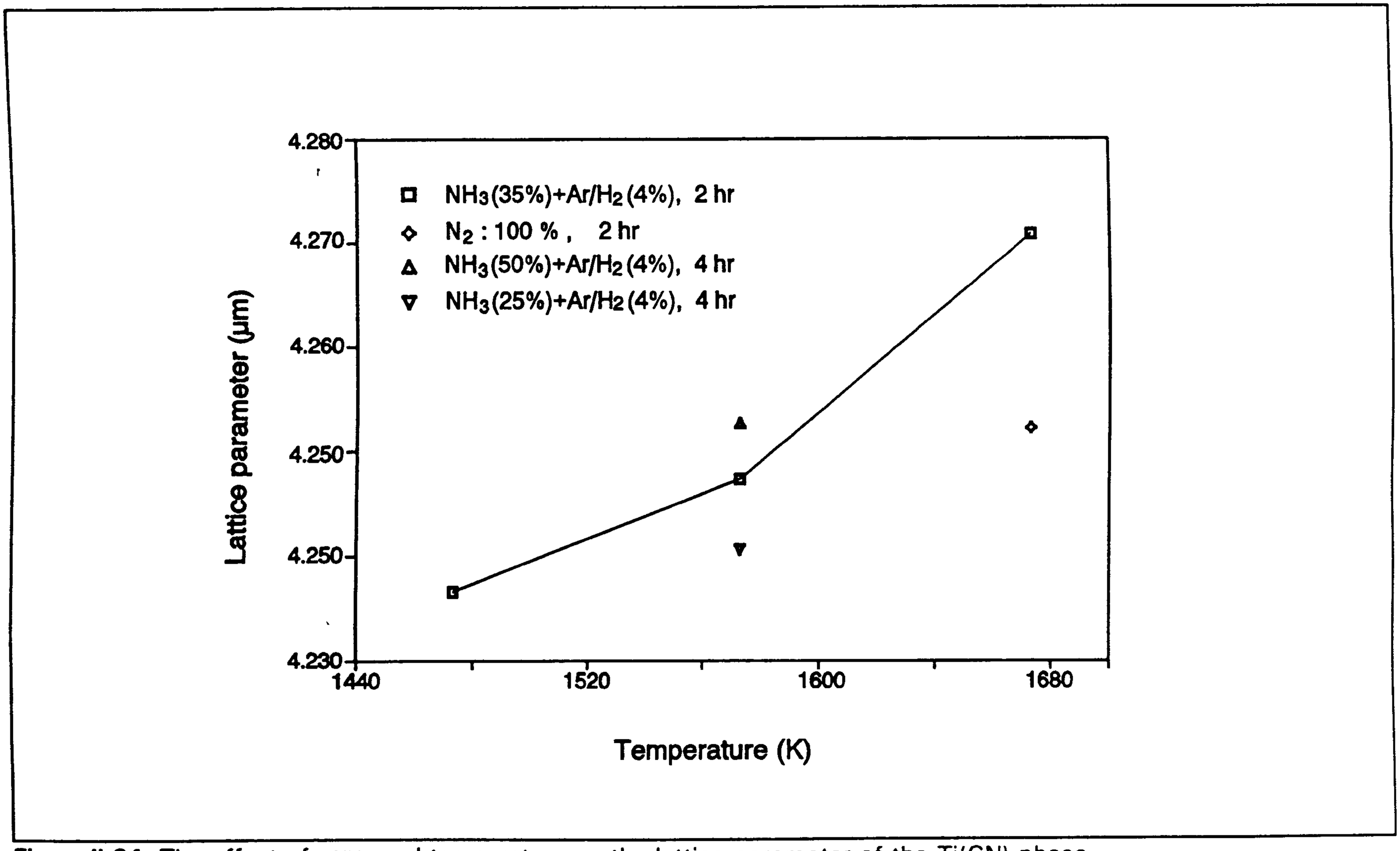

Figure II-24. The effect of pNH_3 and temperature on the lattice parameter of the Ti(CN) phase.

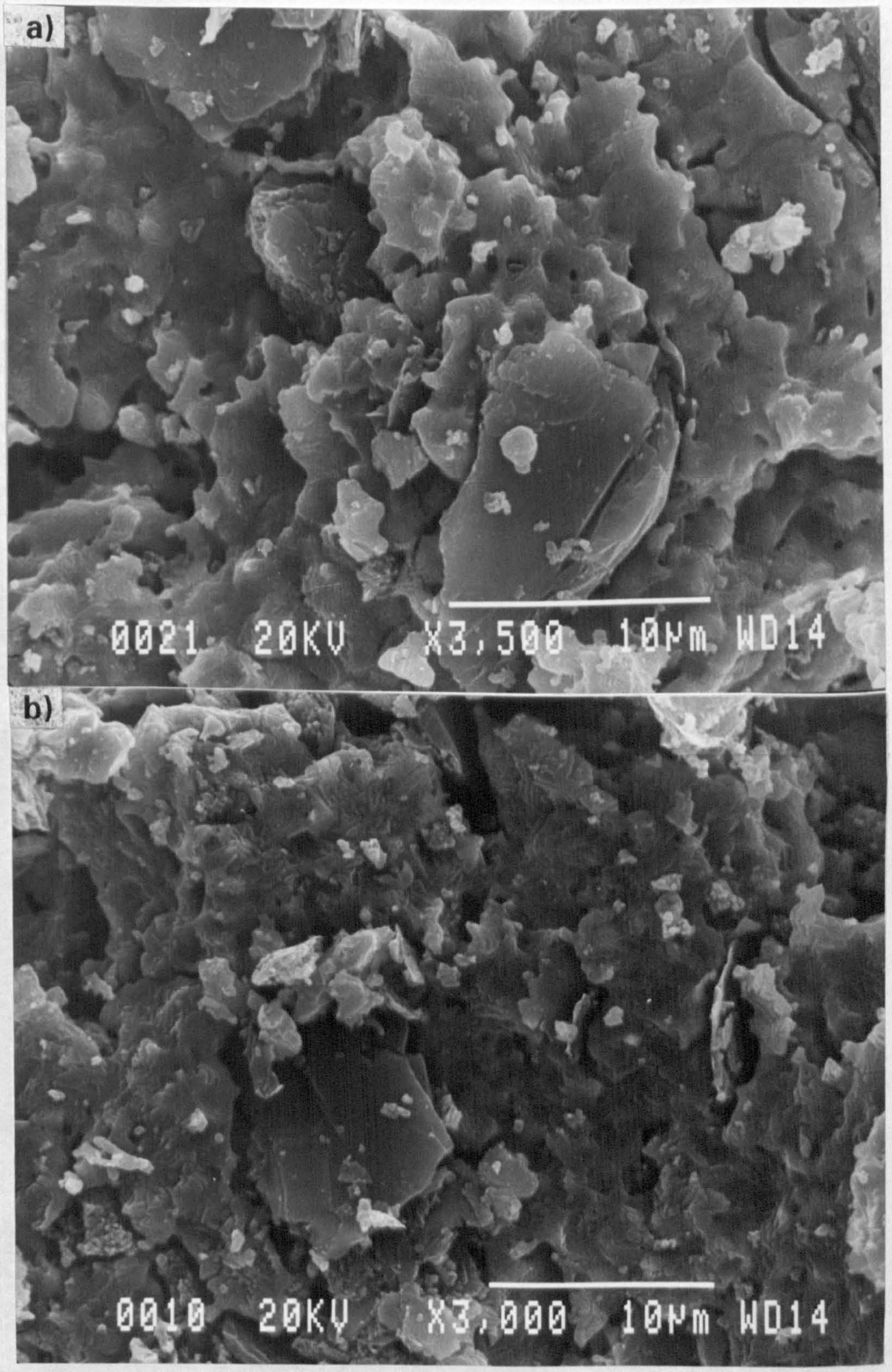

Photo. II-1. Scanning electron micrograph of the reaction product with graphite after different time intervals: (a) 10min, (b) 1hour, (c) 8hours and (d) 24hours. (T = 1673K, starting material: $TiO_2 + 3C$)

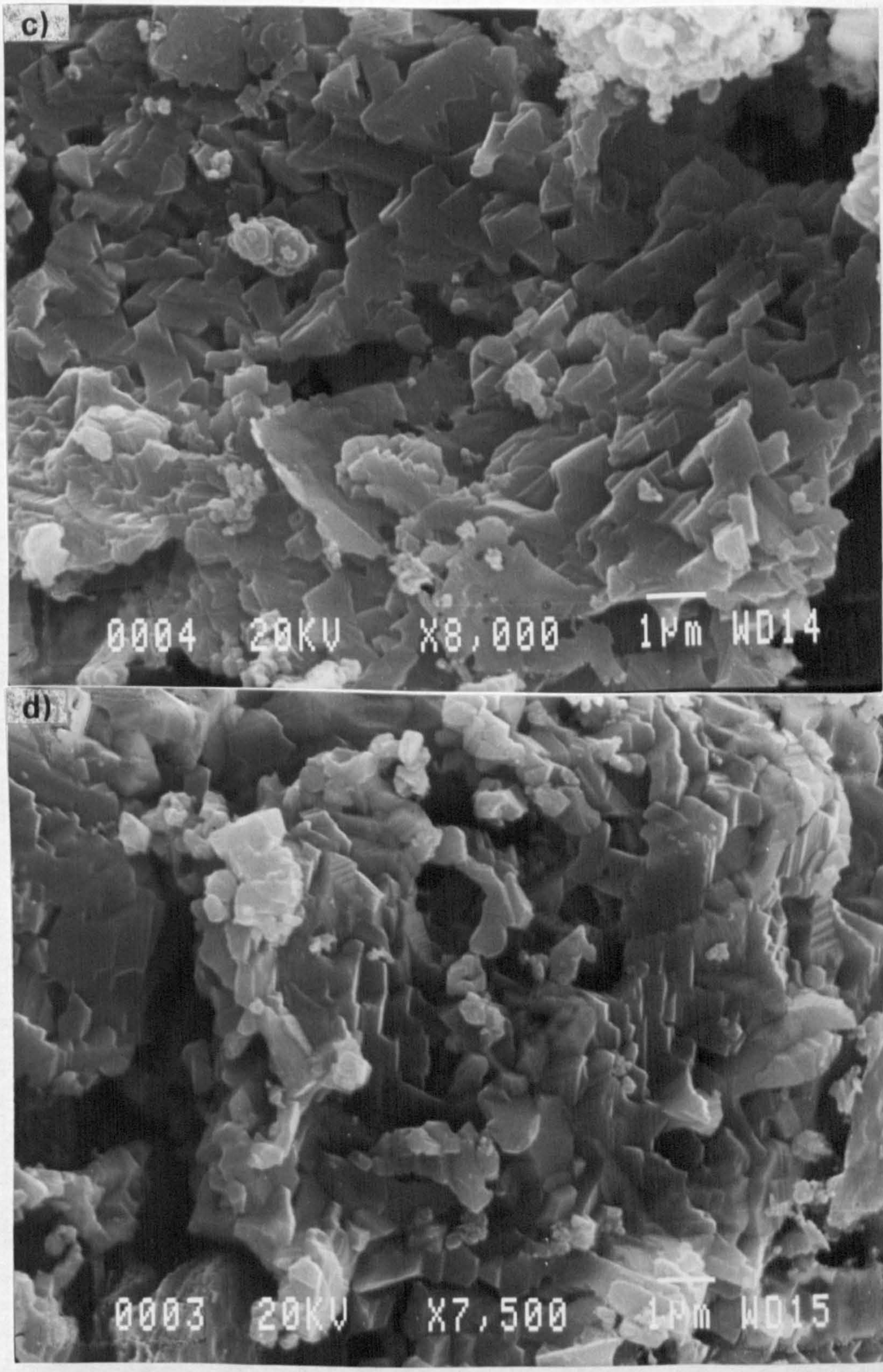

Photo. II-1. (continued from the previous page)

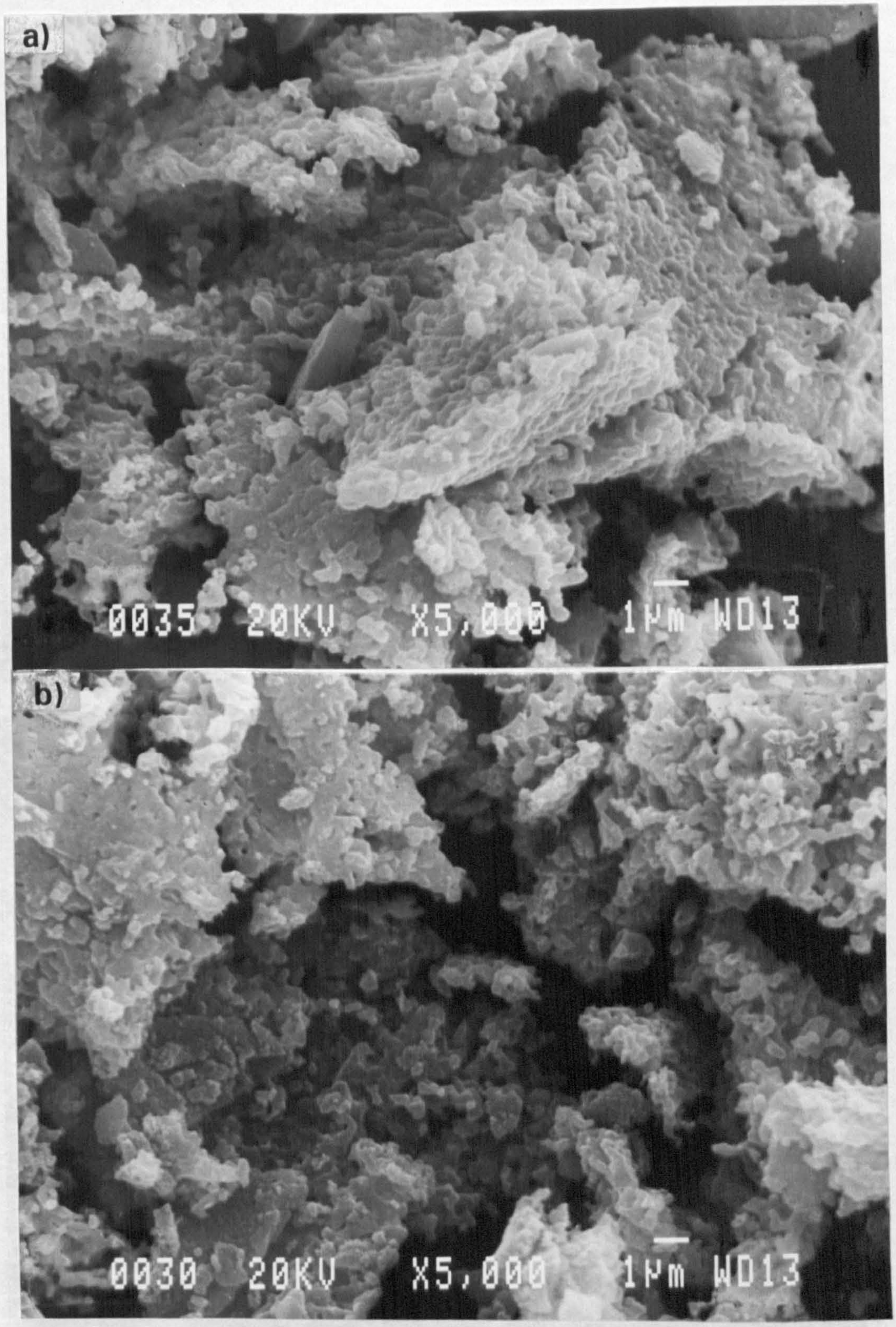

Photo. II-2. Scanning electron micrograph of the reaction product with active carbon after different time intervals: (a) 10min, (b) 1hr, (c) 8hrs and (d) 24hours. (T = 1673K, starting material: $TiO_2 + 3C$)

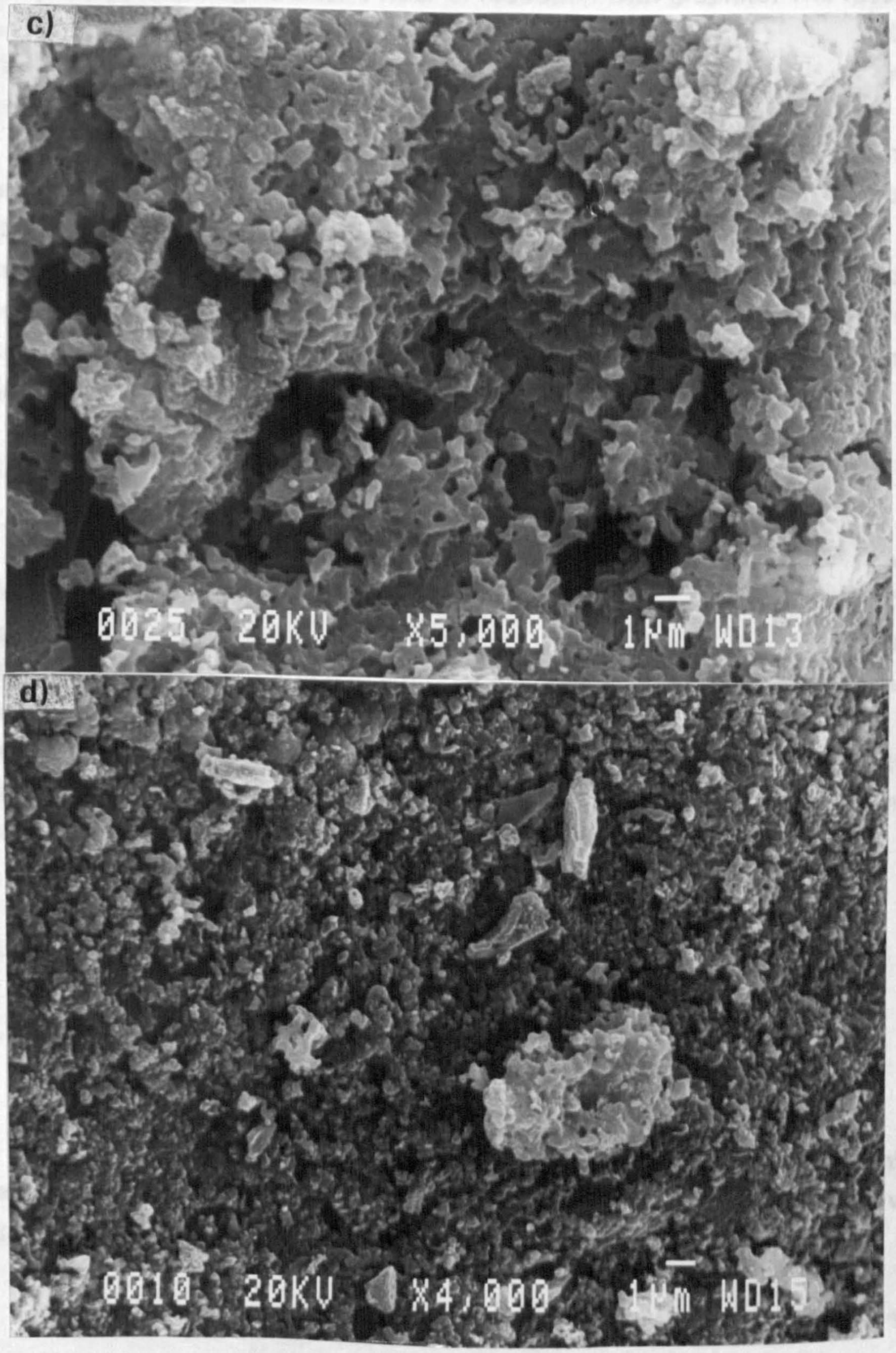

Photo. II-2. (continued from the previous page)

morphology that begins after 1 hour of reduction with graphite. The facetted phase was not observed while the reduction was carried out by active carbon. The carbonitride particle size appears to be in the range 100 nm to 500 nm at 1473K.

With graphite, as the temperature rises, the microstructure changes from partially sintered oxide to facetted structure, which appears to be structurally-coherent with the oxide and finally to completely dispersed fine carbonitride structure.(see **Photo II-3**) A similar feature is observed with active carbon except the microstructure is much finer at any temperature even in the initial sintered stage. Active carbon flakes appears to provide extensively large reduction sites.(see **Photo II-4**)

5.6.2 The effect of reactivity of carbon

The grain morphology shown in Photo.II-2 of $Ti(C_xN_{1-x})$ is related with the reactivity of carbon. The active carbon yielded submicrometer size of the carbonitride phases at all temperatures. There is only a slight indication of sintering between the particles. While with graphite (Photo.II-1), a significantly large amount of sintering and grain growth appears to have taken place. The crystals have a facetted surface that are full of ledges as shown in Photo II-1(c,d). Limited growth can occur easily by the condensation of atoms from the vapour phase or by surface diffusion.

6. DISCUSSION

6.1 Free Energy Change for the Formation of Titanium Carbonitride, Oxycarbide and Oxynitride

Ouensanga[80] measured the free energy of formation (ΔG_f°) of titanium oxycarbide phase at 1580K. In this investigation the following reaction was considered.

$$TiC_xO_{1-x} + 2(1-x)C = TiC + (1-x)CO \qquad \textbf{(2-19)}$$

which at a constant temperature and CO partial pressure yields a unique composition of the oxycarbide phase. We have also compared the measured

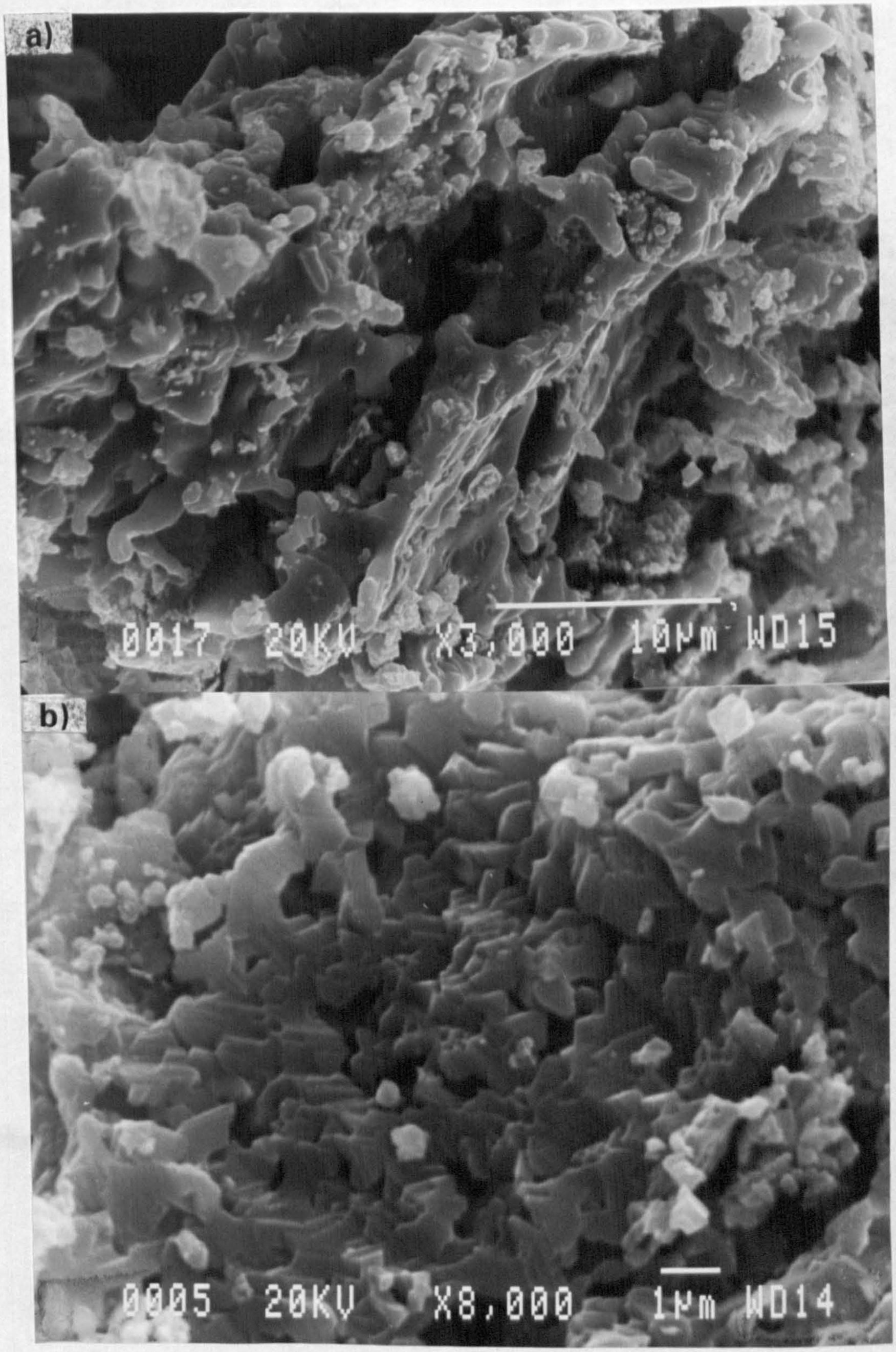

Photo. II-3. Scanning electron micrograph of the reaction product with graphite at different reaction temperature : (a) 1573K, (b) 1673K and (c) 1773K after 8 hours reaction. (starting material:$TiO_2 + 3C$)

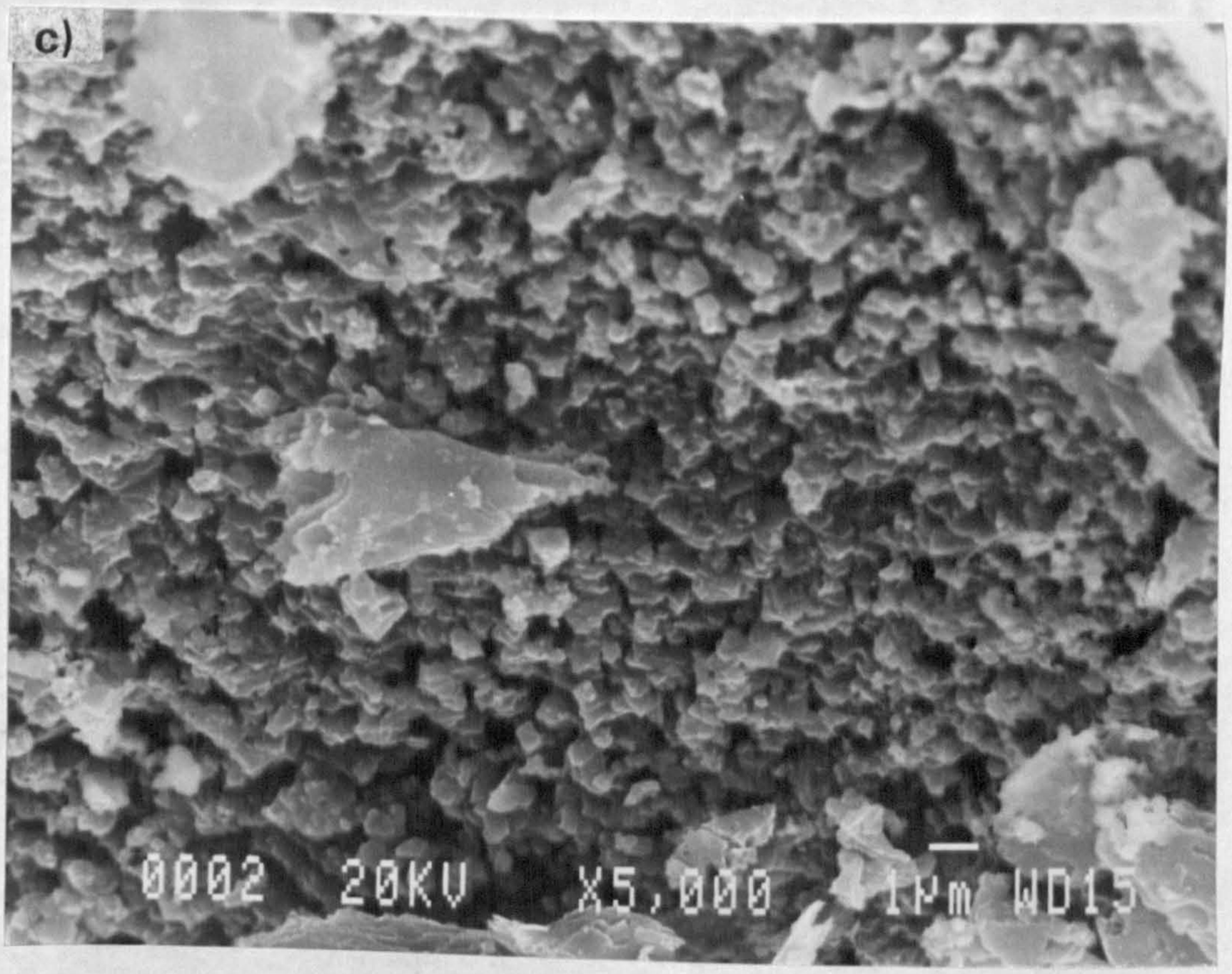

Photo. II-3. (continued from the previous page)

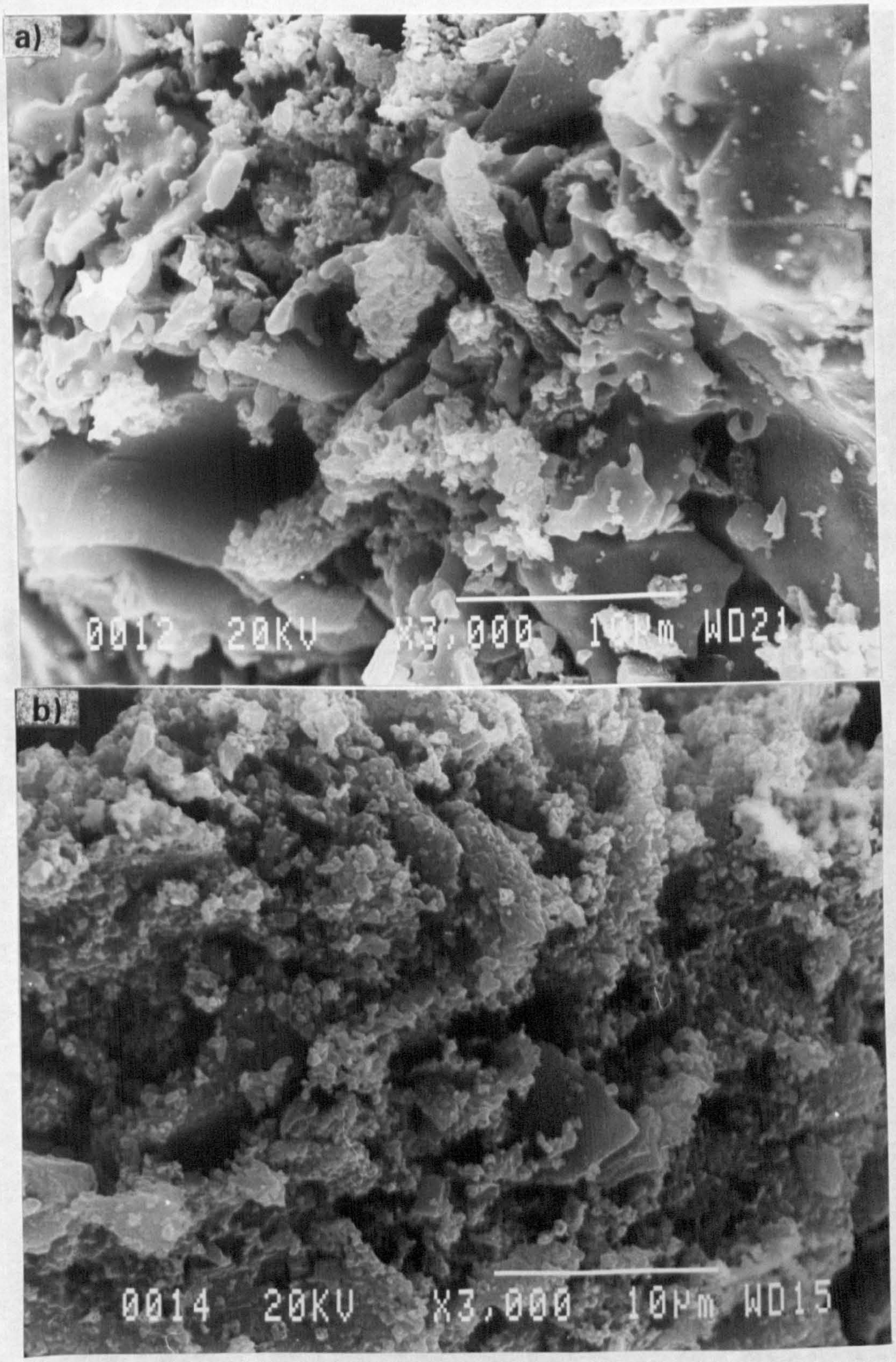

Photo. II-4. Scanning electron micrograph of the reaction product with active carbon at different reaction temperatures: (a)1473K, (b)1573K, (c)1673k and (d)1773K after 8 hours.(starting material: $TiO_2 + 3C$)

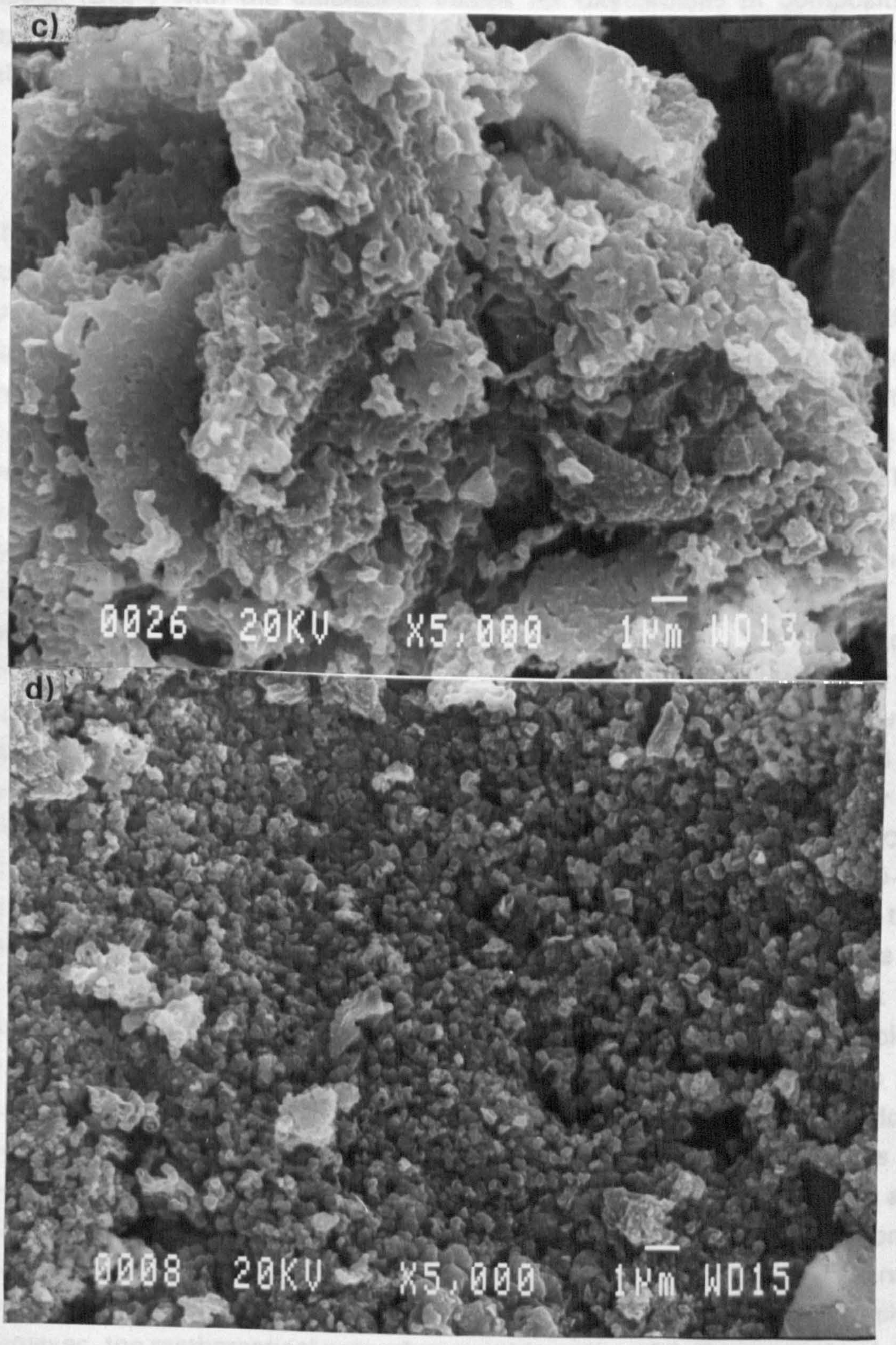

Photo. II-4. (continued from the previous page)

results ($\Delta G_f°$) with the calculated values for oxycarbides of composition reported by Ouensanga. The calculated values are obtained from the following relationship :

$$\Delta G_{TiC_xO_y} = X_{TiC} \cdot \Delta G_{TiC} + X_{TiO} \cdot \Delta G_{TiO} \qquad \textbf{(2-20)}$$

At T = 1580K, using the thermodynamic data from the compilation of Turkdogan[77], the values of ΔG_{TiC} and ΔG_{TiO} are -164.933 and -397.622 $kJ \cdot mol^{-1}$, respectively. The calculated and measured values are compared in **Table II-15** below. Note that the calculated value has an additional term of free energy which is added with $\Delta G_{TiC_xO_y}$. This arises due to the contribution of the configurational entropy of mixing i.e $\Delta G_{mix} = RT\{X_{TiC} \cdot \ln X_{TiC} + X_{TiO} \cdot \ln X_{TiO}\}$ in the idealised interstitial mixture of oxygen and carbon in B_1 structure (i.e TiC or ß-TiO defect lattice structure). The calculated configurational free energy appears to be systematically smaller than the empirically determined free energy due to the configurational entropy term. The higher value of configurational entropy term indicates two possibilities: oxygen and carbon are not only randomly distributed on the interstitial sites but also there might be a possibility of O-C interaction, lead to a small third term in the free energy equation. The second possibility may be due to the presence of vacancies as the third species. The free energy of vacancies will then modify either to $RT\{X_{TiC} \cdot \ln X_{TiC} + X_{TiO} \cdot \ln X_{TiO} + X_V \cdot \ln X_V\}$ or to $RT\{X_{TiC} \cdot \ln X_{TiC} + X_{TiO} \cdot \ln X_{TiO} + X_{OC} \cdot \ln X_{OC}\}$ where 'O-C' indicates the concentration of 'O-C' pair. The difference in the calculated and measured ΔG_{mix} without the contribution of vacancies or O-C pair interaction is considered on the basis of the above mathematical procedure. On the basis of close agreement of between the measured and calculated values of the energy of oxycarbide phase with composition, we have also calculated the free energies of formation of TiC_xN_{1-x} and TiO_xN_{1-x} phases. The procedure based on random mixing approach can also be extended to ternary interstitial compounds of titanium. The calculated values of the free energy of the mixed interstitials are summarised below in **Table II-16**. Note that the method of calculation is only true for those systems where random mixing is predominant. As the tendency for clustering of similar species or pair-wise interaction of dissimilar species increases, the mathematical procedure would not be valid. On the basis of the understanding of the structure of non-stoichiometric titanium carbides and nitrides, it is also possible to propose that the $\Delta G_{Ti_{1-x}C_x}$ can be written as:

$$\Delta G_{Ti_{1-x}C_x} = \Delta G_{TiC} \cdot X_C + X_V \cdot \Delta G_{Ti} + RT\{X_C \cdot \ln X_C + X_V \cdot \ln X_V\} \quad (2\text{-}21)$$

where ΔG_{Ti} is the free energy of formation of titanium.

Table II-15. The calculated and measured values of free energies of formation of TiOC as a function of composition at 1580K.

Composition	Calculated value		Measured value[80]	
	$\Delta G_f°$ ($J \cdot mol^{-1}$)	$\Delta G_{mix}°$ ($J \cdot mol^{-1}$)	$\Delta G_f°$ ($J \cdot mol^{-1}$)	$\Delta G_{mix}°$ ($J \cdot mol^{-1}$)
$TiC_{1.0}$	-164933	0	-164933	0
$TiC_{0.96}O_{0.04}$	-174241	-2206	-176071	- 1954
$TiC_{0.90}O_{0.10}$	-188202	-4271	-192410	- 4489
$TiC_{0.85}O_{0.15}$	-199837	-5553	-205807	- 6422
$TiC_{0.78}O_{0.24}$	-220779	-7239	-229651	- 9598
$TiC_{0.72}O_{0.28}$	-230086	-7789	-240254	-11012
$TiC_{0.70}O_{0.30}$	-234740	-8025	-245534	-11698
$TiC_{0.67}O_{0.33}$	-241721	-8331	-253463	-12736

Table II-16. The calculated values of free energy of the mixed interstitials at 1580K.

Composition		Total free energy ($\Delta G_f° + \Delta G_{mix}°$, $J \cdot mol^{-1}$)	
x	1-x	TiC_xN_{1-x}	TiO_xN_{1-x}
1	0	-164933	-186591
0.8	0.2	-175838	-235371
0.6	0.4	-182438	-279845
0.4	0.6	-186769	-322051
0.2	0.8	-188833	-361990
0	1	-186591	-397622

6.2 The Activation Energy for the Reduction of TiO_2

The presence of Ti_3O_5 during the reduction of TiO_2 indicated that the

non-stoichiometric Ti_3O_5 phase is the most stable intermediate oxide. In the majority of the experiments, neither TiO nor Ti_2O_3 appears to be in equilibrium with either Ti_xN_{1-x} or $Ti(C_xN_{1-x})$. However the rate of reduction of TiO_2 appears to be dependent on the reactivity of carbon. At the initial stage, it is the direct reduction of TiO_2 by carbon which prevails and it is feasible that CO forms as a result of direct reduction but mechanistically direct reduction cannot be sustained after the physical contact between the carbon and titanium oxide is lost. Subsequent reduction can only progress when CO generation occurs via the Boudouard reaction. During the direct reduction, an active carbon surface plays a significant role in promoting the reaction. Graphite, being very inactive, takes a relatively long time to initiate the oxidation of carbon as can be seen from the rate of reduction curves in Figure II-13 in section 5.1. In **Figure II-25**, the values of slopes from the %R vs time curves shown in Figure II-13 and II-14 are plotted for the derivation of activation energy. Calculation of the activation energy is based on the initial sharp increase in the weight loss from the pellets. This is also compared with the self-diffusivity of oxygen in rutile (TiO_2) phase and derived values of the overall activation energy for the formation of TiN phase reported by White et al[76] and Li and co-workers[21]. The comparison of the slopes of the straight lines point out that the temperature coefficient of the rates of reduction is almost identical within the limits of experimental error therefore suggesting that the nucleation of CO, as expected from the Boudouard reaction, is not the rate controlling step. We also find from the Arrhenian plot that the intercept for active carbon is higher than for graphite which means that the number of reaction sites is expectedly larger in active carbon than with graphite. The activation energy for graphite and active carbon are 115 $kJ \cdot mol^{-1}$ and 125 $kJ \cdot mol^{-1}$, respectively. The overall activation energy for the reduction process is approximately 120 ± 5 $kJ \cdot mol^{-1}$ of TiO_2.

The activation energy for the diffusion of oxygen in the rutile lattice was calculated in order to compare it with the measured value. For this the defect structure model proposed in reference [81] was considered. The most common behaviour for many oxide materials, such as titanium oxide is as intrinsic non-stoichiometric semiconductors at equilibrium with an oxidizing or reducing atmosphere. Diffusion through vacant sites in non-stoichiometric oxides is usually classed as metal-deficient or oxygen-deficient. Titanium oxide (TiO_2) is considered as an oxygen-deficient oxide. For oxide structures with anion vacancies, the following reactions can be considered[81]:

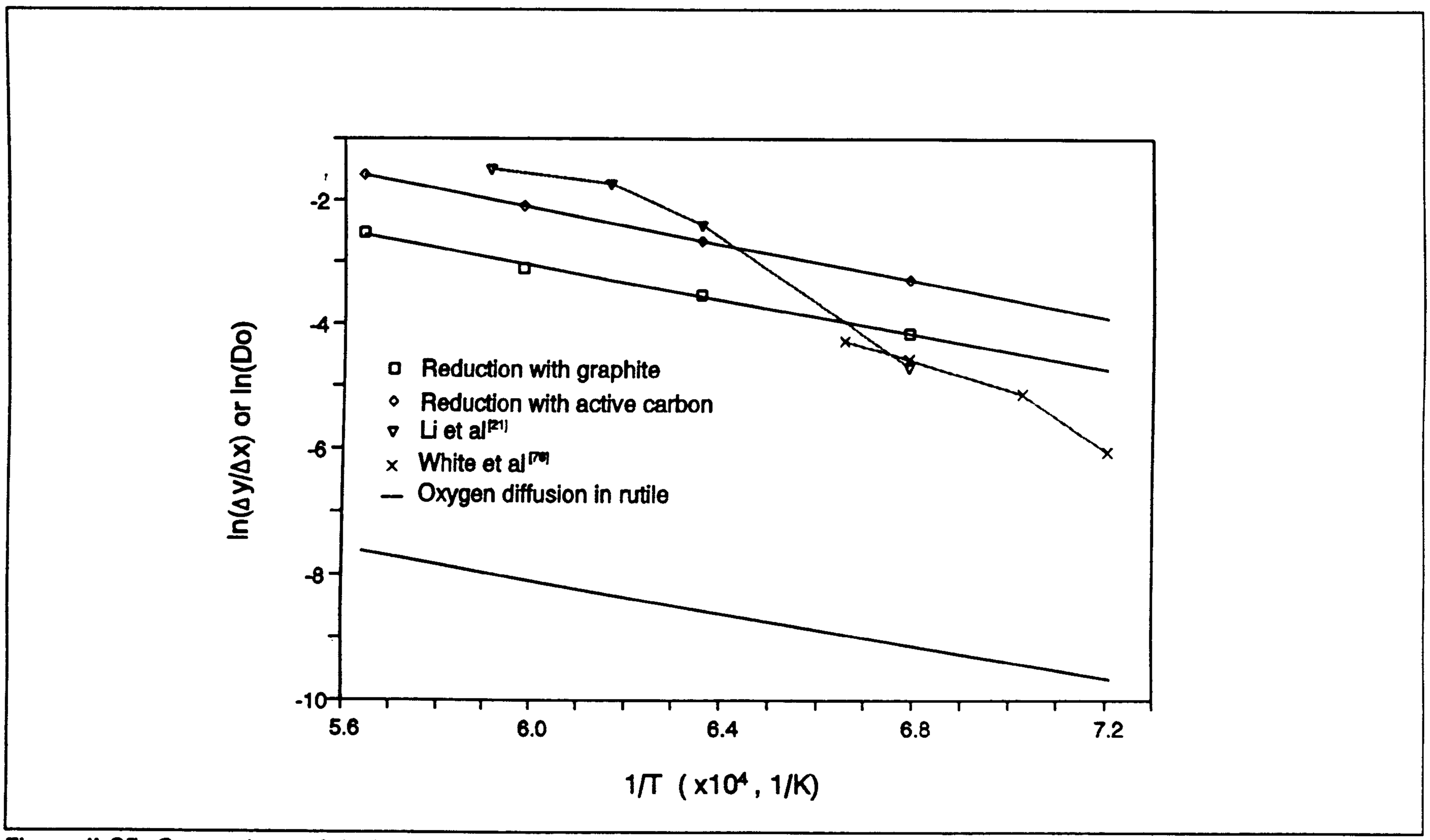

Figure II-25. Comparison of Arrhenius plots for the reduction of TiO_2 to TiC_xN_{1-x}, self diffusivity of oxygen (D_o) in rutile and derived values[21,76] of activation energy.

$$O_o = 1/2O_2(g) + Vö + 2e' \quad (2\text{-}22)$$

$$[Vö] \approx (1/4)^{1/3} \cdot Po_2^{-1/6} \cdot \exp[-\frac{\Delta G°}{3kT}] \quad (2\text{-}23)$$

Thus the oxygen diffusion coefficient is :

$$D_o = \gamma \nu \lambda^2 [Vö] \exp[-\frac{\Delta G°}{3kT}] \quad (2\text{-}24)$$

$$= \gamma \nu \lambda^2 (1/4)^{1/3} Po_2^{-1/6} \exp[-\frac{\Delta G_o}{3kT}] \exp[-\frac{\Delta G^+}{kT}] \quad (2\text{-}25)$$

where Vö : fraction of the vacant oxygen sites

ΔG_o: free energy of solution

ΔG^+: activation energy

D_o : oxygen diffusion coefficient ($cm^2 \cdot sec^{-1}$),

γ : geometric factor (0.1)

ν : frequency factor (10^{13} sec^{-1})

λ : jump distance (3.248×10^{-10} m)

N : Avogadro's number (6.02×10^{23} atoms$\cdot$mole^{-1})

k : Boltzmann's constant (1.38×10^{-22} J$\cdot$K^{-1})

The activation energy for the diffusion of oxygen in the rutile lattice is approximately 110 kJ and compares favourably with the derived value of the thermal barrier for the reduction process. The thermal barrier encountered therefore could be attributed to the process of excess defect sites available in the Ti_3O_5 structure which is oxygen-deficient, the deficiency being the function of the oxygen partial pressure. The migration of oxygen ions in the oxide lattice at an isotherm under a fixed oxygen potential takes place and is strongly dependent upon the value of CO/CO_2 ratio (=oxygen potential) maintained or prevailing during the reduction process. It is for this reason we find that the slopes of Arrhenius lines for graphite and active carbon are virtually similar because the overall redox potential with coal and graphite does not seem to change the oxygen diffusion process significantly in the sub-oxide lattice. This is definitely true if we consider only the initial stage of the reduction curves in Figures II-13 and 14. We also point out that TiO_2 and Ti_3O_5 crystal structures are rather similar. The latter is a monoclinic distortion of the tetragonal lattice. From the structural point of view, the activation energy for

oxygen diffusion in two crystals should therefore appear to be virtually similar.

6.3 The Reduction Sequence of Titanium Oxide with Carbon in the Nitrogen Atmosphere

The reduction sequence of titanium oxide with carbon in the nitrogen gas atmosphere was described in **Tables II-9** and **II-10** which were TiO_2, $Ti_{10}O_{19}$, Ti_9O_{17}, Ti_8O_{15}, Ti_7O_{13}, Ti_6O_{11}, Ti_5O_9, Ti_4O_7 and Ti_3O_5. The last sub-oxide that reduces to form $Ti(CN)_x$ is Ti_3O_5. This observation is consistent with the results of White et al[74] although they claimed that the existence of Ti_3O_5 is not possible from the phase diagram nor do the thermodynamic calculations support their view. Below we prove that the stability of the Ti_3O_5 phase by both methods, and confirmed the observations of all Ti_nO_{2n-1} phases as shown in section 5.1. Although some workers[5,6,20] support the concept of progressive reduction to lower sub-oxide, they failed to observe Ti_2O_3 and TiO as intermediates by the carbothermic reduction in their experiments. In these experiments, the lower sub-oxide, Ti_2O_3 and TiO were not detected by X-ray powder diffraction method. **Figure II-26** shows the $\log p_{CO}$ vs 1/T for titanium oxide, nitride and carbide phases. The number in the diagram designates the corresponding reaction in **Table II-17**. From the calculated equilibrium temperatures and partial pressure of CO in the table, it can be established that the Ti_2O_3 and TiO phases are unlikely to form (cf.reactions (7-9)). This is due to the higher prevailing equilibrium partial pressure of CO (p_{CO}), for example at 1573K (cf. p_{CO} for $TiO_2/Ti_4O_7/Ti_3O_5$ equilibrium) in the reaction chamber as a consequence of Ti_3O_5 and TiN formation reactions. Indeed, for the formation of Ti_2O_3 and TiO, the value of p_{CO} must be lower than equilibrium partial pressure of CO, ie 4.78×10^{-1} and 2.10×10^{-2} atm, respectively. By comparing the equilibrium partial pressure of CO, we can deduce whether a specific sub-lattice phase is likely to be stable. It is for this reason that the Ti_2O_3 phase was found to be stable and in equilibrium with the oxycarbide in the investigating carried out by Terry et al[3] and Coley et al.[27] Additionally the presence of Fe-Ti-C alloy ensured the lower equilibrium partial pressure of oxygen than reported in Table II-17 for the stability of TiO and Ti_2O_3 phases.

ß-TiO has a lattice parameter in the range (0.4168-0.4201 nm) and up to 40% substitution of nitrogen in TiN by oxygen can occur without change in the lattice parameter.[29] White et al[74] discussed that in the presence of

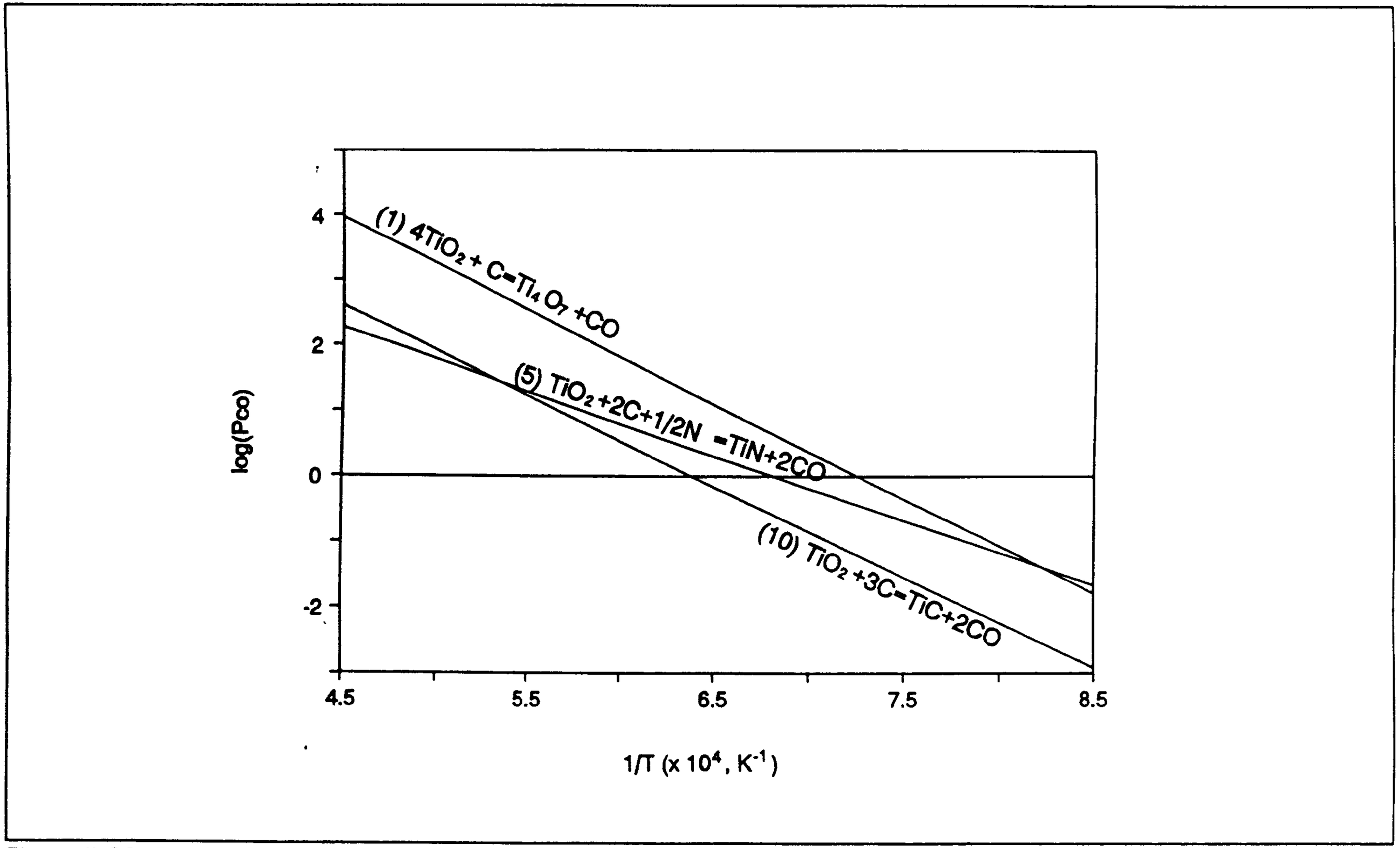

Figure II-26. Relationship between $logp_{CO}$ and 1/T for titanium nitride, carbide and oxide phases.

Table II-17. The reduction steps for titanium oxide to sub-oxides, nitride and carbide, and their equilibrium temperatures and equilibrium p_{CO} values at 1573K.

Reaction	$T_{eq.}$(K)	p_{CO}(at 1573K,atm)
(1) $4TiO_2 + C = Ti_4O_7 + CO$	1378	1.96×10^{1}
(2) $3Ti_4O_7 + C = 4Ti_3O_5 + CO$	1448	6.18×10^{0}
(3) $2Ti_3O_5 + C = 3Ti_2O_3 + CO$	1636	4.78×10^{-1}
(4) $Ti_2O_3 + C = 2TiO + CO$	1831	2.10×10^{-2}
(5) $TiO_2 + 2C + 1/2N_2 = TiN + 2CO$	1469	2.76×10^{0}
(6) $Ti_4O_7 + 7C + 2N_2 = 4TiN + 7CO$	1448	2.19×10^{0}
(7) $Ti_3O_5 + 5C + 3/2N_2 = 3TiN + 5CO$	1500	1.89×10^{0}
(8) $Ti_2O_3 + 3C + 2N_2 = 2TiN + 3CO$	1479	2.21×10^{0}
(9) $TiO + C + 1/2N_2 = TiN + CO$	960	2.26×10^{1}
(10) $TiO_2 + 3C = TiC + 2CO$	1567	1.08×10^{0}
(11) $Ti_4O_7 + 11C = 4TiC + 7CO$	1606	6.61×10^{-1}
(12) $Ti_3O_5 + 8C = 3TiC + 5CO$	1612	6.13×10^{-1}
(13) $Ti_2O_3 + 5C = 2TiC + 3CO$	1610	6.30×10^{-1}
(14) $TiO + 2C = TiC + CO$	1463	3.45×10^{0}

nitrogen, TiO should form TiN either by direct substitution of nitrogen for oxygen or via an intermediate oxynitride. From the reasons of phase stability described above, Ti_2O_3 and TiO phases are unlikely to participate in the reduction process. The oxynitride phase therefore can directly form from Ti_3O_5 phase. A similar reason could also be applied to other possible either oxygen-rich or oxygen-deficient ternary titanium based interstitials. The stability of the oxynitride phase can be considered by writing the following reaction:

$$Ti_3O_5 + 4.4C + 1.2N_2 = 3TiO_{0.2}N_{0.8} + 4.4CO \qquad (2\text{-}26)$$

The free energy of oxynitride can be calculated as follows:

$$\Delta G_{TiO_{0.2}N_{0.8}} = 0.2 \cdot \Delta G_{TiO} + 0.8 \cdot \Delta G_{TiN} + RT\{0.2 \cdot \ln 0.2 + 0.8 \cdot \ln 0.8\} \qquad (2\text{-}27)$$

At T = 1573K, the free energy of $TiO_{0.2}N_{0.8}$ formation is -31.8 kJ. The free

energy change of equation (2-26) and equations (8),(9) in the Table II-7 at 1573K are 642.5kJ, -10.3kJ and -40.8kJ, respectively, which proves that the TiO phase is not an intermediate phase.

6.4 Lattice Parameter Change During Reaction

Above we have reported in Figure II-20 to II-24 that the lattice parameter of titanium carbonitride (TiC_xN_y) changed with the reduction condition. Licko et al[6] reported that with increases in reaction temperature, the concentration of carbon in Ti(CN) solid solution also increased. Our results, however, showed that the lattice parameter of TiC_xN_y changed at each reaction stage. **Figure II-27** shows a schematic diagram for the diffusion of carbon and oxygen across the intermediate phase. The diagrammatic illustration is based on the observed variation of lattice parameter with time during the reduction process. Detailed analysis of the composition dependence of the lattice parameter of the carbonitride phase indicated that at a smaller degree of reduction (%R), the carbo-nitride phase was saturated with carbon.

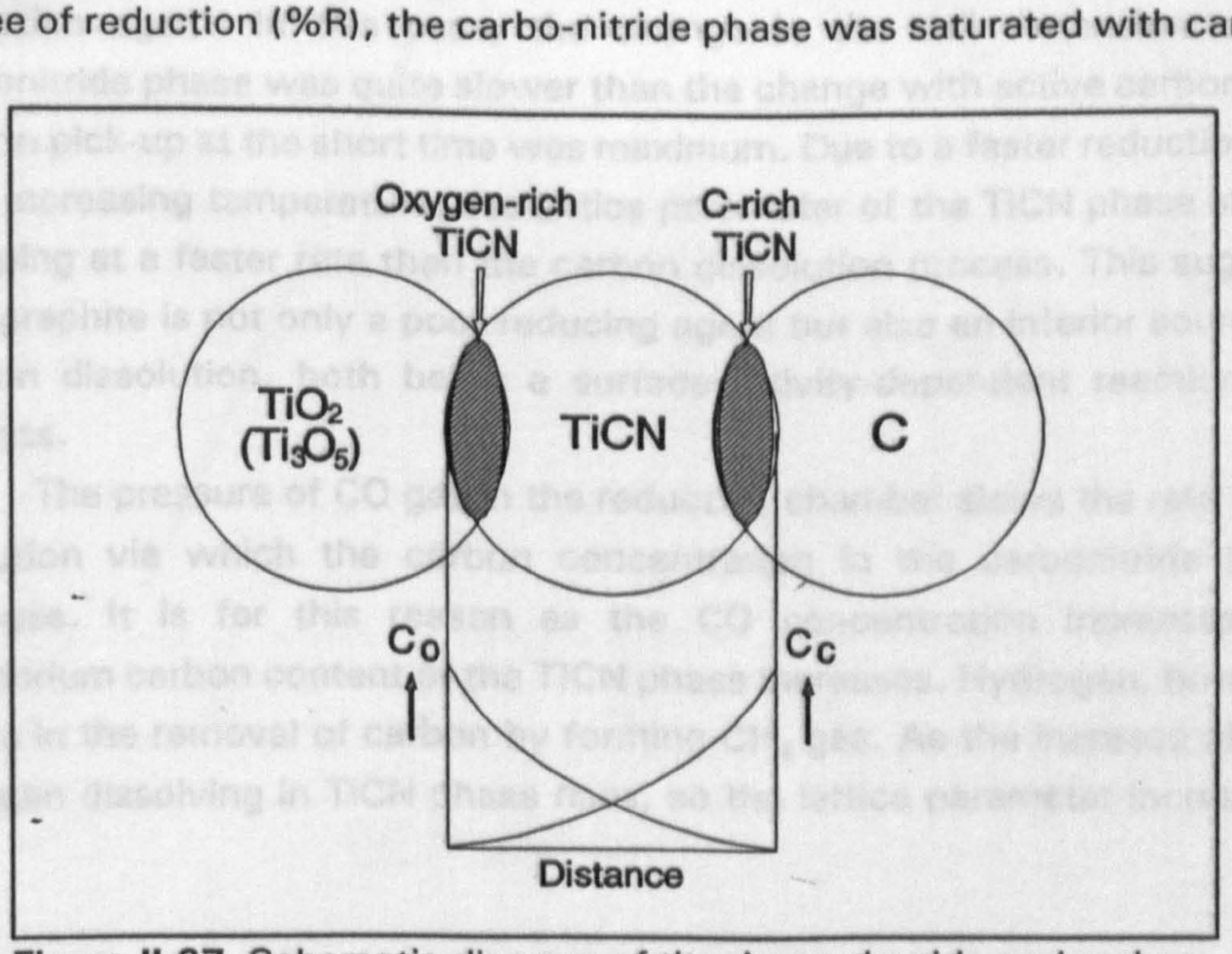

Figure II-27. Schematic diagram of titanium suboxide and carbon.

This indicated that as the rate of reduction slowed down, the excess carbon was rejected from the carbo-nitride lattice. The rate of reduction with graphite,

as shown above, is much slower than the activated charcoal. The particle size of carbon, its reactivity and gas composition, therefore, are the most important variables that determine the percentage conversion of oxides to carbonitride and initial carbon pick up by the carbonitride phase. The carbon-saturated TiCN acts as a reducing agent or as a medium for carbon transport for the continuation of the reduction reaction. This is the reason that after initial sharp rise in the lattice parameter, the lattice parameter of the carbonitride phase decreased (see Figure II-20). Once the equilibrium carbon composition in the carbonitride phase in contact with Ti_3O_5 had been reached, the carbon content was insufficient to sustain the further reduction. This meant that for the sustenance of the reduction process, carbon diffusion must take place. This was possible because of the presence of unreacted active carbon. The change in the lattice parameter of TiCN phase produced from active carbon also varies with temperature. The variation in the cell dimension with time in the temperature range 1473K to 1673K follows the pattern of the reduction reaction shown in Figure II-14 (cf.Figure II-20)

The mechanism of carbon diffusion also holds good for graphite as a reduction agent. In this case, the change in the cell dimension of the carbonitride phase was quite slower than the change with active carbon. The carbon pick-up at the short time was maximum. Due to a faster reduction rate with increasing temperature, the lattice parameter of the TiCN phase started dropping at a faster rate than the carbon dissolution process. This suggests that graphite is not only a poor reducing agent but also an inferior source for carbon dissolution, both being a surface-activity-dependent reaction rate process.

The pressure of CO gas in the reduction chamber slows the rate of CO evolution via which the carbon concentration in the carbonitride lattice changes. It is for this reason as the CO concentration increases, the equilibrium carbon content of the TICN phase increases. Hydrogen, however, arises in the removal of carbon by forming CH_4 gas. As the increase of NH_3, nitrogen dissolving in TiCN phase rises, so the lattice parameter increases.

6.5 The Computed Phase Equilibria Between TiC and TiN Phases

The liquidus and solidus phase boundaries between the titanium nitride and carbide phase are plotted in **Figure II-28** by using the following equations

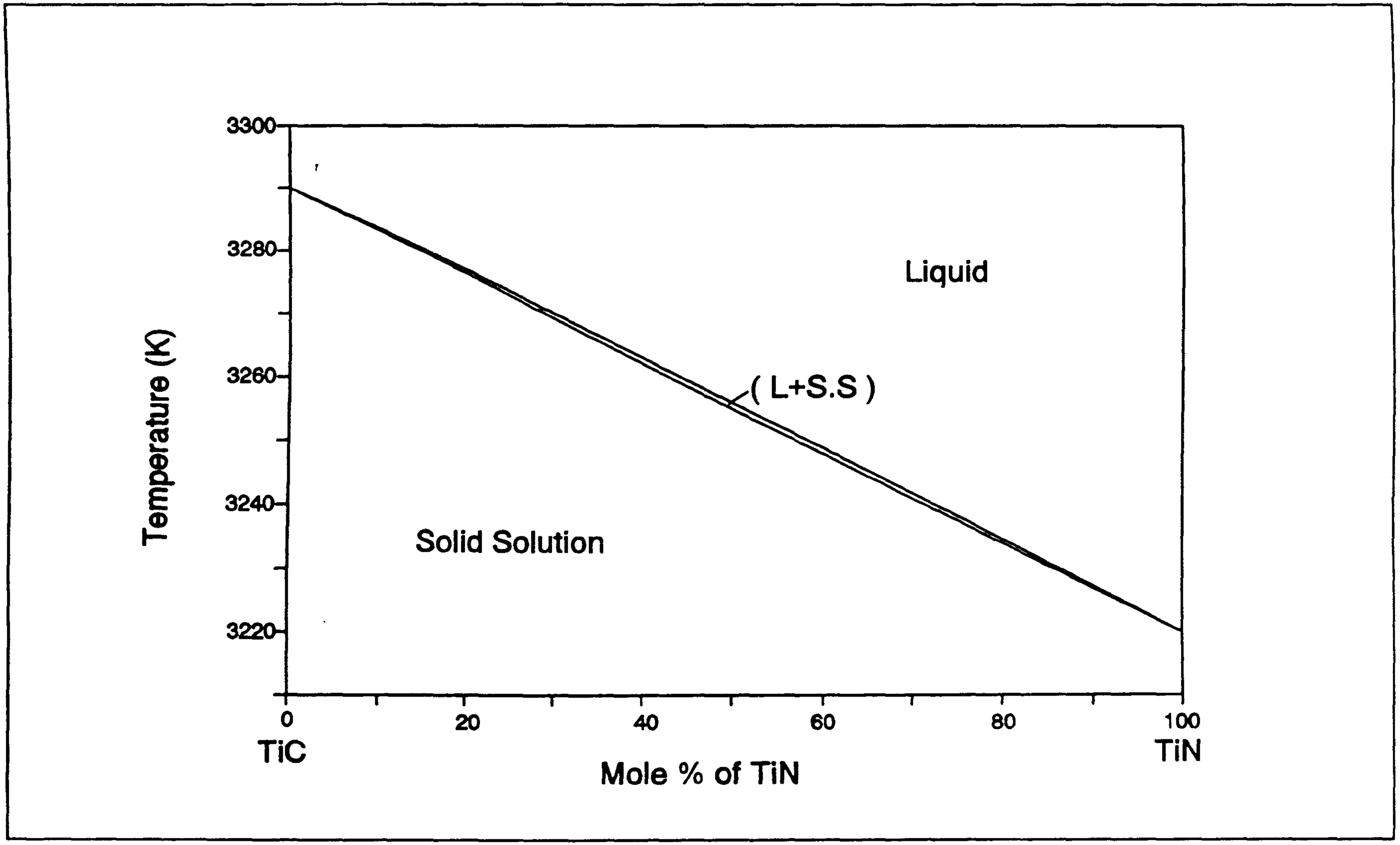

Figure II-28. The calculated liquidus and solidus phase boundaries in TiN-TiC system.

which were derived by considering the equilibrium between the solid and liquid phases at a given temperature[82]. TiC and TiN being identical in chemical nature and having similar crystal structures, their phase mixture is expected to exhibit extended solid and liquid solubility.

For equilibrium between solid and liquid

$$\ln\frac{a_{L,\,TiC}}{a_{S,\,TiC}} = \left(\frac{-\Delta H_{F,\,TiC}}{R}\right)\left(\frac{1}{T} - \frac{1}{T_{F,TiC}}\right) \qquad (2\text{-}28)$$

where $a_{L,TiC}$: the activity of TiC in the liquid

$a_{S,TiC}$: the activity of TiC in the solid, at equilibrium

$\Delta H_{F,TiC}$: enthalpy of fusion for the TiC phase

R : the gas constant

T : an arbitrary temperature (K)

$T_{F,TiC}$: the temperature of fusion of TiC (K).

As the solid solution formed can only occur due to ideal mixing;

$$a_{TiC} = \gamma_{TiC} \cdot X_{TiC}$$

and for an ideal solution, $\gamma = 1$

Therefore, $a_{L,TiC} = X_{L,TiC}$ and $a_{S,TiC} = X_{S,TiC}$

where X is the mole fraction.

Therefore equation (2-28) now becomes;

$$X_{L,TiC} = X_{S,TiC} \cdot \exp\left[\left(\frac{-\Delta H_{F,TiC}}{R}\right)\cdot\left(\frac{1}{T} - \frac{1}{T_{F,TiC}}\right)\right] \qquad (2\text{-}29)$$

$$X_{L,TiN} = X_{s,TiN} \cdot \exp\left[\left(\frac{-\Delta H_{F,TiN}}{R}\right)\left(\frac{1}{T} - \frac{1}{T_{F,TiN}}\right)\right] \qquad (2\text{-}30)$$

as $X_{L,TiC} + X_{S,TiN} = 1$, and $X_{S,TiC} + X_{S,TiN} = 1$

Thus, if

$$A = \exp\left[\left(\frac{-\Delta H_{F,TiC}}{R}\right)\left(\frac{1}{T} - \frac{1}{T_{F,TiC}}\right)\right] \qquad (2\text{-}31)$$

$$B = \exp\left[\left(\frac{-\Delta H_{F,TiN}}{R}\right)\left(\frac{1}{T} - \frac{1}{T_{F,TiN}}\right)\right] \qquad (2\text{-}32)$$

Then

$$X_{S,TiN} = \frac{(A-1)}{(A-B)} \qquad (2\text{-}33)$$

$$X_{L,TiN} = X_{S,TiN} \cdot B \qquad (2\text{-}34)$$

Both TiC and TiN are congruently melting phase with enthalpies of fusion, ΔH_F = 71128 J mole^{-1} and ΔH_F = 66944 J mole^{-1} at 3290K and 3220K[65], respectively. Because of a small difference in the melting point between the two phases, the (liquid + solid) phase field is rather narrow. We find that the complete mutual solid solubility is possible and this was also confirmed from the x-ray powder diffraction analysis (cf.Figure II-19).

6.6 The Effect of Catalyst

In most carbothermic reduction experiments, the formation of CO gas on the carbon surface is known to be a major barrier to chemical reaction. For this reason reactions were catalysed with $FeCl_3$. Chrysanthou et al[83] explained the effect of a catalyst as follows. The rate of carbothermic reduction of oxides is determined by the rate of CO gas evolution via the Boudouard reaction. The reaction of carbon with CO_2 also relies on the catalytic mechanism. The donation of electrons to a carbon ring in the graphitic structure during catalytic oxidation is the most accepted theory.[84] Here transition and alkali metals (in this case Fe) donate one of their outermost electrons to the carbon-carbon bond in the ring. The electronic exchange is also believed to occur when their compounds such as chlorides and carbonates are used as catalysts. The charge transfer rises the potential energy of the ring structure, and if oxygen is present, a lower energy state is acquired by the adsorption of an oxygen atom, thus forming a (CO)· bond which is much weaker than the C-C bond. This is believed to be the most important step in the oxidation of carbon. On addition of $FeCl_3$ during the reduction of TiO_2 in the reactions considered, the iron chloride decomposes to Fe and chlorine gas. This takes place above 1073K. Alternatively the hydrated $FeCl_3 \cdot 6H_2O$ oxidises to form hematite (Fe_2O_3) and HCl gas. Fe_2O_3 then reduces to metallic iron which acts as a catalyst. The metallic iron produced is then involved in the following catalytic reaction :

$$C + e^- = C^- \quad \textbf{(2-35)}$$

$$C^- + [O]_{ad} = (CO)^- = (CO) + e^- \quad \textbf{(2-36)}$$

Here, *'ad'* designates the adsorbed oxygen.

In the case of transition metals, such as Fe, the following transition occurs:

$Fe^{2+} \rightarrow Fe^{3+}$ (a 3d to 4s transition.)

In the case of alkali metals, the metals acquire a 1^+ valance state after donating their outermost electron.

The above mechanism of catalysis also underlines the principle of catalytic oxidation based on the molecular adsorption of oxygen on the carbon surface because the adsorption of a gas on a solid substrate is a physico-chemical phenomenon which also depends upon the exchange of electronic charge between the substrate and the adsorbent. Graphite has fewer potential sites for oxygen adsorption than activated charcoal (activated charcoal has a much higher surface area and therefore more unsaturated carbon-carbon bonds). This is also evident from the analysis of catalysis of activation energy for the reduction reaction. The addition of $FeCl_3$ to the samples containing graphite was essential for the reduction reaction. A further increase in the number of active sites available in the samples containing activated charcoal is also likely when a small amount of $FeCl_3 \cdot 6H_2O$ is added.

6.7 Microstructure

The microstructure of the carbonitride phase produced from two different types of reducing agents differs significantly in the final stage. The microstructure of the carbonitride obtained from the reduction of oxides with the activated charcoal has a much finer structure that appears to develop from a partially facetted matrix. In the case of graphite as a reducing agent, the end product is sintered and heavily facetted. It is also evident from the microstructural examination that there is no interface between the sub-oxides and the carbonitride phase. This, in the first instance, appears to be rather surprising, but close examination of X-ray diffraction results suggest that the microstructure of the oxide phase progressively transforms from TiO_2 to Ti_3O_6 and evidently to TiCN.

The lack of phase boundary perhaps arises due to a small difference in the surface energy of the two sub-oxides and the carbonitride phase. This is further evident from the difference in the free energy of the non-stoichiometric oxides and TiCN phase. In the final stage of the reduction/nitridation with activated charcoal, when the carbonitride phase becomes saturated with carbon, the phase boundaries and surfaces become more distinct. This is perhaps the reason for the evolution of a finer microstructure with activated charcoal. Tentatively we propose that the evidence for facetting and sintering is due to the presence of higher concentration of surface oxygen in the sub-oxide/carbonitride interface. At the end of the reaction, the oxygen concentration drops significantly and hence the agglomeration tendency drops dramatically.

7. CONCLUSIONS

Titanium nitride powder was produced in the powder form by the carbothermic reduction process. The synthesised titanium nitride by carbothermic reaction was identified as a $Ti(C_xN_{1-x})$ having a range of composition. The rate of reduction of TiO_2 appears to be determined by the rate of oxygen diffusion in the sub-oxide lattice and the derived value of activation energy from the Arrhenius plot is 120 $kJ \cdot mole^{-1}$ of TiO_2. Ti_3O_5 was found as a precursor for the formation of titanium nitride. The use of $FeCl_3$ catalyst and activated charcoal in the mixtures of oxides increased the yield of the titanium nitride phase by enhancing the rate of reduction of oxides. The morphology of titanium carbonitride particles is dependent upon the reactivity of carbon and temperature. A satisfactory agreement between the calculated and experimental phase relationships has been found in the Ti-C-N system.

CHAPTER III. SYNTHESIS OF BORON NITRIDE AND CARBIDE BY CARBOTHERMIC REDUCTION OF BORIC OXIDE

1. INTRODUCTION

Boron nitride is primarily found in hexagonal (h-BN) form that resembles graphite structure, whereas the sphalerite (c-BN) and wurtzite (w-BN) forms are related to cubic diamond and hexagonal diamond crystal types[85], respectively. Each of these crystallographic structures has a number of unique physico-chemical properties, and its properties are of considerable interest to engineers. Hexagonal boron nitride has a layer structure as in graphite. It has strong covalent bonding within the layers and Van der Waals-type weak bonding between the layers. Weak bonds between the layer structure provide easy slip, which is manifested in its anti-friction properties. The sphalerite and wurtzite forms of boron nitride are characterized by a tetrahedral distribution of atoms in their lattices and also by a high density packing of atoms. This accounts for extreme hardness of these modifications and hence their extensive use as abrasive materials is justified.[86] If some of the h-BN phase is allowed to convert into diamond form, the designed microstructure will provide a good wear resistance as well as exhibit antifriction properties on a machined-finished surface. Hexagonal boron nitride has a very high melting point, a low specific gravity, thermal expansion coefficient, moderately high hardness, excellent dielectric strength and exceptionally high thermal conductivity. The material can be easily machined with conventional cutting tools and used as solid lubricants and boundary layer surface coatings. This is the reason why BN is known as a good antifriction and high temperature structural material. Cubic boron nitride exhibits sp^3 hybridisation of B-N bonds and has attractive electronic properties. The properties of BN make it suitable as reinforcement in a wide range of low density matrices.

Boron carbide (B_4C) has a comparable physical and chemical properties with other competing high temperature ceramic materials. It is for this reason that the material is used as hard phase in high technology industries.[87]

A wide variety of boron and nitrogen reagents have been used to prepare h-BN. Typical examples are salt decomposition, carbothermic reduction, oxide (or metal, metal boride) nitridation. An alternative method of

production of advanced ceramic materials utilises vapour deposition techniques. The polymer pyrolysis routes are also a competitive route for BN synthesis. Cubic boron nitride can be produced under high temperature and pressure, by shock compaction, ion-assisted vapour deposition, and other high energy techniques. The reduction of boron anhydride (or acid) in the presence of carbon (or with magnesium) yields boron carbide. Thin solid films, fibres or single crystals are obtained by chemical vapour deposition technology. A vapour mixture of BCl_3, CH_4 and H_2 gas can be reacted in plasma or laser to form carbide films. The controlled reductive dehalogenation of halides with sodium metal as a low temperature route to form nitride was also tested.

The preparation of nitrogen ceramics from metal oxides by carbothermic reduction have some advantages not only due to the availability of several different cheap raw materials but also for the versatility of the process. The properties of BN are closely related to the morphology of nitride phase and the latter can be controlled during synthesis process. The main aim of this project is to synthesise boron nitride and carbide powders and whiskers by carbothermic reduction of oxides in a nitrogen atmosphere and to understand a relation between the processing parameters and phases produced.

2. LITERATURE SURVEY

2.1 Boron Nitride

2.1.1 Introduction

The physical and chemical properties of boron nitride are very similar to those of carbon. Graphite-like hexagonal boron nitride (h-BN), wurtzite structure BN (w-BN) and cubic zinc blende structure BN (c-BN) are known as polymorphs of boron nitride. These correspond to graphite, hexagonal and cubic diamond, respectively. Hexagonal boron nitride, h-BN, which is also called g-BN or α-BN, crystallizes in the graphite structure, and is a soft, white material. The interesting properties are the high thermal conductivity in combination of with its excellent electrical properties, its inertness to many metal melts, and its application as a solid lubricant and as a refractory.

The dense modifications, c-BN and w-BN, are mainly used in hard sinter materials in abrasive for metal phase. Their semiconducting properties are also

gaining some interest. Cubic BN was first discovered by Wentorf.[88] The successful laboratory synthesis of diamond from graphite in 1955[89,90] led to the synthesis of a new form of boron nitride having a zinc-blende structure from h-BN starting material.[88,91] This is the diamond analog of boron nitride, and the second hardest material after diamond. It is also called cubic boron nitride (c-BN), sphalerite BN (ß-BN) or zinc-blende boron nitride (z-BN). The synthesis of the c-BN phase was achieved at high pressure and high temperature.[90,92,93] Now-a-days c-BN is produced industrially in commercial quantities by General Electrics in the U.S.A., by DeBeers (in South Africa, Ireland and Sweden), and by several other industrial organizations in Japan and in the U.S.S.R.[94] C-BN is an important engineering material, the less-reactive character of c-BN with iron makes it somewhat more applicable for engineering materials than diamond. It is used in powder form for abrasive operations, and as sintered cutting tool inserts for high speed machining of hardened steel, chilled cast iron, and nickel and cobalt-base superalloys.

Another polymorphic modification of BN, wurtzite-type BN (w-BN or *γ*-BN), was later produced in the laboratory by static high pressure technique[95], and by shock methods.[96,97] This form is the BN analog of the third modification of carbon, namely the hexagonal diamond,[98] produced in the laboratory also by static and dynamic high pressure methods. These are also abundant in meteorites.[99] W-BN is also produced on an industrial scale, mostly in fine powder form and by shock process in Japan, USSR and USA.[94] It is a good precursor material for sintered c-BN and w-BN cutting tools. The three forms of boron nitride are synthetic laboratory-made materials and are not found in nature. Turbostratic boron nitride (t-BN) is known to be an intermediate form of the crystallisation process of amorphous boron nitride (a-BN).[100,101] T-BN has a diffused structure of boron and nitrogen networks which have three dimensional disorder and have lattice parameters somewhat larger than those of h-BN. Occasionally in the t-BN structure, depending upon the process, a high volume fraction of sp^3 hybridisation is observed. This yields an interesting combination of properties of sp^2 and sp^3 hybridisation.

2.1.2 The crystal structure of boron nitride

Hexagonal boron nitride has a layer structure as graphite. For the fully ordered graphitic modifications, the lattice constants for boron nitride and carbon are similar: **(BN)**: a = 2.504Å, c = 6.661Å; **(C)**: a = 2.456Å,

c = 6.696Å.[85] Although the structure of h-BN is analogous to the graphitic form of carbon, the h-BN structure differs, as shown in **Figure III-1**, by having plana, six-membered rings stacked directly on top of each other, with boron atoms in one layer serving as nearest neighbours to N atoms in adjacent layers. In the graphitic carbon structure, the carbon atoms in adjacent layers are offset. Boron and nitrogen atoms occupy alternate vertices of the hexagons and also alternate along the c-direction. The layer sequence in h-BN is '-ABAB-'. It has strong primary covalent sp^2 bonds within the layers, but depend on weak van der Waals-type bonds to hold the layers together. Due to this highly difference anisopropic properties result and h-BN exhibits higher compressibility along the c-axis than along the a-axis.[102]

Upon compression at high temperatures, the reduction in interplanar spacing along the c-axis is accompanied by deformation of the hexagons taking place by splitting of each (001) planar layer of the h-BN lattice into two planes, one of boron atoms, the other of nitrogen atoms, displaced from each other along the c-axis. The sequence -ABAB- of the h-BN lattice therefore splits into layer sequence -A'BB'A- of the wurtzite lattice.[103] In both c-BN and w-BN, the B-N bonds are strong, covalent sp^3 bonds, each of the B and N atoms is tetrahedrally coordinated and all bonds are equivalent. Corrigan et al[104] insist that the c-BN lattice is not obtained from h-BN (or w-BN) lattice by simple compression. The transformation is reconstructive, involving breakage and reformation of bonds, actually taking place via chemical attack and dissolution-reprecipitation from specific (molten) solvent materials (which lower the very high activation energy barrier), or at very high pressures and temperatures (typically 100 kbar, 2273K or 65 kbar 2673K). The structures of w-BN and c-BN are shown in **Figure III-2**.

2.1.3 Synthetic routes to boron nitride

2.1.3.1 Hexagonal boron nitride

One of the main applications for h-BN is for the construction of high-temperature crucibles and other pressure-sintered parts. These articles are prepared from powder samples by using hot-pressing techniques. A wide variety of inexpensive boron and nitrogen reagents have been used to prepare h-BN. Some representative reactants and conditions are as follows[85,106]:

(a) Reaction of boric oxide (or sodium borates) with ammonia above 1173K

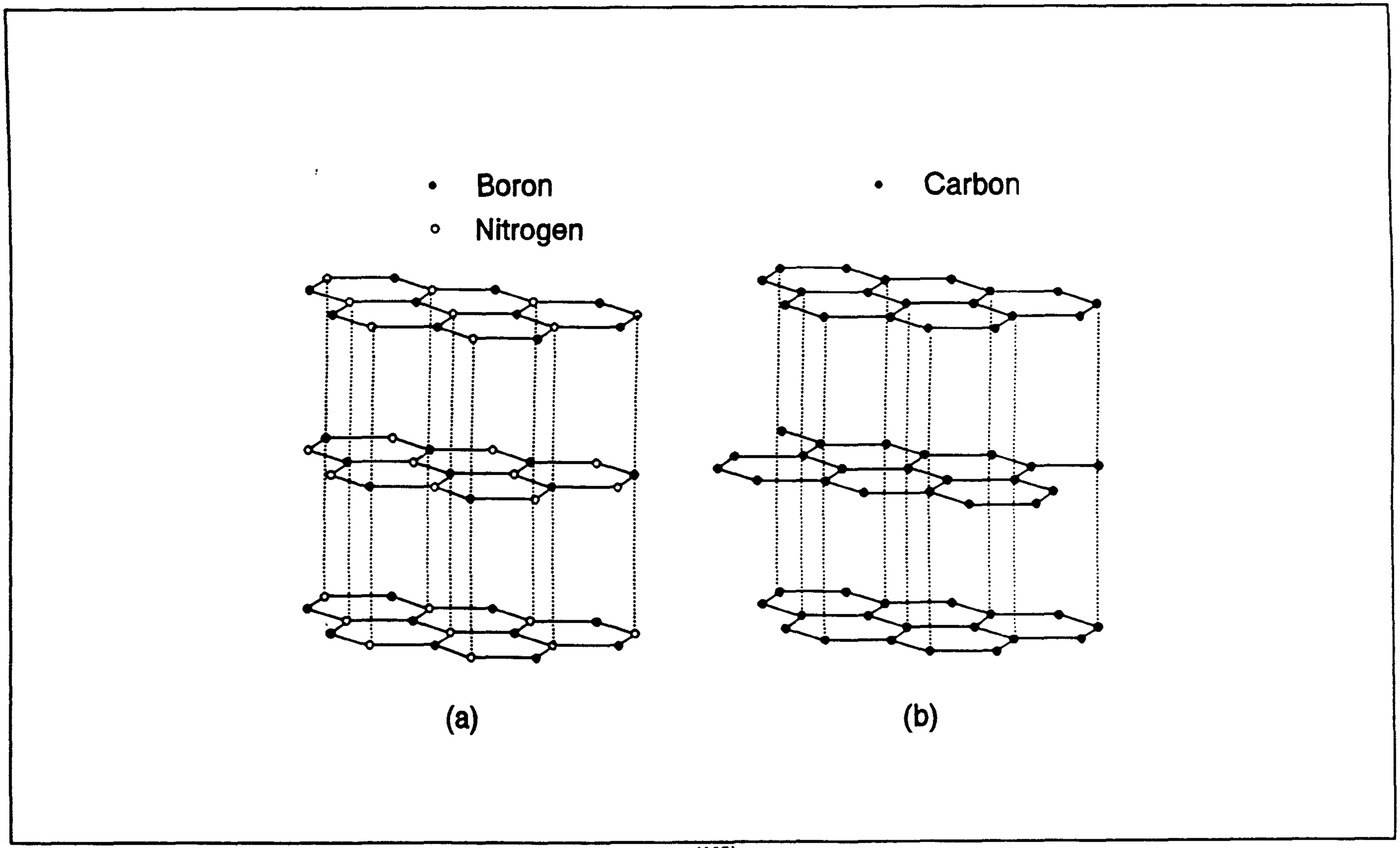

Figure III-1. Crystal structures of (a) h-BN and (b) graphite.[105]

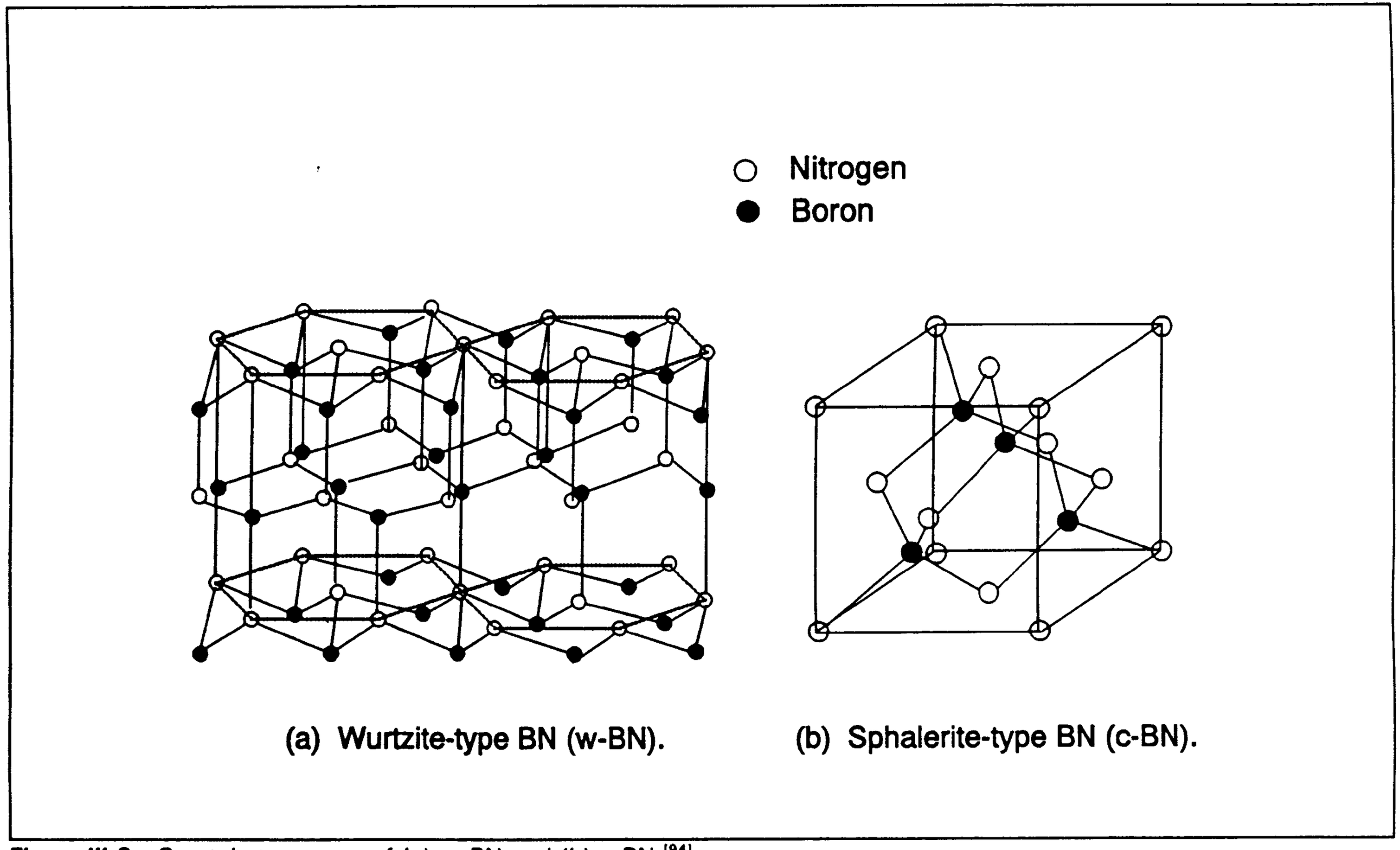

Figure III-2. Crystal structures of (a) w-BN and (b) c-BN.[94]

yields hexagonal BN. A second heat treatment for purification and stabilization is then carried out above 1773K under nitrogen gas. **(b)** Boric acid or borax reacts with organic nitrogen compounds, e.g. urea, biuret, guanidine, cyanamide, dicyanamide, thiourea, or melamine and produce h-BN. **(c)** Metallic boron powder can be nitrogenated with dry nitrogen gas above 1473K to BN. This is an exothermic reaction. **(d)** Carbothermic reduction reaction of boric acid with carbon above 1773K in the N_2 atmosphere yields h-BN and CO gas. **(e)** Like metallic boron, metal borides exothermically react with either NH_3 or N_2 above 1473K. Boric oxide acts as catalyst during the synthesis reaction. **(f)** Similarly metal borohydrides and NH_4Cl above 1173K react with each other in the N_2 atmosphere and form BN. **Table III-1** summarises the above processes.

Table III-1. A summary of reactions for the synthesis of hexagonal boron nitride.

Reaction	Working Temperature
(1) $B_2O_3 + 2NH_3 = 2BN + 3H_2O$	> 1173K
(2) $B_2O_3 + CO(NH_2)_2 = 2BN + CO_2 + 2H_2O$	> 1773K
(3) $B + 1/2N_2 = BN$	> 1473K
(4) $B_2O_3 + 3C + N_2 = 2BN + 3CO$	> 1773K
(5) $3CaB_2 + B_2O_3 + 4N_2 = 8BN + 3CaO$	> 1473K
(6) $KBH_4 + NH_4Cl = BN + KCl + 4H_2$	> 1173K

It is reported that amorphous BN is often obtained along with turbostratic or mesographitic modifications that possess disorder in the layered, hexagonal, graphite-like structure.[101,107] In some cases, these disordered materials can be converted to highly ordered h-BN by proper thermal annealing.[108] Fully ordered h-BN is only obtained with careful attention to processing details that seems to vary with each synthetic approach. Since some crucial properties are dependent on crystallinity, it is important to recognize and assess the degree of ordering. Pikalov and Germanskii[109] investigated the effect of parameters of the carbothermic process on the crystalline structure of h-BN and established the dependence of P_3, three-dimensional orderliness, on the integral intensity relationship of the *110* and *112* lines. For $P_3 = 0.79\text{-}0.99$ this dependence is conveniently described with the equation: $P_3 = 0.75 + 0.43\ln(I_{112}/I_{110})$. Formation of h-BN by

the carbothermic process is a complex heterogeneous process including the stages of reduction and nitriding. Pikalov[110] examined the carbothermic process and assumed that the formation of the h-BN in the carbothermic process takes place in two stages: reduction of the boron oxide by carbon with the formation of boron carbide and CO; chemical interaction of boron carbide with B_2O_3 and nitrogen with the formation of boron nitride and CO. But the latter reaction is two independent reactions, one is nitridation of boron carbide and the other is reduction nitridation of boron oxide.

Most alternative preparations of advanced ceramic materials have utilised vapour deposition techniques, including conventional chemical vapour deposition (CVD), metal organic chemical vapour deposition (MOCVD), low-pressure chemical vapour deposition (LPCVD), plasma-assisted (or plasma-enhanced) chemical vapour deposition (PACVD), laser-assisted chemical vapour deposition (LCVD), sputter process, and ion-assisted process. In most of these approaches, volatile precursors containing the final elements of interest (e.g. B and N) are passed over a substrate and a ceramic phase is deposited as an amorphous or crystalline thin film or fine powder, depending on the conditions employed. The chemical combinations that have been most commonly employed in vapour deposition production of amorphous and crystalline BN powders and films include B_2H_6/NH_3, $B_2H_6/NH_3/H_2$, BF_3/NH_3, BCl_3/NH_3, $BCl_3/NH_3/H_2$, borazene ($H_3B_3N_3H_3$), trichloroborazene ($Cl_3B_3N_3H_3$), and $B_{10}H_{14}/NH_3$. Luce et al[111] synthesized ultrafine powders of boron nitride in the nanometre size range by laser driven reactions in BCl_3-NH_3 mixtures. These mixtures have been used to deposit films on a wide range of substrates including transition metals, structural ceramics, electronic ceramics, and glasses. A condensed-phase pyrolysis of molecular reagents, a molecular boron-nitrogen compounds, have been prepared and preceramic polymer routes also exercised.

2.1.3.2 Dense forms of boron nitride

The diamond-like modifications are metastable under standard conditions. Dense forms of boron nitride can be produced by high temperature-high pressure methods with or without catalyst[108], by shock compaction[112], ion-assisted vapour deposition[113] or related high-energy techniques.[114] Once formed, diamond-like BN is kinetically stable in a manner similar to diamond. The direct conversion of h-BN into c-BN was first performed by Bundy and

co-workers.[95] They found that the w-BN formed from h-BN at room temperature under compression above 10 GPa, and the c-BN could be synthesised by heating above 2000K under pressure. The difference in density between c-BN and w-BN is <1% under normal conditions.[115] Both crystal structures contain a tetrahedron with sp^3 hybridisation. Therefore, the mechanical properties of w-BN are expected to correspond to those of c-BN. The w-BN powders were synthesised by shock compression.[104,115] The w-BN is the metastable phase and is transformed into c-BN under high pressure and temperature conditions. The stability of shock-synthesized w-BN at high pressures has been studied by Tani et al[116], Hiraoka et al[117], Corrigan and Bundy[104] and Akashi et al[118]. Their results agree qualitatively. The w-BN transforms to c-BN at pressure above 5.5 GPa and temperatures above 1573K. As it has been reported that c-BN is stable in the range from 1373K to 1773K and above 5.5GPa, w-BN should be metastable in the temperature range 1373-1573K. Several investigators have reported that graphite-like boron nitride transforms to w-BN[119] and also to c-BN by multiple shock compression of g-BN.[120] Sato et al[121] reported that rhombohedral boron nitride transforms to zinc blende-type by normal shock compression. Cubic boron nitride has been prepared from h-BN using magnesium fluoronitrides as well as magnesium-lithium, manganese and zirconium fluoronitrides as flux-precursors.[122] The conversion yields are much higher than those observed when pure magnesium nitride, Mg_3N_2, is used. BN is anisotropic and extremely difficult to fabricate and sinter, especially, cubic boron nitride.[123] **Figure III-3** showed the phase relation of boron nitride and carbon at high temperature and pressure.

2.1.4 The properties of boron nitride and applications

Hexagonal boron nitride has a unique combination of properties, for instance, low density (2270 $kg \cdot m^{-3}$), high temperature stability up to 3273K, chemical inertness, especially its resistance to acids and molten metals. It is stable in air up to 1273K and in inert gases like N_2, CO and Ar up to 2997K. The material exhibits superb stability to thermal shock, workability of hot-pressed shapes, extremely low electrical conductivity, which makes it an excellent insulator, and has a high thermal conductivity.[106] The layered structures of BN and graphite, with very strong in-plane covalent bonding and weak interplane attractions, are unique in ceramic materials, and this feature

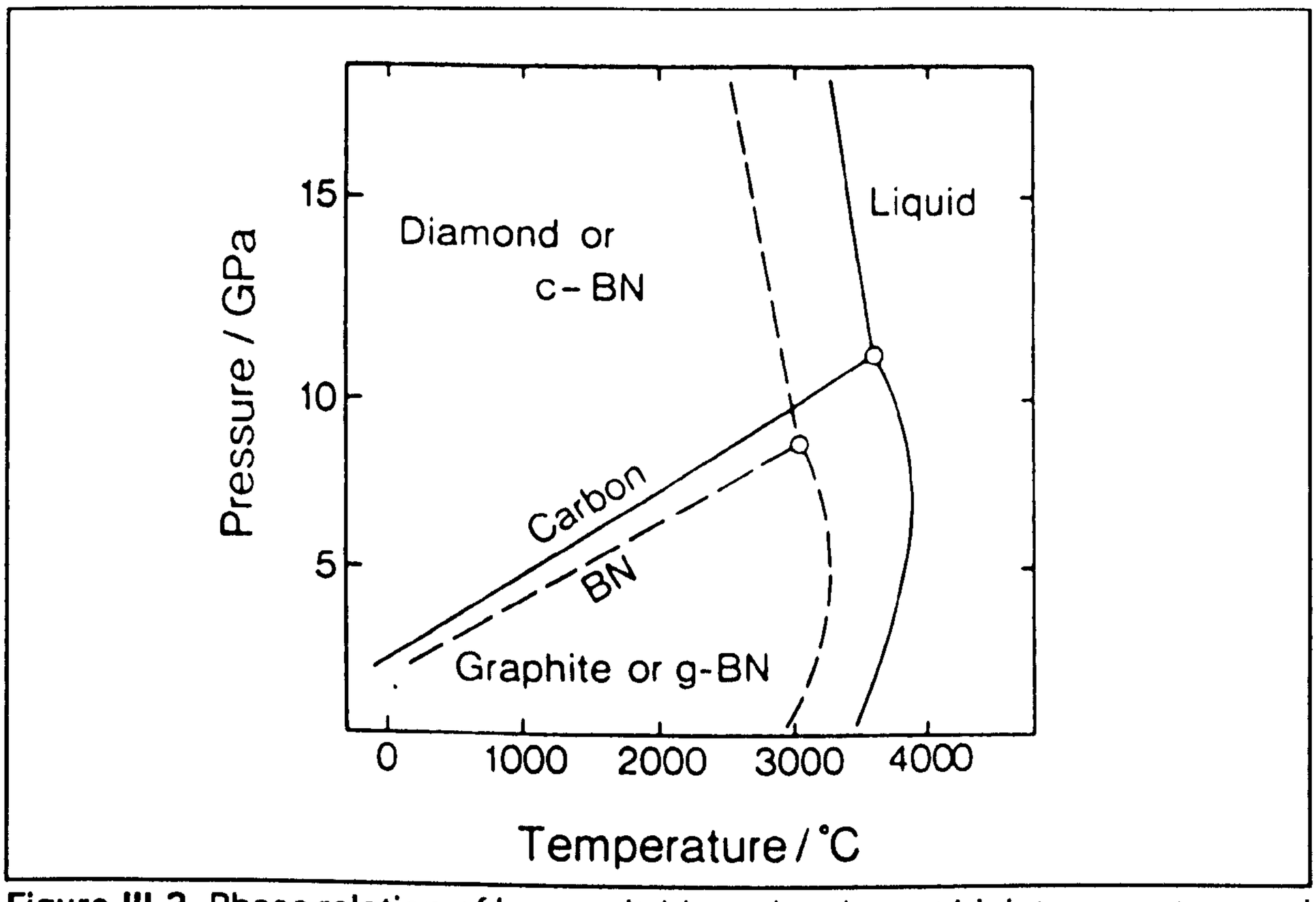

Figure III-3. Phase relation of boron nitride and carbon at high temperature and pressure.

results in a number of quite anisotropic mechanical, thermal and electronical properties. For example, pyrolytic BN has a high compressive strength, excellent thermal shock resistance in the temperature region 298 to 2273K, and it has a specific heat of 1002.4 $J \cdot kg^{-1} \cdot K^{-1}$, which is comparable to that of magnesium and aluminum. Like graphite[1124], the thermal expansion and thermal conductivity are highly anisotropic. It should be noted that the distinct anisotropic thermal properties of the BN are responsible for its widespread use in fabrication of high-temperature crucibles. Its layer structure, which slip easily between layers, has resulted in many tribological applications of this material. H-BN can be easily machined with conventional cutting tools and provide low-friction, self-lubricating surfaces for a wide variety of seals. Because of its stability at high temperature and inertness towards carbon and carbon monoxide up to 2073K, it is used as a refractory ceramic. H-BN is also used as solid lubricants and as boundary layer surface coatings. The properties of boron nitride are strongly dependent on the crystalline modification.[1100] In powder or compacted forms, boron nitride has a silky feel, monoliths may be readily machined, and the material is nontoxic. Unlike graphite, which is characteristically black, h-BN, when pure and defect free, is transparent. The

opaque, white colour typically found in macroscopic samples is not intrinsic, but rather it results from impurity and defect states in the electronic band gap.[125] The density of anisotropic pyrolytic BN could be as low as 2000 $kg \cdot m^{-3}$ compared with the theoretical density[107] of 2270 $kg \cdot m^{-3}$. This density is the lowest of all ceramic materials. Boron nitride apparently does not display a normal melting behaviour. Thermodynamic data for h-BN have been summarized[108]: $C_p(298\ K) = 17.5\ J \cdot mol^{-1} \cdot K^{-1}$, $H°_{298} - H° = 2623\ J \cdot mol^{-1}$, $S°_{298} = 14.80\ J \cdot mol^{-1} \cdot K^{-1}$, $\Delta H(298K) = -252.63\ kJ \cdot mol^{-1}$.

The electronic properties of BN and graphite are distinctly different. Graphite is a black, highly reflective semimetal with anisotropic resistivity. The conductivity of BN is much smaller at lower temperatures, thus making the material a useful insulator.[126] The electrical properties are highly dependent on its purity and it is for this reason that the resistivity of BN may be influenced by annealing in nitrogen atmosphere.[127] At higher temperatures, the resistivity decreases, and the material eventually becomes a semiconductor. It may be possible to realise some useful properties from the semiconducting properties for high temperature, extreme environment applications. The material has a larger electronic band gap than silicon carbide.

It is clear that the chemical reactivity of BN is very dependent on BN sample preparation, purity, crystallinity, and microstructure. It appears that, for pyrolytic BN, air oxidation (as measured by weight loss due to volatilisation of B_2O_3) is negligible below 1173K. However, the oxidation becomes significant in the range 1373-1473 K (4.8 $mg \cdot cm^{-2}$ in 180 min at 1473 K).[128] Metallurgically prepared BN shows slight oxidation below 1423K and more extensive weight loss at 1273K.[128] Commercial pyrolytic BN also has been reported to undergo weight loss due to oxidation.[126] Calcining powdered BN in air, on the other hand, shows significant formation of B_2O_3 at 1073K.[129] BN is reported to react with Al_2O_3 at 1973K and SiC at 1073K.[130] Because of the poor sinterability of BN, a number of studies of reactions between BN and metals, alloys, and metal nitrides have appeared[108] in the literature. Some properties of hexagonal boron nitride are summarised in **Table III-2**.

Pure c-BN is colourless and a good electrical insulator. Doping with Li_3N or the elements such as Be, Si, C or P turns c-BN yellow to black colour and also changes other properties, such as conductivity or toughness[106]. Rapoport[94] collected physical and chemical properties data and some of them are presented in **Table III-3**.

Table III-2. The properties of boron nitride and carbide.[131,132]

Property	h-BN	HIP h-BN
Density ($x10^3$, $kg \cdot m^{-3}$)	2.27(theoretical)	2.2
Melting point (K)	2600(decomp.)	
Heat of formation ($kJ \cdot mol^{-1}$)	-254.0 ± 10.5	
Entropy ($J \cdot mol^{-1} \cdot K^{-1}$)	15.36 ± 0.21	
Specific heat ($J \cdot mol^{-1} \cdot K^{-1}$)	17.460	
Thermal expans.co.($x10^{-6}$,K^{-1})	41(∥), -2.3(⊥)	4.4
Thermal conductivity($J \cdot m^{-1} \cdot s^{-1} \cdot K^{-1}$)	15(∥)	50(at 298K)
	29(⊥)	20(at 1273K)
Electric resistivity ($\Omega \cdot cm$)	$\sim 10^{13}$(at 298K)	$6.3x10^{13}$(at 298K)
		10^8(at 1273K)
Dielectric constant (e)	4.0 ~ 4.3	5.4
Dielectric loss (tan δ)	0.0005, 10^{10} c/s	$3x10^{-4}$(100kHz,1V)
Comp. strength ($x10^{-3}$,$kg \cdot cm^{-2}$)	1 ~ 3	
Young's modulus(E) (GPa)		32(at 298K)

Table III-3. Crystallographic and mechanical properties of cubic boron nitride.[94]

Property	Value
Crystal structure	cubic, zinc-blende
Lattice constant	c-BN : $a_o = 3.6157 \pm 0.001$ Å
	Diamond: $a_o = 3.56696 \pm 0.00005$ Å
	w-BN : $a_o = 2.549 \pm 0.003$ Å
	$c_o = 4.216 \pm 0.003$ Å
Ionic distance	(B-N) : 1.57 Å
	(C-C) : 1.54 Å (Diamond)
Density ($x10^3$,$kg \cdot m^{-3}$)	c-BN : 3.4879 ± 0.0030
	Diamond: 3.515
	w-BN : 3.454 ± 0.009
Hardness (GPa)	60-70 (Knoop scale)
	Diamond > 80
	Si_3N_4 > 24
	Al_2O_3 > 19

2.2 Boron Carbide

2.2.1 Introduction

Boron carbide was discovered by Joly[133] in 1858 and in early days its mistaken stoichiometry was B_3C. However in 1934, the correct stoichiometric formula, B_4C was assigned. The compound belongs to the important group of non-metallic hard materials which includes alumina, silicon carbide, diamond and cubic boron nitride. The homogeneity range that has been confirmed from an experimental phase diagram lies in the stoichiometry B_4C and $B_{10.4}C$. The commercial boron carbide, however, has a composition close to B_4C. The experimental phase diagram[134] indicates that the carbide melts congruently at 2763K at 13.3 at% carbon. The hardness of boron nitride is only next to diamond and c-BN. Some important properties of B_4C are compiled below in **Table III-4** and have been taken from reference [106]. In addition to its high melting point, the material has a high specific strength, large neutron cross-section and is a semiconductor.

2.2.2 The crystal structure of boron carbide

The crystal lattice belongs to the $D3d^5$-R3m space group. The rhombohedral unit cell shown in **Figure III-4** has 15 atoms corresponding to $B_{12}C_3$. More recent data have contested these results and subsequent NMR studies have indicated that for a crystal of $B_{12}C_3$ stoichiometry, the central position in the C-C-C chain (see Figure III-4, site b) was partially occupied (60%) by boron atoms. Furthermore, IR absorption spectroscopy by Becher and Thevenot[135] have confirmed the existence of the C-B-C chain in compounds such as B_4C and $B_{5.62}C$. The carbide structure is composed of twelve atom icosahedral clusters which are linked by direct covalent bonds and through three-atom intericosahedral chains. The phase is known to exist in the carbon concentration range 8.8 to 20 atom percent. The non-stoichiometry has been possible by the substitution of boron and carbon atoms for one another within both the icosahedra and intericosahedral chains. This arises due to the small size difference between carbon and boron atoms. The lattice parameters of two different categories of boron carbide is compiled in **Table III-5** and is given after Thevenot[87]. Based on detailed structural analysis,

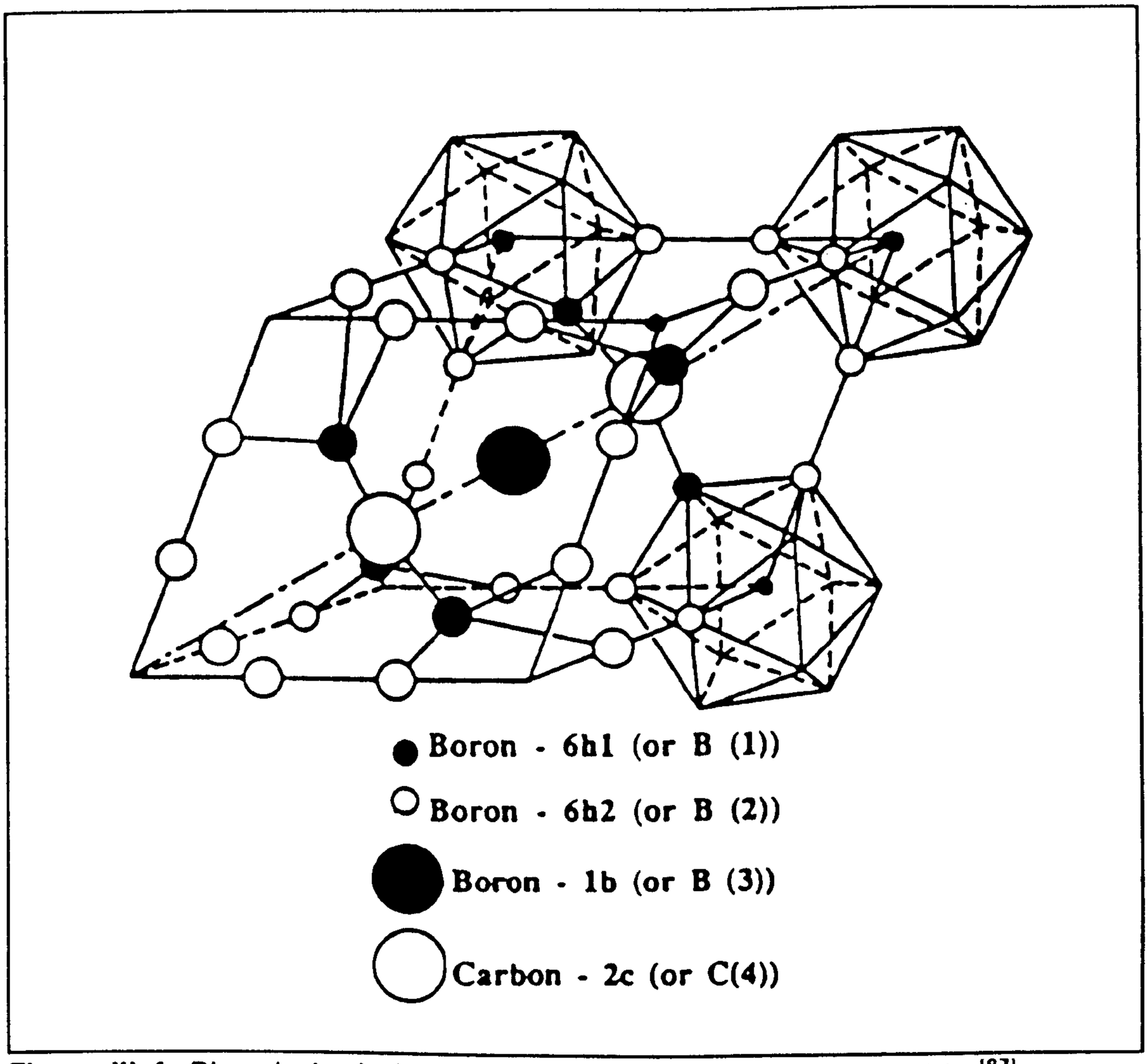

Figure III-4. Rhombohedral crystalline structure of boron carbide.[87]

Thevenot derived an empirical relationship between carbon content (C_c, at%) and number of carbon atoms (n_t) in each unit cell:

$$n_t = 15.47 - 0.019\ C_c \qquad (3\text{-}1)$$

Table III-4. Selected properties of hot-pressed and sintered boron carbide

Property	Hot-pressed B_4C	Sintered B_4C	
		B_4C (1 wt%C)	B_4C (3 wt%C)
Total carbon content	21.7	22.5	24.8
Porosity(%)	< 0.5	< 2	< 2

Bulk density ($kg\text{-}m^{-3}$)	2510	2440	2460
Mean grain size (μm)	5	8	7
Flexural strength 4-point($MN\text{-}m^{-2}$)	480 ± 40	351 ± 40	353 ± 30
Young's modulus (GPa)	441	390	372
Shear modulus(GPa)	188	166	158
Poisson's ratio	0.17	0.17	0.17
Fracture toughness $MPa\text{-}m^{½}$, K_{Ic}	3.6 ± 0.3	3.3 ± 0.2	3.2 ± 0.2

Table III-5. Lattice parameters of boron carbides. H and R designate hexagonal and rhombohedral crystal lattices respectively.

Carbon-saturated ß-rhomobohedral boron	Limited boron-rich B_4C	
	H	R
$a_H = 10.929Å$	$a_H = 5.651Å$	$a_R = 5.213Å$
$c_H = 23.921Å$	$c_H = 12.196Å$	$\alpha = 65.650°$
$V_H = 2474.20Å^3$	$V_H = 337.29Å^3$	$V_R = 112.43Å^3$

2.2.3 Synthetic routes for boron carbide

The sub-section is divided into two parts covering both the industrial processes and laboratory preparative routes. The annual production of boron carbide in the non-communist countries is believed to be of the order of 500 tons.

2.2.3.1 Industrial practice

The reduction of boron anhydride or boric acid is carried out with carbon and the overall reaction is:

$$2B_2O_{3\ (vapour)} + 7C_{solid} = B_4C_{solid} + 6CO_{gas} \qquad (3\text{-}2)$$

The briquettes of boric anhydride and carbon are fed into the central zone of an arc furnace where the temperature exceeds 2473K. At these temperatures, metallic boron is produced as an intermediate phase that readily combines with carbon to yield boron carbide of $B_{4.3}C$ composition. The carbide forms in the molten state and is crushed. This is followed by attrition and sifting to select a particular size range. This is a closed circuit operation.

Alternatively boron anhydride is reduced with metallic magnesium in the presence of carbon black. The reaction is strongly exothermic and as a result B_4C and magnesia are produced. Magnesia is removed from the reaction product together with unreacted magnesium metal and MgB_2 by sulphuric and hydrochloric acid treatment. The particle size of stoichiometric boron carbide is 0.1 to 5 μm. A typical processing temperature may be between 1273K and 1473K.

$$2B_2O_{3\ (vapour)} + 6Mg_{liquid} + C_{solid} = B_4C_{solid} + 6MgO_{solid} \qquad (3\text{-}3)$$

Magnesium borate is one of the stablest intermediate phases that can only be removed in the presence of carbon above 1473K and it is this phase that could transform into magnesium diboride.

2.2.3.2 Laboratory synthesis routes

Most laboratory methods for the production of boron carbide employ either organometallic compounds of boron or BCl_3 that are reacted in the gaseous state with hydrocarbon and hydrogen gas. The powder produced have wide stoichiometry range (B/C = 15.8 to 3.9) and this depends upon the composition of the inlet gas mixture. The particles produced by thermal decomposition have spherical shape with 20 to 30 nm size range.

The organometallic precursor gas route with BCl_3 or BBr_3 can also be used for depositing films of carbide either by microwave plasma or direct current arc plasma. The chemical vapour route also provides an opportunity to manufacture whiskers and long fibres of boron carbide. The chemical reaction involved in the powder production and film and whisker growth is:

$$4BCl_{3\ (gas)} + CH_{4\ (gas)} + 4H_{2\ (gas)} = B_4C_{(solid)} + 12\ HCl_{(gas)} \qquad \textbf{(3-4)}$$

Details of laboratory synthesis routes have been reviewed by Thevenot.[136]

3. THERMODYNAMICS OF SYNTHESIS REACTIONS

3.1 The B-N-C-O Phase Equilibria

3.1.1 The reducing condition leading to the formation of boron carbide and nitride from boron anhydride

The phase equilibrium diagrams in the B-N-C-O system were constructed by plotting $-RT\ln pN_2$ (kJ) against the reciprocal of the absolute temperature for the following equilibrium relationships shown in **Table III-6.**

Table III-6. The values of the standard Gibbs free energy change ($\Delta G°$) for the reduction condition of boron anhydride to BN and B_4C and for the nitridation of boron carbide.

Reactions	$\Delta G°$ (kJ)
a) $B_2O_3 + N_2 + 3C = 2BN + 3CO$	384.426 - 0.292 T
b) $B_2O_3 + B_4C + 2C + 3N_2 = 6BN + 3CO$	-576.555 + 0.053 T
c) $B_4C + 2N_2 = 4BN + C$	-960.981 + 0.345 T
d) $2B_2O_3 + 7C = B_4C + 6CO$	1729.833 - 0.929 T
e) $B_2O_3 + 2NH_3 = 2BN + 3H_2O$	92.592 - 0.100 T

We have assumed that the activity of carbon is unity and the total partial pressure of CO gas is 1 atmosphere. From **Figure III-5**, we find that the univariants (a),(b) and (c) listed in Table III-6, intersect each other at point 'B'. This means that the phase field ABD defines the stability region for boron carbide. Whereas BN and B_2O_3 are stable above DBD' and below ABD' lines respectively. The point 'B' is the invariant point where three boron-containing condensed phases are in equilibrium with the gas phase mixture of CO and nitrogen. We have also plotted CC' univariants which defines the equilibrium between all boron compounds, carbon and nitrogen and CO gas mixture. As

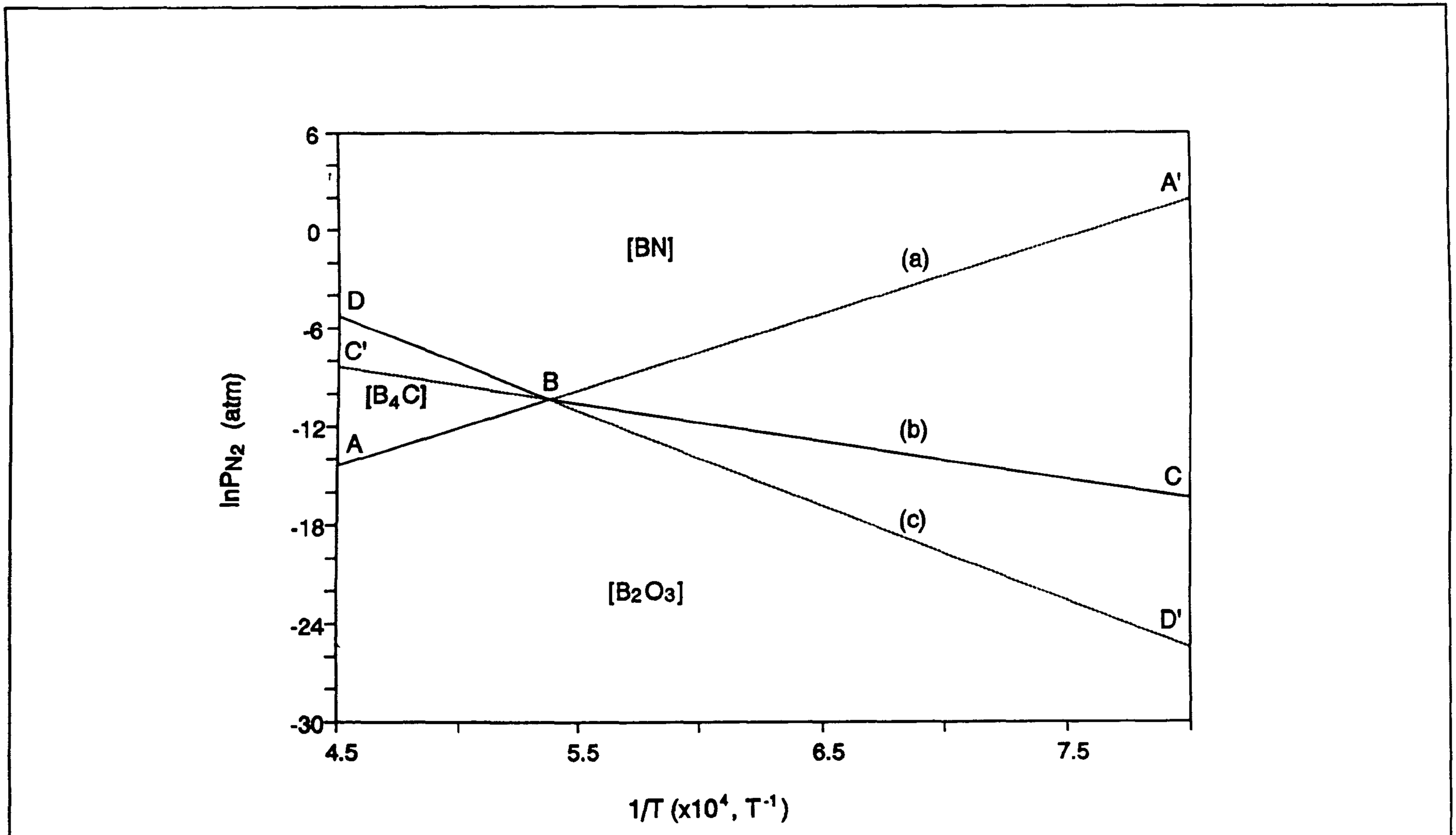

Figure III-5. The phase equilibrium diagram in the B-N-C-O system.

expected from the Gibbs phase rule, the CC' line must go through point B. This is shown in Figure III-5. The CC' line points out that the stability of boron carbide has significantly reduced at lower temperatures and this is only possible because B_4C and B_2O_3 vapour can combine to form BN phase. The importance of the phase equilibrium calculations will become apparent in the *Results and Discussion* section. The new phase fields are as follows:

a) above curve DBC, BN is stable;
b) in the region ABD, B_4C is stable;
c) and below curve ABC, B_2O_3 is stable.

3.1.2 Equilibrium between metallic boron, B_4C, BN, carbon and the gas phase

An alternative method of establishing the phase relationships in the B-N-C-O system is to consider a set of independent chemical reactions that involves both the relevant condensed phase and a gas phase composed of BO, CO and N_2 gas. The equilibria we have considered are listed in **Table III-7** below.

Table III-7. Phase equilibria equations in the presence of BO gas.

Reaction	$\Delta G°(J)$
A) $BO + \frac{1}{2}N_2 + C = BN + CO$	-361,209 + 90.63 T
B) $4BO + 5C = B_4C + 4CO$	-484,854 + 17.61 T
C) $BO + C = B + CO$	-110,587 + 3.01 T
D) $B_2O_3 + C = 2BO + CO$	1,106,844 - 473.38 T
E) $B_4C + BO = 5B + CO$	-69,082 - 2.55 T
F) $B_2O_3 + B_4C = 4B + 2BO + CO$	1,152,152 - 390.16 T
G) $B_2O_3 + B_4C + 2N_2 = 4BN + 2BO + CO$	145,863 - 128.49 T

Additional reactions can also be considered but there are only five independent reactions relating four boron-containing condensed phase ie B_2O_3, B, B_4C and BN. The other two dependent equilibria are (F) and (G) also shown in **Table III-7**. Once the necessary equations are defined , the univariants (log p_{BO} vs T) curves can be constructed by arbitrarily fixing the partial pressures of CO and

N_2 gases. The total pressure is one atmosphere and the thermodynamic activity of carbon is unity. The partial pressure of CO in all reactions in Table III-7 is 1 except reaction (a) where we have arbitrarily fixed the partial pressure of nitrogen and carbon monoxide such that $p_{CO}/(p_{N2})^{1/2} = 1$. This is to simplify the calculation of univariants described above. In **Figure III-6**, points 'a', 'b' and 'c' are the invariant points between BN, B_4C, B and B_2O_3 plus carbon respectively. At these points, the condensed phases are in equilibrium with CO and N_2 gas mixture.

For a complete representation of the B-C-O phase equilibria, reactions (B) to (F) should be considered. The partial pressure of BO for the stability of carbide and metal phases is of the order of 10^{-3} and higher. Furthermore, incorporation of reaction (A) and exclusion of reaction (G) will lead to the definition of the phase fields in the B-C-N-O system. This is shown in Figure III-6 where the metastability of BO gas is also indicated. The invariant point 'a' determines the stability of BN and boron anhydride phases over a wide temperature range. Only above 1315K, BN crystals can be thermodynamically stable and below this temperature B_2O_3 is a stable phase. A similar approach can be taken by considering the appropriate free energy equation in order to define the phase stability of boric anhydride gaseous phase. This species is known to exist above 1000K. Figure III-6 is fairly illustrative and indicates the operational temperature range for the synthesis of ceramic and metal phase. This diagram confirms why electric arc furnace operation yields B_4C phase above 2473K.

In **Figure III-7**, the univariants for the carbothermic reduction and ammonia nitridation are plotted. The nitridation with ammonia has the lowest free energy in the low temperature range and it will therefore favour the formation of BN. This is also apparently one of the ways for the synthesis of h-BN. At higher temperatures than 1500 K, the univariant nitridation with nitrogen gas becomes more stable and eventually above 2000K boron carbide is the most stable phase. This is consistent with the above phase relationship shown in Figure III-5.

4. EXPERIMENTS

Granulated boron oxide (B_2O_3) of 99.999% purity supplied by Aldrich Chemical Company was used as the starting material with carbon. The granule

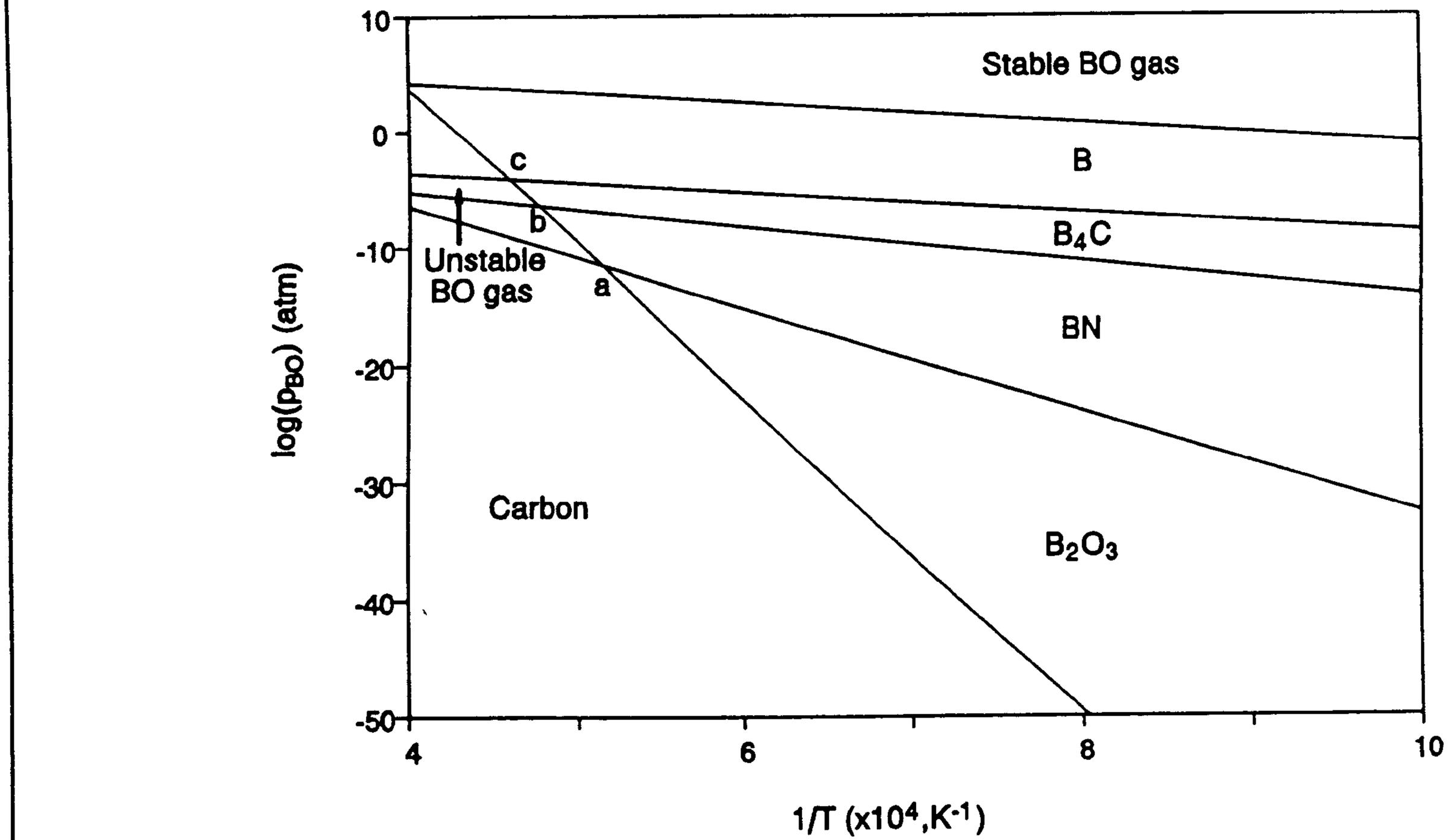

Figure III-6. The phase equilibrium diagram in the B-C-O system.

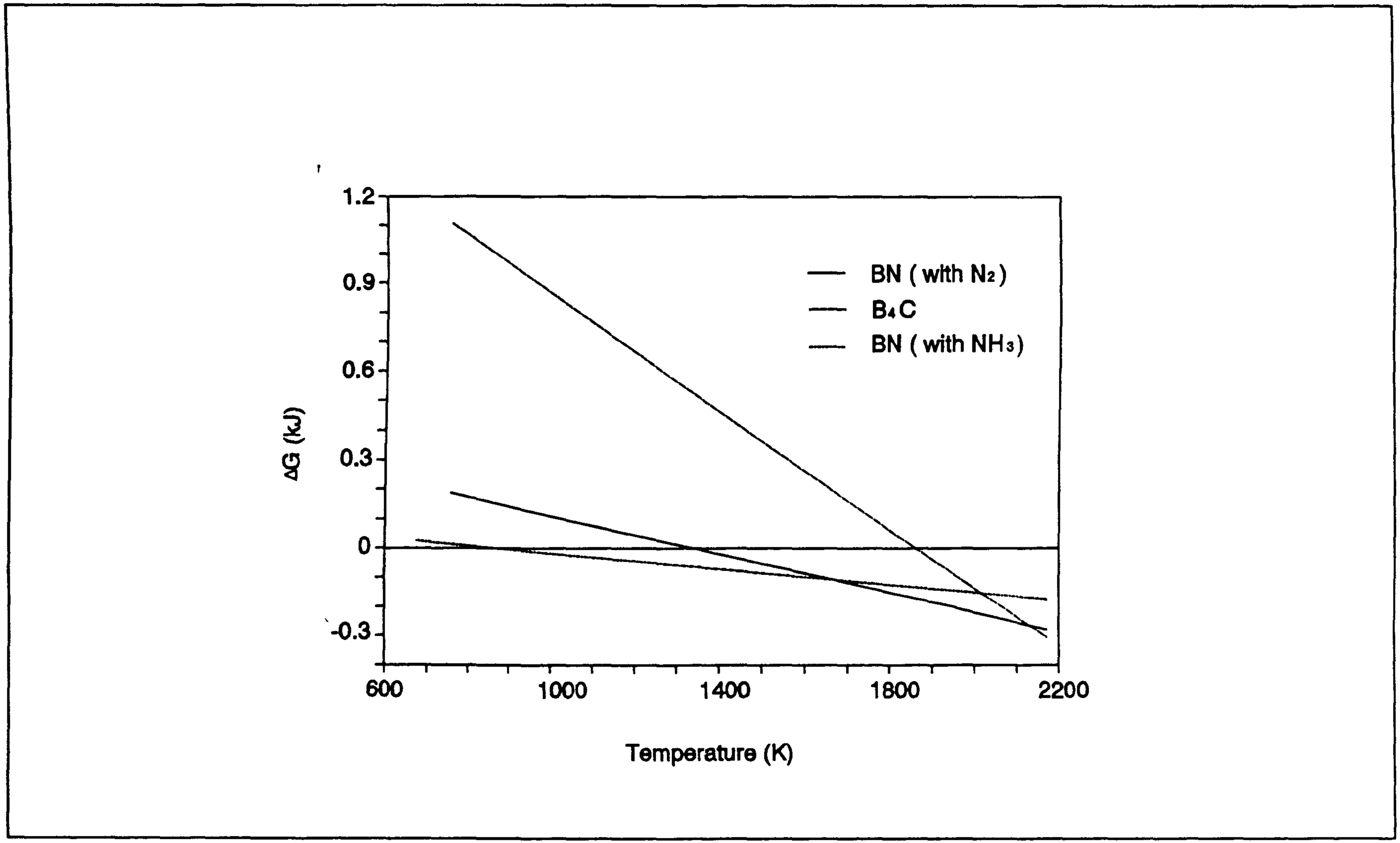

Figure III-7. The standard free energy change diagram for the formation of BN and B_4C.

size was 1-5 mm. The particles were crushed in a steel mortar for 10 minutes and ground for more than 30 minutes in an agate mortar for the production of finer particles. The grinding was carried out inside a controlled atmosphere glove box in order to avoid contamination from ambient moisture. Other types of boric anhydride from Aldrich Chemical Company (B_2O_3 pellet, diameter :2.5cm, 99.99%) and from Fluka Chemicals AG (>98% purity) were also tested for reduction experiments.

For the sustenance of the reaction $B_2O_3 + 3C + N_2 = 2BN + 3CO$, more than the stoichiometric amount of carbon was added in a series of mixtures. However in order to understand the mechanism of the reduction reaction, we also added less than the stoichiometric amount of carbon in the starting mixture. This was necessary to analyze the volatilisation loss of boric anhydride either as B_2O_3 gas or BO gas. A resistance-heated tube furnace shown in Chapter II (Figure II-11) and a radio frequency induction coil (**Figure III-8**) were used for heating the pelletized mixture in a controlled nitrogen atmosphere. Several different heating rates, ranging from 3 to 300 K-min^{-1}, were employed for the reduction experiment.

A few mixture were tested with NH_4HF_2 (Fluka Chemicals AG., 90-95%) and with NH_4Cl (BDH Ltd, >99%) as catalyst for promoting the nucleation of non-graphitic type boron nitride during reduction. The catalytic reagents were either added to the starting mixture or located in the lower temperature part of the furnace so that it can sublime at a gentle rate with the incoming stream of gas. The experimental technique employed in this chapter is essentially the same as that described in Chapter II.

5. RESULTS

In this section, the results from the reduction of boric oxide under different conditions are presented. These results are based on the X-ray powder diffraction analysis and microscopy. The total reduction time was defined from the moment, the pellet/powder mixture was raised in the hot zone of the vertical furnace until the time it was withdrawn from the isothermal zone. A few experiments were carried out by using the radio frequency coil. In this case, the total heating time was taken as the reduction time.

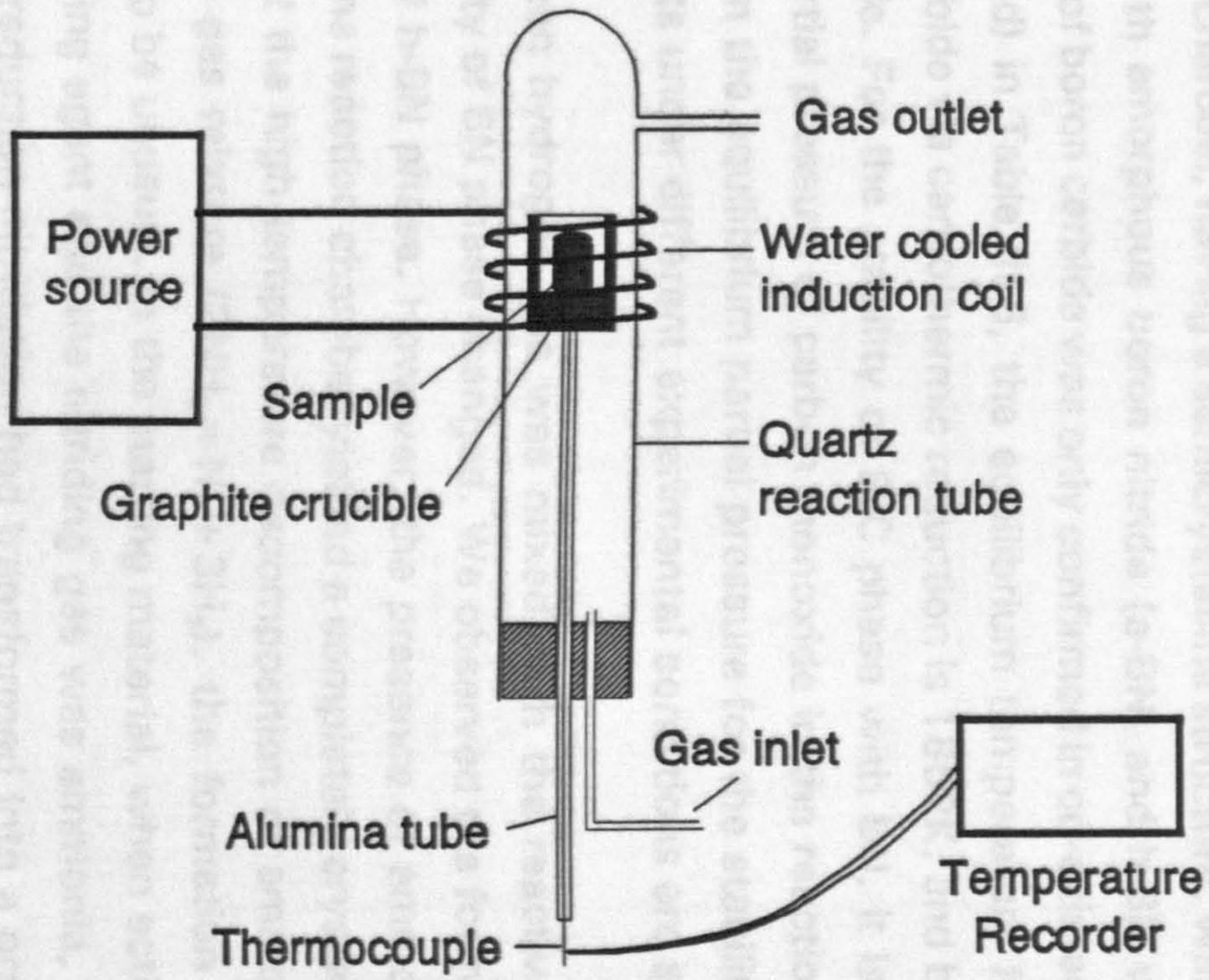

Figure III-8. A schematic diagram of the induction furnace.

5.1 The Effect of Gas Composition and Type of Carbon Used on the Phases Produced

In the nitrogen atmosphere with several stoichiometric ratios of carbon (1 to 4 moles of carbon) for the formation of BN by carbothermic reduction, hexagonal boron nitride (h-BN) phase was produced. The formation of h-BN was particularly favourable in the presence of graphite. However, when activated charcoal, having a semicrystalline structure, was used as a reducing agent, both amorphous boron nitride (a-BN) and h-BN were observed. The presence of boron carbide was only confirmed in co-existence with a-BN. From reaction (d) in Table III-6, the equilibrium temperature for the formation of boron carbide via carbothermic reduction is 1862K, and below this the phase is unstable. For the stability of B_4C phase with BN, it is important that the actual partial pressure of carbon monoxide in the reaction chamber must be lower than the equilibrium partial pressure for the stability of boron carbide. The results under different experimental conditions are summarised in **Table III-8**.

When hydrogen gas was mixed with the reactive nitrogen gas, the crystallinity of BN phase changed. We observed the formation of a-BN phase instead of h-BN phase. However, the presence of ammonia gas as nitriding agent in the reaction chamber yielded a completely crystalline h-BN structure. In view of the high temperature decomposition of ammonia to nitrogen and hydrogen gas mixture ($2NH_3 = N_2 + 3H_2$), the formation of crystalline h-BN appears to be unusual. In the starting material, when activated charcoal was the reducing agent and the nitriding gas was ammonia, residual carbon left after the reduction-nitridation had transformed into a graphitic structure. It appears that the graphitization of activated charcoal might have been initiated due to the presence of ammonia gas which is sp^2 hybridized. Furthermore the reduction of boric anhydride with ammonia in a graphite crucible yielded crystalline graphitic carbon with h-BN.

5.2 The Effect of Carbon Content in the Mixture and Reduction Temperature

The presence of graphitic carbon at temperatures $\leq$1573K yielded graphitic carbon and boric anhydride glass. Above this temperature, the

Table III-8. The effect of gas composition on the structure of BN phase formed. (Type of carbon used : activated charcoal. In ammonia/argon-hydrogen experiment, the flow rate of NH_3 is 50ml/min and Ar/H_2 100 ml/minute)

Starting materials	Temp (K)	Time (hr)	Gas composition	Produced phases
$B_2O_3 + 3C$	1573	4	N_2	h-BN
			$N_2 + H_2(15\%)$	a-BN
			$N_2 + H_2(50\%)$	a-BN
		1	$NH_3 + Ar/H_2(4\%)$	h-BN, Gra
$B_2O_3 + 4C$	1473	8	N_2	a-BN, B_4C
	1523	4		a-BN, B_4C
	1573	5		a-BN, B_4C
	1673	8		a-BN, B_4C
	1573	4	$N_2 + H_2(15\%)$	a-BN
	1573	4	$N_2 + H_2(50\%)$	a-BN
	1673	8	$N_2 + H_2(15\%)$	a-BN
	1573	0.5	$NH_3 + Ar/H_2(4\%)$	Gra, h-BN

tendency to form h-BN phase increased and eventually h-BN and boron carbide existed in equilibrium with the graphitic carbon (see **Table III-9**). On the other hand, active carbon or charcoal at and above 1473K yielded only amorphous BN and B_4C in nitrogen atmosphere when the molar ratio of boric oxide to carbon was 1:4. With proportions of carbon to oxide lower than 4, h-BN phase formed with active charcoal in nitrogen atmosphere (see Tables III-7 and III-8).

Only with low stoichiometric proportions of carbon (<1:3), the reduction-nitridation of boric anhydride was incomplete. Due to this, the unreacted anhydride turned into a glassy phase or volatilized as such a high temperature. Above a critical temperature (ie 1573 K), the tendency for the formation of either h-BN or a-BN was enhanced. This appears to be consistent with the reaction rate law ie the reduction rate increases with the increasing

Table III-9. The effect of reactivity and content of carbon on the phases produced. (Nitrogen flow rate : 500 ml/min)

Carbon		Temp (K)	Time (hr)	Gas composition	Produced phases
Type	Content				
Active carbon	1C	1573	4	N_2	h-BN
	2C	1573	4	N_2	h-BN
	3C	1573	4	N_2	h-BN
	4C	1523	8	N_2	a-BN, B_4C
		1573	8		a-BN, B_4C
		1673	8		a-BN, B_4C
		1773	8		a-BN, B_4C
Graphite	2C	1573	4	N_2	Gra, B_2O_3
	4C	1523	8	N_2	Gra, B_2O_3
		1573	8		Gra, h-BN, B_2O_3
		1673	8		Gra, B_4C, h-BN
		1773	8		Gra, B_4C, h-BN

temperature and reduction surface area. The time, as one of the reaction rate parameters, had a very little effect on the phase constitution of the reaction product. Unfortunately in all the boron nitride experiments, it was difficult to accurately record the weight of the pellet after reduction experiment stopped. This was particularly due to poor pellet-forming tendency of the powder mixture and the type of gas used which also contributed to the weight loss from the containment graphite crucible. This is the reason that none of the data tables in this chapter include the results of percentage reduction (%R).

From our results, a set of specimen X-ray powder diffraction patterns have been complied and these are shown in **Figure III-9**. The phases identified are labelled. From the X-ray powder diffraction pattern, the difference in the structure of amorphous BN and h-BN becomes apparent.

From **Tables III-8** and **III-10**, we find that when activated charcoal was used as a reducing agent, the formation of BN started much closer to the

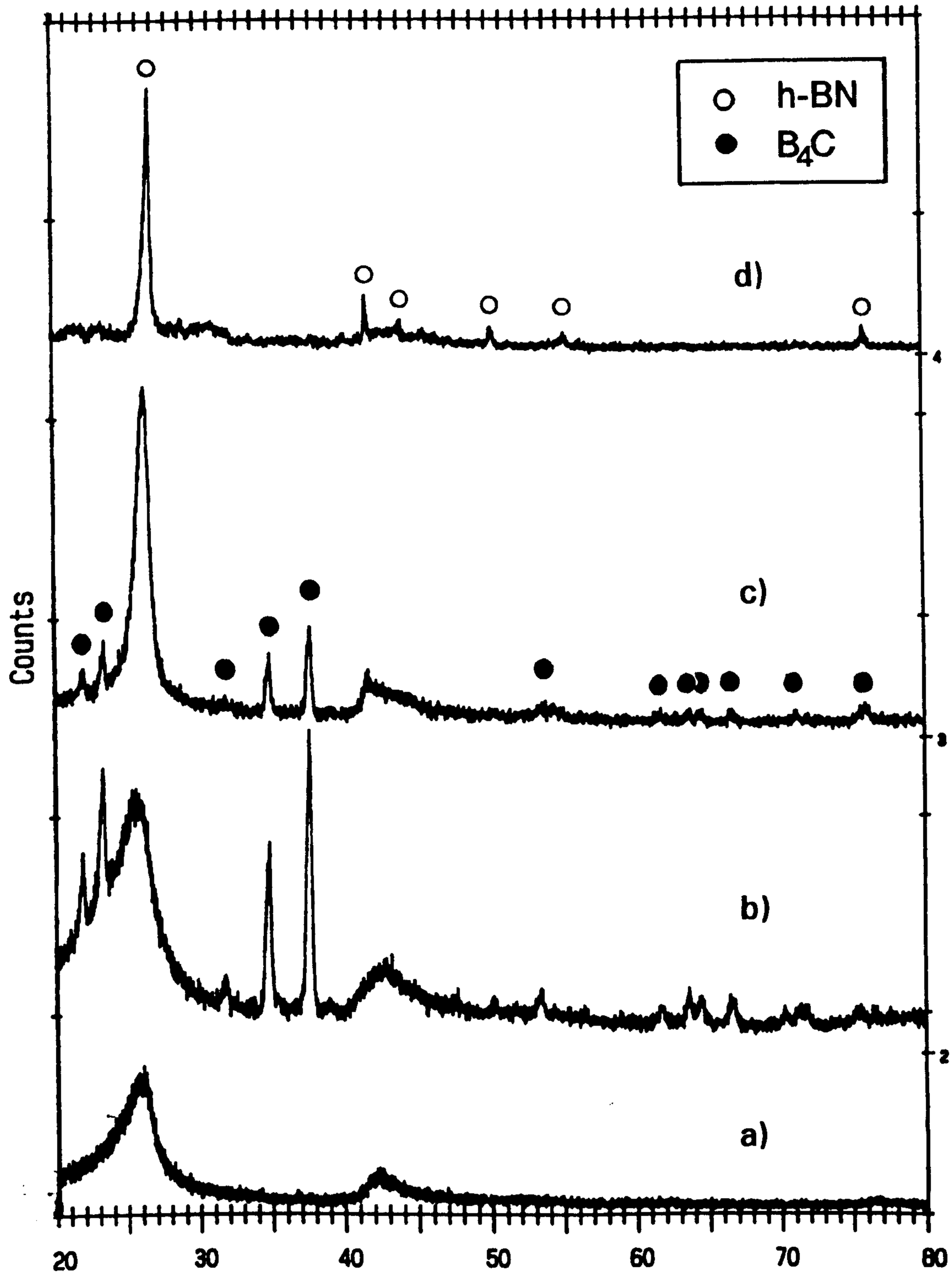

Figure III-9. X-ray diffraction patterns of boron nitride and carbide.
((a) $B_2O_3 + 3C$, $N_2 + H_2$(50%), 1673K, 4hrs (b)$B_2O_3 + 4C$,
N_2, 1773K, 8hrs (c) $B_2O_3 + 3C$, N_2, 1673K, 24hrs
(d) $B_2O_3 + 3C$, N_2, 1573K, 4hrs. C:Activated charcoal)

Table III-10. The effect of reaction temperature and time on the phases produced. (Type of carbon used: activated charcoal. H_2 and N_2 compositions are indicated in the gas composition column of the table. Total flow rate of gas: 500 ml/min)

Start materials	Temp (K)	Time (hr)	Gas composition	Produced phases
B_2O_3+2C	1373	2	N_2	B_2O_3 glass
	1473	2		B_2O_3 glass
	1573	2		B_2O_3 glass
	1573	4		h-BN
	1673	2		h-BN, B_4C
	1673	24		h-BN, (B_4C)
B_2O_3+3C	1573	4	N_2	h-BN
B_2O_3+3C	1473	4	$N_2+H_2(50\%)$	a-BN
	1523	4		a-BN
	1573	4		a-BN
	1623	4		a-BN
	1673	4		a-BN
B_2O_3+4C	1473	8	N_2	a-BN, B_4C
	1523	8		a-BN, B_4C
	1573	4		a-BN, B_4C
	1573	8		a-BN, B_4C
	1673	4		a-BN, B_4C
	1673	8		a-BN, B_4C
	1773	8		a-BN, B_4C
B_2O_3+4C	1573	4	$N_2+H_2(15\%)$	a-BN
	1573	4	$N_2+H_2(35\%)$	a-BN
	1573	4	$N_2+H_2(50\%)$	a-BN
	1673	8	$N_2+H_2(15\%)$	a-BN

predicted thermodynamic equilibrium temperature (1316K, see Table III-6, reaction a)). At the end of the reaction, irrespective of the stoichiometric ratios of carbon to oxide shown in tables above, no free carbon was detected by X-ray powder diffraction pattern.

5.3 Effect of Reaction Time and Carbon Content in the Mixture

With a lower than 4 stoichiometric proportions of carbon to oxide in the mixture, the nitridation in nitrogen atmosphere at 1673K produced h-BN with B_4C phase within two hours of reduction. This was confirmed by X-ray powder diffraction technique. However when the experiment was allowed to proceed for a longer period of time, for example 24 hours, the relative intensity of boron carbide phase diminished significantly. This can be seen from the powder diffraction pattern shown in Figure III-9. Above oxide to carbon ratio of 1:3, there was no significant change in the relative intensities of the phases formed. We also did not observe any change in the degree of crystallinity of amorphous boron nitride phase.

Boron carbide phase appeared to be stable in all experiments with mixtures containing B_2O_3:C = 1:4. The carbide phase did not transform to BN neither with a change in temperature nor with time.

5.4 Investigation on the Relative Stability of B_4C Phase in the Nitriding Atmosphere

In this experimental investigation, the presence of boron carbide was particularly surprising since the phase is unstable in nitrogen atmosphere as discussed in Section 3 under the phase equilibria in the B-C-N-O system. For this reason a few verification experiments were carried out at 1673K. The B_4C crystal was heat treated in an atmosphere of nitrogen and hydrogen gas where the composition of the gas mixture was 50 vol% N_2 and 50 vol% H_2. The powder sample after heat treatment was analyzed by X-ray powder diffraction technique. By comparing the powder diffraction pattern before and after the annealing experiment, we observe a subtle change in the diffraction pattern. The powder pattern indicated that the carbide phase had become more crystalline. This could be only due to the loss of excess active carbon from boron carbide-residual active charcoal mixture. The crystallinity of boron carbide after annealing is known to increase and this has been recently reported by Thevenot.[87]

An additional reduction-nitridation experiment was also carried out. In this experiment, boric anhydride and active carbon mixture (1:3) was heated in a stream of nitrogen/hydrogen mixed gas for a short period of time (30

minutes). After this stage, the pellet was cooled down to room temperature from T = 1673K. The X-ray powder diffraction pattern confirmed the presence of boron carbide phase which coexists with a-BN.

5.5 The Formation of w-BN under One Atmospheric Pressure Condition and Elevated Temperatures

A few mixtures were tested with NH_4HF_2 and NH_4Cl_2 as ammonium-salt-halide agents in the gaseous phase in order to promote the nucleation of the wurtzite form of boron nitride during reaction. The reagents were either added into the starting mixtures or placed in the cooler part of the vertical tube furnace, so that the volatilisation can occur at a slow rate. In this way a halogen gas atmosphere could be insured for a longer period of time. In the first method, however, the volatilisation is expected to be spontaneous.

The summary of experimental conditions for the micrographs included in this section is given below in **Table III-11.**

Table III-11. Reduction of boric oxide with activated charcoal (AC) and graphite (Gr) in the presence of ammonium-salt-halide agents. (AC:50 wt%/Gr 50 wt% were added. The nitriding gas was nitrogen. Flow rate: 500 ml/min)

Photos	Pellet Mixture	Gas Composition	Phases Identified
Photo.III-1	$B_2O_3 + 3C$ (AC + Gr) 1673K, 24 hour	$N_2 + NH_4Cl$*	Graphite, B_4C, BN Whisker growth
Photo.III-2	$B_2O_3 + 3C$ (AC + Gr) 1673K, 24 hour	$N_2 + NH_4HF2$*	Graphite, B_4C, BN Whisker growth
Photo.III-3	$B_2O_3 + 2C(AC) + NH_4HF_2$ 1673K, 2 hour	N_2	BN, B_4C Whisker growth

(*: *The ammonium salts were kept in the cooler part of the vertical furnace for a slow volatilisation and the vapour was mixed with the incoming gas*)

After reduction, the reaction product was examined by X-ray powder diffraction and scanning and transmission electron microscopic techniques. In

the powder pattern, there was no significant evidence for the presence of either w-BN or c-BN. The scanning electron micrographs of the reaction product revealed the presence of moderate quantities of whiskers with diamond and blade-type cross-sections. These can be seen in **Photo.III-1**. They appear to be typically 30-40 μm long and 1-5 μm in cross-section. Additionally rhombohedral disc-like crystals also grew. Their shapes and sizes can be appreciated from **Photo.III-2** and **III-3**. The composition of these crystals are not precisely known. This is because the crystals appear to be made of light elements such as boron, carbon and nitrogen, which could not be detected by the energy dispersive technique. Although it was possible to quantify light elements by wavelength dispersion technique, this method required an extensive calibration for all lighter elements present in the crystal. It is for this reason the section has been left incomplete due to the lack of time.

An attempt was also made to analyze the unusual crystals by transmission electron microscopic technique. The bright field image was obtained in a 200kV microscope and the selected area diffraction pattern (SADP) was obtained to characterise the d-spacings of the crystals under examination. The diffraction spots were calibrated with alumina crystals and the camera length was accordingly corrected to obtain accurate values of d-spacings. These are shown in **Photo. III-4** to **III-7**. The figure insets are the representative SADPs. The d-spacings were determined and the corresponding diffraction vectors are shown on the respective schematic diagrams of the SADP. The hexagonal symmetry of the diffraction vectors is similar to the diffraction pattern of (111) planes of the fcc lattice for carbon diamond and c-BN crystals reported by Angus[137] and Walmsley[138]. The SADPs in **Photo III-4** insets agrees well with both (002) planes of w-BN and (111) planes of c-BN crystals. The measured d-values for these SADP insets were 2.078Å and 2.089Å compared with the reported values 2.114Å and 2.087Å for (002) of w-BN and (111) of c-BN, respectively. Considering that the accuracy of d-spacings determined from TEM diffraction pattern is less than the X-ray powder diffraction pattern, the d-values fall satisfactorily within the reported d-spacings for the two metastable forms of BN crystals. Provided a large quantities of the metastable BN phases could be produced, it could not be possible to detect them by X-ray diffraction technique. The problem is further compounded by the fact that the lighter elements have a smaller structure factor therefore the diffraction intensities are significantly lower.

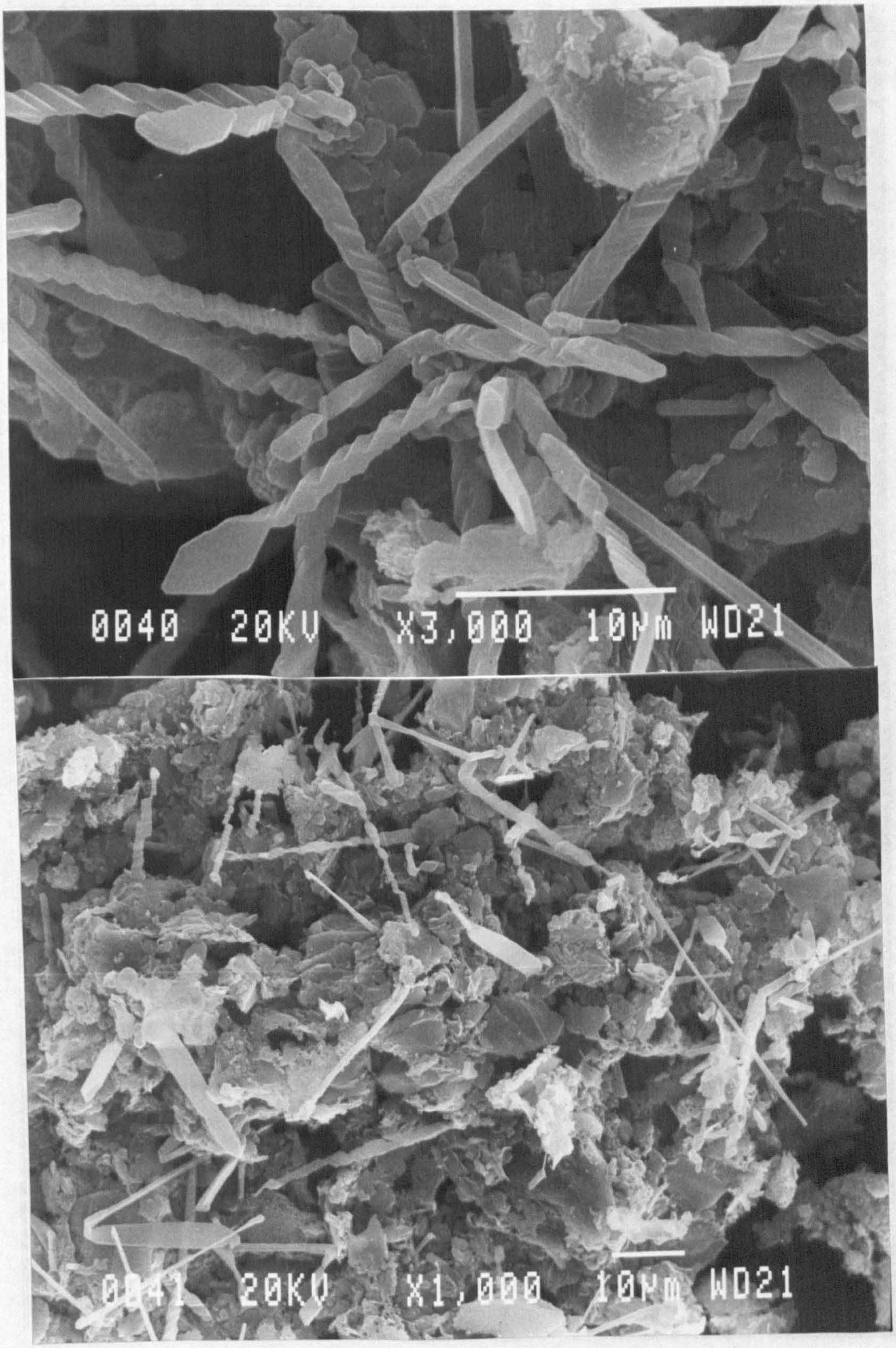

Photo.III-1. The scanning electron micrographs of the reaction product.
($B_2O_3 + 3C(AC + Gr)$, 1673K, 24 hour, $N_2 + NH_4Cl$)

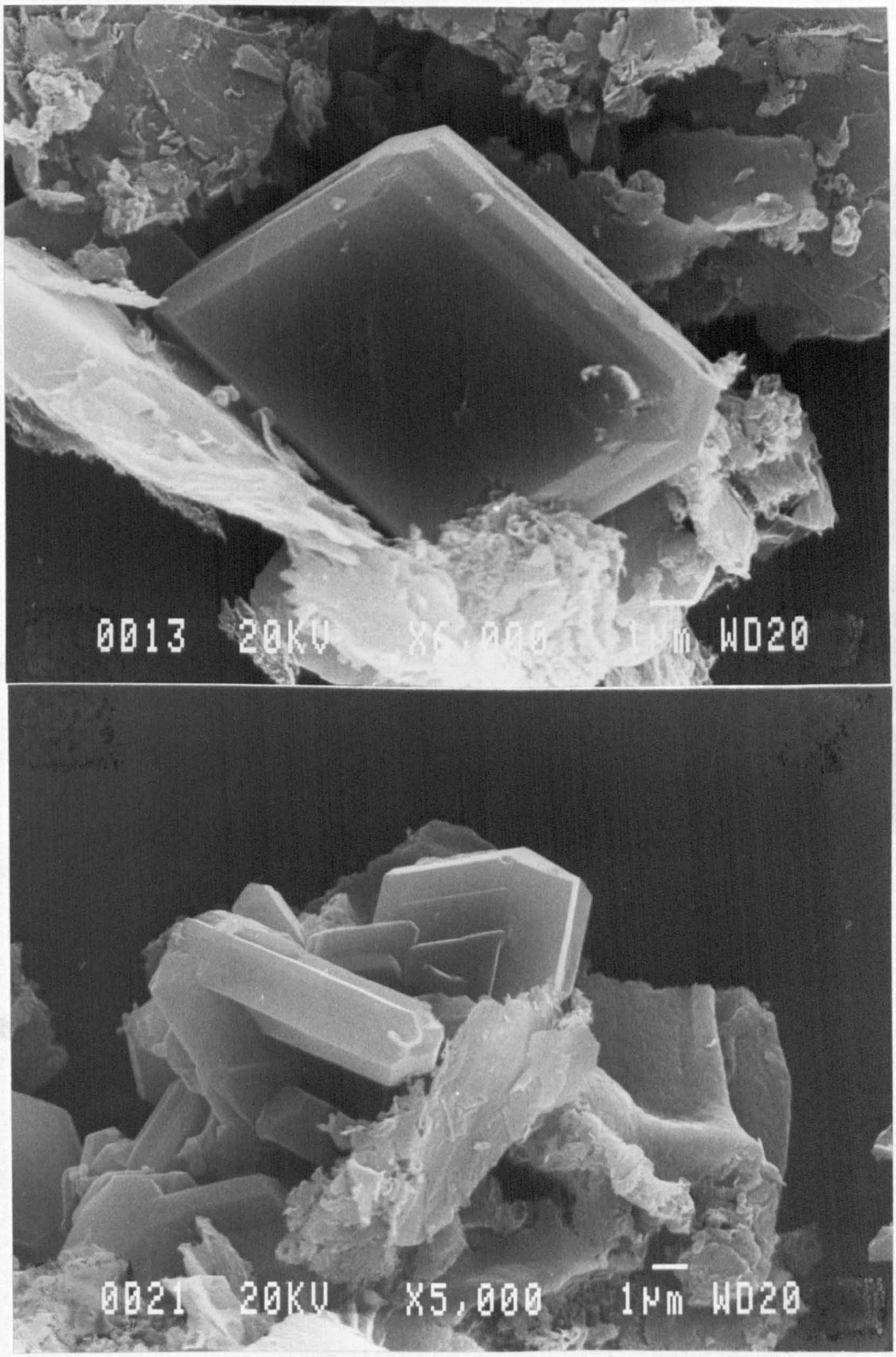

Photo.III-2. The scanning electron micrographs of the reaction product.
($B_2O_3+3C(AC+Gr)$, 1673K, 24 hour, $N_2+NH_4HF_2$)

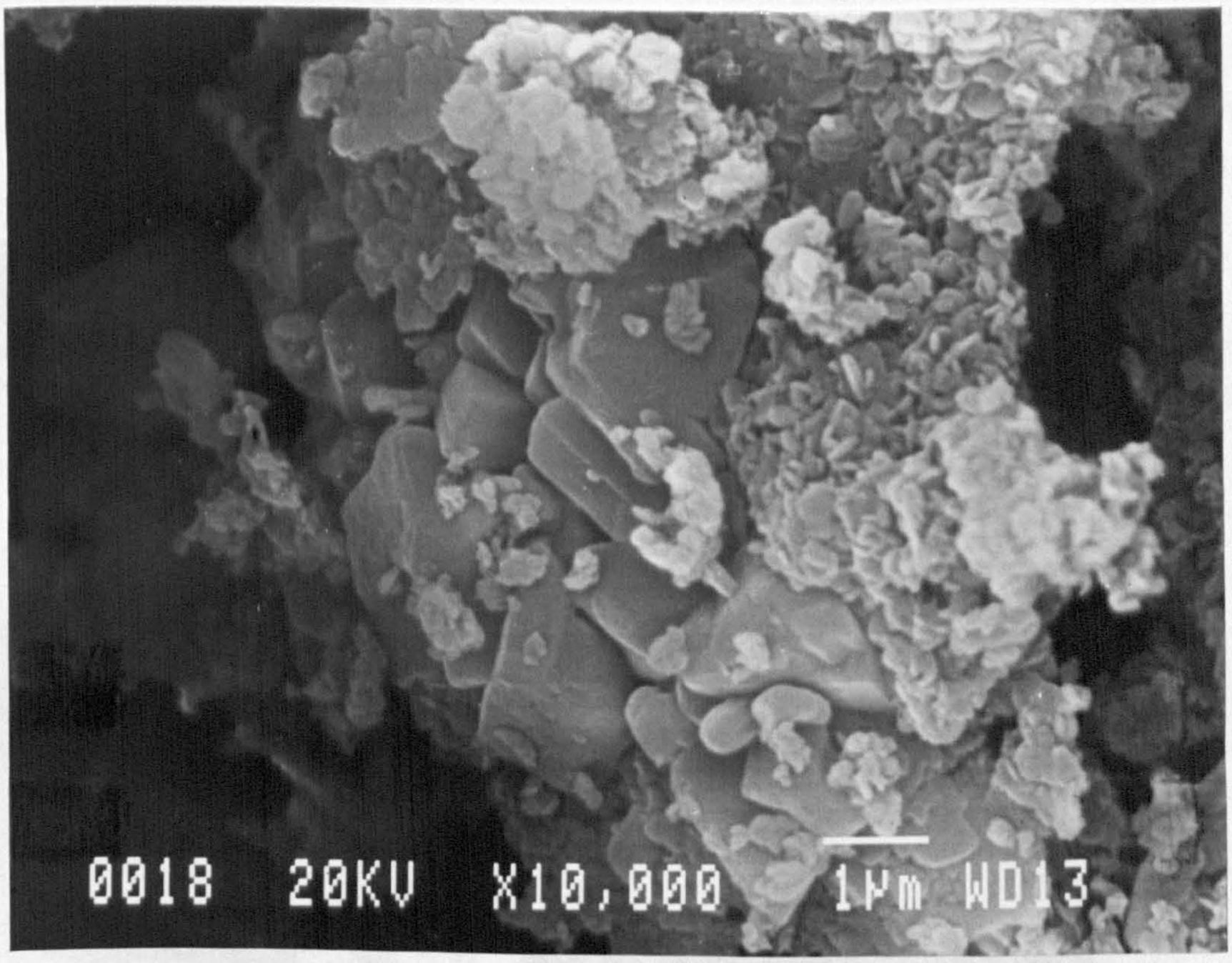

Photo.III-3. The scanning electron micrographs of the reaction product.
($B_2O_3 + 2C(AC) + NH_4HF_2$, 1673K, 2 hour, N_2)

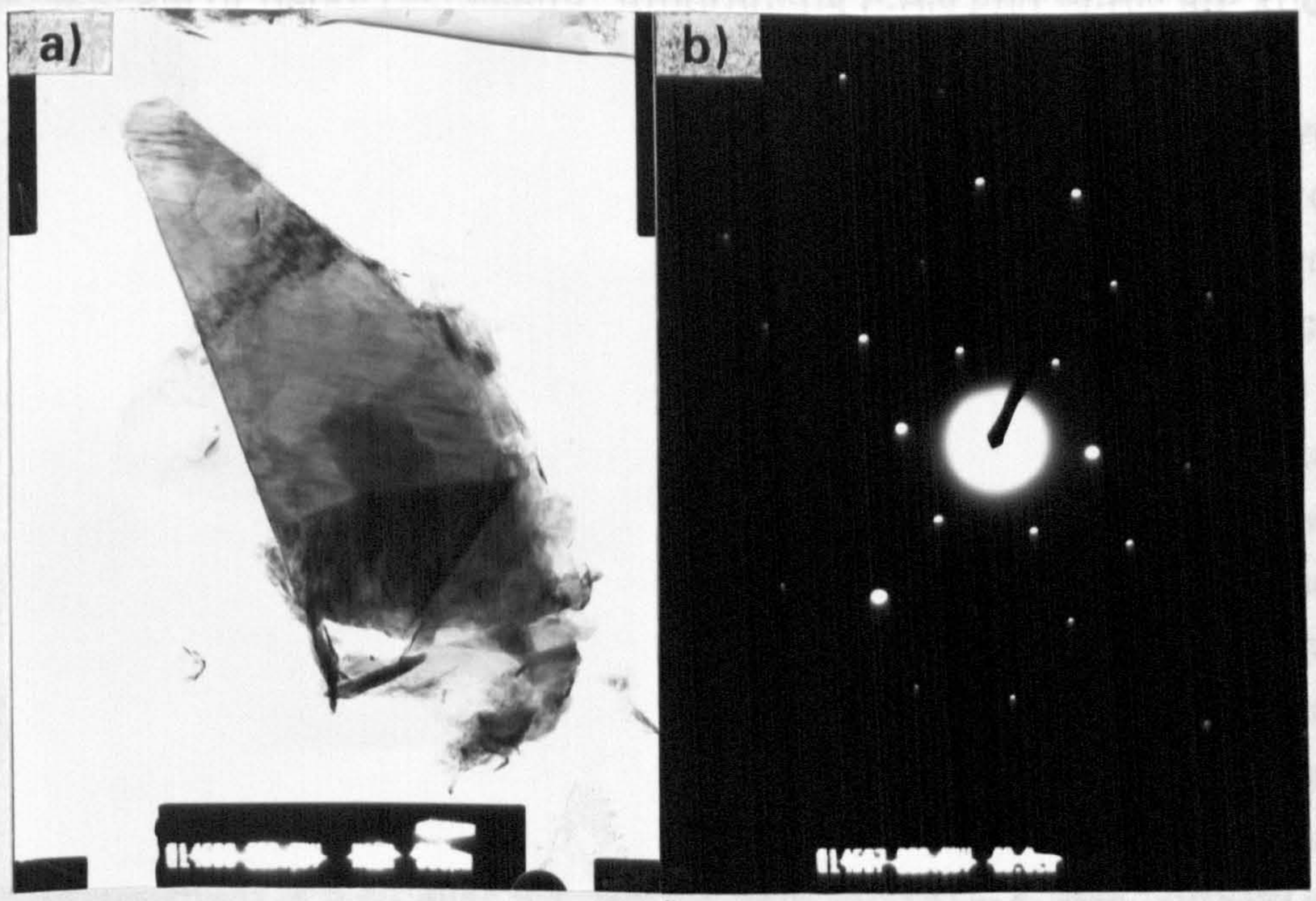

Photo.III-4. (a)Bright field image(x12k) and (b)selected area diffraction pattern.
(B_2O_3+3C(AC+Gr), 1673K, 24 hour, $N_2+NH_4HF_2$,

The SADP in **Photo. III-5** also shows the evidence for microtwins i.e the strong diffraction spot/weak-satellite-pair. The bright field image shows the contrast along the length of the whisker. There are three diffraction rings in the diffraction pattern. These ring patterns correspond to d-spacings, 2.09Å and 1.15Å. The outermost ring corresponds to the d-spacing of graphite for (112) planes. The central ring pattern could possibly due to either c-BN or w-BN and has a crystallographic relationship with graphite matrix. The ring pattern suggests nanocrystallinity of materials whereas their width point out the scale of nanocrystallinity. Amorphous c-BN and w-BN are known to form the vapour phase as reported by Kokudate et al.[139]

The transmission electron micrograph analysis also revealed some crystal structure information for the whiskers with rhombohedral cross-section. The bright field micrographs and selected area diffraction patterns are shown in **Photo. III-6** and **III-7**. The SADP of the micrographs confirms the presence of faults and stress accumulated in the crystals. These can also be ascertained from the streaking of the diffraction spots. It is likely that the whiskers have stress accumulated along the growth direction and this is not uncommon. A similar type of diffraction pattern was also observed during the growth of silicon carbide whiskers[83]. The d-spacings of these two types of crystals are shown on the corresponding schematic diagrams and the measured values do not agree with the reported d-values of either boron carbide or boron nitride. These we call the "*unknown*" crystals. The best approximant is a smaller B_4C lattice with $d(0\underline{1}1) = 4.39$Å, $d(003) = 3.90$Å and $d(012) = 3.69$Å (**Photo III-6**). The pure B_4C lattice has $d(0\underline{1}1) = 4.499$Å, $d(003) = 4.0330$Å and $d(012) = 3.783$Å. Other diffraction pattern in **Photo III-7**, the d-values are: $d(0\underline{1}1) = 4.34$Å, $d(003) = 3.91$Å and $d(012) = 3.68$Å. The d-spacing data based on boron carbide approximant hypothesis indicates that the composition of the crystals may be slightly different from c-saturated or B-rich B_4C. On the basis of the comparison of d-spacings of the approximant with that of the pure carbide phase, we find that on an average there appears to be a reduction of 2.5 to 3.0% in the cell dimension of the pure carbide lattice. Using the following relationship for the hexagonal crystal lattice (**Equation III-5**), the lattice parameters of the unknown crystals were determined and these are summarised in **Table III-12** below.

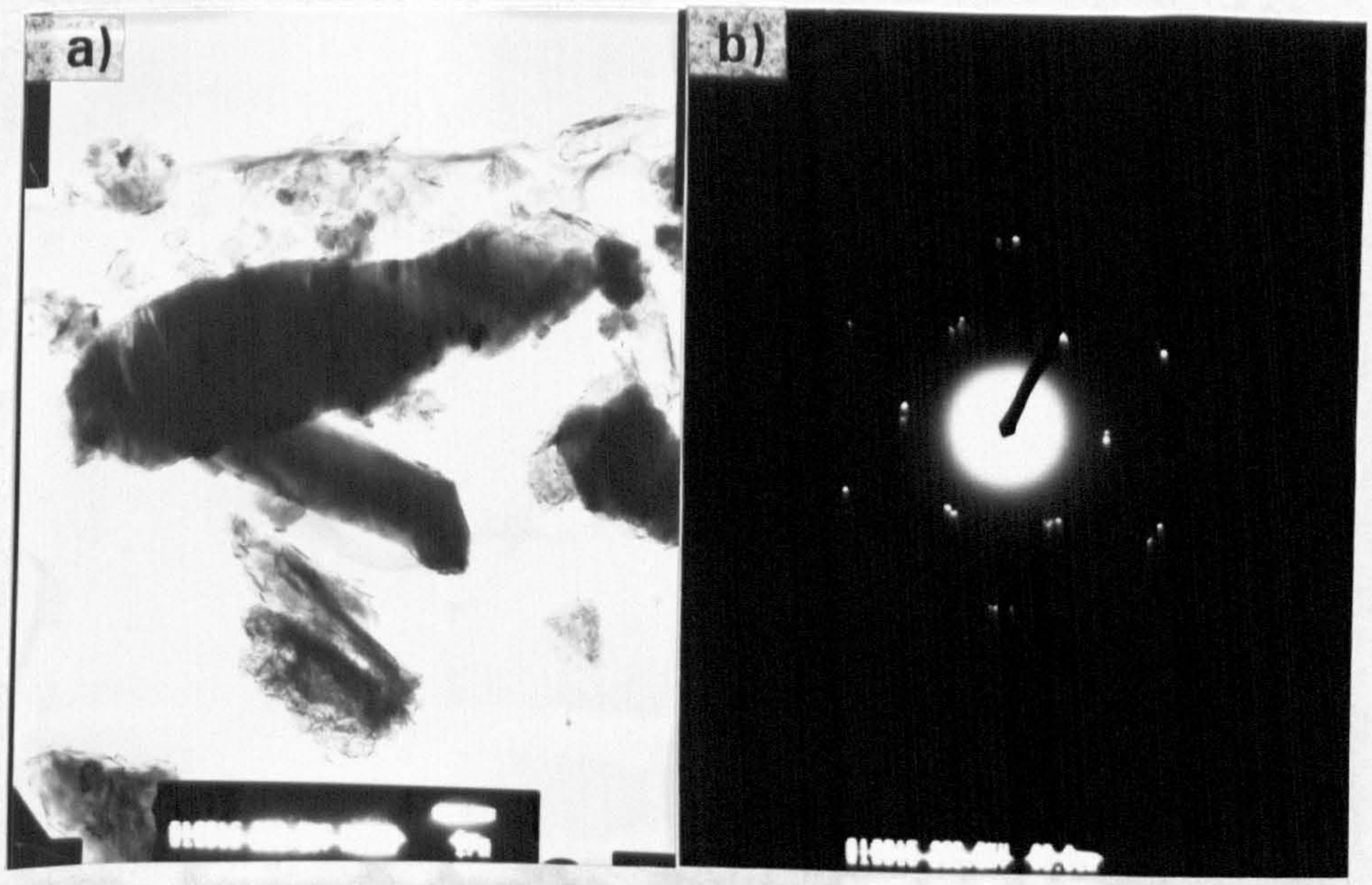

Photo.III-5. (a)Bright field image(x6k) and (b)selected area diffraction pattern.
(B_2O_3+3C(AC+Gr), 1673K, 24 hour, N_2+NH_4Cl,

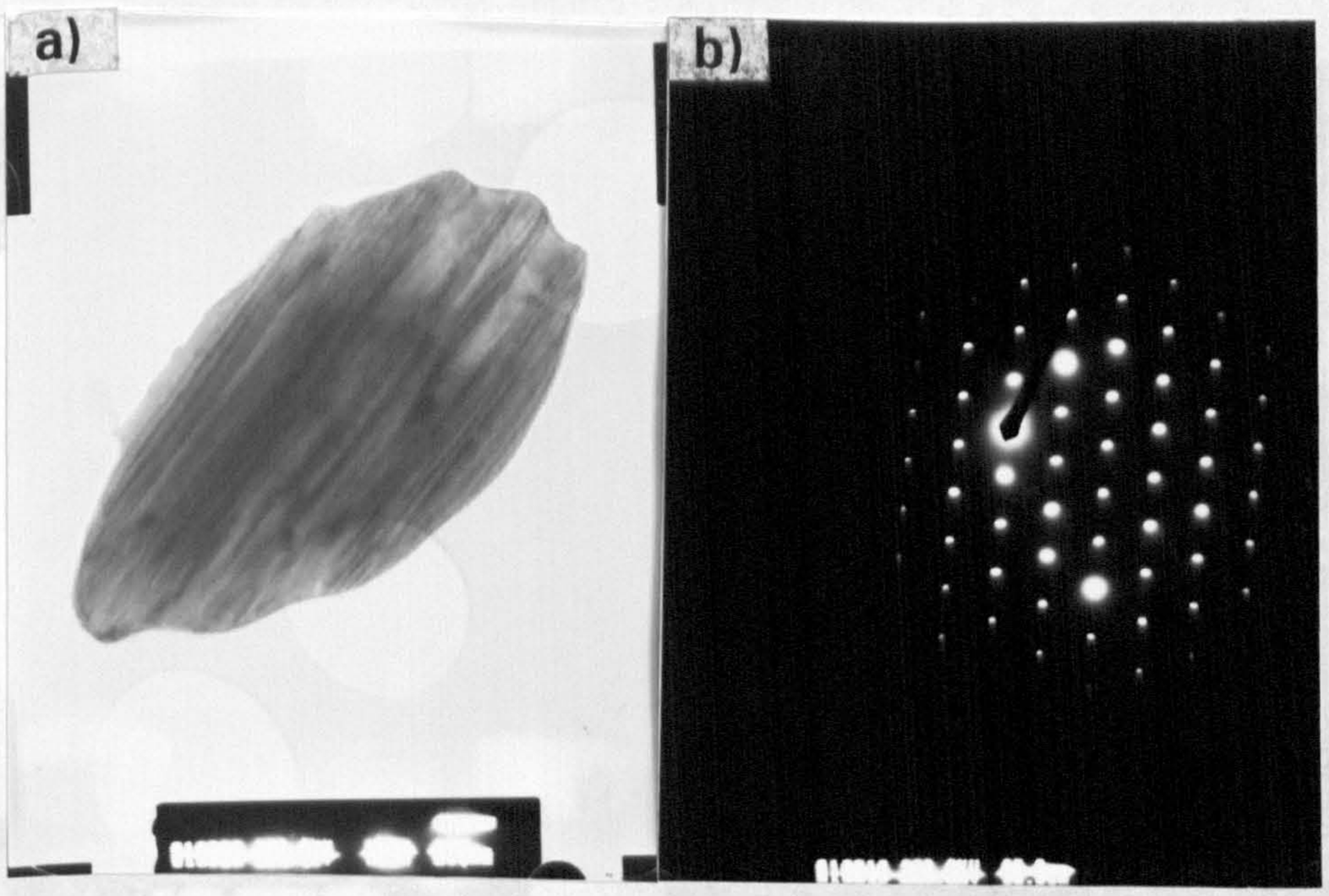

Photo.III-6. (a) Bright field image (x30k) and (b) selected area diffraction pattern.
($B_2O_3 + 3C(AC + Gr)$, 1673K, 24 hour, $N_2 + NH_4HF_2$,

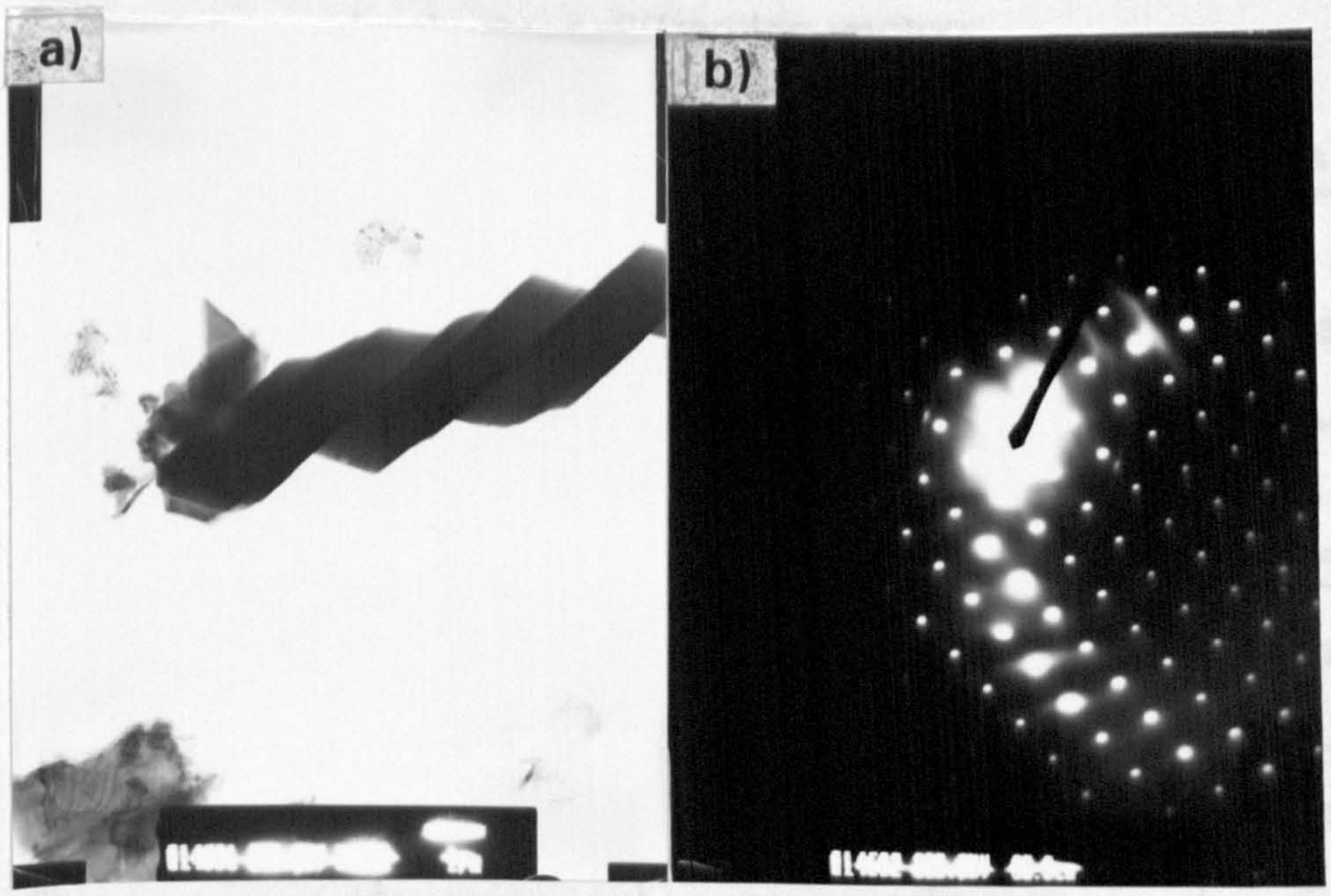

Photo.III-7. (a)Bright field image(x6k) and (b)selected area diffraction pattern.
(B_2O_3+3C(AC+Gr), 1673K, 24 hour, N_2+NH_4HCl,

$$\frac{1}{d^2} = \frac{4}{3}\left(\frac{h^2+hk+k^2}{a^2}\right) + \frac{l^2}{c^2} \qquad (3\text{-}5)$$

The Bragg reflection (003) permitted the estimation of the c-axis of the hexagon using the above equation whereas 0$\underline{1}$1 and 012 reflection with the value of c-axis yielded the value of a dimension. The 0$\underline{1}$1 reflection is a low angle reflection and has a correspondingly larger error. For a better accuracy of the lattice parameter results, we have used only 012 planes for the determination of the a-dimension. Unfortunately a similar procedure could not be adopted for c-axis from the SADPs shown above which permits the determination of only three diffraction vectors.

Table III-12. The calculated lattice parameter of unknown crystals. (10Å = 1nm)

Name	d spacing (Å)			lattice parameter (Å)
	0$\underline{1}$1	003	012	
B_4C C-saturated	4.499	4.033	3.783	a = 5.607 c = 12.095
Fig.III-6	4.38	3.90	3.69	a = 5.50 c = 11.70
Fig.III-7	4.39	3.91	3.68	a = 5.46 c = 11.74

5.6 Microstructural Evolution of Boron Nitride and Boron Carbide Phases during the Reduction-Nitridation of B_2O_3

The experimental conditions for the photo micrographs discussed in this subsection are summarised in the following **Table III-13** below. The table also includes the results from X-ray powder diffraction analysis from which the phases produced after reduction were identified.

The microstructure of the reaction product formed in nitrogen atmosphere, for example, are shown in **Photo.III-8, III-9** and **III-10**. In **Photo III-8**, we see the evidence for the nucleation of crystals. The "dotted phase" are the nuclei of h-BN which have formed on already-growing h-BN crystals.

In the microstructure shown below, the smaller nuclei grow into a mass of dense platelets (light-grey areas). Evidently the crystal nucleation and growth are occurring simultaneously. In this particular case, because the amount of activated charcoal used was only sufficient to convert B_2O_3 to BN (oxide:carbon = 1:3), towards the end of the reduction reaction, a few nuclei might have formed but were unable to grow. It is perhaps due to this reason that they stand out in the micrograph as a unique feature. By comparing the micrometer bar, it appears that the nuclei are in the 10-30 nm size range. Whereas growing crystals have over 200 nm to 2000 nm range.

Table III-13. Reduction-nitridation of boric oxide with activated charcoal (AC) and graphite (Gr) in the mixture. (The nitriding gases were nitrogen and ammonia. N_2 Flow rate: 500 ml/min at STD)

Figures	Pellet Mixture	Gas Composition	Phases Identified
Photo. III-8	$B_2O_3 + 3C(AC)$ 1573K, 4 hours	N_2	h-BN
Photo. III-9	$B_2O_3 + 4C(Gr)$ 1773K, 8 hours	N_2	Gra, h-BN, B_4C
Photo. III-10	$B_2O_3 + 4C(AC)$ 1773K, 8 hours	N_2	a-BN, B_4C
Photo. III-11	$B_2O_3 + 2C(AC)$ 1773K, 2 hours	$NH_3 = 50ml/min$ $Ar + 4\%H_2 = 100$ ml/min	h-BN, B_4C (B_4C was present in small proportions)

The growing crystals also appear to have rapidly sintered into larger clusters of 10 μm. This is evident in all micrographs of BN produced in a nitrogen atmosphere. The microstructures in **Photo III-9** reveal the presence of uniform size of B_4C crystals and pan-cake like graphitic structure (dark phase). H-BN appears brighter in the micrograph. The growth of whiskers are quite apparent from micrograph shown in **Photo.III-10**. The whiskers of BN and rhombohedral *'unknown'* crystals are growing from the mass of B_4C crystals. In the higher magnification micrograph, the growth of two types of crystals, namely "blade-shape" and rhombohedral facetted whiskers are apparent. There

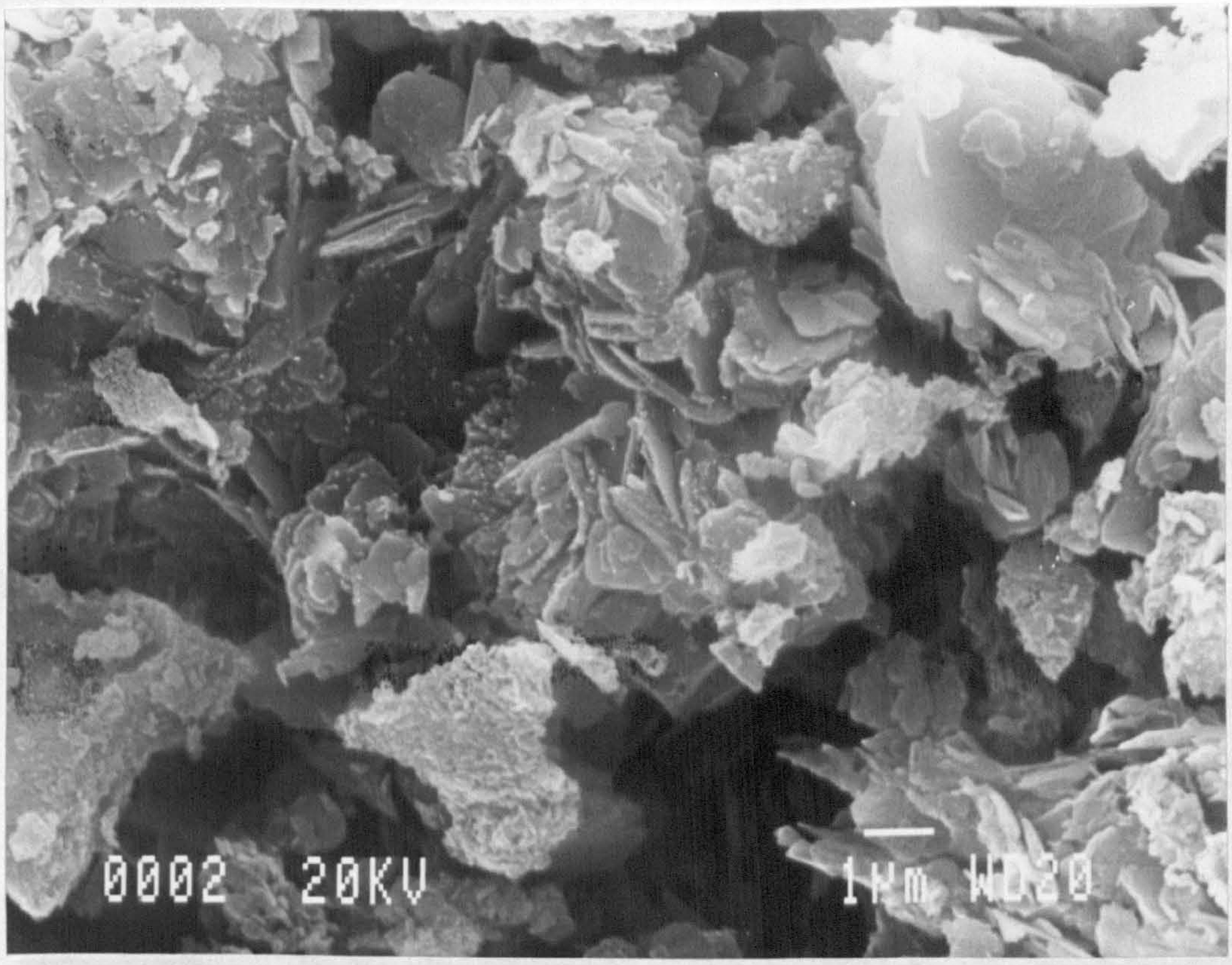

Photo.III-8. The scanning electron micrographs of the reaction product.
($B_2O_3 + 3C(AC)$, 1573K, 4 hours, N_2)

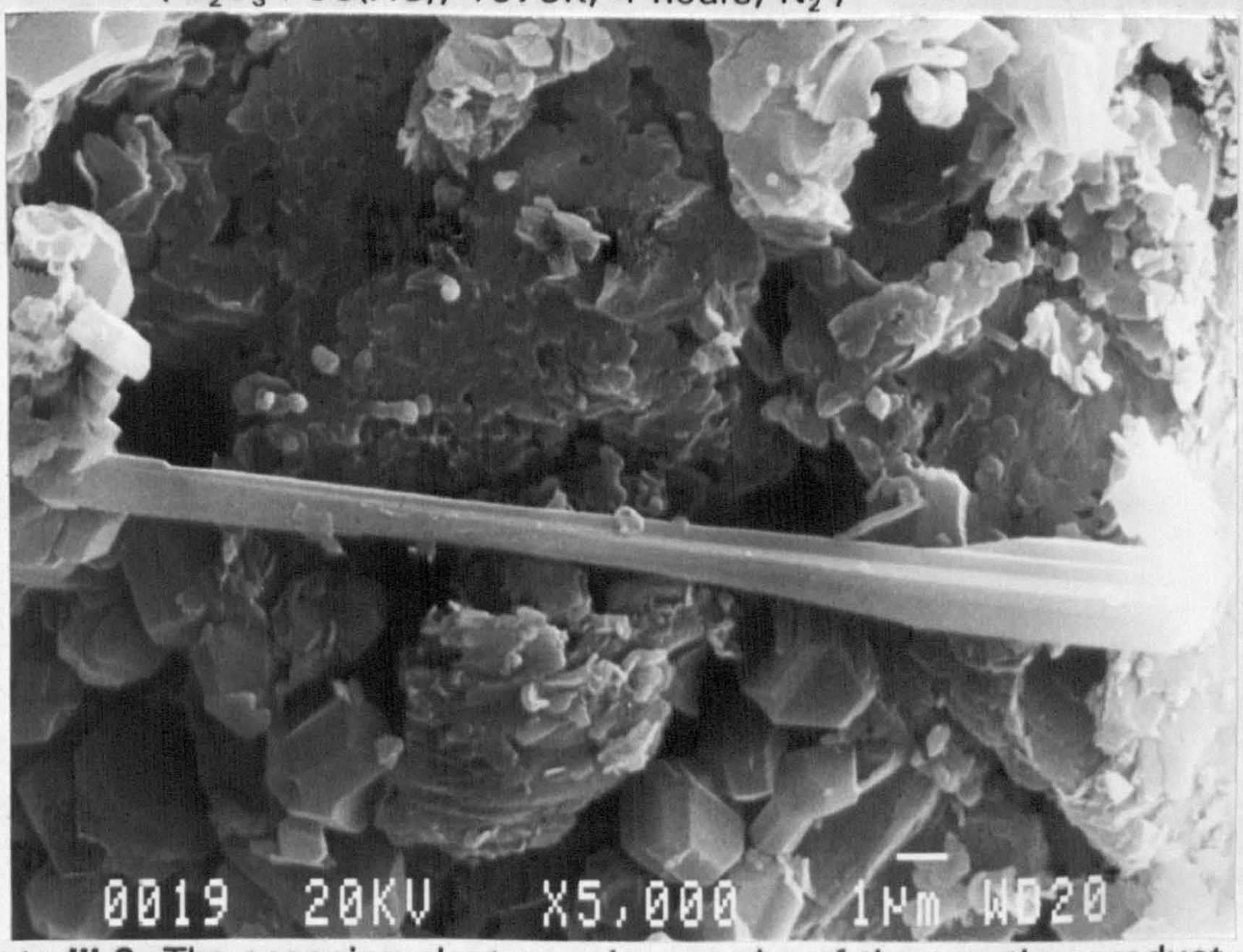

Photo.III-9. The scanning electron micrographs of the reaction product.
($B_2O_3 + 4C(Gr)$, 1773K, 8 hours, N_2)

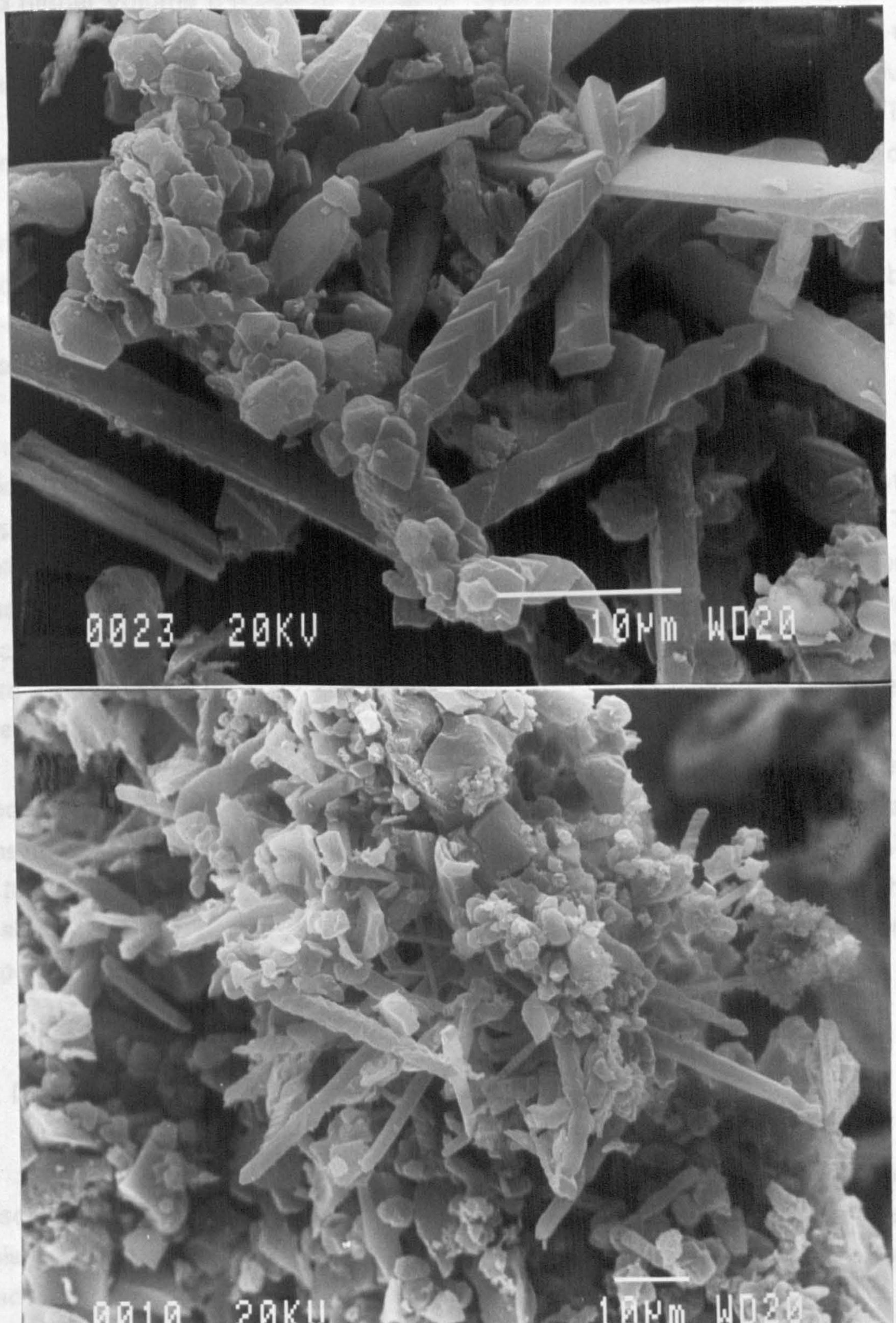

Photo.III-10. The scanning electron micrographs of the reaction product.
(B_2O_3+4C(AC), 1773K, 8 hours, N_2)

is a higher volume fraction of the latter type in the micrograph.

Photo.III-3 is a micrograph of h-BN and B_4C crystals produced in the presence of ammonium hydrogen fluoride. The experimental details are given in Table III-11 in section 5.5. No whisker growth was observed. The micrograph reveals that h-BN crystals have formed from B_4C crystals and due to the lack of sufficient amount of carbon in the starting mixture, the conversion appears to be incomplete. The main difference in the microstructure and Photo.III-8, III-1 and III-2 was the amount of carbon present which is essential for complete conversion as well as for the whisker growth process.

Photo III-11 show the microstructure of BN crystals produced in the ammonia atmosphere. The micrographs are in sharp contrast with the microstructure produced from N_2 gas atmosphere. The nucleation of crystals appears to be occurring heterogeneously along "tubular-like" columns. The hole in the along the growth axis is evident. There are much larger number of nuclei of h-BN in ammonia atmosphere than with nitrogen as shown above in the micrographs. Also the nuclei in NH_3 atmosphere have grown at a faster rate than with nitrogen gas. The dense crystalline mass produced underneath the growing nuclei are typically 50μm.

Literature[140] has cited an article that tubular carbon whiskers grow under the presence of high chemical potential of carbon in the vapour phase. The morphology of tubular h-BN appears to be similar. While producing h-BN in NH_3, we have also noticed the formation of tubular carbon whiskers which is shown in **Photo III-12.** The morphology of carbon whiskers is similar to that reported in the literature.

6. DISCUSSION

The reduction of boric anhydride (B_2O_3) under different conditions discussed above yielded boron carbide and various forms of boron nitride. In this section, the mechanism of formation of BN crystals and amorphous BN and the stability of B_4C under nitriding conditions will be discussed.

6.1 Mechanism of B_2O_3 Volatilization and Reduction in the Vapour State

Boron oxide (B_2O_3) has a tendency to volatilize above its melting point

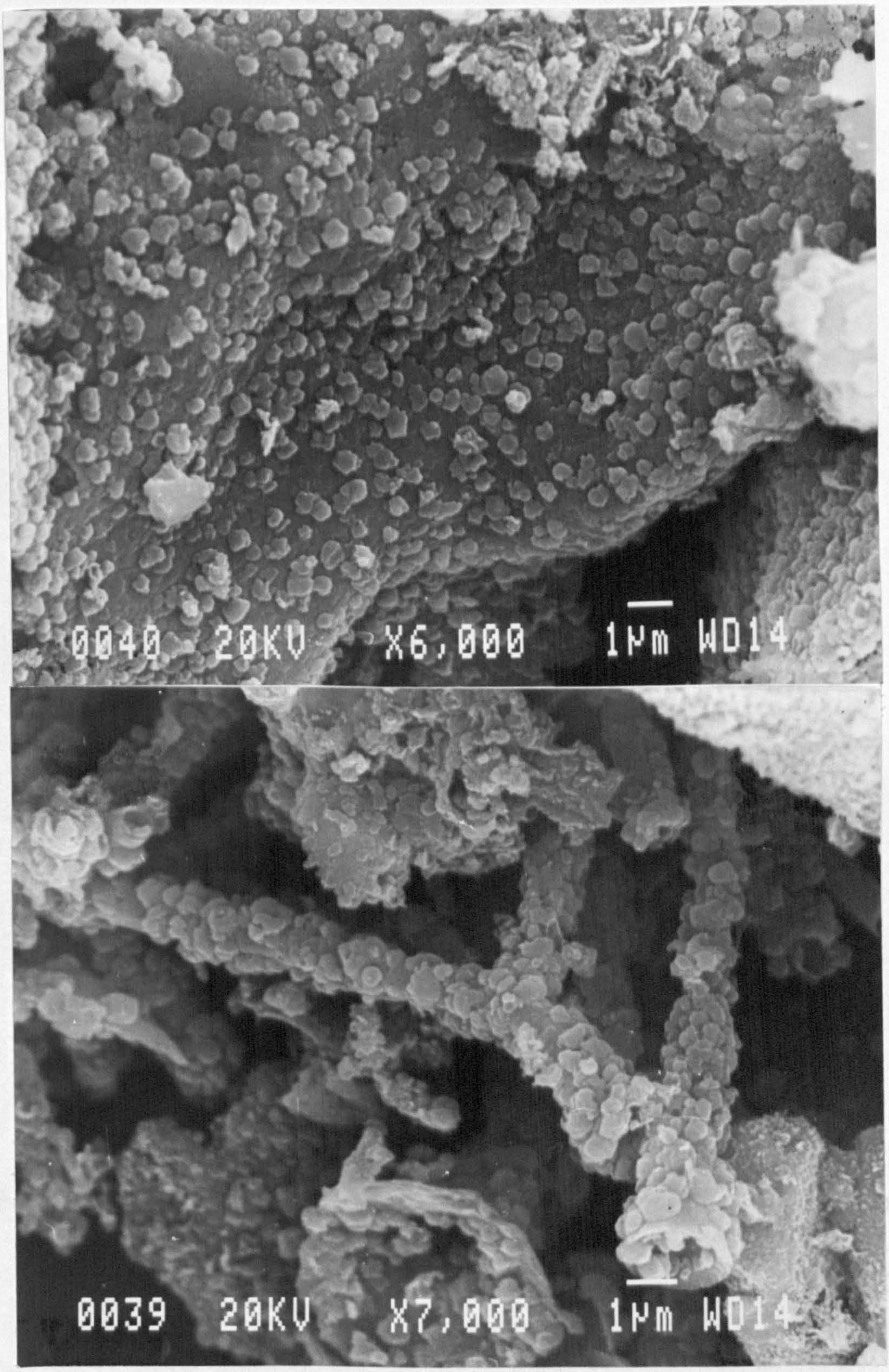

Photo.III-11. The scanning electron micrographs of the reaction product.
($B_2O_3 + 2C(AC)$, 1773K, 2 hours, $NH_3 + Ar/4\%H_2$,
$NH_3 = 50ml/min$, $Ar + 4\%H_2 = 100ml/min$)

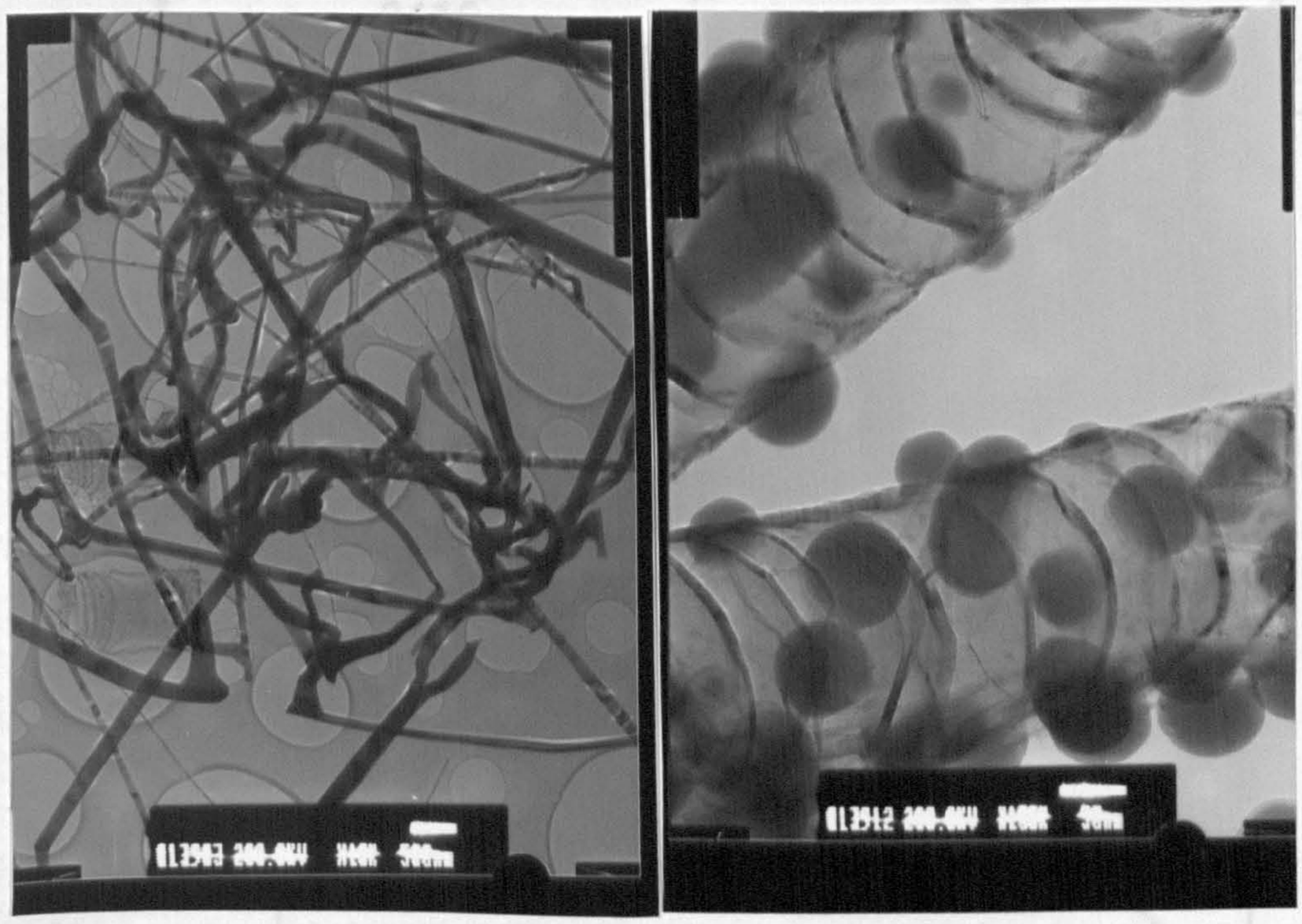

Photo.III-12. The transmission electron micrographs of the graphite whiskers produced in the NH_3(50ml/min) + N_2(350ml/min) at 1573K.
(B_2O_3 + 2C(AC), 1573K, 1hour, magnification:(a)10k,(b)100k)

Table III-14. The calculated values of vapour pressure of B_2O_3.

Temperature (K)	$P_{B_2O_3}$ (atm)
1463	4.935×10^{-4}
1543	4.935×10^{-3}
1946	1.480
2083	5.625
2273	23.69
2419	78.95

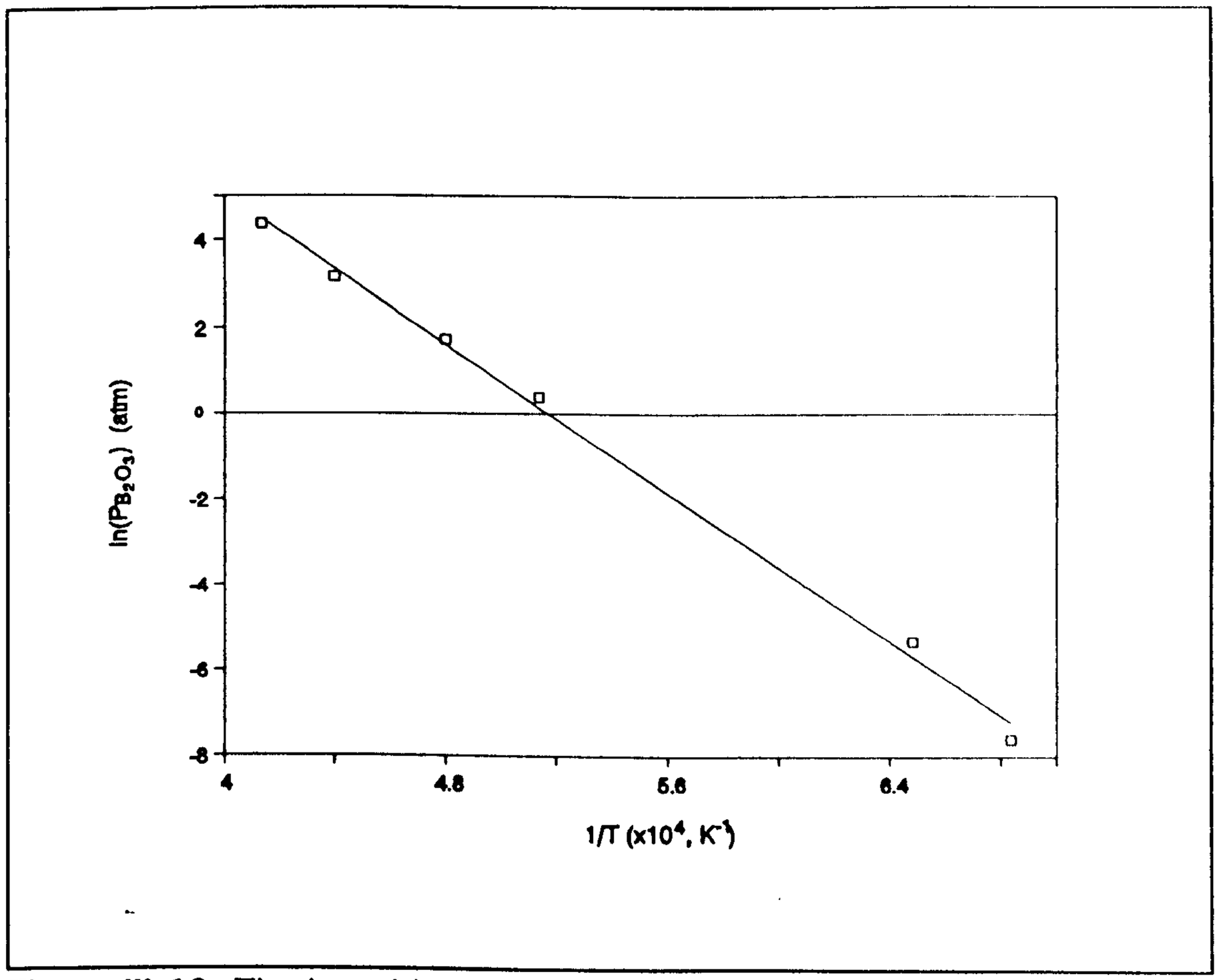

Figure III-10. The logarithm values of vapour pressure against the reciprocal of absolute temperature.

723k, and its vapour pressure can be expressed by the following mathematical relationship derived from the data given in reference [106]. The tabulated values of vapour pressure in atmospheres are given below in **Table III-14**. By plotting $\log(p_{B_2O_3})$ against the reciprocal of absolute temperature (T), the values of the enthalpy and entropy of evaporation can be derived for the volatilization reaction: $B_2O_3(l) = B_2O_3(g)$. The linear relationship is shown in

Figure III-9. The equation for the free energy of vaporization of B_2O_3 liquid to B_2O_3 gas is 360.053-0.186T kJ·mo1^{-1}·K^{-1}. The vapour pressure of B_2O_3 in the reaction chamber used for BN synthesis is going to be significant above 1423K. Most of our experiments were carried out well above this temperature. There is another likely species of boron oxide gas that is commonly known as "BO" gas and has been reported to be stable only under reducing or inert gas conditions. "BO" gas can therefore form from B_2O_3 gas at elevated temperatures via $B_2O_3(g) + C = 2BO(g) + CO(g)$ for which the standard Gibbs free energy change is equals to 746.79-0.287T kJ·mol^{-1}. Experimental results from the reduction-nitridation suggest that the presence of above gaseous species in the reaction chamber is critical for the formation of BN and B_4C crystals. In the reducing atmosphere in the reduction chamber which is flushed with a stream of purge gas, the partial pressure of BO gas at a given temperature is determined by the presence of CO gas. At a constant temperature, as the value of CO partial pressure decreases, the pressure of BO gas in the reaction chamber will increase by following the equilibrium relationship:

$$K = \frac{(p_{BO})^2 \cdot p_{CO}}{p_{B_2O_3} \cdot a_C} \qquad (3\text{-}6)$$

provided the activity of carbon and B_2O_3 gases are arbitrarily fixed. It is therefore expected that each reduction-nitridation experiment corresponds to a unique BO, CO and B_2O_3 partial pressures because of a variation in the reduction parameters such as carbon content and temperature.

6.2 Formation of BN and B_4C During Reduction-Nitridation of Boric Anhydride at High Temperatures in N_2 Atmosphere

In the presence of a reducing agent, B_2O_3 gas reduces to BO gas as discussed above. The presence of BO gas provides a larger surface area for reduction reaction via which either BN or B_4C forms. The phase equilibria in the B-C-N-O system, discussed in section 3 of this chapter points out the regions of phase stability. In **Figure III-6**, the B_2O_3 vapour phase has not been considered and its presence will modify the phase fields. From our

experimental results, we propose the following mechanism for the formation of BN phase: The reduction of B_2O_3 gas to BO gas takes place at elevated temperatures ($T > T_{eq.}$). Once the BO gas is available, in the presence of unreacted carbon particles which are surrounded by a BO-rich gas, the formation of B_4C takes place. The presence of B_4C crystals in the powder diffraction pattern confirms our hypothesis. The formation of B_4C via BO gas takes place by:

$$4BO(g) + 5C(s) = B_4C(s) + 4CO(g) \qquad (3\text{-}7)$$

The B_4C reaction overwhelms the reduction-nitridation process in the initial stage of the reaction. This has also been confirmed experimentally by performing a short-time reduction-nitridation experiment discussed in the subsection 5.4. Our experimental results also pointed out that when the proportion of carbon to B_2O_3 is less than 3:1, the relative intensity of the powder diffraction peak for the B_4C phase diminished with prolonged reduction time. This indicated that the B_4C was converting to BN phase (see Photo.III-3); the relative diffraction intensity of this nitride phase increased at the expense of B_4C. On the basis of these evidence, we propose that the initial period of reduction leading to B_4C synthesis is followed by conversion of B_4C to BN in the presence of the BO gas in the surrounding pore volume space.

$$B_4C + BO + 5/2N_2 = 5BN + CO \qquad (3\text{-}8)$$

$$\Delta G^\circ = -1,322,822 + 435.5T \ J \cdot mol^{-1} \text{ of } B_4C.$$

The BN formation reaction in equation (3-8) competes with the formation of BN directly from the BO and nitrogen gas:

$$BO + C + 1/2N_2 = BN + CO \qquad (3\text{-}9)$$

$$\Delta G^\circ = -361,380 + 90.7T \ J \cdot mol^{-1} \text{ of BN.}$$

The lowest temperature, at which the presence of BO, B_4C phase was confirmed, was 1473K. Below we have compared the partial pressure of CO gas at 1473K for reactions given in equation (3-7), (3-8) and (3-9). For unit activity of carbon and $P_{BO} = 10$ atm, an arbitrarily chosen value, the calculated

values of partial pressure of CO are 0.015, 1.2×10^2 and 1.4×10^{18} atm for (3-7), (3-8) and (3-9), respectively. From the comparison of calculated partial pressures of CO gas for the equilibria shown in equations (3-7), (3-8) and (3-9), it is evident that the reduction-nitridation of B_4C with BO in N_2 atmosphere will dominate the other two reactions after the initial stage. This is concluded from Le chatelier principle which points out that for the continuation of reaction in equations (3-7) and (3-8), the partial pressure of CO must be lower than 0.015 atm.

6.3 Reduction-Nitridation of B_2O_3 in the Presence of Carbon in Ammonia Atmosphere

The nitridation of B_2O_3 with NH_3 in a reducing atmosphere differs in two ways: (a) Firstly the partial pressure of nitrogen produced from decomposed ammonia is consistently higher than the partial pressure of pure N_2 used at 1 atmosphere pressure. This higher N_2 pressure favours the decomposition of B_4C phase i.e

$$B_4C + 4NH_3 = 4BN + CH_4 + H_2 \qquad (3\text{-}10)$$

$$\Delta G^\circ = -837{,}135 - 10.54T \ J \cdot mol^{-1}$$

During nitriding reaction with ammonia, an Ar-4%H_2 gas mixture was used. The reaction equilibrium suggests that at a constant temperature and fixed CH_4 and NH_3 partial pressures, the partial pressure of hydrogen, will be closely related with the activity of BN which means that the lower the value of P_{H_2}, the higher activity of BN phase leading to a higher rate of nucleation. This is evident from the micrographs shown in Photo.III-11. On the other hand, the nucleation rate of BN in nitrogen gas is expected to be much lower. In a similar way thermodynamically it can be proved that

$$B_4C + BO + 5NH_3 = 5BN + CO + 15/2H_2 \qquad (3\text{-}11)$$

is more favourable than equation (3-8).

6.4 Conditions for the Formation of a-BN, h-BN and w- or c-BN

The possibility of obtaining a wide variety of BN phase is the most attractive feature of the present investigation. Results detailed in section 5 indicated that the formation of a-BN was only possible when activated charcoal was present in the starting mixture and that too it must be present in quantities more than required from the stoichiometry (B_2O_3:C = 1:3).

In the presence of excess activated charcoal, which has a broken graphite-like network structure, boron nitride phase nucleates epitaxially on the surface of active carbon. The nuclei adopt the local structural order and then continue to grow as an amorphous phase. However, when the ratio of active carbon to oxide drops to 3:1 and lower, in the gas phase, the concentration of B_2O_3 species is expected to proportion of activated charcoal in the starting mixture. Due to this the BO concentration is expected to be lower. The higher concentration of B_2O_3 gas, which has an sp^2 hybridized molecular structure, promotes the formation of sp^2-hybridized h-BN structure. This appears to be a possible reason when graphite replaces activated charcoal, not only the relative concentration of B_2O_3 gas rises due to a slower reduction rate of B_2O_3 to BO gas, but also unreacted graphite favours the nucleation of sp^2-hybridized h-BN structure. When N_2 gas is replaced by ammonia, also having an sp^2-hybridized molecular structure, the formation of h-BN was observed. No amorphous phase was observed. Any amount of B_4C that forms in the initial stage of reduction gradually converts into h-BN phase.

In the results section, we pointed out that the w-BN and c-BN phases formed in the presence of ammonium halide salt vapour. Ammonium halide salts at high temperatures when decompose are likely produce NH_4^+ and F^- species in the gas phase. The presence of NH_4^+ species suggests that the tendency for the formation of c-BN and w-BN phases enhances significantly. Ammonium gas above 1000K, are less stable but they provide gas-phase SP^3 precursor for the nucleation of a metastable form of BN i.e c-BN and w-BN. The process of c-BN and w-BN formation is similar to the formation carbon diamond from CH_4 gas dissociation under reduced pressure. [140]

The conversion of B_4C to BN also offers a route for the formation of metastable forms of BN crystals. This is because some B-C bonds in the B_4C structure shown in Figure III-4 provide a precursor for the transformation of B-C bonds in B_4C to a sp^3 hybridized B-N bond in w- or c-BN. This is evident

from the results of the calculated lattice parameters of the hexagonal lattice of B_4C in Table III-12. The lattice parameter is smaller than the c-saturated B_4C in which the nitrogen atoms have replaced the carbon atoms. This means that the nitrogen atoms are possibly sharing 4-fold coordination bonds with boron atoms in the B_4C structure. So far we have no conclusive evidence that B_4C can be transformed into metastable forms of BN. For this further experimental work is required.

7. CONCLUSIONS

The effect of processing conditions such as the gas composition, reactivity of carbon, reaction temperature and time as well as the nature of starting materials on the synthesis of boron nitride and carbide phases were studied.

The reactivity of carbon, B/C ratio and gas composition are the most important variables that determined the formation, structure and morphology of nitride and carbide phase during reduction. In this study, it has been demonstrated that boron nitride and boron carbide powder and whiskers can be produced by carbothermic reaction. Depending on the composition of the gas, starting materials, temperatures selected and the time of the reaction, powders have different morphology. The proportion of nitride and carbide which has a composite microstructure can be controlled by selecting the processing parameters. Specially the use of ammonia halide salts promotes the formation of metastable forms of boron nitride.

CHAPTER IV. SYNTHESIS OF TITANIUM DIBORIDE AND COMPOSITES

1. INTRODUCTION

The selection of engineering ceramics is determined by favourable thermal, mechanical, thermo-mechanical or wear resistance properties. Metal diborides are one such material and titanium diboride falls in this category. Titanium diboride is a unique material because it combines many properties typical of metals and ceramics. In addition to its high melting point and hardness, the ceramic crystal structure has low electrical resistivities[141] and metal-like thermal conductivity. The material is virtually insoluble and wettable by most transition and groups II, III and IV metals. It resists oxidation to 1673K and is chemically inert to most harsh and corrosive environments. Titanium diboride with the combination of these unique properties is expected to be suitable as refractory alloy constituents and in protective coatings, metal evaporation boats, electrodes and wear resistant tools. Diboride films also have been examined for use as wear-resistant coatings, diffusion barriers, conductive layers and coatings on graphite fibres for use in aluminum composites. Titanium diboride, TiB_2-TiC, and TiB_2-SiC composites find applications as protective coatings, cutting tools, pump parts in the chemical processing industry requiring corrosion and wear resistant seals, lightweight armour material, components for advanced ceramic heat engines, rocket nozzles, parts of outer space structure, and for turbine technology. These applications which require advanced ceramic materials for their high temperature strength up to 2273K and toughness, resistances to thermal shock, low densities, high thermal conductivity and corrosion resistances, and all of which TiB_2 is superior to those of oxide ceramics. TiB_2-SiC composite material is one specific example of a high temperature composite material. The material can be machined by spark erosion or electrical-discharge technique.[142,143] TiB_2 and ZrB_2 have long been proposed for use in Hall-Heroult

cells in the electrolytic production of aluminium as they appear to have superior qualities compared with the normal carbon cathode. This is partly due to the result of their improved corrosion resistance, higher electrical conductivity and greater mechanical strength. A particular advantage of TiB_2 in such an application is its excellent wettability by molten aluminium. This is important for electrical conduction. A molten metal can react with a ceramic only if it is able to make intimate contact with it. It therefore follows that ceramics, which are resistant to wetting, will also be resistant to metal attack. However TiB_2 is readily wetted by molten aluminium but is outstandingly resistant to it. In mixed diborides such as TiB_2-CrB_2, it is thought that the corrosion resistance is further increased as Cr produces a passive layer in the structure by forming CrB_2. Both TiB_2 and CrB_2 have a C-32 structure, and intimately mix to form an extended solid solution. The solid-solubility of diborides therefore enables a significant improvement in oxidation resistance properties of the end members. TiB_2 and ZrB_2 are already used as thermocouple protection tubes in experimental aluminium reduction cells. Presently silicon and titanium carbides are synthesised independently before being mixed with the diboride prior to fabrication of the component.

Titanium diboride products are among the more expensive engineering materials. Firstly, it is difficult to synthesise these materials economically in a pure form. Secondly, the material characteristics of TiB_2 such as its hardness, inevitably lead to high manufacturing costs. At present there are several methods for the preparation of diborides and these are briefly described in Chapter I. The carbothermic reduction synthesis process with metal oxides however has not been studied in detail. In reference [15], the subject area has been only briefly studied. As illustrated in Chapter I and II, the economic benefits are also potentially realizable for the production of pure TiB_2 powders, mixed diborides and composite materials. In particular the diborides can be formed in the partially-densified geometries by adding suitable sintering agents such as high-melting point alloy phase that not only provides adequate bonding but also is expected to improve toughness of the composite materials. This is important for the fabrication of cutting tool inserts. Some powder

synthesis routes are rather expensive and also produce pyrophoric powders. The reducing atmosphere maintained in the carbothermic reduction process reduced the surface contamination of the titanium diboride powders.

In this investigation, an attempt has been made to establish the kinetic and thermodynamic aspects of boride synthesis. The mechanism of growth of TiB_2 particulates also explored and the effect of gaseous atmosphere on the morphological modification is discussed. Furthermore, the phase equilibria have been established for the synthesis of TiB_2/TiN, TiB_2/TiC, TiB_2/TiN/BN composite materials and a few phase field have been empirically verified. It is also presented the results of the formation of diborides and calculated phase equilibria in a mixed diboride system.

2. LITERATURE SURVEY

2.1 Introduction

Titanium diboride (TiB_2) has a high melting point (3063K), microhardness ($H_v = 3370$ $kg \cdot mm^{-2}$ and good electrical and thermal conductivities[144]. It is for these reasons that the material is called a highly refractory compound. The hot-pressed TiB_2 retains strength up to 2273K above which the high temperature creep leads to a substantial drop in the structural strength. The unique combination of properties offers the material a potential for a wider use as engineering ceramics in diverse applications discussed above. Prerequisite to the use of metal diboride for any of the above applications is the preparation of powder that is not only pure, but also has a controlled particle size, shape and state of agglomeration. The morphological factors affect and determine the physical and mechanical properties. TiB_2 has also some disadvantages, such as brittleness, low sinterability due to the low bulk diffusivity, anisotropic thermal expansion due to the hexagonal structure, and localised oxidation.

2.2 Structure of Borides

The borides are a unique group of interstitial compounds. Boron, as an interstitial atom, is relatively large, having a radius of 0.87 Å. The boron atoms in a lattice with other atoms still possess the strongly covalent bonding characteristics between them. This suggests that the basic metal lattice can undergo major modifications in terms of lattice parameters. If the metal to boron ratio is increased from M_2B to MB_{12}, the dimensions in which linkage of the boron atoms occurs increases from 0 (in the M_2B case) to 3 (in the MB_{12} case). **Figure IV-1** shows the sequence of B atom configurations.[145]

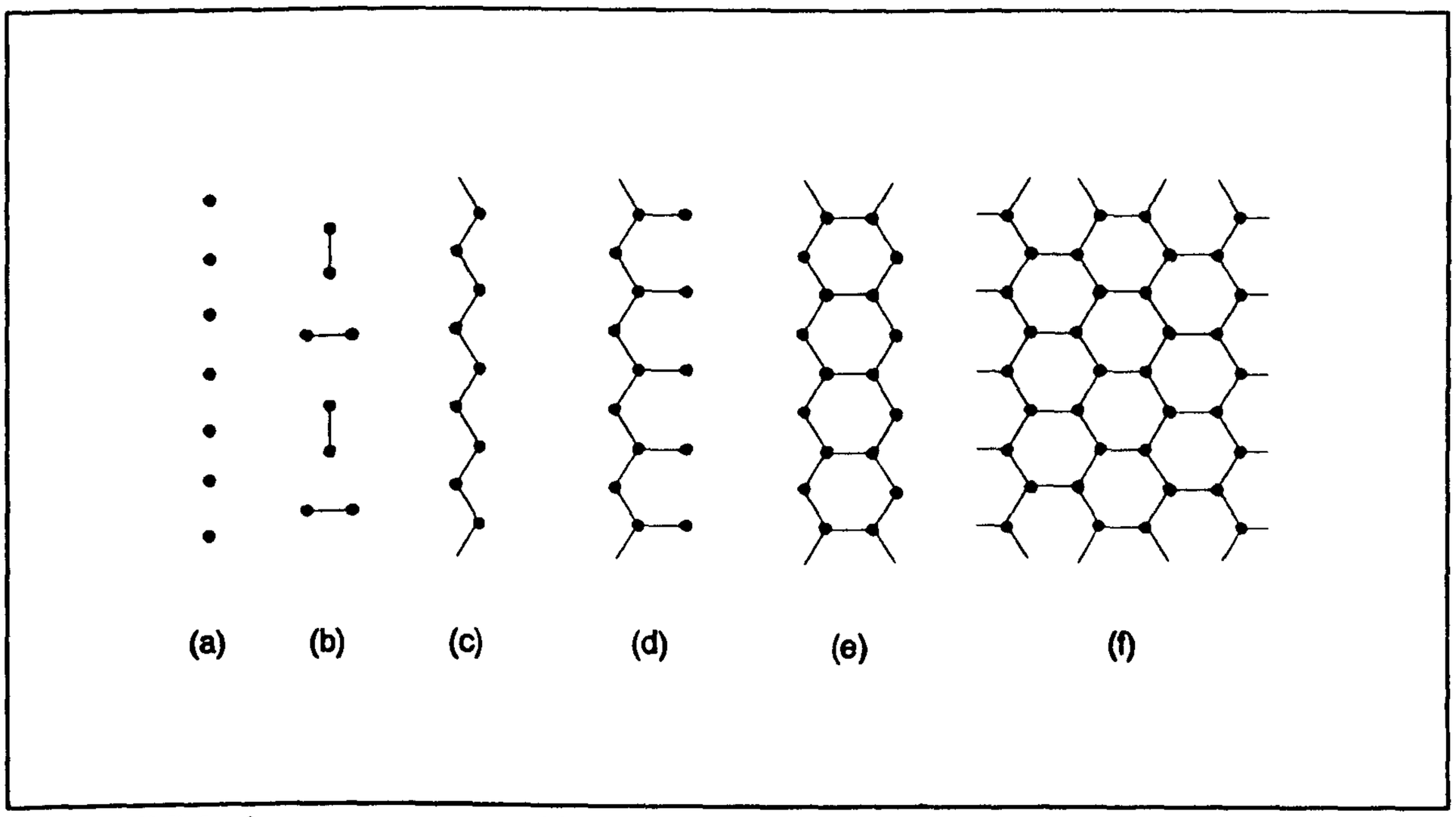

Figure IV-1. Arrangements of boron atoms in various phases. The boron atoms are (a) isolated, (b) form pairs, (c) zig-zag chains, (d) branched, (e) double chains or (f) net or three-dimensional networks.[145]

Titanium diboride forms type *f*, i.e, two dimensional nets of boron atoms. The metal-metal bond, however, still persists throughout and the most important properties are due to their essentially metallic character.[2] The thermal stability of TiB_2 is determined by the nature of its bonding. The B-B bonding is predominantly covalent whereas the Ti-Ti bonding is metallic. The Ti-B bonding

exhibits a mixture of covalent and metallic bonding and there is a simultaneous contribution of metallic and covalent bonding within the concerned and this therefore allows relatively simple geometrical structure.The boride structures are governed by size factor of the elements considerations to be made. Hägg[56] said that the atomic arrangement of interstitial phases is often related to the ratio of radii r_x/r_{metal}. Thus when the ratio has a value between 0.41 and 0.59, the metal atoms are very commonly cubically close packed with the non-metal atoms *(x)* located in the octahedral voids of the metal skeleton. For nearly all borides, the radius ratio exceeds 0.59 and in the few systems where it does not, some lower borides where the atoms are not in contact with each other, the intermediate phases are not isostructural as with the typical interstitial carbides and nitrides. Haggs rule, therefore, becomes less significant when boron-boron links are established. Higher borides demonstrate the strength of the boron-boron bond and the lattices of these compounds can be significantly altered. **Table IV-1** shows radii of two metallic and two non-metallic interstitial atoms.

Table IV-1. Radii of elements used.

Element	Goldschmidt metallic radius (Å)
Ti	1.45
B	0.87
Cr	1.28
C	0.77

As boron is the only electron deficient non-metal ($1s^2\ 2s^2\ 2p^1$), its bonding is a curious blend of types found in metals and non-metals. The boron-boron bonds formed by covalent chains and nets free electrons for transfer from the boron to the metal lattice and this is a major contributing factor to the properties of borides. MB_2 (AlB_2) type borides, TiB_2, CrB_2 etc, have hexagonal

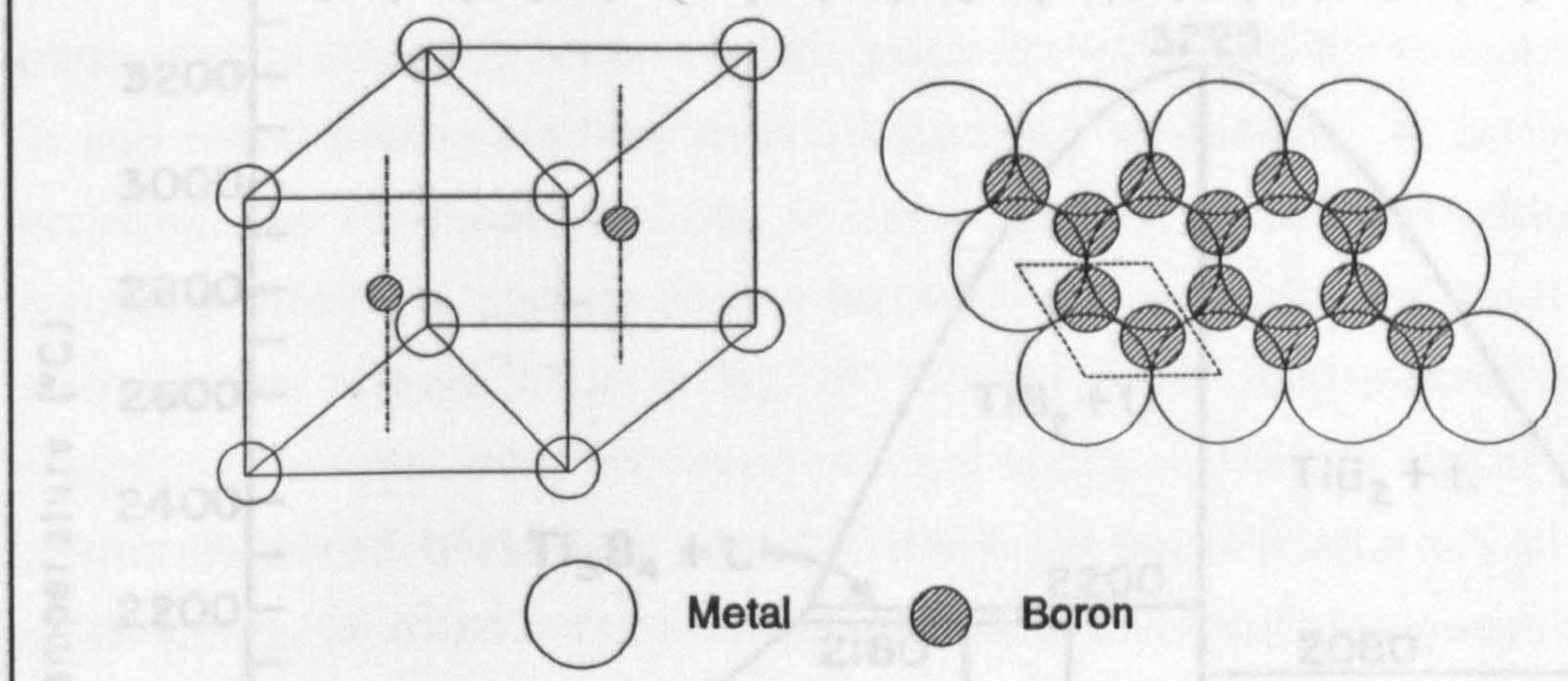

Figure IV-2. Atomic arrangement in an MB_2 type boride projected along c. (one unit cell is outlined by dashed lines).[147]

unit cells and the space group is *P6/mmm*. There are no variable atomic position parameters in this structure, the metal atom is at the origin of the unit cell (0,0,0) and the boron atoms lie along the long diagonal *a-a'* section of the unit cell at Z=1/2 i.e at 1/3, 2/3, 1/2 and 2/3, 1/3, 1/2 (**Figure IV-2**). The metal and the boron atoms are arranged in alternate planar hexagonal layers perpendicular to the *c* axis. Titanium diboride (TiB_2) has a primitive hexagonal unit cell structure of the C-32 or AlB_2 type and forms a network structure.The titanium and boron atoms lie in alternate planar layers. Each metal atom has six equidistant metal neighbours in its plane and 12 equidistant boron atoms, six in the layer above and six below the metal atom. Correspondingly each boron atom has three closest boron neighbours in its plane and also forms six boron-metal bonds. This structure can be regarded as alternating close packed titanium and boron layers with interstitial carbon and/or chromium incorporated. This may cause the boron layers to become puckered, although they still form network-layers. These plane layers are perpendicular to the hexagonal axis. Spear et al[146] produced a phase constitution diagram for the Ti-B system which is shown in **Figure IV-3.** Most of the diborides are very stable phases, readily formed when the appropriate amounts of metal and

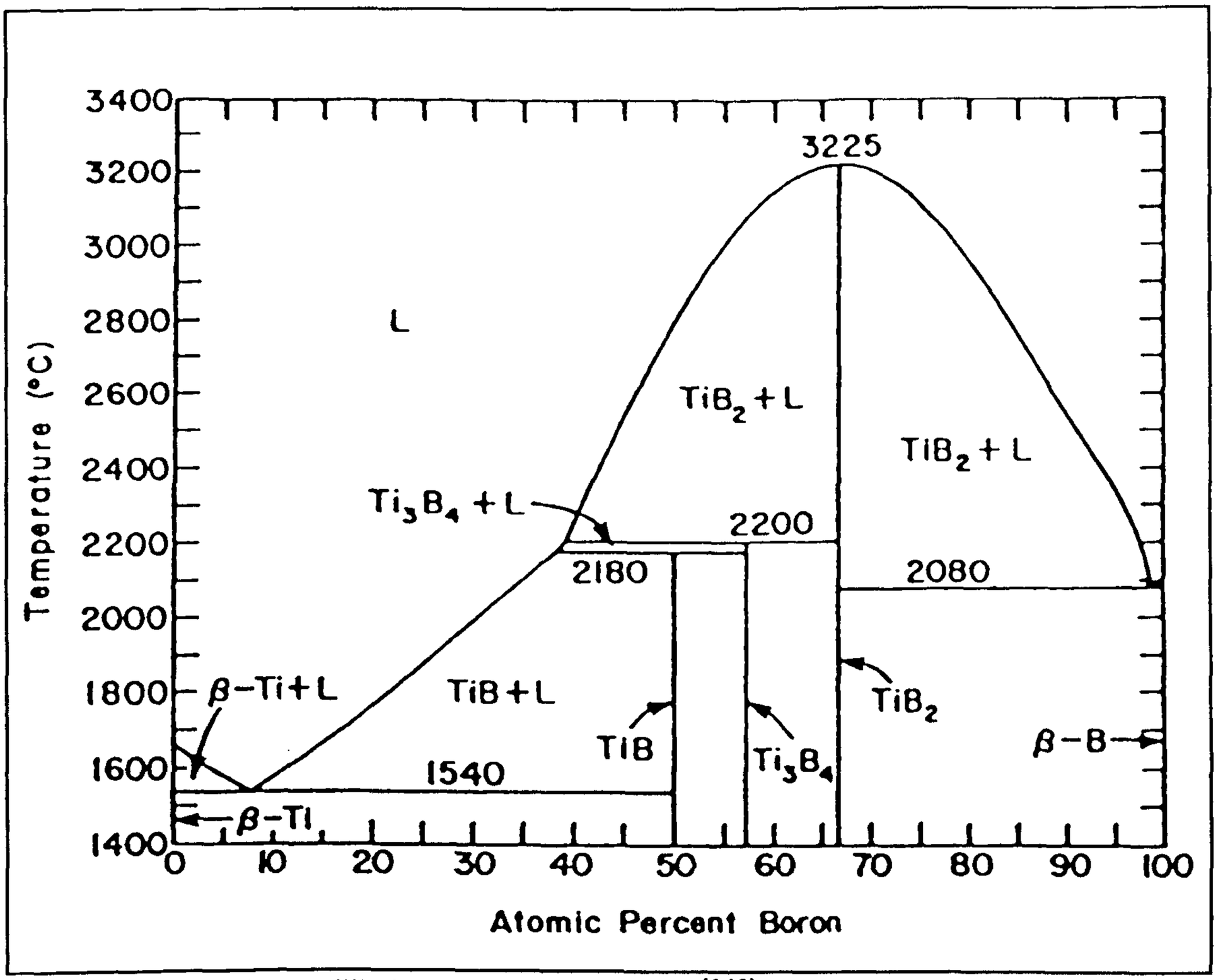

Figure IV-3. Ti-B equilibrium phase diagram.[146]

boron powders are mixed and heated. Among the transition metal borides, stability tends to decrease in going from group *IV* to groups *VI* and *VII* (titanium is in group *IV* and chromium in group *VI*) and also as the atomic numbers within these groups increase. **Table IV-2** shows some typical melting points for some diborides.

Table IV-2. Melting points of some diborides.

Metal	M.P. Diboride (K)	Metal	M.P. Diboride (K)
Ti	3093	Zr	3323
V	2673	Nb	3323
Ta	3473	Cr	2173
Mo	2373	W	2473

Post et al[147] investigated the structural characteristics and solid solubility of TiB_2 with eight other transition-metal diborides. They found that 100 mole percent solid solubility occurred if the percent radius ratio difference between Ti and metal atom was less than 15 percent. In contrast to co-cemented carbides, the toughness of TiB_2 is not improved by solid solutions. Solid solutions decrease grain-boundary mobility and suppress the formation of intermediate phases. The ability of TiB_2 to form solid solutions allows advanced ceramics with improved thermal shock resistance and strength to be manufactured. It has been postulated that the lattice anisotropy and elastic strain energy increase in the solid solutions and that they determine the grain-boundary cohesion in polycrystalline TiB_2.[148] Zdaniewski[148,149] has investigated the effect of solute additions on the lattice constants of TiB_2 alloys. It is reported that increased concentrations cause positive deviation of lattice parameter for various diborides and related this phenomenon to the valance of the solute and the size of the metallic radii.

2.3 Synthesis processes of diboride powders

High purity defect-free material is important for widespread applications. Narrow size distributions, spherical shape, and small particle size lead to better processibility and sintered bodies with improved physical and mechanical properties. Various methods of synthesis described above are defined by their corresponding chemical reactions in **Table IV-3.** *(A)* The first method is a two stage process.[9] In the first stage, the reduction of B_2O_3 with carbon yields boron carbide at 1723K via step (a) shown in Table III-3 whereas in the following stage, the reduction of TiO_2 with B_4C in the presence of excess carbon takes place at 2273K. High temperatures are required at both stages and the energy requirements are high. *(B)* The reaction of the metal halide gaseous phases in hydrogen plasma [10,11] yields TiB_2 and HCl gas. Again this is a two stage process. In the primary process $TiCl_4$ (a highly corrosive liquid) is produced by the reduction-chlorination of TiO_2. This is then used in the

Table IV-3. The chemical reaction of synthesis methods.

Reactions
(A) a. $2B_2O_3 + 7C = B_4C + 6CO$
b. $2TiO_2 + B_4C + 3C = 2TiB_2 + 4CO$
(B) a. $TiO_2 + 2Cl_2 + 2C = TiCl_4 + 2CO$
b. $TiCl_4 + 2BCl_3 + 5H_2 = TiB_2 + 10HCl$
(C) $TiCl_4 + 2BCl_3 + 10Na = TiB_2 + 10NaCl$
$Ti + 2BCl_3 = TiB_2 + 3Cl_2$
(D) $Ti + 2B = TiB_2$
(E) $2TiC(BH_4)_3 = 2TiB_2 + B_2H_6 + 9H_2$
(F) a. $TiO_2 + 3C = TiC + 2CO$
b. $B_2O_3 + TiC + 2C = TiB_2 + 3CO$
(G) $TiO_2 + B_2O_3 + 5C = TiB_2 + 5CO$

secondary process where hydrochloric acid is produced. These highly toxic and corrosive species pose many problems. Hydrochloric acid can combine spontaneously with chlorine (the reaction being explosive) further increasing the undesirability of this process. The energy is supplied to the reaction by means of a plasma arc or CO_2 laser and the installation of the equipment and running costs are considerable. Hydrogen is an expensive gas and is required in large amounts for the reaction to be viable. The operating costs are high and are escalated by the necessity for expensive corrosion resistant materials for the construction of processing equipment. *(C)* The dehalogenation of BCl_3 gas with sodium in the presence of Ti at 923K yields TiB_2 via exothermic reaction.[12,150] *(D)* The self-sustaining exothermic reaction between metallic titanium and amorphous boron has been tried in the laboratory for the synthesis of TiB_2.[14] The method also yields sub-borides. The process seems simple, however, it is expensive due to the requirement of high vacuum installations plus the cost of pure Ti and B powders. The rate of reaction is low as it is kinetically controlled and requires the raw materials to be in a fine

powder form to provide a large surface area. *(E)* Thermal dissociation of metal borohydrides was attempted by Gallagher et al[9] for the formation of various diboride powders. The metal borohydrides, which are very soluble in aromatic and aliphatic hydrocarbons, decompose to the corresponding metal diboride upon heating. At 1673K the reaction took 2 hours and the powders produced were sub-micrometer with a narrow size distribution. It was shown that the powders produced were amorphous when formed, but could be crystallised by heating to around 1773k. A major hazard in using sub-micrometer TiB_2 powder is its pyrophoric nature which makes it extremely hazardous to work with. *(F)* Reduction of boron oxide by metal carbide and carbon.[151] This is a high cost two stage process involving the primary production of titanium carbide. The reactions take place above 1773K. *(G)* In the carbothermic reduction of TiO_2 and B_2O_3, the boride crystals form above 1673K and CO gas evolves.[15] It is a single stage process and the by-product, CO gas, is a useful source of energy. The raw materials cost is significantly lower than for those process described above.

2.4 Densification

It is generally acknowledged that densification of pure titanium diboride ceramic to a reasonably high sintered density is difficult due to its low diffusivity and high melting point.[152] Because of this, it has been impossible to obtain a sintered body with greater than 90% theoretical density using commercially available TiB_2 powder.[153] Previous work has shown that small additions of nickel or iron in TiB_2 can enhance the densification of the ceramic using pressureless sintering or hot-sintering.[153,154] The incorporation of Ni as a densifying aid encourages the formation of a liquid phase and enhances the grain growth.[2] This allows hot-pressing to be performed at 1673K rather than the usual 2273K necessary for pure TiB_2 ceramic densification. The small additions inhibit grain growth incurred at high temperatures and limits the microcracking associated with larger grains. Cobb[155] investigated the

influence of titanium carbide as a sintering aid for TiB_2 on densification and found that it was useful for densification. Baik et al[156] examined effect of oxygen on densification of TiB_2 and results were compared between pressureless and hot-pressing sintering. The adverse effect of oxygen contamination found that oxygen promoted grain coarsening. They explained that the primary oxygen-bearing species, in the case of hot-pressing (1673K to 1973K), is B_2O_3. In the case of pressureless sintering (1973K to 2323K), oxygen remains primarily as titanium oxides, and suggested that the oxygen contamination level must be limited to less than 0.5 wt % in order to achieve theoretical densities and inhibit abnormal grain growth.

Titanium diboride components can be made either by cold-pressing, followed by sintering, or by hot-pressing. The sintering or hot-pressing can be performed under vacuum or in an inert or reducing atmosphere. The fabrication method which produces the highest density and therefore the most favourable mechanical properties is hot-pressing. However, the shapes and the range of size of artefacts produced by this method are limited. Since the products are extremely hard, they are difficult and expensive to machine after manufacture. Because of this, TiB_2 is commonly used in composite materials which contain smaller amounts of other materials, such as the nitrides of boron and aluminum. The minute additions are softer and can be formed by the same methods. The components are subsequently machined to shape. The composite materials are widely used in the form of crucibles and boats for the evaporation of aluminum in the vacuum metallising industry. The densification of TiB_2 by hot-isostatic pressing to produce near-net shapes has been extensively researched by Besson et al.[157] They studied the rheological behaviour of the powder and determined constitutive equations which were subsequently used in a finite-element program to simulate the forming of TiB_2 artefact by Hot Isostatic Pressing (HIP). Observed and calculated final shapes were compared, showing good agreement. Hot isostatic pressing was found to be an efficient way to produce high-quality ceramics.[157] The finite-element program calculated the residual stresses after processing as well as the remaining porosity. This enabled the processing routes and geometries of the

artefact to be obtained. Holcombe and Dykes[158] sintered TiB_2 to over 90 % theoretical density using a microwave sintering process. This was achieved using soak times of 30 minutes or less and sintering temperature of 2173K to 2373K. They found that a 3 weight % addition of CrB_2 inhibited excess grain growth, with typical grain size below 15μm routinely produced. Hardness and fracture toughness data indicated that microwave processing could yield a product equal to or better than conventionally-sintered material and much improved over hot-pressed material. It is, however, believed to be a relatively high cost process. Miyamoto et al[159] adopted a high pressure self-combustion technique and they produced 95 % of theoretical density of TiB_2 compact by this method. Densification occurs by self-diffusion requiring a high grain boundary surface area, i.e a small grain size, to reach theoretical density.

Much work on the strength related properties of titanium diboride ceramics have been covered by Baumgartner and Steiger.[13] They produced greater than 99% of theoretical density of TiB_2 sinter by use of a submicrometer-sized powder produced in an arc plasma. This was achieved using a pressureless sintering method. The physical and mechanical properties of various materials were measured. Microstructure and grain boundary stresses were also considered and were postulated, understandably, that internal stresses caused by anisotropic thermal expansion coefficients highly influence the physical properties of the material. It was also found that the influence on modulus, strength, and electrical and thermal conductivity are most pronounced if the grain size is large enough to induce microcracking. The activation energy for grain growth in titanium diboride is 1.02 $MJ \cdot mole^{-1}$.[13]

Mutual solid solubility readily occurs between some 27 metallic diborides. A problem arises in finding a stable metallic addition in order to promote the sintering process without detrimental effect on the properties of TiB_2. Solid-solution surface layers can be formed by the diffusion of a metallic element with atomic radius larger than that of the matrix metal so that the body can be strengthened by inducing surface compression.[160] This effect is similar to solid-solution strengthening or hardening of alloy where by the

substitutional alloying element depending upon the atomic radius either tension or compression in the crystalline lattice.

2.5 Properties and Applications of Borides.

The properties of borides are intimately associated with the electronic structure of the metallic components. On this basis, the borides constitute a group of ceramic materials with attractive and unusual properties. Their extreme hardness and high melting points resemble those of covalently bonded ceramics, while their high thermal and electrical conductivity, positive temperature coefficient of resistivity and lustre are typical of metals. At cryogenic temperatures some are superconducting. These unusual properties result from the simultaneous contributions of covalent and metallic bonding characteristics in the structure.[2] The temperature coefficient of resistivity is generally found to be positive, as expected of metallic conductors. Almost all borides, including those with a high non-metal content, have been reported as possessing metallic properties, the only probable exceptions being some hexaborides of the alkaline earth metals and the very boron rich borides, containing more than 90 at% boron. The most notable chemical property is its good corrosion resistance towards a number of molten metals. Because of its remarkable resistance to molten aluminium, despite being easily wetted by it, TiB_2 has been used for thermocouple protection tubes in molten aluminium reduction cells and has been considered for use as an electrode material.

Titanium diboride has good thermal shock resistance and has a mean coefficient of linear expansion of 5.9×10^{-6} K^{-1}. It can be used in air up to 1673K, and the rate of oxidation increases dramatically above this temperature. It is resistant to carburization up to 2273K.[161] Owing to their resistance to oxidation and creep, borides have found application in atomic reactor components, where resistance to both high temperatures and chemical attack becomes important. Bonded uranium borides have also been applied in this field. An attractive application of borides lies in fields where their

interconnecting role to other compounds serves well; such as in special ceramics, metal ceramics, transition joints or protective coatings for high temperature alloys. Titanium diboride also has a large crystallographic thermal expansion anisotropy. For instance, along the 'a' and 'c' crystallographic axis, the thermal expansion coefficients are $7.19x10^{-6}\cdot C^{-1}$ and $9.77x10^{-6}\cdot C^{-1}$, respectively.[162] The anisotropy produces considerable internal stress after hot-pressing due to thermal expansion mismatch between grains. These localized residual stresses are relieved by microcracking when a critical grain size is exceeded.[153] The induced microcracking drastically reduces the mechanical properties of the titanium diboride ceramic. To obtain good physical mechanical properties the inhibition of normal and abnormal grain growth is essential. The properties of TiB_2 powder, produced in an arc-plasma reactor and pressureless-sintered, to achieve a range of grain sizes, have been evaluated by Baumgartner.[13] The mechanical properties after exposure to molten aluminium environments were extensively evaluated and it was suggested that impurities within the aluminium penetrated the TiB_2 grains and then preferentially segregated at the grain boundaries. The results are interpreted in terms of crack growth mechanisms and the highest fracture toughness was shown to be achieved from powders synthesized by carbothermic as opposed to arc-plasma processes. Marked brittleness is associated with these phases and constitutes a considerable problem in their technological applications and machining by spark-erosion methods is possible although near-net shaping processes would be of great advantage. It is obvious from the above that titanium diboride products are among the more expensive engineering materials, the powders from which they are produced are generally synthesised by employing expensive techniques and their intrinsic characteristics inevitably lead to high manufacturing costs. This has led to a considerable decrease in the production output. Hot pressing has been, until now, the only useful method to fabricate TiB_2 engineering components.

Sintered diborides presently available are brittle and typical k_{1c} values[6]

are in the range 5 to 6 $MPa{\cdot}M^{1/2}$. It is thought improvements could be achieved in this area if components are near-net shaped rather than being machined as this may introduce flaws. Modifications of properties can be achieved to some extent by the addition of foreign species, for example the incorporation of compounds, such as BN, can be used to fabricate products which are a little softer and can be more easily machined to shape after manufacture.[163] Dense TiB_2 products have recently been developed using a pressureless sintering fabrication method. Such products find use in wide ranging areas as indicated above in introductory section 1. Because fine grain size in aluminum alloys is desirable for fatigue and strength, it is usual to add small amounts of master alloys of Al-Ti-B to the melt in order to promote further refinement. It is thought that the heterogeneous nucleation of

Table IV-4. The properties of TiB_2.[2]

Properties	Values
Structure type	hexagonal
lattice dimensions (Å)	a = 3.028, c = 3.228
No. of molecules per unit cell,M	M = 1
Melting point, K	3263
Heat of formation, $kJ.g^{-1}atom^{-1}$	~ -100.4, (~ -91.6 for mono carbides)
Hardness at 30-50 g load, $kg.cm^{-2}$	3370 (+9 Moh), (3200 for mono carbides)
Density, $kg{\cdot}m^{-3}$	4520
Electrical resistivity, σ,$\mu\Omega$.cm	σ = 10, at 323K rising to 60 at 1273K
thermal conductivity, $J{\cdot}m^{-1}{\cdot}sec^{-1}{\cdot}C^{-1}$	$K = 5.858x10^{-3}$ at 323K, $4.602x10^{-3}$ at 1273K
thermal expansion coefficient, ß, $°C^{-1}$	ß = 6.39×10^{-6} (≈ 293K-873K)

aluminum alloy grains at insoluble particles of TiB_2 in the melt occurs. TiB_2 is added because (111) planes of aluminum grow from (0001) of TiB_2.[164] Titanium diboride has been considered as a promising candidate for ceramic engines and turbines because of its good oxidation resistance up to 1673K, high hardness and excellent thermal shock resistance. Similarly it is replacing silicon carbide and silicon nitride as a coating on gas turbine blades, with high quality coatings being applied by vacuum plasma spraying. This allows the turbine to be used at higher operational temperatures, thereby increasing the efficiency of the system. Its high thermal conductivity over a range of temperatures allows its use as a transfer coating in externally cooled turbine combustion cans. Low friction coefficient was obtained from the sintered TiN-TiB_2 or Ti(CN)-TiB_2 ceramics by Shobu et al[165] because of TiB_2 oxidation, which produces a lubricating, glassy phase of boron oxide on the sliding surfaces. In **Table IV-4**, some of the properties of TiB_2 are summarised.

3. THERMODYNAMICS OF THE SYNTHESIS REACTIONS

3.1 The Formation of TiB_2 by Carbothermic Reduction

The complied thermodynamic data[77] were used to predict the phase stability of titanium boride and titanium and boron nitride in equilibrium with a gas phase as a function of the temperature. The thermodynamic feasibility of the formation of titanium diboride and nitrides phases via the reduction of oxides in the presence of carbon is considered. An example of the derivation of the $-RTlnP_{CO}$ equation is shown below. For the synthesis of TiB_2, we can write

$$TiO_2 + B_2O_3 + 5C = TiB_2 + 5CO \qquad \textbf{(4-1)}$$

for which the Gibbs free energy, $\Delta G°$equals to $\Delta H° - T \cdot \Delta S°$; the values of enthalpy and entropy are 1337.4 kJ $mole^{-1}$ and 0.829 kJ $mole^{-1}K^{-1}$,

respectively. Therefore the equilibrium constant, K_1, can be expressed in terms of $\Delta G_1°$ as shown below.

$$K_1 = \exp(\frac{-\Delta G_1^o}{RT}) = \frac{a_{TiB_2} \cdot (p_{CO})^5}{a_{TiO_2} \cdot a_{B_2O_3} \cdot (a_C)^5} \quad (4\text{-}2)$$

where p designates the partial pressure of the gaseous phase. For unit activities of the condensed phases, ie a_{TiB_2} etc. equal to unity.

$$K_1 = (p_{CO})^5 = \exp\ (\frac{-\Delta G_1^o}{RT}) \quad (4\text{-}3)$$

$$-RT\ln p_{co} = 267.483 - 0.166T \quad (4\text{-}4)$$

The value of P_{CO} equal to 1 atm in equation (4-4) represents the equilibrium temperature ($T_{eq.}$) at which $\Delta G_1°$ equals to zero. From the Le Chatelier principle, the removal of CO gas from the reaction chamber by purging argon gas will ensure a shift in the equilibrium of reaction (4-1) in the forward direction, otherwise the backward equilibrium will dominate.

3.2 The Formation of Composite Materials

The standard free energy change ($\Delta G°$) vs temperature relationship for the formation of titanium diboride (TiB_2), nitride (TiN), carbide (TiC), boron nitride (BN) and carbide(B_4C) phases have been drawn in **Figure IV-4**, and the relevant reactions are summarised in **Table IV-5**. For example, it is evident that TiB_2 is the most stable high temperature ceramic phase whereas BN is the stablest phase in the temperature range 1255 to 1844K. Similar deductions concerning the stability relationship between other phases can also be established. The proximity of $\Delta G°$ values of TiC and TiN phases is indicative of the fact that the two crystalline phases are likely to be similar in their chemical and structural characteristics. The temperature at which two univariants intersects is the invariant point indicating the equilibrium between

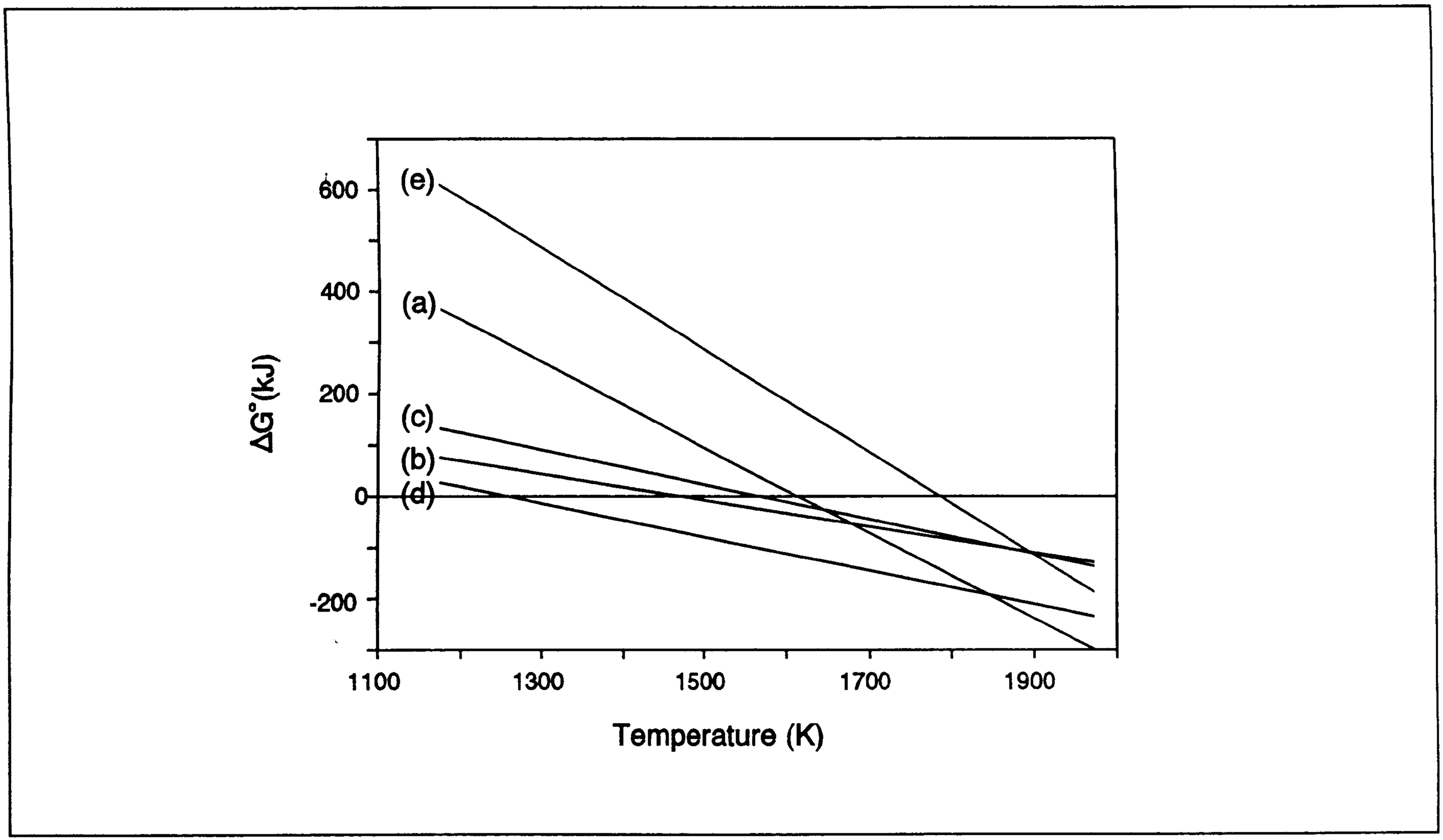

Figure IV-4. The standard free energy change diagram for the formation of TiB_2, TiN, TiC, BN and B_4C.
((*): Number in Table IV-5)

Table IV-5. The values of $-RT\ln P_{CO}$ (kJ) for various carbothermic reactions in the Ti-C-B-O-N system.

Reactions	$-RT\ln P_{CO}$(KJ)	$T_{eq.}$(K)
(a) $TiO_2 + B_2O_3 + 5C = TiB_2 + 5CO$	267.483-0.166T	1613
(b) $TiO_2 + 2C + \frac{1}{2}N_2 = TiN + 2CO$	187.945-0.128T	1469
(c) $TiO_2 + 3C = TiC + 2CO$	263.717-0.168T	1567
(d) $B_2O_3 + 3C + N_2 = 2BN + 3CO$	136.161-0.108T	1255
(e) $2B_2O_3 + 7C = B_4C + 6CO$	296.325-0.166T	1786
(f) $TiN + B_2O_3 + 3C = TiB_2 + 3CO + \frac{1}{2}N_2$	320.508-0.191T	1677
(g) $TiC + B_2O_3 + 2C = TiB_2 + 3CO$	269.994-0.164T	1644
(h) $2BN + TiO_2 + 2C = TiB_2 + 2CO + N_2$	484.466-0.252T	1844
(i) $B_4C + 2TiO_2 + 3C = 2TiB_2 + 4CO$	224.221-0.166T	1353

the two ceramic phases. For example, the TiB_2 univariant intersects TiC and TiN univariants at 1644K and 1677K, respectively. Below these two temperature, TiN and TiC are stable whereas above these temperature, the diboride phase is stable.

4. EXPERIMENT

Pigment grade titanium oxide (TiO_2) described in Chapter II, boron oxides (B_2O_3) whose properties and chemical compositions are described in Chapter III and carbon were the starting materials for the synthesis of pure and mixed ceramic phases. The experimental technique employed in this chapter was similar to that described in **Chapters II** and **III**. The gas atmosphere selected for the synthesis of pure boride and composite powder mixtures was different from the synthesis conditions for titanium nitride and boron nitride. The gas flow rate maintained mainly at 0.5 $l \cdot min^{-1}$ unless otherwise specified. In the tables containing the results of X-ray powder diffraction analysis of phases produced, the phases identified are arrange in the descending order of

their relative diffraction intensities.

5. RESULTS

5.1 The Synthesis of Titanium Diboride

5.1.1 The extent of reduction of titanium and boron oxides with carbon

The percentage reduction of titanium and boron oxides with carbon was investigated by measuring the weight of sample before and after reaction at the selected reaction temperature and time. The degree of reduction (%R) was calculated from the stoichiometry of reaction shown below in **equation (4-5)**:

$$TiO_2 + 1.5B_2O_3 + 6C = TiB_2 + 5CO + 0.5B_2O_3 + C \qquad \textbf{(4-5)}$$

$$\text{Percentage reduction (\%R)} = \frac{\Delta W}{W_o} \times 100 \qquad \textbf{(4-6)}$$

where ΔW is the observed percentage weight loss in a pellet during the course of reaction at any arbitrarily chosen time 't' from the starting time $t = 0$, and W_o is the maximum expected stoichiometric percentage weight loss. Total weight of the reactant is 256.4 gram, while that of the product should be 116.3 gram, from which a maximum weight loss of 140.1 gram is expected. This means that the theoretical maximum W_o is 54.62 %. B_2O_3, however, is easily volatilised as a BO (or B_2O_3) gas. Therefore, it is reasonable to assume that there is no B_2O_3 remaining in the product after reaction, and in this case theoretical maximum W_o is 68.20%. The relationship between the percentage reduction (%R) and time for the reduction of titanium and boron oxides with carbon at 1673K is shown in **Figure IV-5**. The reaction occurred rapidly leading to formation of TiB_2 crystals. For example, in 10 minutes reaction, more than 80 %R was obtained of which TiB_2 was the main phase with small amount of TiC. The reduction was complete within 30 minutes below 1773K and no further change in weight was observed even after 24 hours. The relationship between the extent of reduction (%R) and temperature for the reduction of titanium and boron oxides with carbon for 10 minutes reaction is shown in **Figure IV-6**. As expected, at higher reaction temperatures, the value of %R

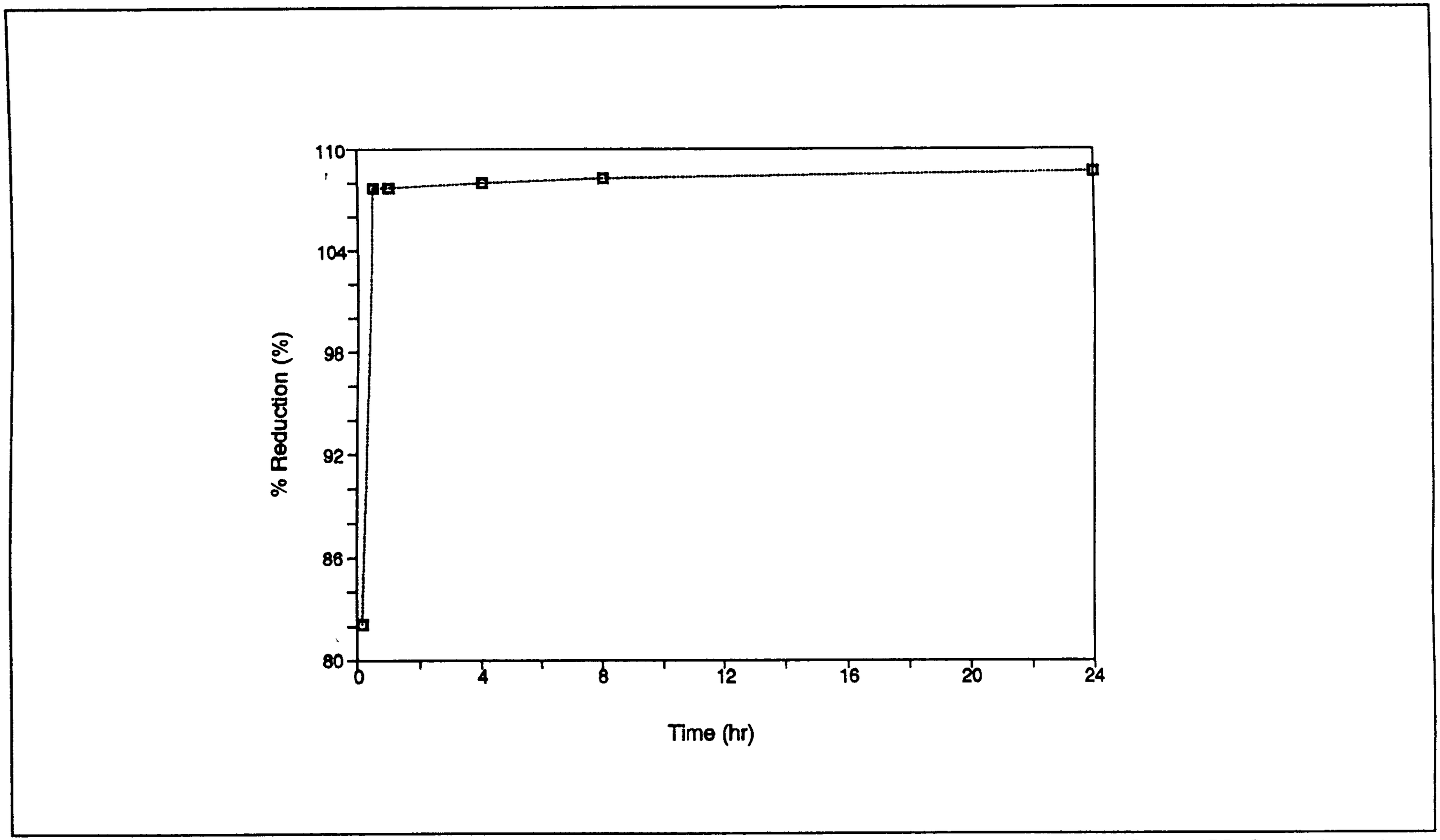

Figure IV-5. Relationship between percentage reduction (%R) and time for the reduction of $TiO_2 + 1.5B_2O_3$ with carbon at 1673K.

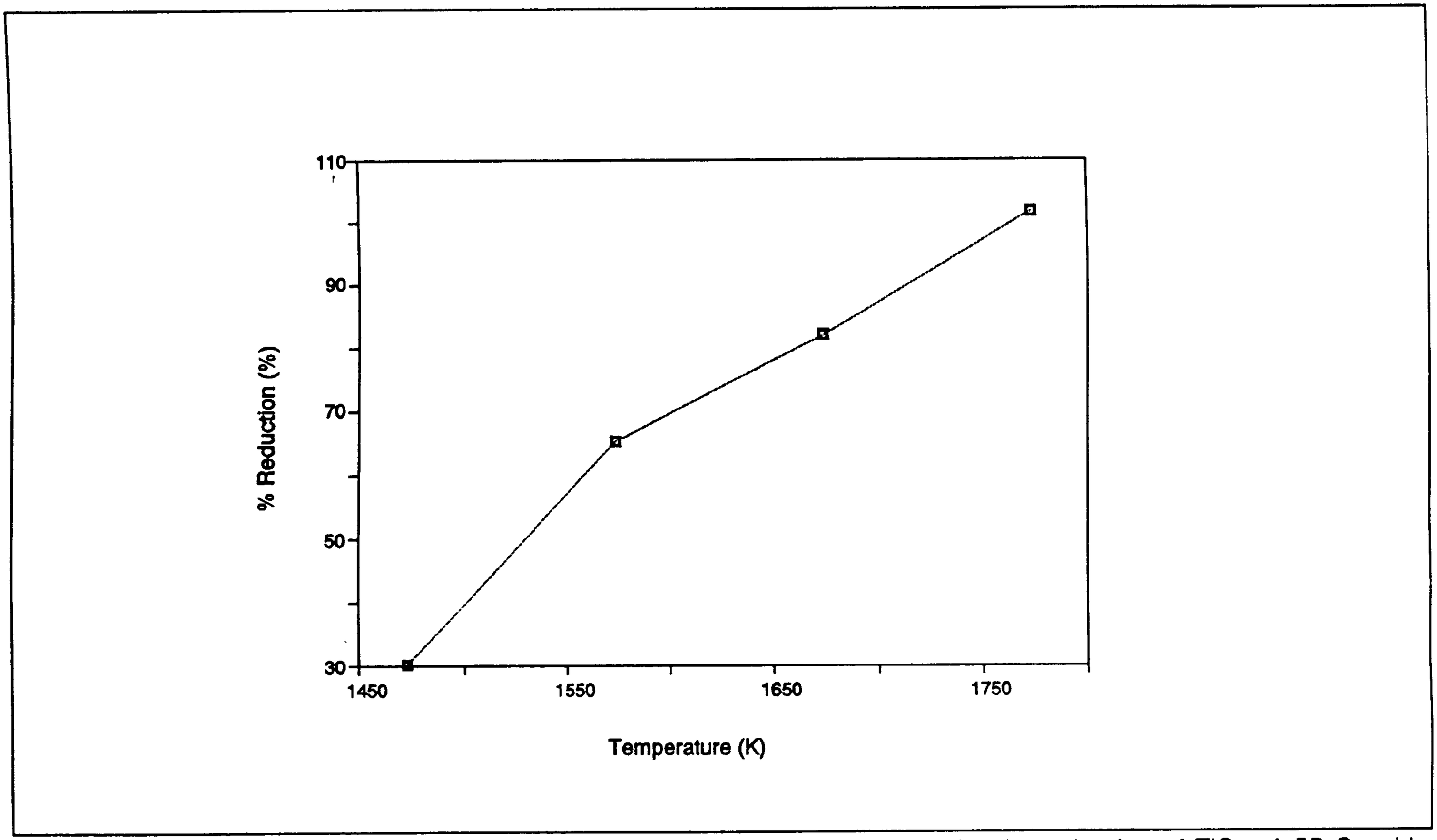

Figure IV-6. Relationship between percentage reduction (%R) and temperature for the reduction of $TiO_2 + 1.5B_2O_3$ with carbon for 10 minutes.

were higher. The rate of reduction is expected to be exponentially dependent on the temperature via Arrhenius relationship.

5.1.2 The effect of reaction temperature and time

When pellets with $TiO_2 + B_2O_3$ in the mixture were reduced with carbon at 1573K in an argon atmosphere, the boride (TiB_2) phase formed. At short reaction time, the formation of $Ti_{1-x}C_x$ phase was noticeable, but with prolonged reaction time, the $Ti_{1-x}C_x$ phase became less stable. **Table IV-6** summarises phases produced as a consequence of co-reduction of titanium and boron oxides. For the synthesis of TiB_2 by carbothermic reaction, $TiO_2 + B_2O_3 + 5C = TiB_2 + 5CO$, the equilibrium temperature is 1613K. From the Le Chatelier principle, the removal of CO gas from the reaction chamber by purging argon carrier gas shifts the equilibrium reaction in the forward direction, so that TiB_2 phase can be produced below the equilibrium

Table IV-6. Summary of phases produced a consequence of co-reduction of oxides.

Starting Materials	Gas	Temp (K)	Time (hr)	Phase
$TiO_2 + 1.5B_2O_3 + 6C$	Ar	1473	0.17	Ti_3O_5, TiC_xO_y
		1573	0.17	TiB_2, TiC
			0.5	TiB_2, TiC
		1673	0.17	TiB_2, TiC
			0.5	TiB_2, B_4C
			1.0	TiB_2, B_4C*
			4.0	TiB_2
			8.0	TiB_2
			24.0	TiB_2
		1773	0.17	TiB_2

(1) carbon source: activated charcoal,

2) *: very small trace,

3) gas flow rate = 0.5 $l \cdot min^{-1}$, unless otherwise specified)

temperature. Ti_3O_5 was the intermediate phase for the formation of titanium diboride at 1473K. TiB_2 was the main phase along with TiC or B_4C in the samples reduced above 1573K for 10 minutes reaction. At relatively low temperature, titanium carbide formed via titanium oxycarbide phase. The formation of TiC via $Ti_3O_5 \rightarrow TiC_{1-x}O_x$ is expected and is thermodynamically feasible. The formation of the boron monoxide gas or B_2O_3 gas is expected above 1373K. In the presence of excess unreacted carbon, the formation of carbide of boron is expected via:

$$2B_2O_3(g) + 7C = B_4C + 6CO \quad \textbf{(4-7)}$$

$$2BO(g) + 5C = B_4C + 4CO \quad \textbf{(4-8)}$$

Either Ti_3O_5 or $TiC_{1-x}O_x$ could then possibly react with either B_2O_3 or BO gas at higher temperatures to form TiB_2. We will further discuss the stoichiometric aspect of the overall reduction reaction. A selected few X-ray powder diffraction patterns of the reduced pellets are shown in **Figure IV-7**. From this the relative intensities of various phases can be compared.

5.1.3 The effect of composition

5.1.3.1 The effect of B_2O_3/TiO_2 ratio

The effect of composition of starting materials, especially B_2O_3/TiO_2 ratio was investigated. At short reaction time, titanium oxide reduced to suboxide (eg. Ti_3O_5) which is subsequently reduced by carbon to form titanium carbide. When pellets with molar ratio of $TiO_2:B_2O_3 = 1:2$ in the mixture were reduced with carbon at 1623K in an argon atmosphere, the boride (TiB_2) phase formed. At $B_2O_3/TiO_2 = 1$, the formation of $Ti_{1-x}C_x$ phase was noticeable, but as the amount of B_2O_3 was raised from the molar ratio of 1 to 2, the $Ti_{1-x}C_x$ phase became less stable. It was observed from the powder diffraction pattern that the molar ratio of $TiO_2:B_2O_3 = 1$ is sufficient for the synthesis of TiB_2 + $Ti_{1-x}C_x$ phase mixture. **Table IV-7** summarises the experimental condition for the formation of two or more refractory phases mixture. The observations are consistence with the overall stoichiometry of the reduction reaction which is a major subject of discussion.

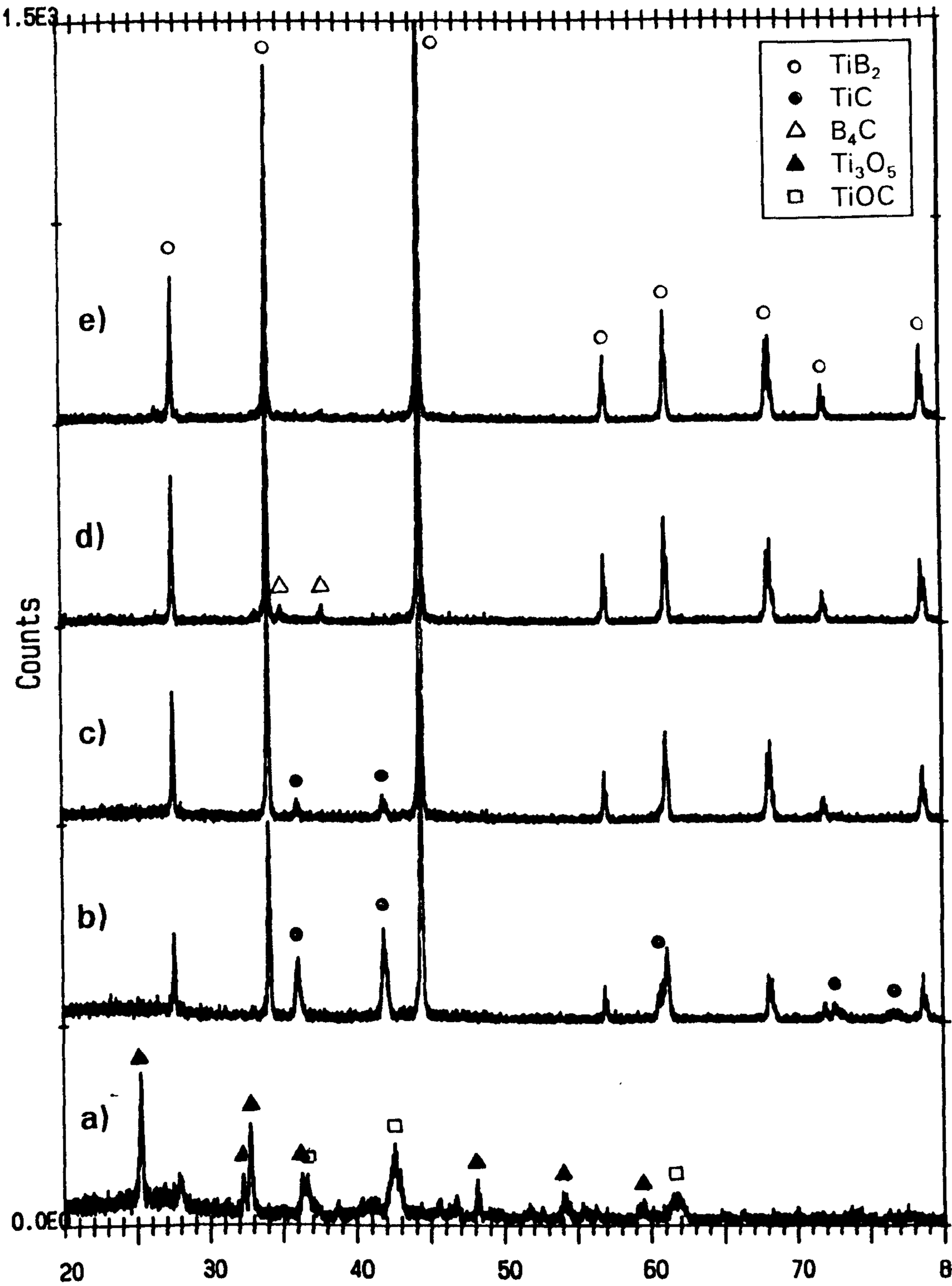

Figure IV-7. X-ray diffraction patterns of the reduced samples at (a) 1473K, 10min, (b) 1573K, 10min, (c) 1573K, 30min, (d) 1673K, 10min, and (e) 1773K, 10min in Ar gas (0.5 $l \cdot min^{-1}$).

Table IV-7. Summary of phases produced a consequence of co-reduction of oxides.

Starting Materials	Gas	Temp (K)	Time (hr)	Phases
$TiO_2 + 2B_2O_3 + 8C^*$	Ar	1773	24.0	TiB_2, C
$TiO_2 + 1.5B_2O_3 + 6C^{**}$		1673	24.0	TiB_2
$TiO_2 + B_2O_3 + 5C^{**}$		1673	24.0	TiC, TiB_2
$TiO_2 + B_2O_3 + 6.5C^*$		1773	24.0	TiB_2, C
$2TiO_2 + 0.5B_2O_3 + 5.5C^*$		1673	18.0	TiC, TiB_2

(*: 50% graphite/50% activated charcoal, **: 100% activated charcoal)

5.1.3.2 The synthesis of TiB_2 with calcium carbide

As a part of the carbothermic reduction reaction of titania and boric oxide (B_2O_3) for the formation of titanium diboride crystalline phase, we have also carried out a limited number of experiments with CaC_2 as a reducing agent. The reduction with calcium carbide facilitates study that of the aspects of both carbothermic and calcio-thermic reduction reaction mechanisms. The synthesis of titanium diboride from calcium carbide reduction is defined below:

$$TiO_2 + B_2O_3 + 2CaC_2 = TiB_2 + 2CaO + 3CO + C \qquad \textbf{(4-9)}$$

The standard Gibbs free energy change is equal to 406.39-0.388T $kJ \cdot mol^{-1}$. The equilibrium of this reaction shifts to the right hand side above 1047K. TiO_2 and B_2O_3 were mixed with CaC_2 in the above stoichiometric ratio and pelletized. The cylindrical pellets were heated inside the radio frequency induction coil described in section 4 (chapter III). The temperature of the pellet was raised above 1273K over a period of 5 minutes at which a minor pyro activity was observed inside the crucible. The inert gas was purged through the reaction chamber while the pellet was reduced. The ignition was spontaneous and localized that lasted a few seconds. The ignition front, unlike aluminothermic reduction, did not propagate right through the pellet. The pyroactivity was more violent when calcium carbide was replaced by metallic calcium. After the ignition phase, no further activity was observed. The pellet

temperature was then raised to an isotherm 1773K at which it was held for a fixed period of time. After the isothermal hold period, the radio frequency coil supply power was turned-off and the sample was allowed to cool in the stream of the argon gas.

Using this method, several pellets were reduced in this way. The reduction was only partially possible in a few samples. However, further isothermal annealing at 1773K resulted in a higher extent of conversion. The reduction, however, was never complete because of the presence of impurity lime in commercially available calcium carbide. The presence of impurity lime slows the conversion rate by forming an unknown complex borate which appeared to be amorphous. This was verified from X-ray powder diffraction patterns in which the extent of crystalline phase and their relative intensities significantly changed as the extent of boride conversion increased. The complex borate phase, however, was found to be unstable above 1673K. The results of the carbide reduction are summarised in **Table IV-8**. When laboratory synthesized calcium carbide was substituted for commercially-available calcium carbide, the reduction reaction reached completion at 1773K,

Table IV-8. Summary of phases produced by carbide reduction.

Starting Materials	Gas	Temp (K)	Time (hr)	Phases
$TiO_2 + B_2O_3 + 3CaC_2$	Ar/H_2 (4%)	1523	0.5	TiB_2, X, Y
$TiO_2 + B_2O_3 + 3CaC_2$		1673	0.25	TiB_2, X, Y
$TiO_2 + B_2O_3 + 3CaC_2$		1673	0.75	TiB_2, Y
$TiO_2 + B_2O_3 + 2CaC_2 + C$		1673	24.0	TiB_2, Y
$TiO_2 + B_2O_3 + 2CaC_2 + C$		1773	0.5	TiB_2, Y

(1) carbon source: activated charcoal,

2) X: borate, Y:Ca-Ti-O phase)

The microstructure of the reaction product is shown and compared with carbothermically-synthesized microstructure under Section 5.5.

5.2 The Formation of Composite Materials

5.2.1 The effect of partial pressure of nitrogen

The results of several phase mixtures formed via the reduction route are summarised in **Table IV-9**. The nitrides, TiN and BN, are evidently the dominant phase produced in the nitrogen atmosphere via carbothermic reduction. But in the inert gas atmosphere, titanium diboride (TiB_2) phase formed with titanium carbide (TiC). X-ray powder diffraction patterns of phases produced are shown in **Figure III-8**.

5.2.2. The effect of composition and reaction temperature during nitridation

Titanium nitride (TiN) phase easily formed by carbothermic reaction of TiO_2 in the nitrogen atmosphere as shown in chapter II, for example, TiN phase formed with titanium suboxide, Ti_3O_5, within 40 min reaction time at 1473K. But TiN did not form with boron oxide in the starting materials even after 24 hours reaction time at 1573K. It is understood that because of the formation of BO gas, the reduction of titanium oxide was retarded. The results of phases formed in the nitrogen atmosphere via the reduction route are summarised in **Table IV-10**.

Table IV-9. Produced phases according to composition of starting materials. (graphite:activated charcoal = 1:1)

Starting Materials	Temp (K)	Time (hr)	P_{N_2}	Produced Phases
$TiO_2 + 2B_2O_3 + 8C$	1773	24	1	TiCN, BN, C
			0.1	TiCN, BN, C
			0.02	TiCN, BN, C
			0.002	TiB_2, TiCN, BN, C
			0.0005	TiB_2, TiCN, C
			0 ($P_{Ar} = 1$)	TiB_2, C

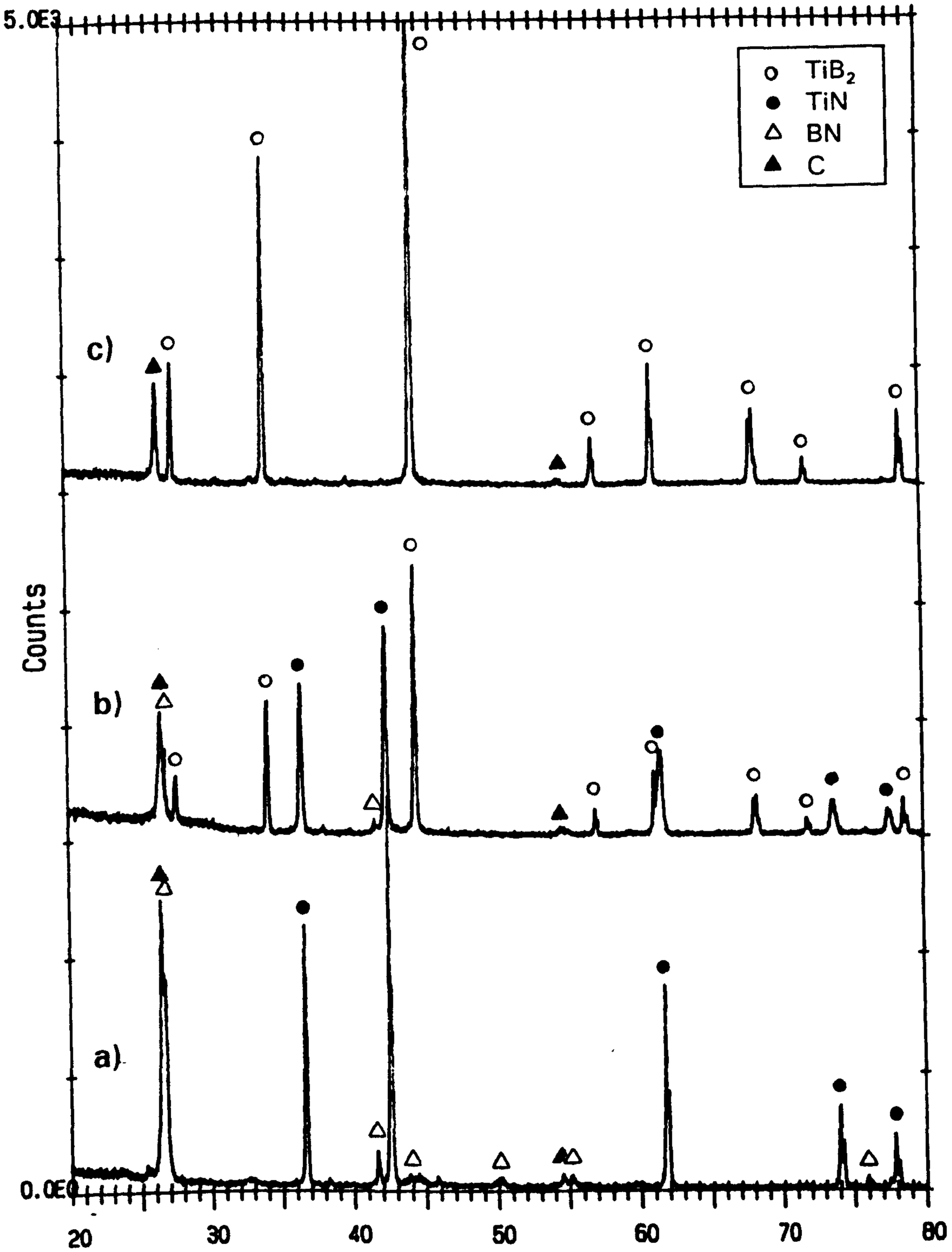

Figure IV-8. X-ray diffraction patterns of the reduced samples.
(P_{N_2} = (a) 0.05, (b) 0.002 and (c) 0 at 1773K after 24 hrs)
($Ar + N_2$ flow rate : 0.5 $l \cdot min^{-1}$)

Table IV-10. Produced phases according to composition and temperature in the nitrogen atmosphere.

Starting Materials	Gas	Time (hr)	Temp (K)	Produced Phases
TiO_2 + 3C*	N_2	0.7 8	1473	Ti_3O_5, TiN TiN, Ti_3O_5
$2TiO_2$ + $0.5B_2O_3$ + 5.5C		24	1573 1673	C, Ti_3O_5, BN** Ti_3O_5, C, TiN
TiO_2 + B_2O_3 + 5C			1473 1773	TiO_2, C, X TiN, C, BN
TiO_2 + $2B_2O_3$ + 8C			1573 1673 1773	C, Ti_3O_5, BN BN, C, Ti_3O_5 TiN, C, BN

(1) *: activated charcoal, otherwise 50% activated charcoal/50% graphite,
2) **: very small amount,
3) X: unidentified Phase)

5.2.3 The verification experiments for the stability of phases in the Ti-B-N system

Titanium nitride and boron nitride crystals converted to titanium diboride (TiB_2) at 1773K in the inert gas (Ar) atmosphere, because TiB_2 phase is the most stable phase at high temperature among them. TiB_2, however, is not a stable phase in nitrogen atmosphere, and transformed to a combination of two

Table IV-11. The stability of TiB_2, TiN and BN phases.

Starting materials	Temp (K)	Time (hr)	Gas Composition	Produced Phases	Weight change
TiN + BN	1773	64	Ar	TiB_2, TiN, BN	-26%
TiB_2 + BN		48	N2	TiN, BN, TiB_2	+21%
TiB_2 + BN		24	Ar + N_2(10%) + H_2(4%)	TiB_2, BN, TiN	+ 4%
TiB_2 + BN		24	Ar + H_2(4%)	BN, TiB_2	(*)

(*: weight loss not measured)

converted nitride phases. This was confirmed after heating the mixtures listed in **Table IV-11** in selected gas atmospheres. The samples were weighed after heat treatment and analyzed by powder diffraction analysis. The pellets reacted in N_2 atmosphere gained weight and the results are shown in Table IV-11.

5.3 Microstructure of TiB_2

5.3.1 Microstructure of TiB_2

5.3.1.1 The effect of reaction temperature and time

The synthesised titanium diboride powder had a hexagonal platelet morphology with layers parallel to the (001) basal plane. The microstructure indicated that the TiB_2 crystals are likely to grow by condensation of the vapour phase. It is well known that in some crystals deposited from the vapour phase, thin plates are often formed, and it is probable that these are separated by faulted layers.[166] In other cases where the crystals have a large structure, it is possible for irregularities in structure to occur as the result of stacking faults which extend across the entire crystal. The grain size of TiB_2 was strongly affected by reaction temperature. It grew up to 10μm diameter at 1773K in 10 minutes. Grain growth occurred mainly along the basal plane direction. **Photo IV-1** showed the morphology of TiB_2 for 10 minute reaction. At 1573K, grains were growing from the reduced oxide matrix, even though not many TiB_2 crystals formed under this condition. TiC phase co-existed along with TiB_2 phase. As the temperature rose, more TiB_2 grains formed and the large grain growth of TiB_2 was observed at 1773K.

At lower reaction temperature, however, irrespective of the reduction time, the grain growth rate of TiB_2 seem to be insignificant. For example, at 1673K, the change in the average size or crystals with increasing reaction time was not noticeable. After 10 minutes of reduction, TiB_2 phase nucleated from the matrix which appears to be sintered and TiB_2 forms a wetted interface with the matrix, i.e, the interface between the crystal and matrix is rather poorly defined. However after 1 hour, the matrix phase completely disappeared. The nucleation and crystal growth from the micrographic analysis appears to be a time-dependent process which might have a classical

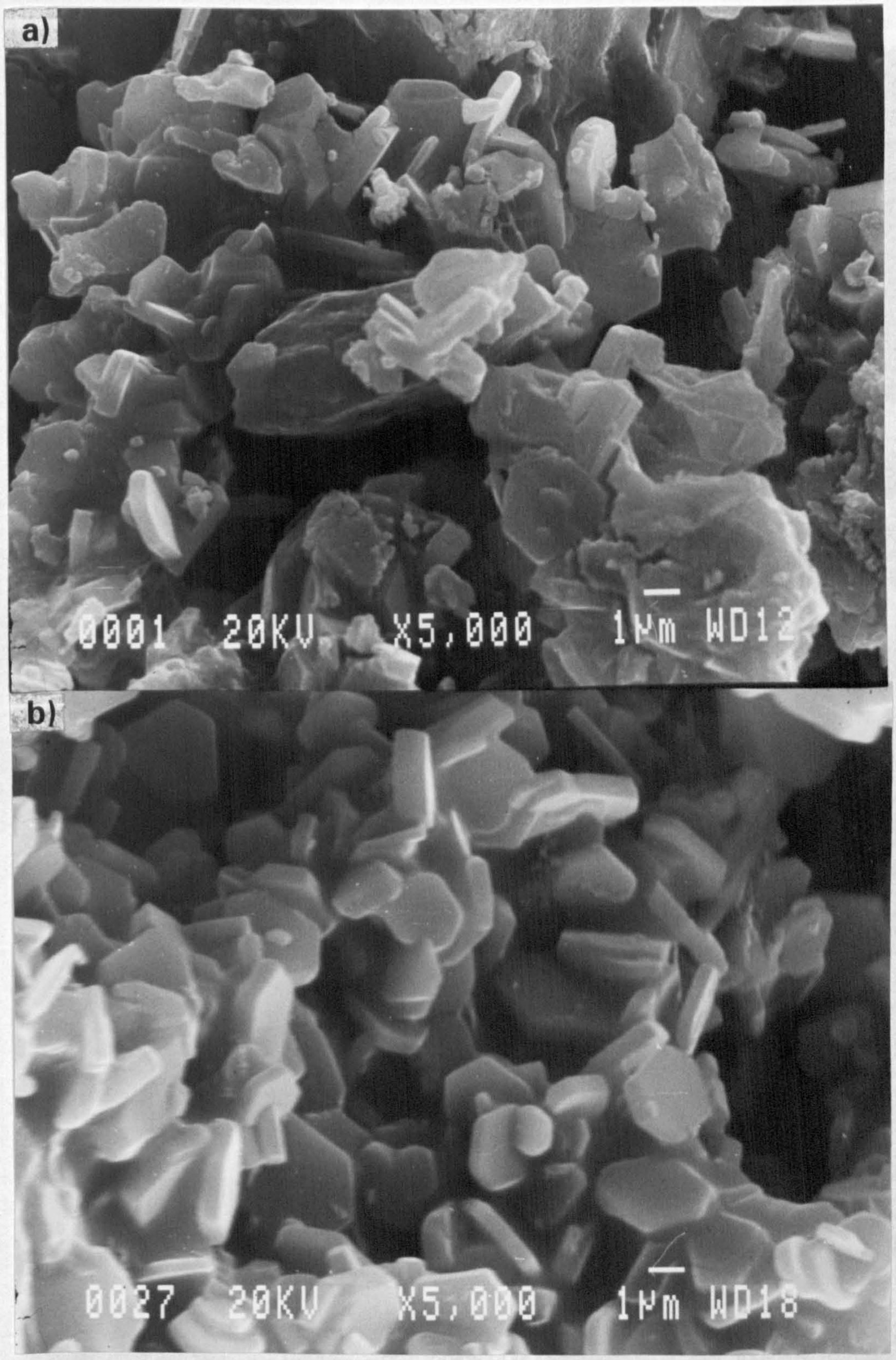

Photo IV-1 Scanning electron micrograph of titanium diboride produced at (a) 1573K, (b) 1673K and (c)(d) 1773K after 10 minutes of reduction in a flowing stream of argon gas.(flow rate:0.5l·min^{-1}, starting material : $TiO_2 + 1.5B_2O_3 + 8C$)

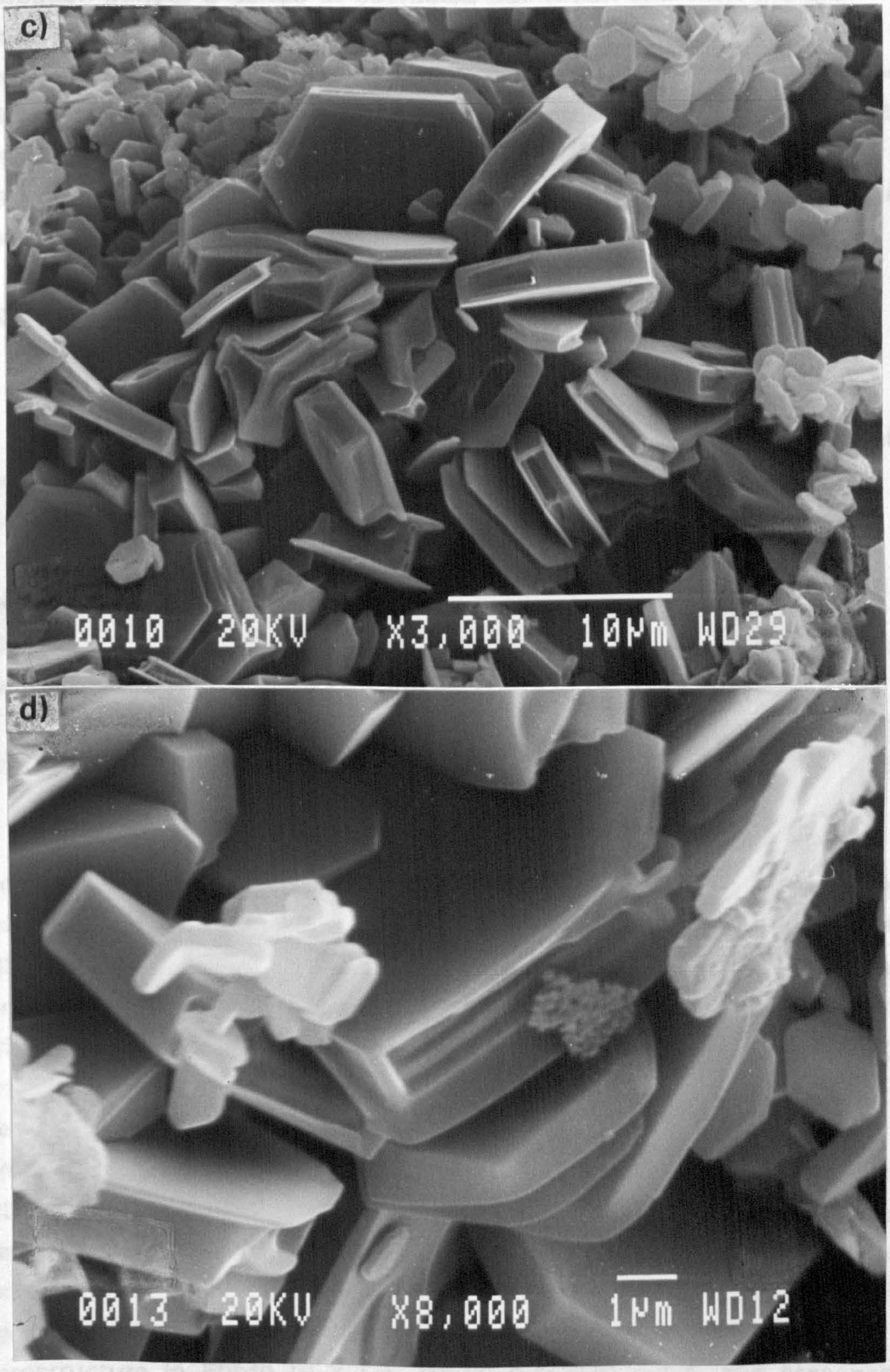

Photo. IV-1. (continued from the previous page)

incubation period, a period of sustained nucleation and then the growth of existing nuclei. Both nucleation and growth steps are dependent upon the mass transport. The crystallite size of TiB_2 formed in this way is between 0.3μm and 4.5μm. This is shown in **Photo IV-2**. The variation of crystalline size with time at 1673K is apparent from the micrograph. After 8 hours, the average crystallite size did not vary significantly. This indicates that the major growth of crystals occur between 1 hr and 8 hrs.

5.3.1.2 The effect of gas composition and reducing agent on the morphology of titanium diboride crystals

In the present investigation, the growth characteristics of titanium diboride crystals was studied. Experiments were carried out under the following conditions:

a) $TiO_2 + B_2O_3 + 8C$ at 1673K for 24 hours in argon gas atmosphere
b) $TiO_2 + 1.5B_2O_3 + 8C$ at 1673K for 24 hours in argon gas atmosphere
c) $TiO_2 + 2B_2O_3 + 8C$ at 1773K for 20 hours in [Ar/H_2(4%):99.95% + N_2:0.05%] mix gas
d) Reduction of titania and boria with calcium carbide in Ar/H_2(4%) gas atmosphere at 1773K.

Under the condition *a)*, the minimum stoichiometric proportion of boric oxide was used for the conversion of titania to titanium diboride. The crystals grew with a pronounced facetting of the basal plane and the growth direction was along the c-axis of the diboride crystals. Due to enhanced volatilization of boric oxide at elevated temperatures, the conversion of TiO_2 to TiB_2 is only partial. The excess TiO_2 converts into TiC which is shown in **Photo IV-3 (a)**. The microstructure of TiC has "flaky-snow dust" type morphology. The TiC formation enhances when an active reducing agent such as charcoal or active carbon is used. However, when the initial composition of pellet changes to *b)*, there is an excess of boric oxide which reacts with TiC and transforms into the diboride phase. The preferred growth of crystals is along a-axis. This is apparent when the microstructure in Photo IV-3 (a) is compared with the microstructure in Photo IV-2 (d). When $B_2O_3:TiO_2 = 2:1$, the presence of nitrogen, as indicated in condition *c)*, appears to promote growth along the c-axis of the hexagonal crystals as shown in **Photo IV-3 (b)**.

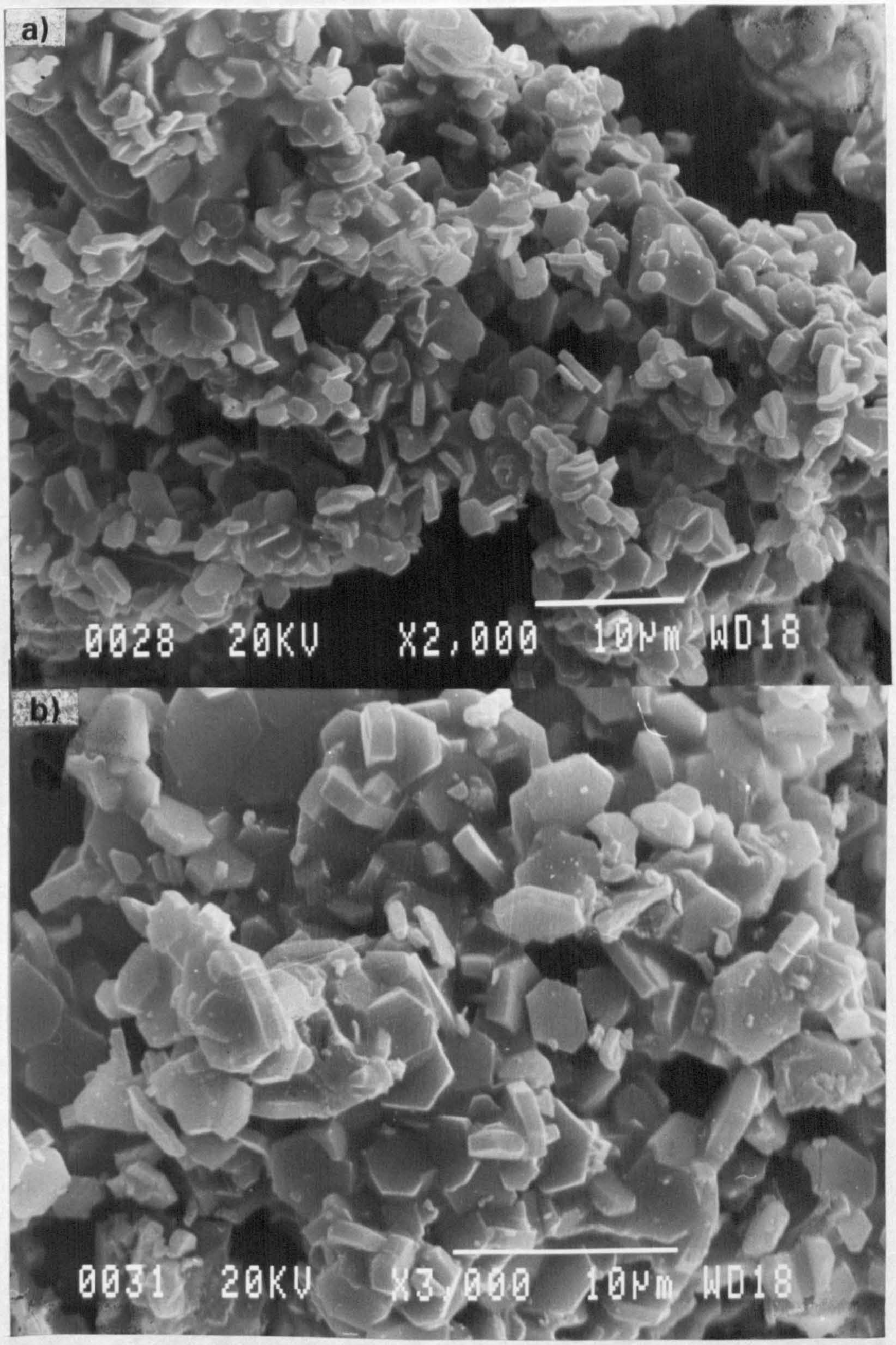

Photo IV-2. Scanning electron micrograph of titanium diboride produced after (a) 10min, (b) 30min, (c) 8hrs and (d) 24hrs of reduction at 1673K in a flowing stream of argon gas. (flow rate:0.5 $l \cdot min^{-1}$, starting material : $TiO_2 + 1.5B_2O_3 + 8C$)

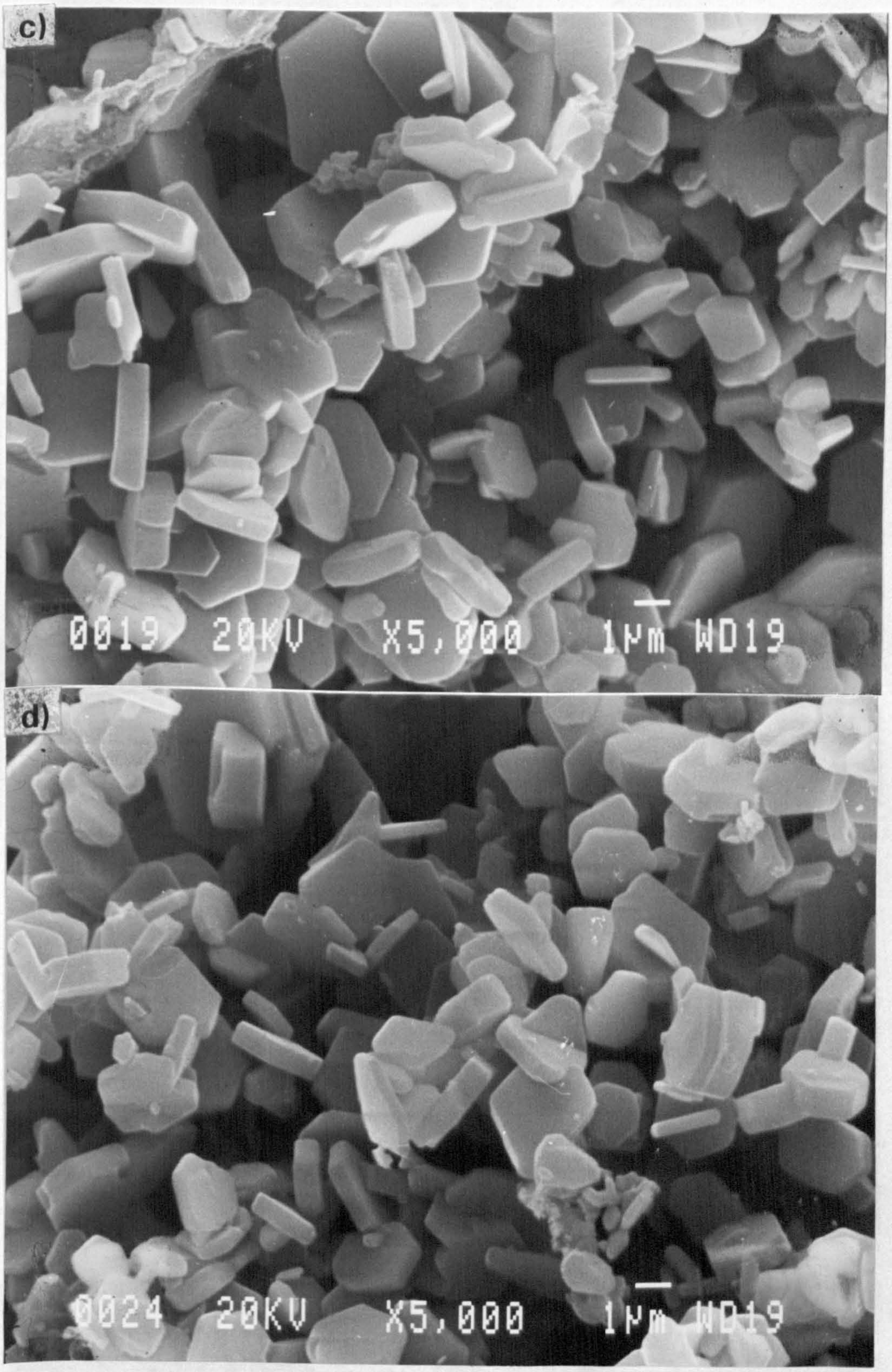

Photo IV-2. (continued from the previous page)

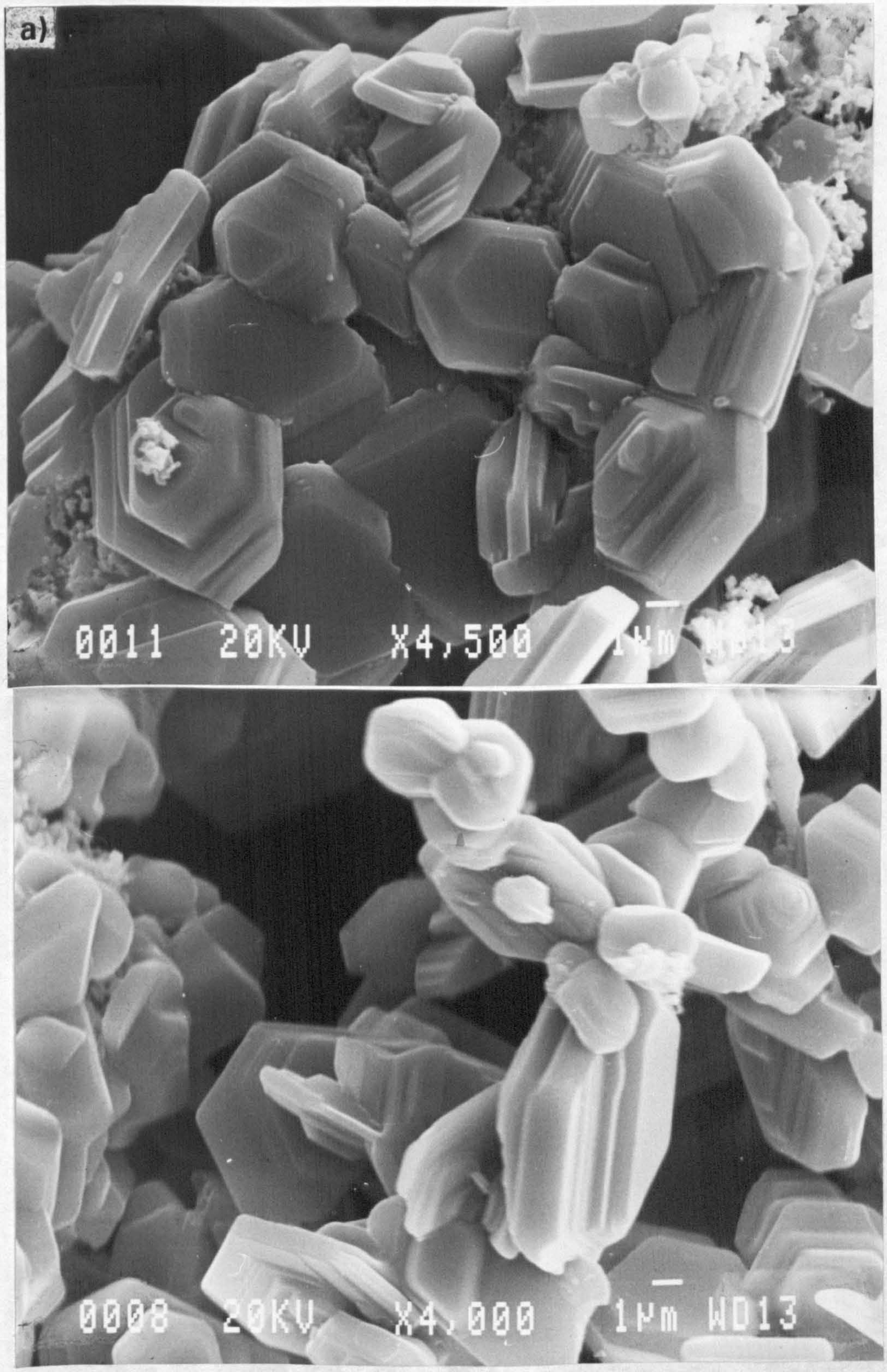

Photo IV-3. Scanning electron micrograph of titanium diboride when B_2O_3/TiO_2 ratio was (a) *1*, after 24 hours at 1673K in Ar and (b) *2*, after 20 hours at 1773K in $Ar/H_2(4\%) + N_2(0.05\%)$ gas. (flow rate:0.5l·min^{-1})

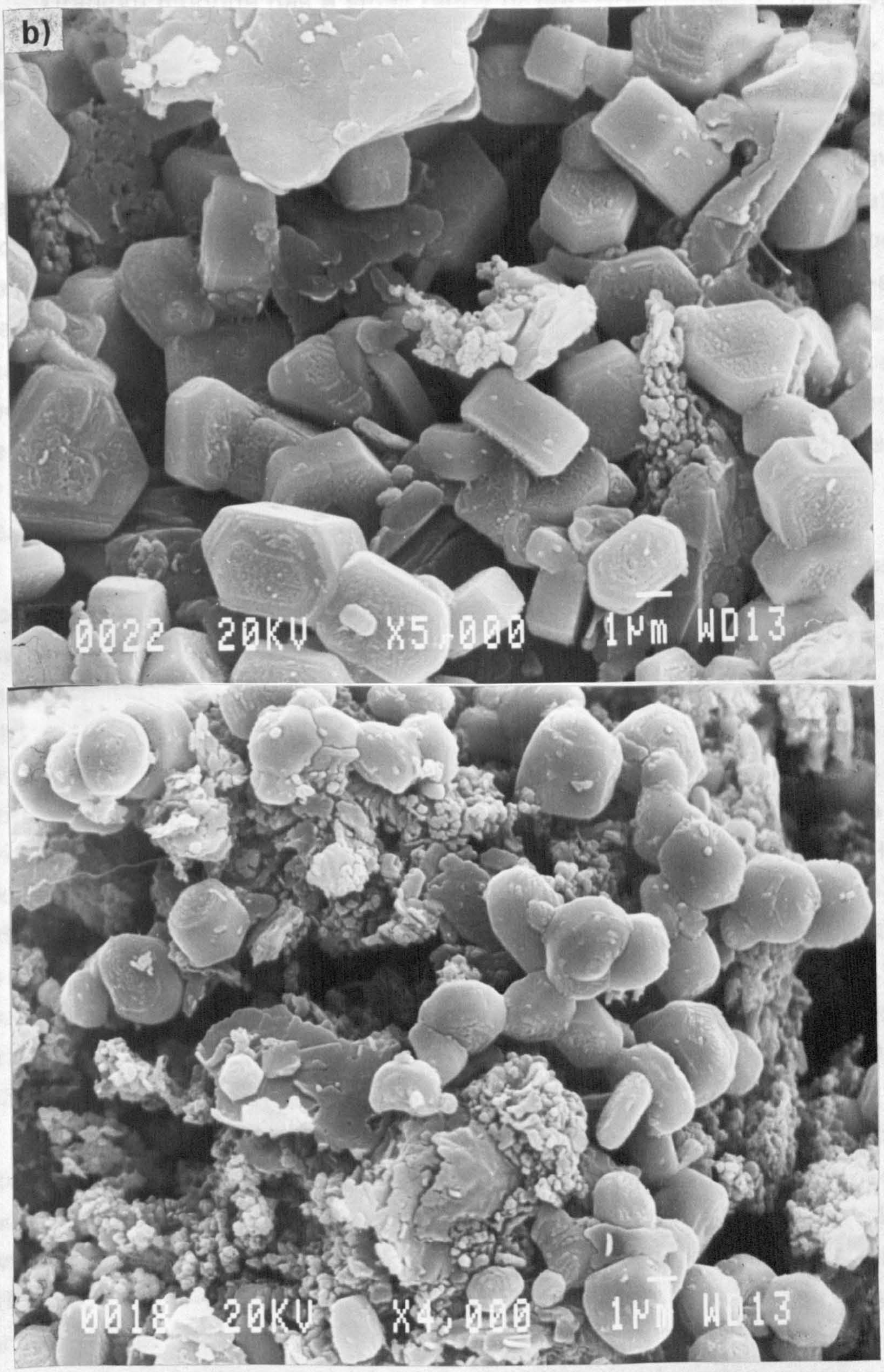

Photo IV-3. (continued from the previous page)

Titanium diboride has a small range of non-stoichiometry. The crystal could be either titanium-rich or boron-rich. Under the conditions *a)* and *b)*, the loss of boric oxide either as BO or B_2O_3 gas enhanced the titanium to boron ratio. Due to this there is a slight excess of titanium atoms in the structure which can only occupy sites along the a-axis in the MB_2 structure. The growth rate along a-axis is faster than c-axis due to a marginally larger concentration gradient of the titanium atoms in the reducing atmosphere. The diboride structure has a relatively smaller defect concentration along the a-axis whereas the interstitial defect concentration is more likely to change because it can be controlled via the gas phase. Boron deficiency in the lattice is expected when the volatilisation rate of boric oxide is expected to increase. The basis for the stability of an interstitial defect structure is similar to that of the metal ion deficiency in oxides and sulphides that is governed by the gas phase.

The presence of nitrogen in the gas phase enhances the relative growth rate along the c-axis as shown in Photo IV-3 (b). The crystallites of boride grow faster along the c-axis because nitrogen atoms compete for interstitial sites with boron. Indeed it is also possible that the solubility of nitrogen gas in the diboride structure increases due to complex interaction between Ti and B atoms. The presence of 0.05% nitrogen in the gas mixture promotes the nitridation process under which it is possible to form TiCN and BN from the boride microstructure. This is via $TiB_2 + (N_2) + xC = TiNC_x + BN$ or $TiN + BN$ reaction in the absence of carbon. Provided the partial pressure of nitrogen gas in the atmosphere reaches the critical value for compound nitride formation, the stability of a solid-solution carbonitride compound phase is possible. The presence of carbonitride on the surface of crystals in the initial stage of nitriding and inter-granular titanium carbonitride phase is apparent from Photo IV-3 (b).

The average size of titanium diboride crystals obtained from the reaction between the oxides and calcium carbide, as indicated under condition *d)*, was much larger than with the carbothermic reduction process and up to 35 μm diameter. This can be seen from the comparison of micrographs in **Photo IV-4** with Photo IV-3 (b). In the carbide reduction process, the average crystal diameter size of 30 μm sharply contrasts with the 2 to 4 μm diameter size crystals produced from carbothermic reduction at the same temperature ($T = 1773K$). The growth of crystals in the carbothermic reduction process

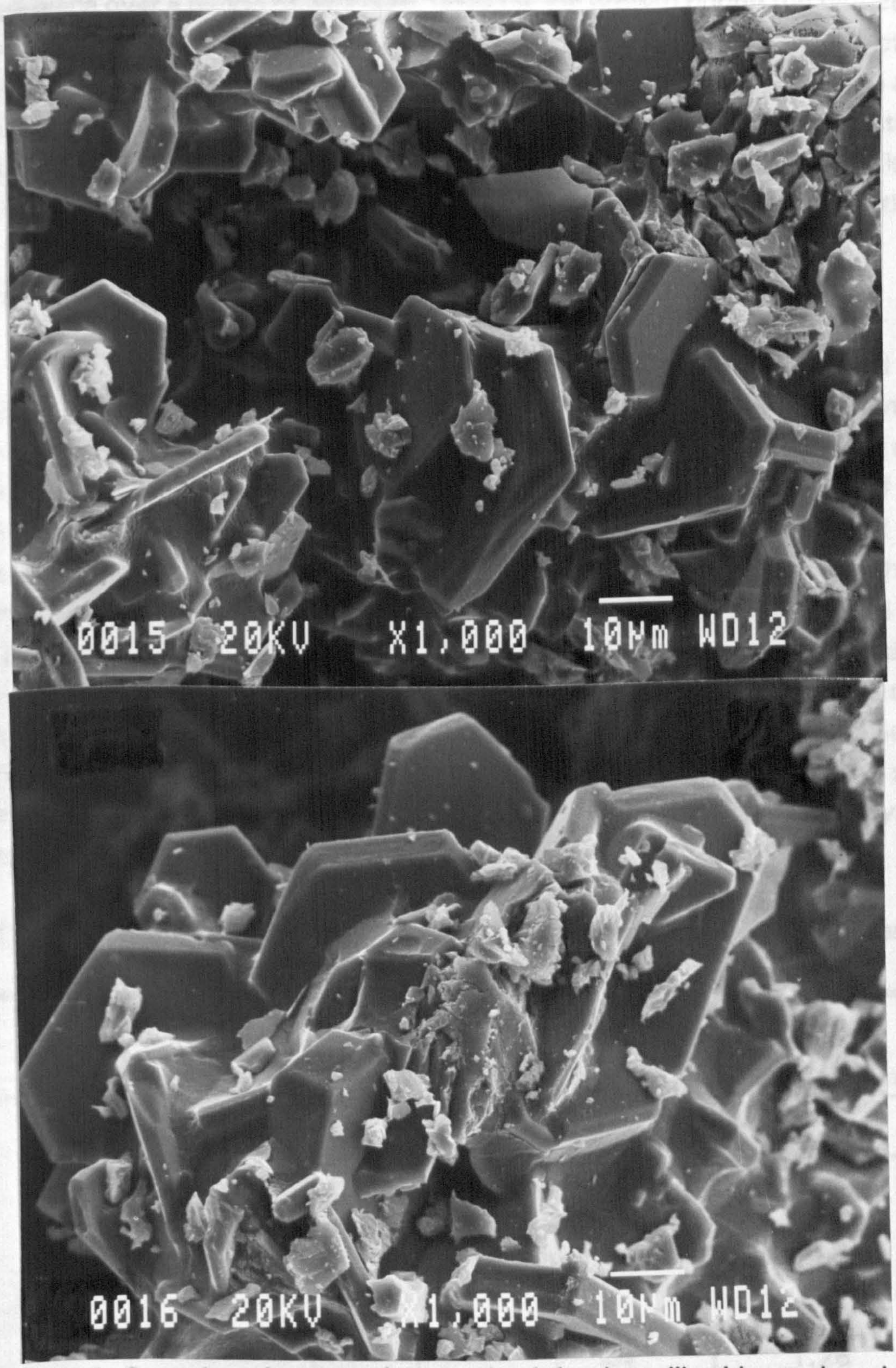

Photo IV-4. Scanning electron micrograph of titanium diboride produced by carbide reduction after 30 min at 1773K.(flow rate:0.5 $l \cdot min^{-1}$, starting material:$TiB_2 + B_2O_3 + CaC_2 + 2C$)

took place over a period of 24 hours, whereas the growth during the reduction with CaC_2 was only 30 minutes at 1773K. Under the above two reduction conditions, the average measured thickness of the crystals were 1.75 μm and 3.52 μm, respectively. From the measured dimensions of the TiB_2 crystals, indicated above, it is apparent that the planar growth rate along the a-axis of the hexagonal lattice appears to be faster than the growth rate in c-direction.

5.3.2 The determination of average crystallite size of TiB_2 crystals

The particle characterisation of boride powder was attempted by determining the average size of crystals at a given temperature. The number of crystals selected for measurement of crystallite size varied between 10 and 20. This is a relatively small number in terms of the true representation of the powder particle size. However it is an approximate guide to understand the rate of crystal growth. The following **Table IV-12** summarizes the data at three different experimental temperatures. The average crystallite size in micrometers is also given at each time and temperature. The standard deviation of thickness was 0.4 μm. **Figure IV-9** is an example which suggests that the growth rate at 1673K is insignificantly small, the average size remains virtually constant between 0 hours and 8 hours. Beyond this period, the size increases with time non-linearly. At higher temperature, the average crystal size was bigger after 10 minutes reduction.

Table IV-12. The average crystallite size in micrometers at each time and temperature.

Composition	Gas	Temp. (K)	Time (hr)	Average grain size(μm)
$TiO_2 + 1.5B_2O_3 + 6C$	Ar	1573	0.17	0.44
		1673	0.17	0.86
			0.5	0.87
			1	0.87
			8	0.87
			24	1.26
		1773	0.17	1.60

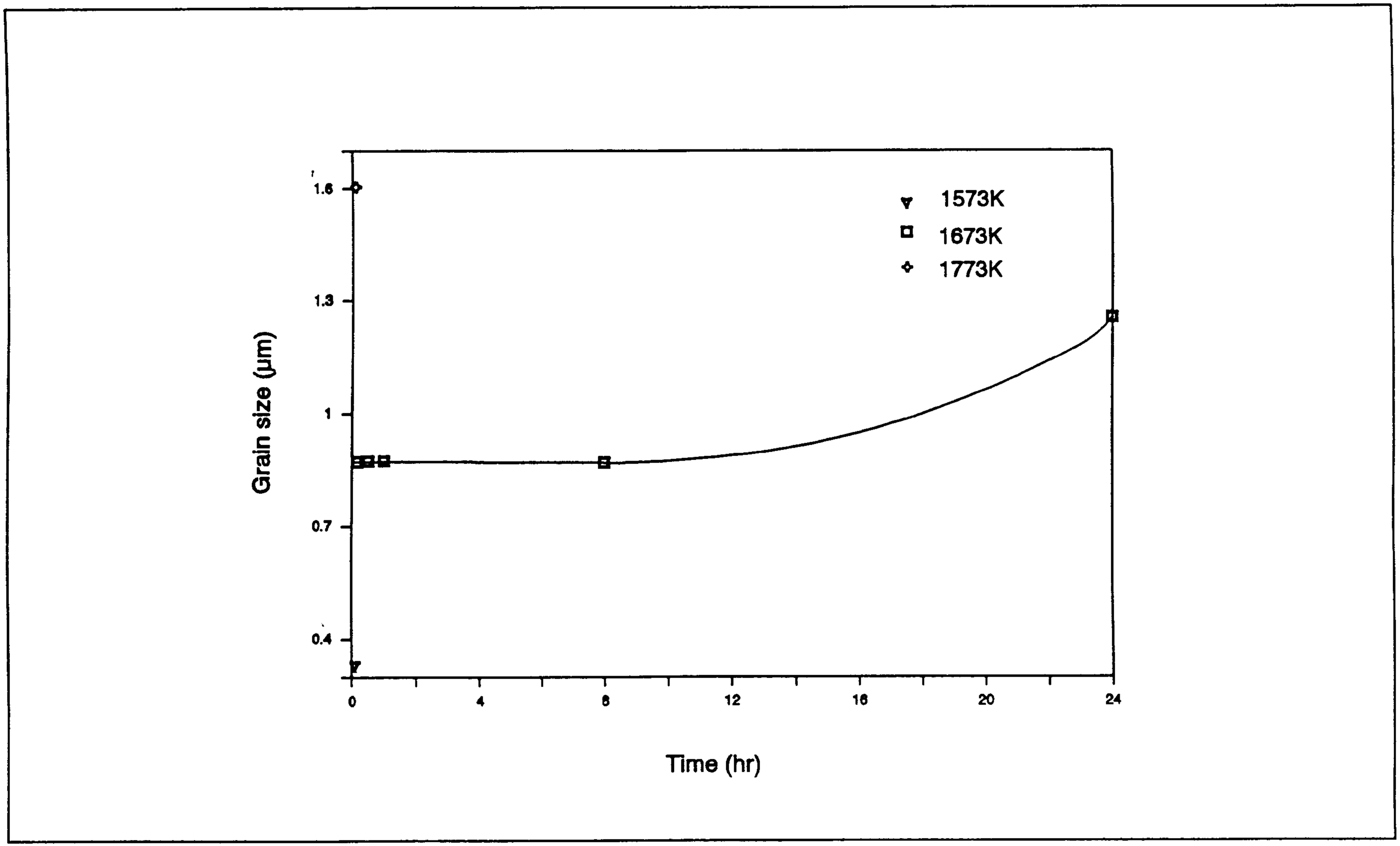

Figure IV-9. Average thickness of TiB_2 grains according to reaction time. (starting material: $TiO_2 + 1.5B_2O_3 + 6C$)

5.3.3 Microstructure of composite materials

The synthesised TiB_2 particles along with nitrides shown in **Photo IV-5** have a hexagonal platelet morphology and a few micrometer size. Titanium nitride or carbide exists with titanium diboride has submicrometer particle size. The morphology of TiC phase formed in co-existence with TiB_2 is similar to those of TiN. The BN phase formed as a result of controlled nitriding has a flake-like morphology. The microstructure shown here has two ceramic phases co-produced during synthesis reaction in the different gas atmosphere.

5.3.4 The morphology of transformed ceramic powders

The commercially available titanium diboride, nitride and boron nitride was heat treated under argon, nitrogen or mixed gas atmosphere. **Photo IV-6** showed the morphology of (a) TiB_2 reagent before heat treat and (b) TiN, BN and TiB_2 phases which are heat treated under nitrogen gas atmosphere from TiB_2 and BN reagents mixture. Because of the stability of titanium nitride in the nitrogen atmosphere, the surface of titanium diboride transformed to titanium nitride phase. The morphology of TiN is quite similar to that of TiN formed from the carbothermic reduction reaction.

5.3.5 Mixed diborides of chromium and titanium

Mixed diboride powders of chromium and titanium were produced by mixing chromium oxide with titanium oxide and boron oxide in different stoichiometric ratios in the starting material. The reduction was conducted in a similar way to that described above for pure boride. The lattice parameters of the mixed diboride phase were determined. (see **Table IV-13**). The presence

Table IV-13. Change in fractional lattice parameter *c* of TiB_2-CrB_2 solid solution.

Cr wt%	c (Å)	c/a	$\Delta c/c_0 \times 10^3$
13.71	3.188	1.052	-13.1
17.48	3.219	1.062	-3.5
20.94	3.221	1.063	-2.6

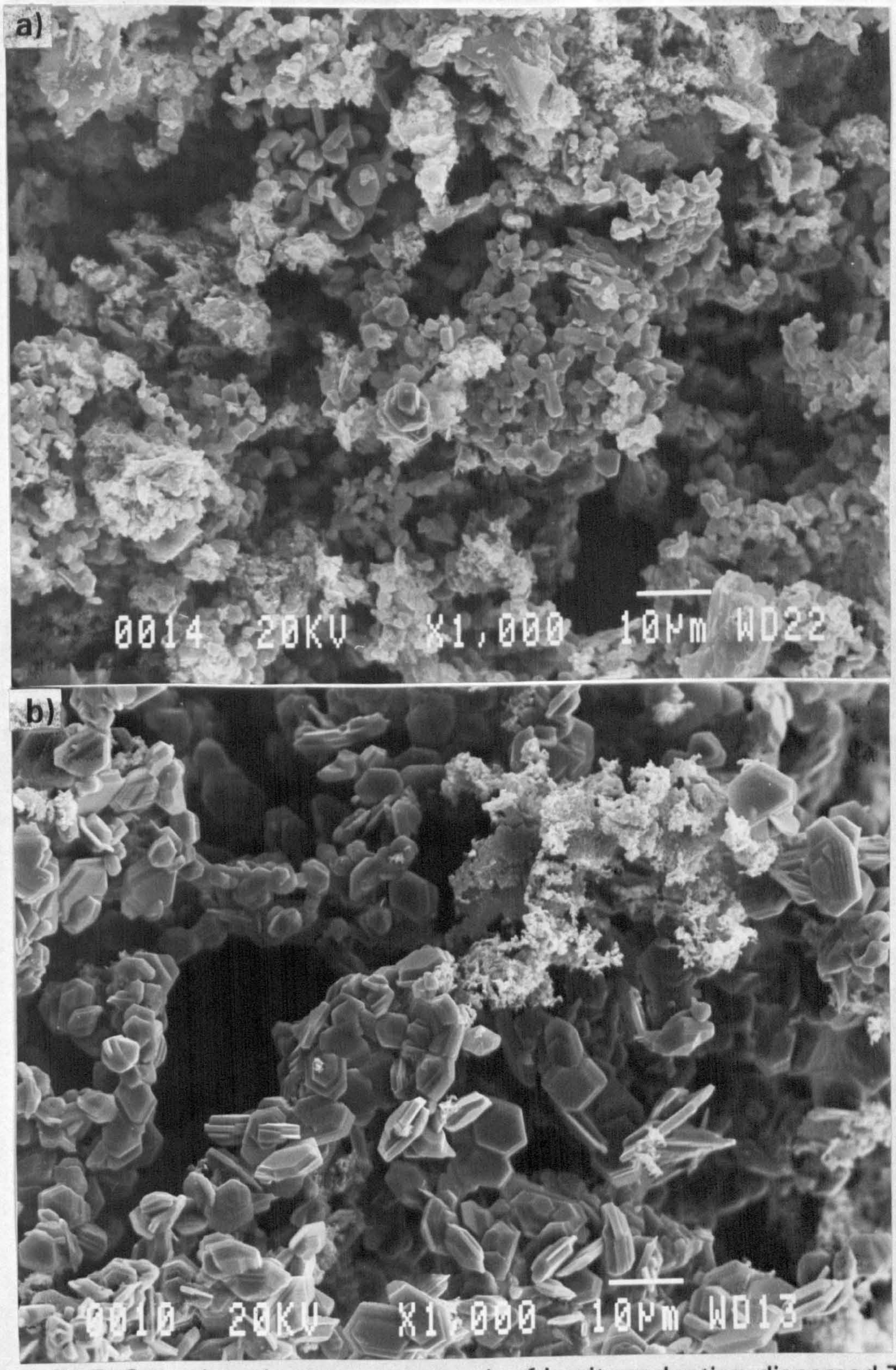

Photo IV-5. Scanning electron micrograph of in-situ reduction dispersed TiB_2 with (a) TiN and (b) TiC. ((a)$TiO_2 + 2B_2O_3 + 8C$ at 1773K in Ar, (b)$TiO_2 + B_2O_3 + 8C$ at 1673K in [$Ar/H_2(4\%)$] + $N_2(10\%)$ after 24hrs.

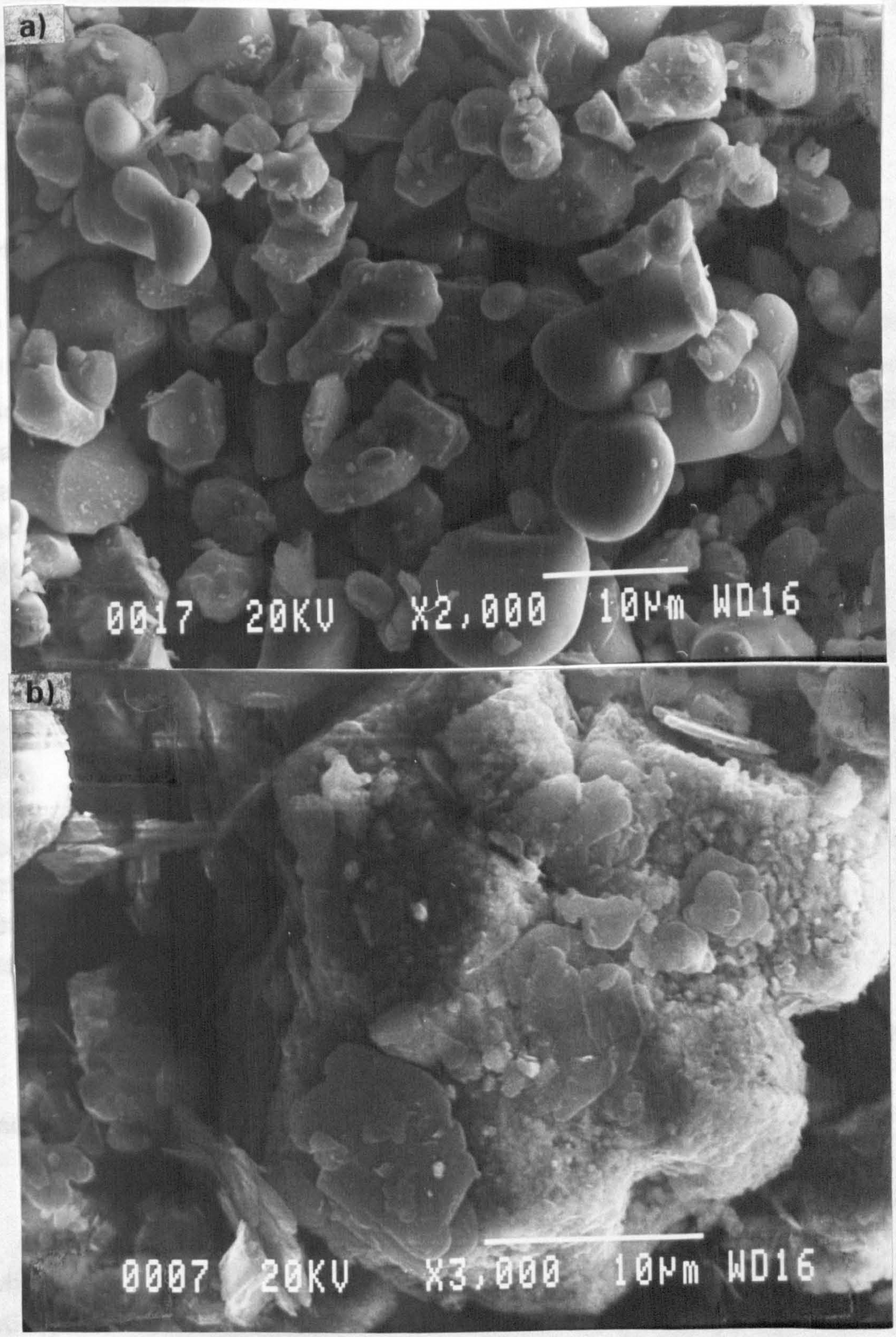

Photo IV-6. The morphology of TiB_2 and BN reagent mixture (a) before and (b) after heat treatment at 1773K for 48 hrs in nitrogen gas atmosphere. (N_2 flow rate:0.5l·min^{-1})

of chromium appears to have a large effect on the morphology of diboride crystals.

6. DISCUSSION

6.1 The Mechanism of TiB_2 Synthesis Reaction

Titanium dioxide and boron oxide reduce to lower oxides in the presence of carbon above thermodynamic equilibrium temperatures. The phase constitution above the equilibrium temperature are determined by the partial pressure of carbon monoxide gas generated as a result of the reduction reaction. For example, rutile was reduced above 1273K, as indicated in chapter II, it progressively loses oxygen and transforms into non-stoichiometric sub-oxides. The reduction sequence is as follows:

$$TiO_2 \rightarrow Ti_4O_7 \rightarrow Ti_3O_5 \rightarrow Ti(OC)_x \rightarrow TiC \qquad \textbf{(4-10)}$$

In the presence of nitrogen or ammonia gas, the last two reaction products are titanium oxynitrides/oxycarbonitrides and titanium carbonitrides/nitrides. The reduction process raises the activity of titanium metal in the sub-oxide lattice. Boron oxide (B_2O_3) similarly reduces to (BO) gas and in this way raises the activity of boron. Once the thermodynamic chemical potential of titanium and boron rises to a critical level, the formation of TiB_2 crystals takes place. The reduction of boric oxide is a critical step:

$$B_2O_3 + C = 2BO + CO \qquad \textbf{(4-11)}$$

and the equilibrium constant, K_{11} is given by

$$K_{11} = \exp[-\Delta G^\circ_{11}/RT] = P_{CO}\cdot(P_{BO})^2 \qquad \textbf{(4-12)}$$

where p is the partial pressure of the gas species in the reaction chamber and ΔG°_{11} is the standard Gibbs free energy change at an isotherm T. For unit activity of boric oxide and carbon, P_{BO} at 1773K is $1.2\text{x}10^{-4}$ atmosphere. It is important to note from the X-ray diffraction results that only Ti_3O_5 can be equilibrium with TiB_2 phase. When the reduction of oxide mixture TiO_2:B_2O_3

=1:1 take place in the presence of carbon, the reduction of TiO_2 to Ti(OC) or TiC takes place with Ti_3O_5 as an intermediate non-stoichiometric oxide phase. An important aspect in addition to the formation of sub-oxides, to note is the volatilisation of boric oxide liquid to boric oxide gas and its subsequent reduction to BO gas. The free energy of formation of boric oxide liquid to boric oxide gas is 360.05-0.186T $kJ \cdot mol^{-1}$ as indicated in Chapter III. This means that boric oxide liquid plays an insignificant role at high temperatures.

On the basis of the results of X-ray powder diffraction pattern, the mechanism of reduction of titanium dioxide to titanium diboride is as follows and can be defined by the following set of chemical reactions.

At low temperatures in the 1573K temperature range:

$$Ti_3O_5 + 3B_2O_3(g) + 14C = 3TiB_2 + 14CO \qquad \textbf{(4-13)}$$

reaction can occur. However, the reaction will only sustain in the presence of a physical contact between the non-stoichiometric oxide and carbon. It also appears to be evident is that when the ratio of TiO_2/B_2O_3 in the pellet is unity, only a part of the total carbon reacts with boric oxide and produces BO gas. In the same way, the rutile phase reduces to Ti_3O_5. The formation of the oxycarbide intermediate phase succeeds the reduction of Ti_3O_5. The presence of this phase is essential and provides a diffusion medium for carbon and oxygen. This is promoted by the available vacant sites from the non-stoichiometry of the oxycarbide phase. The absence of the titanium monoxide (TiO) phase under reducing conditions may support that both Ti_3O_5 and oxycarbide are more stable under reducing conditions. The oxycarbide phase is the intermediate phase for the transport of carbon and oxygen atoms and from this phase, the formation of diboride phase takes place. The proposed mechanism is consistent with the experimental results shown in Table IV-6 and Figure IV-7. This means that carbon and oxygen diffusion can take place through the $Ti(C_{1-x}O_x)$ lattice and either boric oxide or BO gas can pore diffuse to facilitate the formation of titanium diboride.

$$Ti(C_{1-x}O_x) + B_2O_3 + 3C = TiB_2 + (4-x)CO \qquad \textbf{(4-14)}$$

At temperatures higher than 1573K, the reduction mechanism changes because the generation of BO gas becomes thermodynamically more favourable. Therefore the oxycarbide phase can then directly react with the

mixture of BO and CO gas.

$$Ti(O_{1-x}C_x) + 2BO + CO = TiB_2 + CO_2 \quad \textbf{(4-15)}$$

or

$$Ti(O_{1-x}C_x) + 2BO + C = TiB_2 + CO \quad \textbf{(4-16)}$$

The CO_2 gas produced in this way can be regenerated in-situ via the Boudouard reaction ie $CO_2 + C = 2CO$ gas. The overall mass transport process can therefore be summarised by the following schematic diagram shown in **Figure IV-10**. The process (B) is less likely to occur because CO_2 is a less stable gas at higher temperatures. The presence of BO or B_2O_3 gas in the reducing atmosphere implies that the interstitial diffusion rate of carbon and oxygen in the oxycarbide lattice is expected to increase at least by the same order of magnitude as the drop in the activity of boron from BO gas to TiB_2.

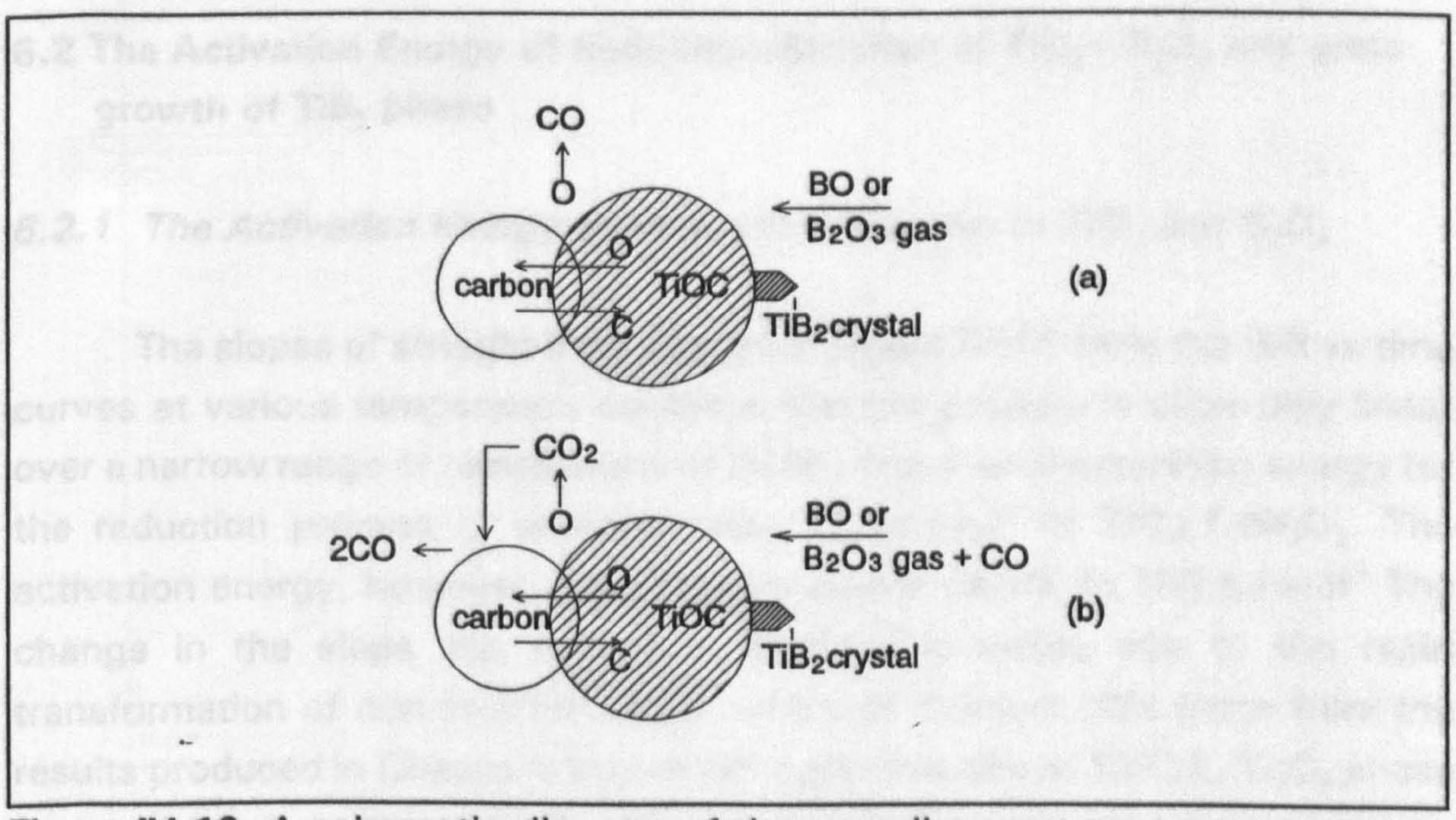

Figure IV-10. A schematic diagram of the overall mass transport process.

This means that the oxygen and carbon diffusion in the oxycarbide lattice rises due to the chemical potential gradient. By examining reactions given in **Equations (4-15)** and **(4-16)**, it is important that the generation of BO gas must compete with the rate of consumption of BO leading to the formation of TiB_2 phase. The calculation of the free energy change at different temperatures for

reactions given by Equations (4-15) and (4-16) show that the equilibrium CO partial pressure for TiB_2 phase is higher than for the stability of TiC or $TiOC_{1-x}$. It is due to TiC or TiO phase can not co-exist with TiB_2 because the partial pressure of CO is higher. The calculated CO partial pressures are shown in **Table IV-14** below.

Table IV-14. The equilibrium partial pressure of CO for various carbothermic reactions.

Reactions	P_{CO}(atm) at 1573K
(a) $Ti_3O_5 + 2C = 3TiO + 2CO$	4.95×10^{-2}
(b) $Ti_3O_5 + 2.3C = 3Ti(O_{0.95}C_{0.05}) + 2.15CO$	7.76×10^{-2}
(c) $Ti(O_{0.95}C_{0.05}) + 2BO + 2.95C = TiB_2 + 3CO$	1.73×10^{10}

6.2 The Activation Energy of Reduction Reaction of $TiO_2 + B_2O_3$ and grain growth of TiB_2 phase

6.2.1 The Activation Energy of Reduction Reaction of TiO_2 and B_2O_3

The slopes of straight lines plotted in **Figure IV-11** from the %R vs time curves at various temperature confirms that the process is ostensibly linear over a narrow range of temperature of 200K. The overall activation energy for the reduction process is approximately 52 $kJ \cdot mol^{-1}$ of $TiO_2/1.5B_2O_3$. The activation energy, however, rises sharply below 1373K to 150 $KJ \cdot mol^{-1}$ The change in the slope the Arrhenius relationship arises due to the rapid transformation of non-stoichiometric oxides of titanium. We know from the results produced in Chapter II that at temperatures above 1373K, Ti_3O_5 phase forms at the expense of Ti_4O_7. The change in the activation energy can be attributed to the reduction-reaction-induced transformations in the crystalline lattice. At higher temperature above 1573K, the diffusion of interstitial atoms in these oxides appear to be substantially fast and the enhance chemical reaction yields an activation energy of 52 KJ. The diffusion rate in the oxycarbide lattice rises due to the boron monoxide chemical potential. The low temperature activation energy is within the acceptable value for the nitridation of TiO_2 to TiN. This is referred to in Chapter II.

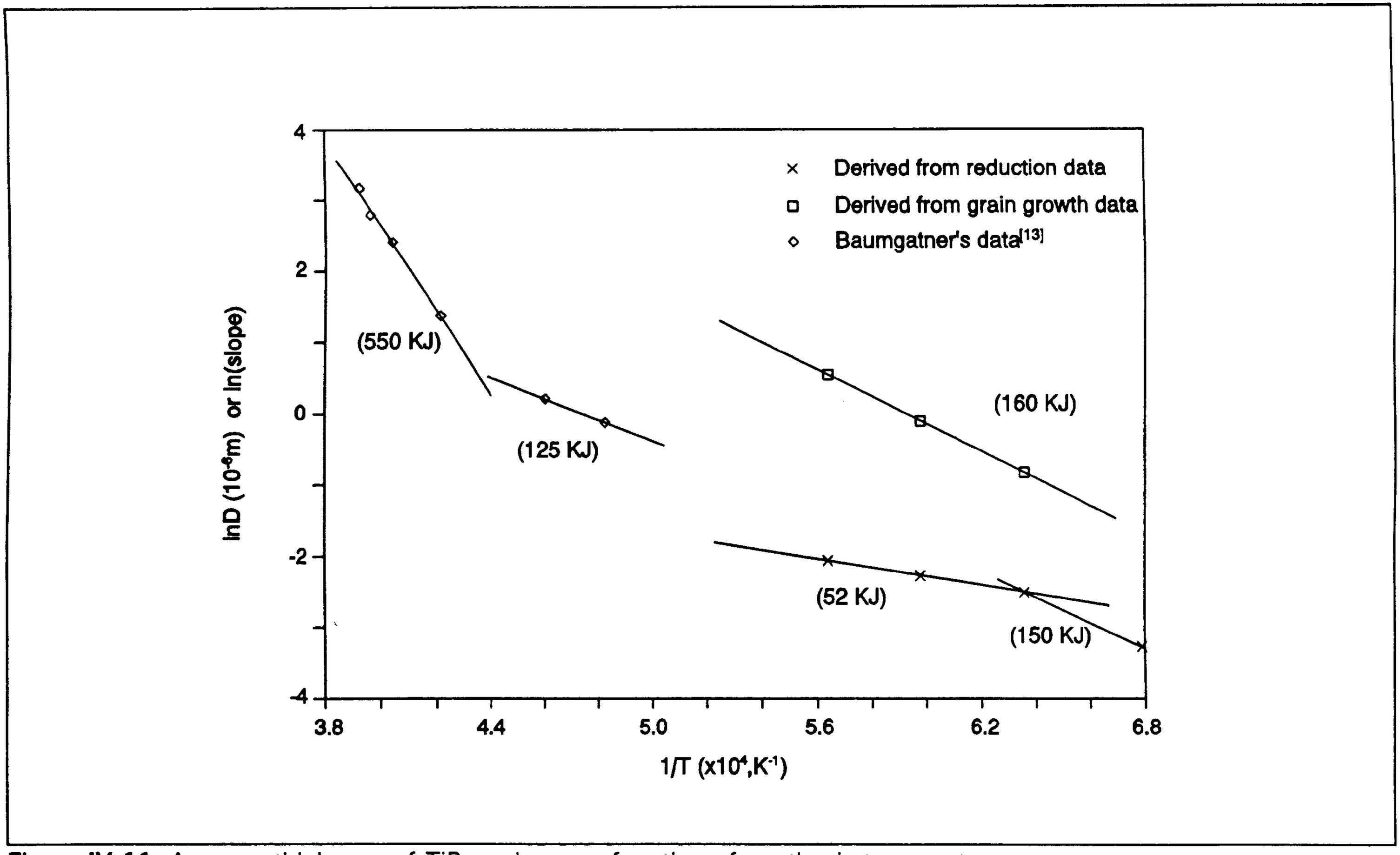

Figure IV-11. Average thickness of TiB_2 grains as a function of synthesis temperature.

6.2.2 The Activation Energy of grain growth of TiB_2 phase

The relationship between the natural logarithm of average thickness of TiB_2 and 1/T yielded the value of the activation energy for the growth of TiB_2 phase. This was approximately 160 KJ. This result was compared with the data reported by Baumgartner et al[13] and plotted in **Figure IV-11**. They measured the average TiB_2 grain size from the sintering experiment which were carried out up to 2600K and the derived value of the activation energy was 1.2 $MJ \cdot mole^{-1}$. Replotting the results of Baumgartner yielded activation energy values for the low and high temperature range. At high temperature, the grain growth rate encounters a thermal activation of 550 KJ whereas the low temperature activation energy was of the order of 125 KJ. The change in the slope occurs at 2373K which is at around 0.66 T_m. The growth rate of TiB_2 at different temperatures is compared with the partial pressure of BO gas at a given temperature. We defined that the growth rate increases with the increasing partial pressure of BO gas. We have assumed that the partial pressure of CO is fixed at 0.1 atmosphere. The derived values of growth rate indicates that the activation energy is of order of 160 KJ. This is comparable to the low temperature activation energy derived from the grain growth rate. The grain growth rate data (by Baumgatner) indicates that the lattice diffusion dominates above 2373K, whereas the surface diffusion governs only below $<0.66\ T_m$. The comparison of activation energy for crystal growth rate indicates that the surface diffusion dominates the growth process. This also appears to be true from the microstructural investigation which shows the presence of spiral and ledge growth. In the classical crystal growth model, whereby a crystalline material grains from a vapour or by VLS mechanism, the growth rate is exponentially dependent on the thermodynamic driving force (ΔG). As the ΔG rises, the rate of crystal growth increases. This is the reason that the crystal growth rate is significantly larger in reduction with calcium carbide.

6.3 The Phase Stability Diagram in Ti-B-N System

After the initial stage, the boride formation progressed via a gas-solid reaction, $2BO_{(gas)} + 1/3Ti_3O_5 + 11/3C = TiB_2 + 11/3CO$. When B_2O_3/TiO_2 is high,

TiC converts into TiB_2 because of the presence of sufficient quantities of BO gas above 1644K which is the temperature of transformation of TiC to TiB_2 in the presence of B_2O_3 by carbothermic reduction. The ratio of phases produced varied depending upon the composition of starting materials, temperature and reaction time. Therefore it is possible to control the production of ceramic mixtures as well as the volume of constituent phases. The equilibrium phase relationship identifies the stability range of various phases in the Ti-B-N system, as shown in **Figure IV-12**. Here the two phase fields surround a three phase $TiB_2 + TiN + BN$ region in which the degree of freedom is one at a constant pressure. The phase field should reduce to a point at a constant temperature and pressure condition. However this is not the case because the phase equilibrium relationship is a pseudo-equilibrium relationship. This is because we have excluded carbon and oxygen as components in the Gibbs phase relationship. However if CO gas is taken as a component, the degree of freedom is 2 in a 3-condensed phase field. The regions of phase stability are compared with the experimental data.

Some experimental results shown in Figure IV-12 include experimental data that lie in different phase fields. For example by considering the reaction:

$$TiB_2 + 3/2N_2 = TiN + 2BN \qquad (4\text{-}17)$$

$$pN_2 = (1/K)^{2/3} \qquad (4\text{-}18)$$

At temperature 1773, pN_2 is 5.95×10^{-3}. Below this partial pressure of nitrogen, the diboride phase should be more stable. This is however not the case. The phase equilibrium in the Ti-B-N system is determined by the combination of univariant lines as indicated in Figure IV-12. This is apparent from the experimental results of controlled nitridation of TiB_2 leading to the formation of TiCN and BN at 1773K (see section 5.2.1). Experimental points 1 to 5 in Figure IV-12 lie in the $TiN + BN$ and $TiB_2 + TiN + BN$ phase fields. Points 1 to 4 are consistent with the calculated phase diagram for which the number of crystalline phases produced the reduction-nitridation agree with the powder diffraction pattern shown in **Table IV-9**. Whereas for the experimental point 5, the BN phase was not identified by X-ray powder diffraction analysis and hence appears to be inconsistent with the calculated phase field. It is also likely that the small quantities of BN might not have been detected by powder diffraction technique. For this a detailed microscopic analysis is required.

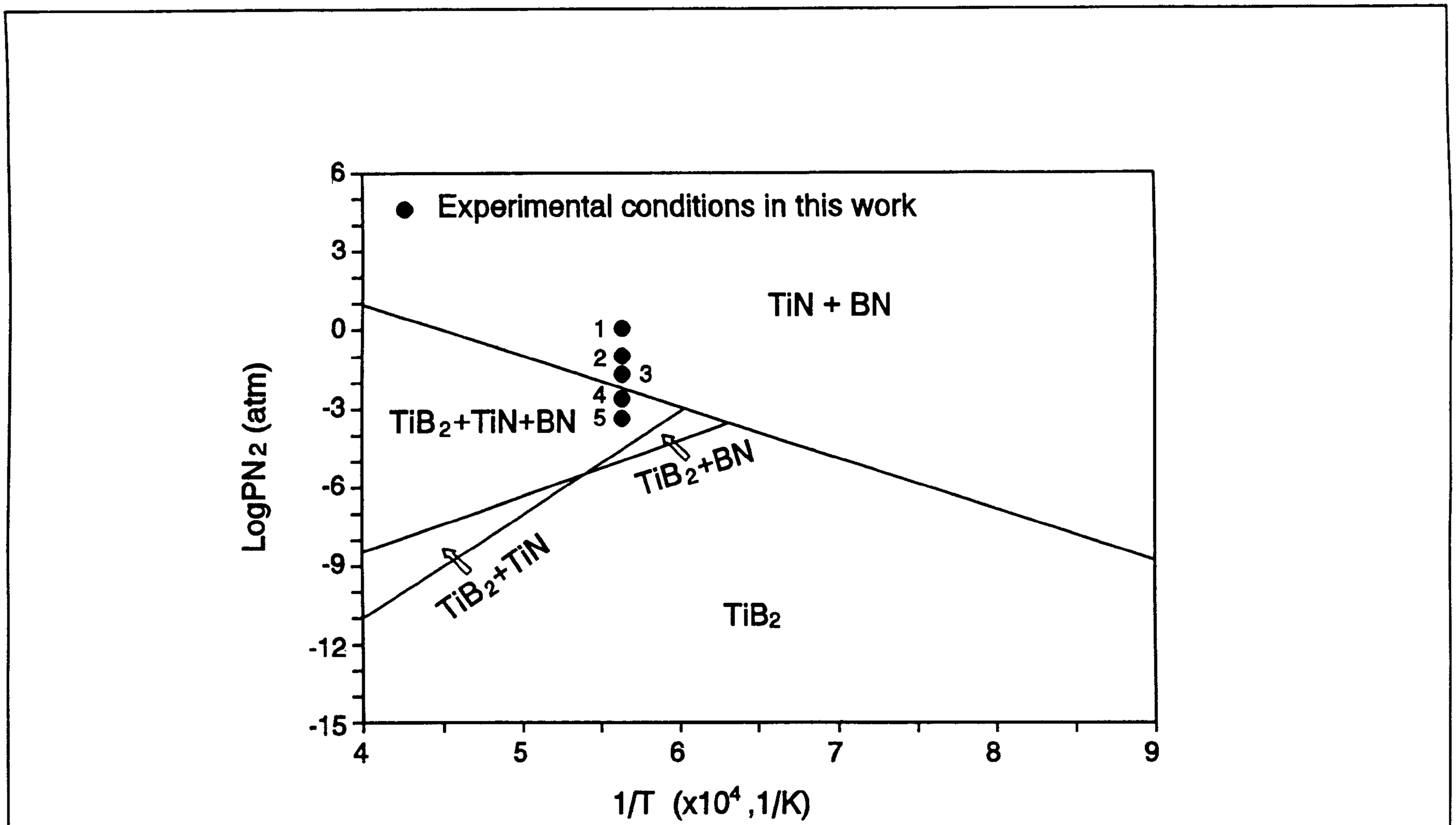

Figure IV-12. The regions of phases stability for the boride and nitrides.

6.4 The Phase Diagram for the TiB_2-CrB_2

The phase diagram for the binary TiB_2-CrB_2 system was calculated and is shown in **Figure IV-13**. Calculation procedures are similar shown to those in section 6.5 in Chapter II. Both TiB_2 and CrB_2 are congruently melting phase with enthalpies of fusion, ΔH_F, of 102.420 $J \cdot mol^{-1}$ and 66.842 $J \cdot mol^{-1}$ at 3253K and 2123K, respectively. Most of the borides exhibit a complete mutual solid and liquid solubility at all temperatures in excess of 2273K. The calculation of the diboride binary phase diagram enables the understanding of the theoretical possible mixing range. We have carried out a limited number of experiments and the determination of lattice parameter is a means to verify the solid solution limits. In the diboride lattice of Ti, Cr atoms replace Ti metals along the (001) basal plane. This occurs which the nucleation and growth of crystals take place. From the calculated phase diagram we find that TiB_2 and CrB_2 melt congruently and are completely intersoluble. It can be seen that the diagram exhibits no maximum or minimum in the liquidus curve. The solidus line between the melting points of TiB_2 and CrB_2 creates an area where liquid and solid solutions, both of variable composition exist.

Mixed diborides such as TiB_2-CrB_2 are important materials from the high temperature corrosion resistance view point. The solid solution phase could form a passivating barrier of Cr_2O_3 to the progressing oxidation front at elevated temperatures. The lattice parameters of the mixed diboride formed by the co-reduction of chromium and titanium oxides are shown in **Figure IV-14**. The experimental data from sintering experiments carried out by Zdaniewski[2] is in good agreement with the estimated lattice parameter using equation $a_{s.s(nm)} = X_{CrB2} \cdot a_{CrB2} + X_{TiB2} \cdot a_{TiB2}$ where 'X' is the mole fraction of the boride phase and 'a' is the lattice dimension. A similar equation was used to estimate the c-parameter of the hexagonal boride lattice. The lattice parameters estimated from the powder diffraction of the co-reduced samples are higher than for equilibrium solid solutions. This is because during the experiments, the sintering time was insufficient to achieve a completely equilibrium microstructure.

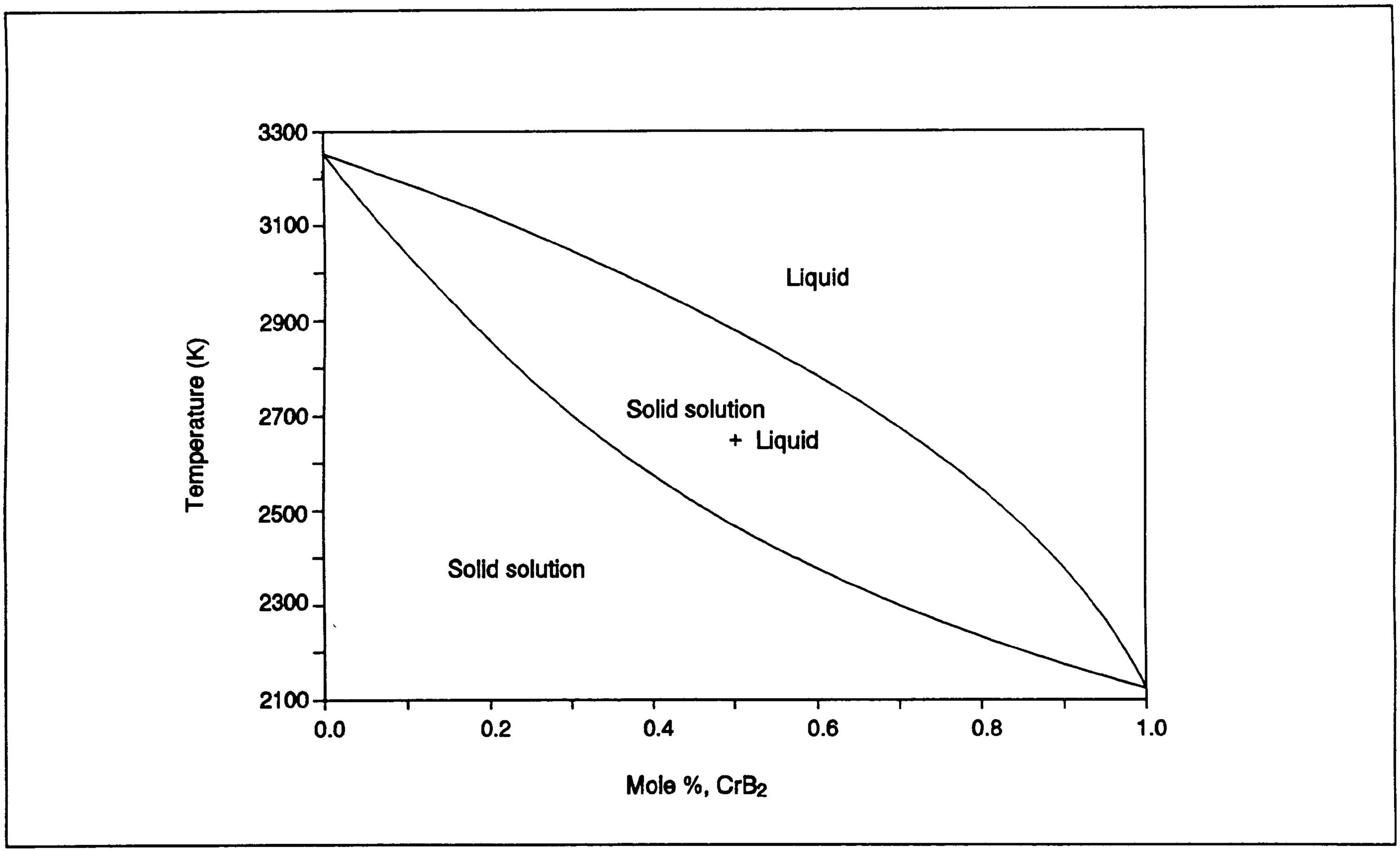

Figure IV-13. The calculated liquidus and solidus phase boundaries in TiB_2-CrB_2 system.

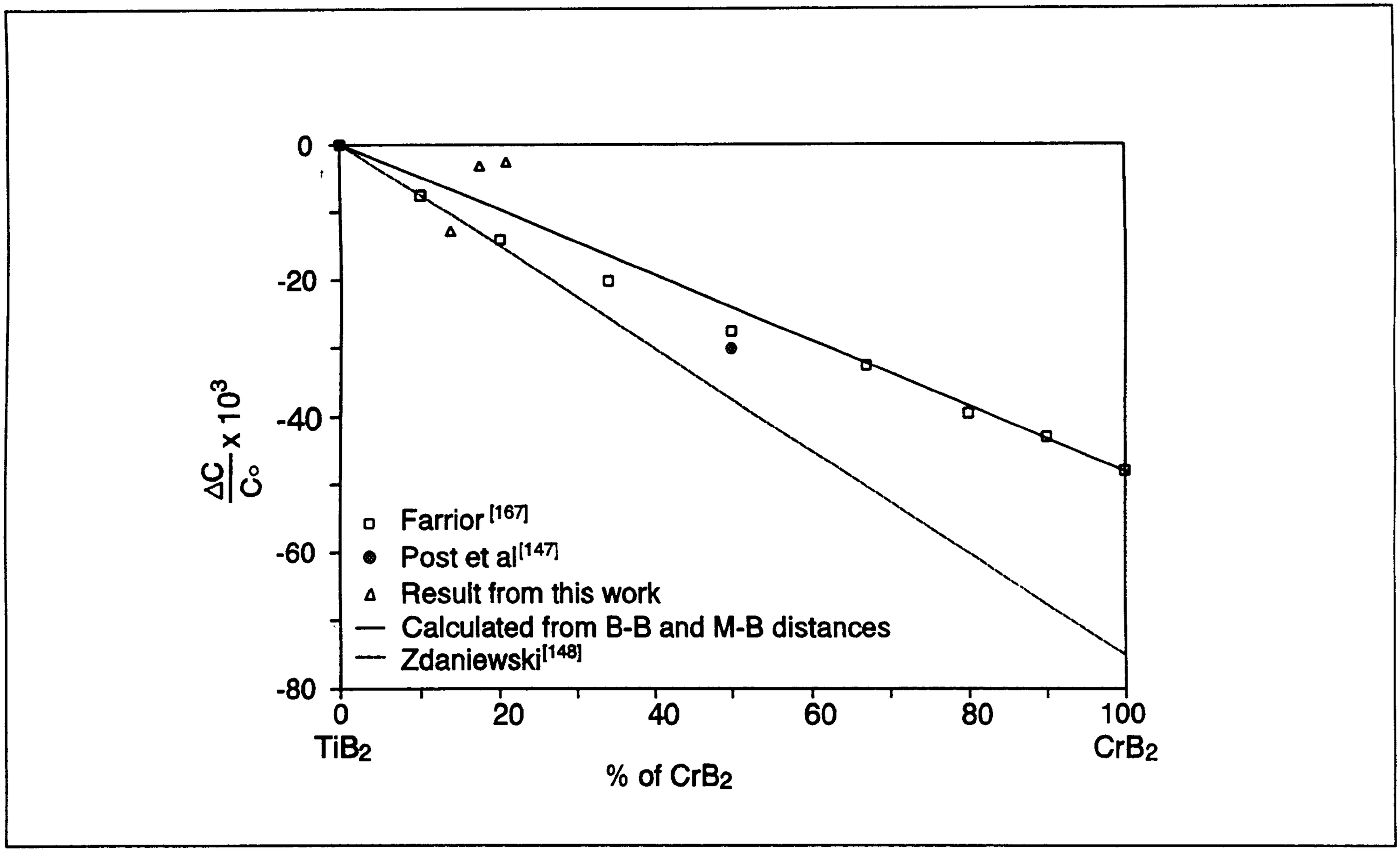

Figure IV-14. The variation of $\Delta c/c_0$ as a function of Cr content.

7. CONCLUSIONS

The titanium boride (TiB_2) phase produced by carbothermic reduction has a hexagonal platelet morphology and during the reduction reactions, once the crystals nucleate they have a tendency to grow. The grain growth rate in the temperature range 1573K to 1773K indicates that the overall activation energy of grain growth is of the order of 160 $KJ \cdot mol^{-1}$ and is significantly lower than the activation energy for the chemical reaction. From the comparison of grain growth rate data, the crystallites of TiB_2 appears to grow via a surface diffusion mechanism. For the production of the composite microstructure, the N_2 partial pressure was found to be the most critical factor. In the composite microstructure, the titanium nitride particle has a submicrometer size whereas the boride particle size is only a few micrometers. The calculated equilibrium phase fields agree with the experimental data and provide a means to select the variables for the reduction condition for designing a required ceramic microstructure. The constituent phases depend on the reduction conditions; for example nitrides in equilibrium with TiB_2 can only form in nitriding atmosphere whereas TiC or B_4C form in inert atmospheres. The investigation also shows the viability of production of composite powder mixture via the oxide co-reduction technique. The carbothermic reaction process of TiO_2 and B_2O_3 in the presence of N_2 atmosphere leads to the formation of ceramic phase mixtures ideal for designing composite materials.

CHAPTER V. CONCLUSIONS

Nitrides and carbides of boron and titanium, and titanium diboride powders can be synthesized by the reduction of ingredient oxides with carbon in a suitable atmosphere. The carbon reduction technology also provides a potential route to manufacture powder mixtures of the above ceramic materials by selecting suitable process variables and conditions. The process on a laboratory scale has yielded the following types of powders and their mixtures. a) TiC_xN_{1-x}, b) TiB_2, c) h-BN and a-BN, d) h-BN or a-BN with B_4C, e) h-BN with c-BN and w-BN whiskers, f) TiB_2-TiN, g) TiB_2-TiN-BN and h) TiN-BN. The maximum quantities of powder produced on a small-scale laboratory trials were 5 grams. The morphology and size of the powders were primarily dependent on process variables such as gas composition, reducing agent etc. The temperature and time had no major effect on the morphology of the crystals formed.

The reduction of TiO_2 to sub-oxide takes place and it is this oxide which transforms into a carbonitride or nitride phase. The experimentally determined overall activation energy of reduction-nitridation reaction is 120 $kJ \cdot mol^{-1}$ and is similar to the energy barrier for oxygen diffusion in the rutile lattice. From the results of nitridation, it is also evident that either the presence of a catalyst or activated charcoal aids the reduction reaction and consequently the particle size of the ceramic phase produced is smaller by an order of magnitude. Typically the average particle size of TiCN produced after the reduction with activated charcoal is less than 0.5 μm whereas with graphite, the average size is found to be 5 μm and above. The carbonitride phase produced has a range of composition and its composition strictly depends upon the operating parameters such as nitrogen gas partial pressure, temperature and type of carbon. The calculated equilibrium phase fields agree with the experimental data and provide a means to select the variables for the reduction condition for designing a required ceramic microstructure.

The reactivity of carbon, B/C ratio and gas composition are the most important variables that determined the formation, structure and morphology of nitride and carbide phase during reduction. In this study, it has been demonstrated that boron nitride and boron carbide powder and whiskers can be produced by carbothermic reaction. Depending on the composition of gas,

starting materials, temperatures selected and the time of the reaction, powders have different morphology. The proportion of nitride and carbide which has a composite microstructure can be controlled by selecting the processing parameters. Specially the use of ammonium halide salts promotes the formation of metastable forms of boron nitride.

The titanium boride (TiB_2) phase produced by carbothermic reduction has a hexagonal platelet morphology and during the reduction reactions, once the crystals nucleate they have a tendency to grow. The grain growth rate in the temperature range 1573K to 1773K indicates that the overall activation energy of grain growth is of the order of 160 $KJ \cdot mol^{-1}$ and is significantly lower than the activation energy for the chemical reaction. From the comparison of grain growth rate data, the crystallites of TiB_2 appear to grow via a surface diffusion mechanism. The carbothermic reaction process of TiO_2 and B_2O_3 in the presence of N_2 atmosphere leads to the formation of ceramic phase mixtures ideal for designing composite materials.

CHAPTER VII. REFERENCES

[1] Y.G.Gogotsi, V.A.Lavrenko : "High Temperature Technology", 6(1988), 2, p79

[2] H.J.Goldschmidt : "Interstitial Alloys", (Butterworth & Co. Ltd., 1967), 255, 225

[3] B.S.Terry and O.Chinyamakobvu : "Carbothermic Reduction of Ilmenite and Rutile as Means of Production of Iron Based Ti(O,C) Metal Matrix Composites", Mater.Sci.Technol., 7 (1991), 842-848

[4] T.Yoshida, K.Kawasaki, K.Nakagawa and K.Akashi : "The Synthesis of Ultrafine Titanium Nitride in an rf Plasma", J.Mater.Sci., 14 (1979), 1624-30

[5] S.Umezu ; "The formation of TiN by the action of titanium oxide and nitrogen", Poc.Imp.Acad.(Tokyo), 7 (1931), 9, 356-356

[6] T.Licko, V.Figusch and J.Puchyova ; "Carbothermal Reduction and Nitriding of TiO_2", J.Europ.Cer.Soc., 5(1989), 257-265

[7] A.Kato, M.Iwata, J.Hojo and M.Nagano : "Fine Titanium Nitride Powders by the Vapor Phase Reaction of the Titanium(IV) Chloride-Ammonia-Hydrogen-Nitrogen System", Yogyo Kyokaishi, 83 (1975), 453; Chem. Abstr., 83: 149700z.

[8] E.K.Storms : "The Refractory Carbides", Academic Press, New York, 1967

[9] M.K.Gallagher, W.E.Rhine, and H.K.Bowen : "Low temperature route to high-purity titanium, zirconium, and hafnium diboride powders and films", in Ultrastructure Processing of Advanced Ceramics, (ed. J.D.Mackenzie and D.R.Ulrich), (1988), 901-906.

[10] R.A.Steiger and F.G.Stroke : U.S. patent number 4180670, (1978).

[11] R.A.Steiger : U.S. patent number 4266977 (1981).

[12] J.J.Ritter : Adv. Ceram, 21(1987), 21.

[13] H.R.Baumgartner, R.A.Steiger : "Sintering Properties of Titanium Diboride Made from Powder Synthesised in a Plasma-Arc Heater", J.Am.Ceram.Soc. 67 (1984), 3, 207-12

[14] F.W.Vahldiek : "Electrical resistivity, elastic modulus and debye temperature of TiB_2", J. Less-comm. Met. 12, (1967) 202-209.

[15] R.F.Hill, J.Lee, L.C.Montgomery and W.M.Shen : "Chemical Synthesis of Ceramic Powders", 1-7

[16] B.Cales ; "Ceramic matrix composites", 2nd Europ. Symposium on Engineering Ceramics, F.L.Riley(ed.), Elsevier Applied Sci., 1989, p198

[17] G.A.Cochran et al : "The Synthesis of a High Quality, Low Cost Silicon Nitride Powder by the Carbothermal Reduction of Silica", Silicon Nitride 93, (ed) M.J.Hoffmann et al, Trans Tech Publications, vol.89-91 (1994), 3-8

[18] M.Srinivasan : "The Silicon Carbide Family of Structural Ceramics", Structure Ceramics (ed.) J.B.Wachtmann Jr., Treatise on Materials and Technology, vol.29, 99-159

[19] M.L.Torti : "The Silicon Nitride and Sialon Families of Structural Ceramics", Structure Ceramics (ed.) J.B.Wachtmann Jr., Treatise on Materials and Technology, vol.29, 161

[20] V.D.Lyubimov, T.V.Shestakova, G.P.Shveikin, S.I.Alyamovskii and Y.G.Zainulin : "High Temperature Reaction of TiO_2 with carbon in Nitrogen Atmosphere", (in Russian), Neorg.Mater., 13 (1977). 1, 58-62

[21] W.Y.Li and F.L.Riley : "The Production of Titanium Nitride by the Carbothermal Nitridation of Titanium Dioxide Powder", J.Europ.Cer.Soc., 8 (1991), 345-354

[22] G.V.White, K.J.D.Mackenzie, and J.H.Jonston: "Carbothermal synsthesis of titanium nitride, Part 1", J.Mat.Sci., 27(1992) 4287-4293

[23] J.Mukerji and S.K.Biswas : "Synthesis, Properties and Oxidation of Alumina-Titanium Nitride Composites", J.Am.Ceram.Soc., 73 (1990), 1, 142-45

[24] A.Bellosi, S.Guicciardi and A.Tampieri : "Delelopment and Characterization of Electroconductivity Si_3N_4-TiN Composites", J.Europ.Cream.Soc., 9(1992), 83-93

[25] F.Hong, R.J.Lumby and M.H.Lewis : "TiN/Sialon Composites via in-situ Reduction Sintering", J.Europ.Ceram.Soc., 11 (1993), 237-239

[26] K.S.Coley : Ph.D Thesis, Uiversity of Lodon, 1986

[27] K.S.Coley, P.Grieveson and B.S.Terry : in Proc. of the Rosenqvist Conference, University of Trondheim, Norway, 1988

[28] B.S.Terry and O.Chinyamakobvu : "Dispersion and Reaction of TiC in Liquid Iron Alloys", Mater.Sci.Technol., 8 (1992), 399-405

[29] L.E.Toth : "Transition Metal Carbides and Nitrides", Academic Press, New York, 1971

[30] K.Agte and K.Moers : Z.Anorg.Allgem.Chem., 198(1931), 133

(13) T.Akashi, A.Sawaoka and S.Saito : J.Am.Ceram.Soc., 61 (1978), 245-246

[31] P.Duwez and F.Odell : J.Electrochem. Soc., 97(1950), 299

[32] P.Schwarzkopf and R.Kieffer : "Refractory Hard Metals", Macmillan, New York, 1953

[33] A.Doi, N.Fusimori and T.Yoshioka : Inst.Phys.Conf.Ser., 75(1986),743

[34] Z.Lianxi, J.Pong and R.Junguo : Chendu Keji Daxue Xuebao, (1985), 65

[35] M.E-Grami and Z.A.Munir : "Effect of Nitrogen Pressure and Dilute Content on the Combustion Synthesis of Titanium Nitride", J.Am.Ceram.Soc., 73 (1990), 8, 2222-27

[36] M.E-Grami and Z.A.Munir : "Effect of Porosity on the Combustion Synthesis of Titanium Nitride", J.Am.Ceram.Soc., 73 (1990), 5, 1235-39

[37] J.B.Holt and Z.A.Munir : "Combustion Synthesis of Titanium Carbide: Theory and Experiment", J.Mater.Sci., 21 (1986), 251-259

[38] L.J.Kecskes and A.Niiler : "Impurities in the Combustion Synthesis of Titanium Carbide", J.Am.Ceram.Soc., 72 (1989), 4, 655-61

[39] S.Adachi, T.Wada and T.Mihara : "Fabrication of Titanium Carbide Ceramics by High-Temperature Self-Combustion Sintering of Titanium Powder and Carbon Fiber", J.Am.Ceram.Soc., 75 (1989), 5, 805-809

[40] K.Honma, H.Okuyama, S.Ohno and M.Uda : "Preparation of Ultra-fine Particles of TiN by Nitrogen-Hydrogen Gas-Mixture Plasma Method", Koon Gakkaishi, 13 (1987), 199

[41] M.Uda and S.Ohno : "Preparation of Ultrafine Particles by Nitrogen Plasma-Molten Metal Reaction", Nippon Kagaku Kaishi, (1984), 802-68

[42] S.Iwama, K.Hayakawa and T.Arizumi : "Ultrafine Powders of TiN and AlN Produced by a Reactive Gas Evaporation Technique with Electron Beam Heating", J.Cryst.Growth, 56 (1982), 265-69

[43] M.Yoshimura, M.Nishoika and S.Somiya : "Synthesis of TiN and TiC Powders by a Reduction/Nitridation Method using Arc Image Heating", J.Mater.Sci.Lett., 6 (1987), 1463-65

[44] G.W.Sears : Acta Met vol. 3 1955 pp 361.

[45] C.Wagner: The Chipman Conference 1962. MIT Press.

[46] T.A.Nolan, L.F.Allard, D.W.Coffey, C.R.Hubbard and R.A.Padgett : "Microstructure and Crystallography of Titanium Nitride Whiskers Grown by a Vapor-Liquid-Solid Process", J.Am.Ceram.Soc., 74 (1991), 11, 2769-75

[47] C.E.Bamberger, P.Angelini and T.A.Nolan : "Formation of Titanium Nitride Whikers by Reaction of Sodium Titanium Bronze with Molten Sodium Cyanide", J.Am.Ceram.Soc. 72 (1989), 4, 587-92

[48] R.J.Lumby and R.F.Coe : Proc. Brit. Ceram. Soc., (1970), 15, 91

[49] G.G.Deeley, J.M.Herbert and N.C.Moore : (1961) Powder Met. , 8, 145

[50] G.E.Gazza : Bull.Am.Ceram.Soc., 54 (1975), 778

[51] B.Saruhan, M.J.Pomeroy and S.Hampshire : Non-Oxide Technical And Engineering Ceramics, Stuart Hampshire(ed.), Elsevier Applied Science, 1985, P69-80

[52] H.Hausner ; "Ceramic Materials and Components for Engins", Proceedings of the Second International Symposium, W.Bunk and H.Hausner(ed.), (1986),p27-38

[53] A.Sawaoka, K.Kondo, N.Hashimodo and S.Saito : Proceedings of the International Symposium on Factors in Densification and Sintering of Oxide and Non-oxide Ceramics, Somiya, S.(ed.), Tokyo, 1979, p.339-344.

[54] C.Martin, B.Cales, P.Vivier and P.Mathieu : "Electrical Discharge Machinable Ceramic Composites", Mar.Sci.Eng., A109(1989), 351-356

[55] S.Kirkpatrick : "Percolation and Conduction", Rev.Mod.Phys., 45 (1973), 4, 574-588

[56] G.Hagg, Z. Phys. Chem., abs. B12, 33(1931)

[57] D.W.Richerson : "Modern Ceramic Engineering", Marcel Dekker Inc., New York and Basel, 1982, p11

[58] G.V.Samsonov and T.S.Verkhoglyyadova : Dokl.Akad.Nauk SSSR, 138 (1961), 342

[59] R.Juza, A. Gabel, H.Rabenau and W.Klose : Z.Anorg. All. Chem. 329, 136(1964)

[60] P.Ehrlich : Z. Anorg. Allg. Chem. 259 (1949), 1

[61] Palty, A.E., Margolin, H., and Nielson, J.P. : "Titanium-nitrogen and titanium-boron systems". Trans. Am. Soc. metals, 46 (1954) 312-29.

[62] A.Brager, Acta Physiocochim. USSR, 11, 617(1939)

[63] F.A-Abautret, B.Pellissier, M.Miloche and P.Eveno : "Nitrogen Self-Diffusion in Titanium Nitride Single Crystals and Polycrystals", J.Europ.Cer.Soc., 8 (1991), 299-304

[64] JCPDS X-ray Powder Diffraction Card Files.

[65] M.W.Chase,Jr., et al., eds : "JANAF Thermochemical Tables" (3rd ed.), J.Phys.Chem.Ref.Data, vol.14 suppl.1, (1985), 640, 1542.

[66] O.Knache, O.Kubaschewski and K.Hesselmann (ed.) : "Thermochemical Properties of Inorganic Substances (2nd edn.)", Springer-Verlag, 1991

[67] S.Andersson, B.Collen, U.Kuylenstierna and A.Magneli : "Phase-Analysis Studies in the Titanium-Oxygen System", Acta Chem.Scan., 11 (1957), 10, 1641-52

[68] S.Andersson and A.Magneli : "Titanium Oxide Phases in the Range $TiO_{1.75}$ to $TiO_{1.90}$", Naturwissen Schaften , 43 (1956), 21, 495-496

[69] S.Asbrink and A.Magneli : "Crystal Structure Studies on Titanium Pentoxide", Acta Cryst., 12 (1959), 8, 575-81

[70] E.Hilti and F.Laves : Naturwissenchaften, 55 (1968), 130

[71] D.Watanabe, J.R.Castles, A.Jostsons and A.S.Malin : Acta Cryst., 23 (1967), 307

[72] P.G.Wahlbeck and P.W.Gilles : "Reinvestigation of the Phase Diagram for the System Titanium-Oxygen", J.Amer.Ceram.Soc, 49(1966), 4, 180-183

[73] A.Ouensanga : "Thermodynamic Study of the Ti-C-O System in the Temperature Range 1400-1600K", J.Less-Comm.Met., 63(1979), 225-235

[74] G.V.White, K.J.D.Mackenzie, I.W.M Brown, M.E.Bowden and J.H.Jonston : "Carbothermal synsthesis of titanium nitride, Part 2", ibid., 27(1992) 4294-4299

[75] K.Borowiec and T.Rosenqvist : "Phase Relations and Oxidation Studies in the System $Fe\text{-}Fe_2O_3\text{-}TiO_2$ at 700-1100°C", Scand.J.Metallurgy, 10 (1981), 217-224

[76] G.V.White, K.J.D.Mackenzie, I.W.M Brown, and J.H.Jonston : "Carbothermal synsthesis of titanium nitride, Part 3", ibid., 27(1992) 4390-4304

[77] E.T.Turkdogan : "Physical Chemistry of High Temperature Technology", (Academic press, New York), 1980, 5-26.

[78] E.T.Turkdogan and J.V.Vinters : Carbon, 8 (1970), 39.

[79] B.D.Cullity : "Elements of X-ray Diffraction", 2nd ed., Addison-Wesley Publishing Co.

[80] A.Ouensanga : "Thermodynamics of the Ti-C-O System at 1580K", J.Less-Comm.Met., 79(1981), 237-241

[81] W.D.Kingery, H.K.Bowen and D.R.Uhlmann : "Introduction to Ceramics", 2nd ed., Hohn Wiley & Sons.

[82] R.A.Swalin, Thermodynamics of Solids (New York.NY:John Wiley & Sons, 1972), 205.

[83] A.Chrysanthou, P.Grieveson and A.Jha : "Formation of Silicon Carbide Whiskers and Their Microstructure", J.Mater.Sci., 26(1991), 3463-3476.

[84] P.L.Walker Jr., M.Shelef and R.A.Anderson : "Catalysis of Carbon Gasification", Chemistry and Physics of Carbon, P.L.Walker Jr. (ed), (Edward Arnold LTD, Lodon), vol.4 (1968), 287-399

[85] R.T.Paine and C.K.Narula; "Synthetic Routes to Boron Nitride", Chemical Reviews, 90 (1990), 1, 73-91

[86] L.N.Rusanova, A.G.Romashin, G.I.Kulikova and O.P.Golubeva : "Boron nitride Ceramics-Problems and Development Perspectives", Soviet Powder Memallurgy and Metal Ceramics, 27 (1988), 1, 21-28

[87] F.Thevenot; "Boron Carbide-A Comprehensive Review", J. Eur. Ceram. Soc., 6(1990), p205-225

[88] R.H.Wentorf : J.Chem.Phys., 1957, 26, 956

[89] F.P.Bundy, H.T.Hall, H.M.Strong and R.H.Wentorf : Nature (London) 1955, 176, 51

[90] H.T.Hall, H.M.Strong and R.H.Wentorf : "Method of making Diamonds", U.S. Patent 2, 947, 610 Aug. 2, 1960

[91] R.H.Wentorf : J.Chem.Phys., 1961, 34, 809

[92] H.T.Hall : "High temperature and high pressure apparatus", U.S. Patent 2, 941, 248 June 21, 1960

[93] H.T.Hall : Rev.Sci.Instr., 1960, 31, 125

[94] E.Rapoport : "Cubic boron nitride", Ann. Chim. Fr., 1985, 10, 607-638

[95] F.P.Bundy and R.H.Wentorf : J.Chem.Phys., 1963, 38, 1144

[96] G.A.Adadurov et al : Soviet Phys.-Doklady, 1967, 12, 173

[97] L.V.Al'tshuler, M.N.Pavlovskii and V.P.Drakin : Soviet Phys., 1967, 25, 260

[98] F.P.Bundy and J.S.Kasper : J.Chem.Phys., 1967, 46, 3437

[99] R.E.Hanneman, H.M.Strong and F.P.Bundy : Science, 1967, 155, 995

[100] A.F.Wells : "Structural Inorganic Chemistry", Clarendon Press, (5th ed.), Oxford, (1975), p874

[101] J.Thomas, N.E.Weston and T.E.O'connor: J.Am.Chem.Soc., 1963, 84, 4619

[102] R.W.Lynch and H.G.Drichamer : J.Chem.Phys., 44 (1966), 181

[103] A.V.Kurdyumov : Sov.Phys.Doklady, 20 (1975), 218

[104] F.R.Corrigan and F.P.Bundy : J.Chem.Phys., 63 (1975), 3812-3820

[105] N.J.Archer : "The Preparation and Properties of Pyrolitic Boron Nitride", High Temperature Chemistry of Inorganic and Ceramic Materials (ed. F.P.Glasser), The Chemical Society, Sep.(1976), 167-180

[106] K.A.Schwetz, and A.Lipp : "Boron Carbide, Boron Nitride and Metal Borides", Ullmann's Encyclopedia of Industrial Chemistry (ed.W.Gerhartz), 1985, 295-307

[107] R.S.Pease : Acta Crystallogra, 1952, 5, 356

[108] A.Meller : Gmelin Handbook of Inorganic Chemistry (ed. K.Buschbeck), Springer-Verlag, 1988

[109] S.N.Pikalov and A.M.Germannskii : "Crystalline Structure of Boron Nitride Produced by the Carbothermic Method", Soviet Powder Memallurgy and Metal Ceramics, 26 (1987) 5, 419-421

[110] S.N.Pikalov : "Mechanism of Formation of Graphite-like Boron Nitride in the Carbothermal Process", Soviet Powder Memallurgy and Metal Ceramics, 27 (1988) 5, 404-406

[111] M.Luce, O. Croix, Y.H.Zhou, M.Cauchetier, M.Sapin and L.Boulanger: "Laser synthesis and characterization of ultrafine boron nitride powders", Europian Ceramic Society Second Conference, September 11-14, 1991, Augsburg (FRG).

[112] T.Akashi and A.Sawaoka : "Shock Compaction of Cubic Boron Nitride Powders", J.Mater.Sci., 22 (1987), 1127-1134

[113] J.Szmidt, A.Jakubowski, A.Michaeski and A.Rusek : Thin Solid Films, 1983, 110, 7

[114] G.Kessler, H.D.Bauer, W.Pampe anf H.J.Scheibe : Thin Solid Films, 1987, 147, L45

[115] T.Soma, A.Sawaoka and S.Saito : Materials Research Bulletin, 9 (1974), 755-765.

[116] E.Tani, T.Soma, A.Sawaoka and S.Saito : Japan.J.Appl.Phy., 14 (1975), 1605-1606

[117] H.Hiraoka, O.Fukunaga and M.Iwata : Yogyokyo kaishi, 84 (1976), 163-170

[118] T.Akashi, A.Sawaoka and S.Saito : J.Am.Ceram.Soc., 61 (1978), 245-246

[119] A.Sawaoka, T.Soma and S.Saito : Japan.J.Appl.Phy., 13 (1974), 891-892

[120] T.Akashi, A.Sawaoka, S.Saito and M.Araki : Japan.J.Appl.Phys., 15 (1976), 891-892

[121] T.Sato, T.Ishii and N.Setaka : J.Am.Ceram.Soc., 65 (1982), C-162-164

[122] G.Demazeau, G.Biardeau and L.Vel : "Synthesis of cubic boron nitride using magnesium or magnesium-based fluoronitrides", Materials Letters, vol.10, No.3 Oct., 1990, pp139-144

[123] B.Akira, A.Sawaoka : "High-tech Ceramics", Gernot Kostorz (ed.), 1988, Academic press, 41

[124] C.F.Fowell, J.H.Oxley, J.M.Jr.Blocher : Vapor Deposition, Wiley, New York, 1966

[125] D.M.Hoffman, G.L.Doll and P.C.Eklund : Phys.Rev.B, 30 (1984), 6051

[126] GTE Products Corp., Exeter : "Pyrolitic Boron Nitride Materials Data Sheet".

[127] V.A.Butenko, V.V.Lopatin and V.P.Chernenko : Inorg.Mater., (Engl.Transl.), 20 (1984), 1428

[128] V.A.Lavrenko and A.F.Alexeev : Ceram.Ins., 12 (1986), 25

[129] N.G.Coles, D.R.Glasson and S.A.Jayaweera : J.Appl.Chem., 19 (1969), 178

[130] D.T-Launay, P.Goeuriot, G.Orange, F.Thevnot and G.Fantozzi : Rev.Int.Hautes Temp.Refract., 20 (1983), 147

[131] R.S.Kalyoncu; "BN Powder Synthesis at Low Temperatures", Cer. Eng.Sci. Proc., 6(1985), p1356-1364

[132] A.Lipp, K.A.Schwerz and K.Hunold; "Hexagonal boron nitride: Fabrication, Properties and Applications", J.Eur.Ceram.Soc., 5 (1989), p3-9

[133] A.Joly : C.R.Hebd.Seances acad.Sci., 97 (1883), 456-458

[134] R.P.Elliot : U.S. AEC ARF-2200-12 (1961)

[135] H.J.Becher and F.Thevenot : "Infrarotspektroskopische Unterschung des Borcarbids und seiner isotypen Derivate $B_{12}O_2$, $B_{12}P_2$ und $B_{12}As_2$", Z.Anorg.Allg.Chem., 410 (1974), 274-86

[136] F.Thevenot; "Laboratory methods for the preparation of boron carbides", in NATO Adv.Res.Workshop (ARW), The physics and Chemistry of Carbide, Nitride and Borides, ed. R.Freer, Manchester, UK, Sep.1989.

[137] J.C.Angus, A.Argoitia, R.Gat, Z.Li, M.Sunkara, L.Wang and Y.Wang : Chemical Vapour Deposition of Diamond, Phil.Trans., Royal Society, Lodon, A (1993), 342, 193-322

[138] J.C.Walmsley and A.R.Lang : "A Transmission Electron Microscope Study of a Cubic Boron Nitride-Based Compact Material with AlN and AlB_2 Binder Phases", J.Mater.Sci., 22 (1987), 4093-4102

[139] Y.Kokudate et al : 3rd IUMRS Inst.Conf., Advanced Materials, Tokyo, Aug. 31-Sep.4, (in press)

[140] B.V.Deryagia and D.V.Fedssayer : Diamond Growth and Films UCIMG, Elsevier Applied Science, London, 1989, in Growth of Graphite from the gaseous phase, 163

[141] A.D.McLeod, J.S.Haggerty and D.R.Sadoway : "Electrical Resistivities of Monocrystalline and Polycrystalline TiB_2", J.Am.Cera.Soc., 67 (1984), 2, 705-708

[142] M.A.Janney : "Mechanical Properties and Oxidation behavioe of a Hot-Pressed SiC-15 vol%-TiB_2 Composite", Am.Ceram.Soc.Bull., 66 (1987), 2, 322-324

[143] C.H.McMurty, W.D.G.Beocker, S.G.Seshadri, J.S.Zhanghi and J.E.Ganier : "Microstructure and Material Properties of SiC-TiB_2 Particulate Composites", Am.Ceram.Soc.Bull., 66 (1987), 2, 325-329

[144] G.V.Samsonov and I.M.Vinitskii : "Handbook of Refractory Compounds", IFI/Plenum, NewYork, 1980, p40, 441, 442

[145] R.Kiessling : "The borides of some transition elements", Acta. Chem. Scand. 4 (1950) 209-227.

[146] K.E.Spear, P.McDowell and F.McMahon : "Experimental Evidence for the Existence of the Ti_3B_4 Phase", J.Am.Ceram.Soc., 69 (1986), 1, C4-C5

[147] B.Post, F.W.Glaser and D.Moskowitz : "Transition Metal Diborides", Acta Metallurgica 2 (1954), [1], 20-25

[148] W.A.Zdaniewski : "Solid Solubility Effect on Properties of TiB_2", J. Am. Ceram. Soc., 70 (1987), 11, 793-97

[149] W.A.Zdaniewski : "Degradation of hot pressed TiB_2-TiC composite in liquid aluminium." , Am. Ceram. Soc. Bull., 65 (1986), 10, 1408-14.

[150] J.Brynestad, C.E.Bamberger, D.E.Heartherly and J.F.Land : "Synthesis of Submicron TiB_2 Powders", High Temp.Sci., 19 (1985), 41-49

[151] J.D.Mackenzie and D.R.Ulrich : "Ultrastructure processing of advanced ceramics", (Wiley interscience, 1988).

[152] J.Casting and P.Costa : Properties and Uses of Diborides, Boron and Refractory Borides, pp390-412, Springer-Verlag, New York, (1977)

[153] E.S.Kang, C.W.Jang, C.H.Lee and C.H.Kim : "Effect of Iron and Boron Carbide on the Densification and Mechanical Properties of Titanium Diboride Ceramics", J.Am.Cera.Soc., 72 (1989), 10, 1868-72

[154] M.K.Ferber, P.F.Becher and C.B.Finch : "Effect of Microstructure on the Properties of Titanium Diboride Ceramics", Comm.Am.Ceram.Soc., Jan. (1983), C2-C4

[155] P.C.Cobb : "Titanium Carbide as a Sintering Agent for Titanium Boride", Materials & Design, 11 (1990), 3, 156-159

[156] S.Baik and P.F.Becher : "Effect of Oxygen Contamination on Densification of TiB_2", J.Am.Ceram.Soc., 70 (1987), 8, 527-530

[157] J.Besson, F.Valin, P.Lointier and M.Boncoeur : "Densification of Titanium Diboride by Hot Isostatic Pressing and Production of Near-Net-Shape Components", JMEPEG, vol.1 (1992), 5, 637-650

[158] C.E.Holcombe and N.L.Dykes : "Microwave sintering of Titanium Diboride", J.Mater.Sci., 26 (1991), 3730-3738

[159] Y.Miyamoto and M.Koizumi : "High-Pressure Self-Combustion Sintering for Ceramics", Comm.Am.Ceram.Soc., Nov. (1984), C224-C225

[160] H.P Kirchener : Strengthening of Ceramics, Marcel Dekker, New York, (1979)

[161] L.K.Walker and C.K.Saha : "Formation of a surface carbide layer during sintering of titanium diboride", J.Am.Ceram.Soc., 71 (1988), 4, C207-209

[162] L.Kaufman and E.V.Clougherty : "Investigation of Boride Compound for Very High Temperature Application", Tech.Rept.RTD-TDR-63-4069, Cambridge, MA, Dec. 1963

[163] R.M.Adams (Ed.) : Boron, metallo-boron compounds and boranes, Interscience publishers, New York. (1964).

[164] P.Schumacher and L.Greer : "Enhanced Heterogeneous nucleation of λ-Al in Amorphous Aluminium Alloys", 8th International Conference on Rapidly Quenched and Metastable Materials, Sendai, Japan, Aug. 22-27, 1993, E10-24

[165] K.Shobu and T.Watanabe : "Frictional Properties of Sintered TiN-TiB_2 and Ti(CN)-TiB_2 Ceramics at High Temperature", J.Am.Ceram.Soc., 70 (1987), 5, C103-C104

[166] William Hume-Rothery and G.V Raynor : "The structure of Metals and Alloys", The Institute of Metals, Richard Clay and Company LTD., 1972, p329, p325

[167] G.M.Farrior : "Diborides in the pseudo-binary system TiB_2-CrB_2; electrical properties" U.S. Dept. of the interior, Bureau of mines report number 6691 (1965).

ACKNOWLEDGEMENTS

I am profoundly grateful to Dr.A.Jha for supervising, suggestions and encouragement which I received throughout this work.

I also expresses my thanks to Professor P.Grieveson and Professor C.Bodsworth for their careful reading, kind advice and encouragement.

I sincerely wish to thank to President D.H.Baik, Dr.C.H.Rhee and all the colleagues in RIST (Research Institute of Science and Technology, Pohang, Korea) for providing opportunity to study this project.

I am greatly indebted to Dr.H.K.Shin who encouraged and gave me a momentum for refreshing my scientific interest.

I am also acknowledge the financial support from the ORS (Overseas Research Student) Awards Scheme in U.K.

Finally, but above all, I couldn't express gratitude sufficiently to my family - parents, my lovely Jihyun, Wonho and especially my wife - for their patient, long suffering and self-sacrificing support during these time.